ResearchOnline@JCU

This file is part of the following reference:

Lu, Jun (2013) *Modelling and control of proton exchange membrane fuel cell.* PhD thesis, James Cook University.

Access to this file is available from:

http://researchonline.jcu.edu.au/40440/

The author has certified to JCU that they have made a reasonable effort to gain permission and acknowledge the owner of any third party copyright material included in this document. If you believe that this is not the case, please contact ResearchOnline@jcu.edu.au and quote
http://researchonline.jcu.edu.au/40440/

JAMES COOK UNIVERSITY
AUSTRALIA

Modelling and Control of Proton Exchange Membrane Fuel Cell

Thesis submitted by

Jun Lu BEng(Hons)

In April 2013

for the degree of Doctor of Philosophy

in the School of Engineering and Physical Sciences

James Cook University

Statement of Access

I, the undersigned, author of this work, understand that James Cook University will make this thesis available for use within the University Library and, via the Australian Digital Theses network, for use elsewhere.

I understand that, as an unpublished work, a thesis has significant protection under the Copyright Act and; I do not wish to place any further restriction on access to this work.

_____21/04/2013_____

Date

Signature

_____Jun Lu_____

Name

Statement of Sources

I declare that this thesis is my own work and has not been submitted in any form for another degree or diploma at any university or other institution of tertiary education. Information derived from the published or unpublished work of others has been acknowledged in the text and a list of references is given.

21/04/2013

Date

Signature

Jun Lu

Name

Statement on the Contribution of Others

Nature of Assistance	Contribution	Names, Affiliations of Co-Contributors
Intellectual support	Thesis supervision	Associate Professor Ahmad Zahedi, Associate Professor Mohan Jacob, James Cook University
Financial support	Scholarship	Chinese Scholarship Council & James Cook University Joint Scholarship
	Research fund	School of Engineering and Physical Sciences & Graduate Research School, James Cook University

Acknowledgements

I would like to begin by acknowledging James Cook University (JCU) and Chinese Scholarship Council (CSC) for providing financial assistance through the JCU-CSC Joint Scholarship.

I wish to express my sincere gratitude to Associate Professor Ahmad Zahedi, my supervisor, and Associate Professor Mohan Jacob, my co-supervisor, for their excellent guidance throughout my degree.

I wish to extend my gratitude to Professor Dr. Yinghe He, Head of Engineering School, and other staff of the Engineering School for their support, encouragement and friendship during my research and writing of this thesis.

Finally, I would like to thank my family back home in China for tolerating my three-year absence, and for giving me excellent motivation to work hard and finish quickly!

ABSTRACT

Proton exchange membrane fuel cell (PEMFC) has been considered as one of the most promising energy sources due to its many desirable properties, including high power density, low operating temperature and fast start-up. However, significant technical challenges exist before PEMFC can be commercialized. Among them, the modelling and control of PEMFC have been recognized as the most critical technical issues. This is because PEMFC‘s inherent nonlinearities, time-varying characteristics and tight operating constraints inevitably give rise to great challenges for system modelling and control. The objective of this thesis is then accurate modelling and efficient control of PEMFC. To accomplish these goals, new modelling and control methods are developed and validated.

First, a new empirical model of PEMFC is developed by mapping performance outputs as a function of various operating conditions through regression analysis of support vector machine (SVM). Further, the empirical modelling approach is integrated with the mechanistic modelling method to develop a combined model of PEMFC, which consists of an empirical submodel for the reference voltage and a mechanistic submodel for the correction voltage. Simulation results demonstrate that these models have desirable properties, including good accuracy, fast response and low computational burden. These characteristics lay the solid foundation for the development of control strategies.

Then, various control strategies are developed, including model predictive control (MPC) for regulating PEMFC outputs to the desired value, extreume seeking control (ESC) for tracking the maximum efficiency point and linearized-model-based control for PEMFC

thermal management. Simulation results demonstrate that each of the control strategies achieves the control objective that it is supposed to accomplish.

Finally, a full picture of future hydrogen economy in China is given, including drivers for transition to the hydrogen economy, energy resources and their potential role in future hydrogen production, government‘s policy and support for the research of hydrogen and fuel cell technology.

Table of Contents

ABREVIATIONS

AFC	Alkaline Fuel Cell
CL	Catalyst Layer
DMFC	Direct Methanol Fuel Cell
ESC	Extremum Seeking Control
GDL	Gas Diffusion Layer
MCFC	Molten Carbonate Fuel Cell
MEA	Membrane Electrode Assembly
MEPT	Maximum Efficiency Point Tracking
MPC	Model Predictive Control
PAFC	Phosphoric Acid Fuel Cell
PEMFC	Proton Exchange Membrane Fuel Cell
PSO	Particle Swarm Optimization
SOFC	Solid Oxide Fuel Cell
SVM	Support Vector Machine

List of Tables

List of Figures

List of Publications

The publications in this list were written during the PhD candidature and include the research results.

Peer-Reviewed Journal Publications

Jun Lu, Ahmad Zahedi, "Air supply control for maximum efficiency point tracking in Fuel cell systems," *Journal of Renewable and Sustainable Energy*, vol. 4, paper no. 033106, pp. 1-15, 2012. (Impact Factor 1.214)

Jun Lu, Ahmad Zahedi, "Constrained model predictive control of PEMFC based on a combined empirical and mechanistic model," *Journal of Renewable and Sustainable Energy*, vol. 4, paper no. 53116, pp. 1-15, 2012. (Impact Factor 1.214)

Jun Lu, Ahmad Zahedi, "Building the hydrogen economy in China: drivers, resources and technologies," *Renewable and Sustainable Energy Reviews*, vol. 23, pp. 543-556, 2013. (Impact Factor 6.018)

Jun Lu, Ahmad Zahedi, "Thermal modelling and management of proton exchange membrane fuel cell," *Energy Sources, Part A Recovery, Utilization and Environmental Effects*, in press. (Impact Factor 0.715)

Peer-Reviewed Conference Publications

Jun Lu, Ahmad Zahedi, "Maximum efficiency point tracking control for fuel cell power systems," *in Proceedings of 2010 International Conference on Power system Technology*, pp. 1-6, 2010.

Jun Lu, Ahmad Zahedi, "Modelling and control of PEMFC based on support vector machine," in *Proceedings of 2011 Australasian Universities Power Engineering Conference*, pp. 1-6, 2011.

Jun Lu, Ahmad Zahedi, "Model predictive control for PEMFC based on least square support vector machine," *in Proceedings of 2012 Asia-Pacific Power and Energy Engineering Conference*, pp. 1-4, 2012.

Jun Lu, Ahmad Zahedi, "Support vector machine based predictive controller with swarm intelligence for PEMFC," in *Proceedings of 2012 Australasian Universities Power Engineering Conference*, pp. 1-6, 2012.

Jun Lu, Ahmad Zahedi, "Predictive control of PEMFC based on a combined empirical and mechanistic model," *in Proceedings of 2012 International Conference on Power system Technology*, pp. 1-6, 2012.

Ahmad Zahedi, **Jun Lu**, "Economic evaluation of grid-connected solar PV production cost in New Zealand," *in Proceedings of 2012 International Conference on Power system Technology*, pp. 1-4, 2012.

Chapter 1 Introduction

1.1 Overview of fuel cells

Fuel cells are electrochemical devices that convert the chemical energy of a reaction directly into electrical energy. In a typical fuel cell, fuel (hydrogen, methanol, natural gas, etc) is fed continuously to the anode (negative electrode) and an oxidant (often oxygen from air) is fed continuously to the cathode (positive electrode). The electrochemical reactions take place at the electrodes to produce an electric current through the electrolyte, while driving a complementary electric current that performs work on the load. As opposed to a battery wherein the chemical reactants are exhausted, the fuel cell is an energy conversion device which can theoretically produce energy so long as the fuel/oxidant supply to the electrodes is maintained. In addition, fuel cells produce electrical energy directly from chemical energy. As a result, fuel cells are not limited by the thermodynamic limitation of conventional heat engines, such as the Carnot cycle efficiency. Since NASA first adopted fuel cell systems as the electric power generating units for their spacecrafts in the 1950s~1960s, fuel cells have sparked much interest and activity as alternative power generators [1].

Fuel cells are classified into six types based on the type of electrolyte: proton exchange membrane fuel cell (PEMFC), direct methanol fuel cell (DMFC), alkaline fuel cell (AFC), phosphoric acid fuel cell (PAFC), molten carbonate fuel cell (MCFC), and solid oxide fuel cell (SOFC). The type of electrolyte determines the electrode reactions and the type of ions that carry the current across the electrolyte. In addition, the choice of electrolyte dictates the operating temperature range of the fuel cell. Aqueous electrolytes are limited to

temperatures of about 200 °C or lower because of their high vapor pressure and rapid degradation at higher temperatures. The operating temperature also plays an important role in dictating the degree of fuel processing required. In low-temperature fuel cells, all the fuel must be converted to hydrogen prior to entering the fuel cell. In addition, the anode catalyst in low temperature fuel cells (mainly platinum) is strongly poisoned by CO. In high-temperature fuel cells, CO and even CH_4 can be internally converted to hydrogen or even directly oxidized electrochemically. Table 1.1 provides an overview of the key characteristics of the main fuel cell types, while major advantages and disadvantages of each fuel cell type are summarized in Table 1.2 [2] [3].

Table 1.1 Key characteristics of the main fuel cell types

	DMFC	PEMFC	PAFC	MCFC	SOFC	AFC
Electrolyte	Polymer	Polymer	H_3PO_4	$KLiCO_3$	ZrO_2 withY_2O_3	KOH
Electrodes	Carbon	Carbon	Carbon	Ni and Ni_2O_3	$CatiO_3$	Ni
Temperature (K)	300-360	<360	<470	870-920	1120-1320	300-350
Charge carrier	H^+	H^+	H^+	CO_3^{2-}	O^{2-}	OH^-
Sensitivity of CO/S	Yes/ Yes	Yes/ Yes	Yes/ Yes	No/<10ppm H_2S (anode) <1ppm SO_2 (cathode)	No/<1ppm	Yes/ Yes
Fuel	H_2	H_2	H_2	H_2 and CO	H_2 and CO	H_2
External reforming	Yes	Yes	Yes	No, for some fuels	No, for some fuels	Yes
Size range (KW)	0.001-0.01	1-250	100-1000	100-2000	5-2000	1-100
Utilization type of energy	Electricity	Electricity Heat	Electricity Heat	Electricity Heat &steam	Electricity Heat &steam	Electricity
Efficiency (%)	20-25	-40	-45	45-50	45-50	50-60
Projected system cost ($/kW)	_	1000-2000	5000 (current)	2000-3000	2000-3000	1900

Table 1.2 Advantages and disadvantages of the main fuel cell types

Type	Advantages	Disadvantages
PEMFC	- Quick system start-up and shut down - Proper portable applications - Electrolyte has outstanding resistance to gas crossover - Highest power density of all the fuel cells	- Expansive catalyst (platinum) - Difficulties in thermal/water management - Poor CO, S, and NH_3 tolerance - Complex system configuration (external fuel processing system)
DMFC	- Simple structure - Good for low power/long operating hours	- Poor cell efficiency - Poor for high power/short term operation
PAFC	- Mature technology - Cogeneration is available - Excellent reliability and long-term running - Relatively inexpensive electrolyte	- Slow reduction in the cathode side (requires platinum catalyst) - Electrolyte is a corrosive liquid - Complex system configuration
MCFC	- Fuel flexibility - Non-precious metal catalyst - High quality waste heat for cogeneration - Higher system efficiency than PEMFC/PAFC	- Corrosive and mobile electrolyte - High temperature promotes material problems (degradation/lifetime issues) - High contact resistance and cathode resistance limit power density
SOFC	- Fuel flexibility - Non-precious metal catalyst - Solid electrolytes allow various shapes of cell - High quality waste heat for cogeneration	- High temperature causes material problems such as thermal expansion - Sealing issues - Limited range of material selection - Relatively expansive components and Fabrication
AFC	- Highest efficiency of all the fuel cells - Low manufacturing and operation costs - Mature technology	- Poor CO_2 tolerance - Electrolyte is a corrosive liquid - Complex system configuration

1.2 Overview of proton exchange membrane fuel cell

Since the first application of PEMFC systems was initially reported in the New Generation of Vehicles program (PNGV) in the US in 1993 [4], PEMFC research has been attracting increasing attention worldwide. PEMFC has shown great potential for transportation application due to its many advantages, such as long stack life, high power density, low operating temperature, fast start-up, suitability for discontinuous operation [5-8]. In addition, a hydrogen-powered PEMFC does only emit water with no carbon dioxide or other pollutants.

Figure 1.1 shows the schematic of components and working principle of a single cell in the PEMFC stack. As can be seen, cathode (positive electrode) and anode (negative electrode) are separated by electrolyte (e.g., a polymer membrane). Each electrode is made up of a thin catalyst layer (CL) which contains the electro-catalyst, and a porous gas diffusion layer (GDL). The GDL, in addition to serving as a mechanical support for the thin catalyst layer, allows for the diffusion of the reactant gases to, and removal of products from the catalyst sites. The membrane and the electrodes together are commonly referred to as the membrane electrode assembly (MEA).

Now, consider the working principle of PEMFC. On the cathode side, oxygen diffuses through the GDL towards the electrolyte and is reduced, while hydrogen is oxidized on the anode side. The migration ion H^+ forms at the anode and carries the charge through the proton exchange membrane towards the cathode side. On the other hand, the electrons pass through the current collectors into an external circuit towards the cathode, and water is produced on the cathode side. An electrical circuit is created by the ion transfer through the electrolyte and the electron transfer through the external circuit.

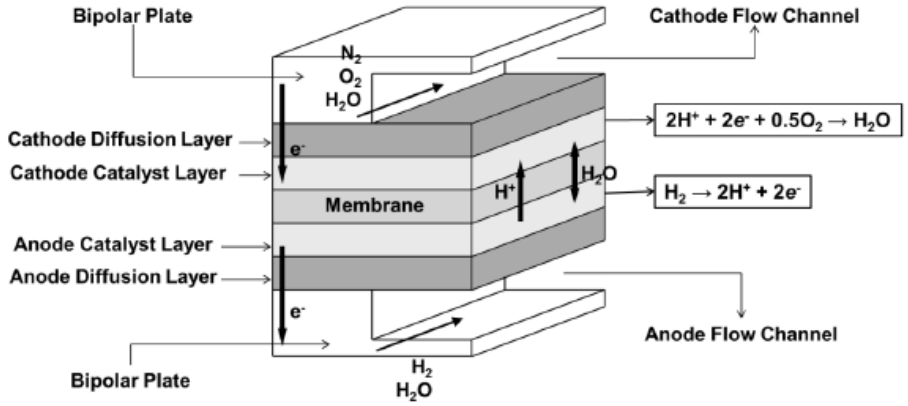

Figure 1.1 Schematic of components and working principle of a cell in PEMFC stack

The bipolar plate (interconnector) is used for separating the cells in a stack, connecting them electrically in series, and providing flow channels (see Figure 1.2). In addition, some of the flow channels on the plate may act as cooling channel for the purpose of thermally management in the stack. The stack is connected to an external circuit via a current collector (see Figure 1.3). The reactants are supplied to the electrodes using the manifolds.

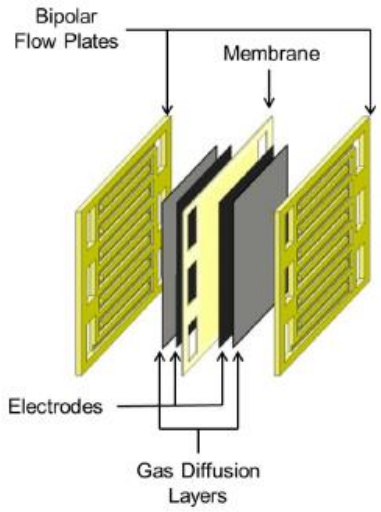

Figure 1.2 Exploded view of a basic unit of a PEMFC stack

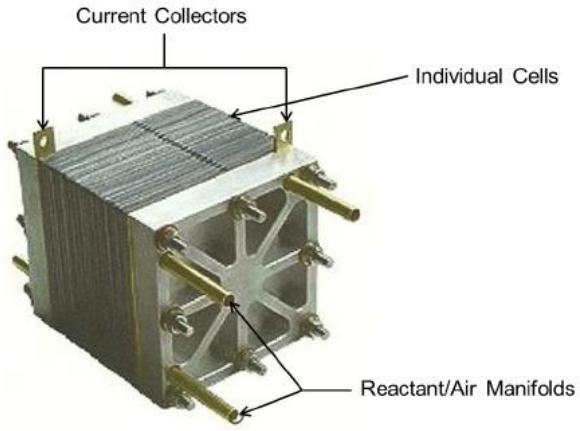

Figure 1.3 External view of a PEMFC stack

1.3 Scope of the thesis

This thesis addresses four major themes regarding the development of PEMFC: (1) modelling, (2) control, (3) maximum efficiency point tracking (MEPT), (4) thermal modelling and management. In addition, key issues of building hydrogen economy in China, including drivers, resources and technologies, are reviewed. The significance of these problems is briefly explained in the following section.

One of the most important aspects in developing PEMFC is the mathematical modeling. The mathematical model serves as an indispensible tool for studying static and dynamic behaviour of PEMFC, designing the cells, evaluating control strategies and designing experiments; it helps reduce the number of experimental tests required to study the cells systematically [9]. Simulation studies can determine the effects of various operating conditions on the performance of PEMFC. Therefore, modelling is considered as the first priority and discussed in Chapter 2.

Another fundamental aspect in developing PEMFC is the control strategy. The basic control goals of PEMFC are: (a) maintaining the output voltage when variations in operating conditions occur, (b) supplying the required power in the presence of rapid variations in the external loads. Another control problem particularly for PEMFC is the phenomenon of oxygen starvation, which may occur when there is a sudden large increase in the load power. In this case, the partial pressure of oxygen drops significantly, accompanied by a rapid decrease in cell voltage, which in turn shortens the life of PEMFC [9]. Therefore, a proper controller is required to effectively prevent oxygen starvation. To achieve these objectives, a series of control strategies are designed and tested in Chapter 3.

The core factor that affects its commercialization potential is the cost of electricity provided by PEMFC system. The cost of electricity is determined by the capital cost of the PEMFC system, the cost of fuel and the efficiency of the whole system. The PEMFC system that always operates at the maximum efficiency produces the least expensive electricity. As a result, the ability to increase the operational efficiency is a crucial issue for the design of a cost-effective fuel cell system with high market competitiveness [10]. Therefore, the maximum efficiency point tracking of PEMFC system is discussed in chapter 4.

Thermal management is crucial for the safe operation of PEMFC as current PEMFC operates in a narrow temperature range of 60 – 80°C and tolerates only a small temperature variation [11]. This range is dictated by the material properties of the proton exchange membrane, most commonly Nafion. Abnormal operating temperature may devastate the performance or even cause permanent damage to the cell. Therefore, thermal study is conducted in Chapter 5.

As an emerging giant of the world economy and international energy markets, China is transforming the global energy system by dint of its sheer size and its growing weight in international energy trade. How rapidly China‘s energy needs develop and how they are met will have far-reaching consequences for the rest of the world. The major concern for improving energy security and reducing greenhouse gas emissions, together with the rapid development of fuel cell technologies in recent years, is focusing China‘s opinion on options for future hydrogen economy. As such, Chapter 6 reviews drivers, resources, and technologies for building the hydrogen economy in China. The results will help us understand China‘s energy system and its impact on global environment and energy trade.

1.4 Challenges and objectives

1.4.1 Modelling

The PEMFC system is a complex system with highly coupled electrochemical, thermodynamics and fluid dynamics. Especially, PEMFC system‘s inherent nonlinearities, time-varying properties and tight operating constraints give rise to great challenges for system modelling [12]. These characteristics make traditional linearization-based models and control methods only valid in the neighborhood of the optimal operating point. In real world applications, however, PEMFC does not usually operate at the optimal steady-state designed by the fuel cell manufacturer [13]. The operating point of PEMFC may change frequently over a wide operating range due to the fluctuating power demands or varying operating conditions. Therefore, novel nonlinear modelling and control method must be employed.

Models of PEMFC in the literature can be classified into two categories: mechanistic models and empirical models. Mechanistic models refer to those using basic physical or electrochemical equations for investigating the details of operation in PEMFC. These models usually have very complicated expression with some key physical parameters that are even immeasurable. In addition, these models require iterative methods to solve the underlying differential and partial differential equations, thereby making them computationally intensive. In essence, mechanistic models are suited for the design and optimization of the cell components, rather than for control purpose.

On the other hand, empirical models behave like a black box, focusing only on input-output relationship. These models allow quick prediction of the PEMFC‘s performance given operating conditions, which lays down a solid foundation for the

real-time calculation of the control algorithm. From this perspective, empirical models are more suitable for control study.

Based on the discussion above, it can be concluded that empirical model is the better choice for this research due to the requirement of control study. Accordingly, the specific objectives for developing the empirical model of PEMFC are to:

- Acquire PEMFC operation data including manipulated inputs, disturbance inputs and performance outputs.
- Develop the empirical model of PEMFC with the operation data. Pre-processing of the raw data may be required.
- Validate the performance of the proposed empirical model. A performance comparison between the novel empirical model and the conventional model is preferred.

1.4.2 Control

As with modelling, the major barriers for the control strategy are PEMFC‘s nonlinearities and time-varying properties. One approach to circumvent these problems is investigating the system in real time. Thus, time-dependent parameters can be more readily tracked and a model structure can be more accurately estimated. Model predictive control (MPC), characterized by its receding horizon strategy, is the one employing such method. The basic idea of receding horizon strategy involves real-time estimation of system states and solution of the control problem for the given state; the first part of the resulting input signal is implemented and the whole process is repeated.

In addition, the tight operating constraint of PEMFC also poses challenges for the controller design. In PEMFC system, several constraints must be respected. First of all, the supply of sufficient hydrogen and air must be ensured at all times. Moreover, the hydrogen and air supply must be coordinated in a way that the pressure difference across the fuel cell membrane is small to avoid membrane damage. In other words, the partial pressure difference between oxygen and hydrogen should be maintained in a safe range. On the other hand, a major advantage of MPC over other control schemes is its ability of handling constraints in a systematic and straightforward manner [14]. This is because that the MPC formulates the control problem as the optimization of an objective function. By employing a proper optimization algorithm, the resulting constrained optimization problem can be effectively solved.

To summarize, MPC has great potential to handle PEMFC‘s inherent nonlinearities, time-varying characteristics and tight operating constraints. Accordingly, the specific objectives for developing MPC strategy are to:

- Design the MPC strategy based on the PEMFC empirical model developed previously.
- Select an efficient optimization algorithm to solve the optimization problem formulated by MPC. Modification of the optimization algorithm may be required to handle the constraints.
- Test the performance of the proposed MPC strategy. Both static scenario and dynamic scenario must be considered.

1.4.3 Maximum efficiency point tracking

The efficiency of the fuel cell system nonlinearly depends on various operating conditions. Among them, the air flow supplied to the fuel cell system is one of the most significant factors in determining the efficiency. The conventional method of controlling the air flow is to stabilize the oxygen supply at a predetermined constant rate for the optimal efficiency. However, in practice, the optimal point can deviate from the pre-set value due to the varying operating conditions, such as the uncontrollable load [15]. Therefore, the major barrier of achieving maximum operating efficiency lies in the real-time estimation of the optimal air supply level. Moreover, sufficient air supply must be ensured at all time to prevent oxygen starvation. As a result, a maximum efficient point tracking (MEPT) controller is required for estimating and tracking the time-varying maximum efficient point. Accordingly, the specific objectives are to:

- Analyse the efficiency of PEMFC under various operation conditions and obtaining the efficiency curves with peaks indentified.
- Design the MEPT controller that can handle the time-varying maximum efficient point.
- Validate the performance of the proposed MEPT controller. The result must be compared with that of steady-state efficiency analysis.

1.4.4 Thermal modelling and management

Despite a large number of publications on thermal modelling of PEMFC, models suitable for thermal management are still lacking. Most existing models are mechanistic models,

ranging from one dimensional non-isothermal models [16] to three dimensional non-isothermal models [17], [18]. These models are developed for investigating the temperature distribution within the cell, rather than for temperature control. As a result, the first barrier is the lack of a control-oriented thermal model of PEMFC. On top of that, a temperature controller that can handle the nonlinearities and disturbances is required. Accordingly, the specific objectives are to:

- Develop a control-oriented thermal model of PEMFC
- Design a thermal controller that can handle the nonlinearities and disturbances
- Validate the performance of the proposed thermal model and controller

1.4.5 Building the hydrogen economy in China

China is unique in terms of its vast area, huge population and rapid economic growth. These situations provide both opportunities and challenges for the transition towards the hydrogen economy. In order to clarify a clear vision of future hydrogen economy in China, three factors that should be paid special attention to are: drivers, resources and technologies. Accordingly, the specific objectives are to:

- Identify China‘s main drivers for the transition towards the hydrogen economy
- Review China‘s energy supply matrix and analysing the potential role of different energy resources in future hydrogen economy

- Review China‘s policy and government support programs for the R&D of hydrogen and fuel cell technologies. Research achievements are also required to be summarized.

1.5 Organization of the thesis

In Chapter 2, the modelling of PEMFC is discussed. First, the major concerns in the development of PEMFC models are summarized and some of the most representative examples of PEMFC models in the literature are reviewed. Then, the theory of support vector machine (SVM) is briefly introduced and the empirical model of PEMFC is developed using SVM. Finally, the combined empirical and mechanistic model is proposed.

In Chapter 3, the control of PEMFC is addressed. First, a literature review on PEMFC control strategy is conducted. Then, the principle of MPC is briefly reviewed and the model predictive controller for PEMFC is designed. Next, the theory of particle swarm optimization (PSO) is introduced and the novel MPC strategy is designed based on the particle swarm optimizer. Finally, the constrained MPC strategy is designed based on the combined model developed previously. The standard PSO algorithm is modified to solve the constrained optimization problem formulated by MPC.

In Chapter 4, the maximum efficiency point tacking problem is formulated and a MEPT controller is designed. First, the steady-state efficiency analysis is conducted and efficiency curves under different operating conditions are obtained. Then, the theory of extremum seeking control (ESC) is introduced and the MEPT controller is designed based on extremum seeking control algorithm. Finally, the whole system is simulated and results are discussed.

In Chapter 5, the thermal management of PEMFC is discussed. First, general issues of thermal management in PEMFC are analyzed and the existing thermal models and control methods are reviewed. Then, the control-oriented thermal model of PEMFC is developed and the model-based thermal controller is designed. Finally, the whole system is simulated and results are discussed.

In Chapter 6, key issues concerning China‘s transition towards hydrogen economy are reviewed. First, a brief presentation of China‘s geographic and economic data, together with its energy consumption profile, is given. Then, China‘s main drivers for the hydrogen economy are discussed. A section on China‘s energy supply matrix and potential sources for hydrogen production follows. Finally, the interests in hydrogen and fuel cell technologies within China are reviewed.

Chapter 7 summarizes the major contributions of this thesis and presents the conclusions. Future work is also suggested.

References

[1] J. M. Andujar, F. Segura, "*Fuel* cells: history and updating. A walk along two centuries," *Renewable Sustainable Energy Rev.*, vol.13, pp. 2309-2322, 2009.

[2] National Energy Technology Laboratory, U.S. Department of Energy, *Fuel Cell Handbook*, University Press of the Pacific, 2005.

[3] R. O'Hayre, S. Cha, W. Colella, F. Prinz, *Fuel Cell Fundamentals*, New York: Wiley, 2006.

[4] P. Costamagna, S. Srinivasan, "Quantum jumps in the PEMFC science and technology from the 1960s to the year 2000 Part I. Fundamental scientific aspects." *J. Power Sources*, vol. 102, pp. 242–252, 2001.

[5] P. Costamagna, S. Srinivasan, "Quantum jumps in the PEMFC science and technology from the 1960s to the year 2000 Part II. Engineering, technology, development and application aspects," *J. Power Sources*, vol. 102, pp. 253–269, 2001.

[6] S. G. Chalk, J. F. Miller, F. W. Wagner, "Challenges for fuel cells in transport applications," *J. Power Sources*, vol. 86, pp. 40–51, 2000.

[7] V. Mehta, J. S. Cooper, "Review and analysis of PEM fuel cell design and manufacturing," *J. Power Sources*, vol. 114, pp. 32–53, 2003.

[8] S. Gamburzev, A. J. Appleby, "Recent progress in performance improvement of the proton exchange membrane fuel cell (PEMFC)," *J. Power Sources*, vol. 107, pp. 5–12, 2002.

[9] M Bavarian, M Soroush, I. G. Kevrekidis, J. B. Benziger, "Mathematical modeling, steady-state and dynamic behavior, and control of fuel cells - a review," *Ind. Eng. Chem. Res.*, vol. 49, pp. 7922–7950, 2010.

[10] W. Na and B. Gou, "The efficient and economic design of pem fuel cell systems by multi-objective optimization," *J. Power Sources*, vol.166, pp. 411-418, 2007.

[11] S. G. Kandlikar, Z Lu, ―Thermal management issues in a PEMFC stack - A brief review of current status,‖ *Appl. Therm. Eng.*, vol.29, pp. 1276-1280, 2009.

[12] J. G. Williams, G. Liu, S. Chai, and D. Rees, "Intelligent control for improvements in PEM fuel cell flow performance," *Int. J. Autom. Comput.*, vol. 5, pp. 145-151, 2008.

[13] J. Golbert, and D. R. Lewin, "Model-based control of fuel cells (1): Regulatory control," *J. Power Sources*, vol. 135, pp. 135-151, 2004.

[14] L. Wang, F. Wan "Structured neural networks for constrained model predictive control." *Automatica*, vol. 37, pp. 1235–1243, 2001.

[15] M. Jang, J. Lee, J. Kim, J. Park, B. Cho, ―Maximum Efficiency Point Tracking Algorithm Using Oxygen Access Ratio Control for Fuel Cell Systems,‖ *J. Power Electron.*, vol. 11, pp. 194-201, 2011.

[16] M. Wohr, K. Holwin, W. Schurnberger, M. Fischer, W. Neubrnad, G. Eigenberger, ―Dynamic modeling and simulation of a polymer membrane fuel cell including mass transport limitation,‖ *Int. J. Hydrogen Energy*, vol. 23, pp. 213-218, 1998.

[17] T. Berning, N. Djilali, ―Three-dimensional computational analysis of transport phenomena in a PEM fuel cell—a parametric study,‖ *J. Power Sources*, vol. 124, pp. 440-452, 2003.

[18] T. Berning, D.M. Lu, N. Djilali, ―Three-dimensional computational analysis of transport phenomena in a PEM fuel cell,‖ *J. Power Sources*, vol. 106, pp.284-294, 2002.

Chapter 2 Modelling

Mathematical modeling is an indispensable tool for studying static and dynamic behavior of fuel cells, optimizing the design of the cell and evaluating control strategies. With the help of mathematical models, the number of experimental tests required can be reduced to a large extent. Through simulation studies, one can easily understand the effects of various operating conditions, cell temperature distribution or thermal stresses, etc. As such, modelling of PEMFC has received much attention over the last decade.

The major contributions of Chapter 2 includes: (1) The novel empirical models of PEMFC are developed using support vector machine (SVM). SVM is a nonlinear generalization algorithm, which learns from experimental data to establish input-output relationship through regression analysis. The SVM models of PEMFC map the performance outputs as a function of various operation conditions and predict future output without the knowledge of internal details. (2) The hybrid modelling approach is proposed based on the combination of prior knowledge, under the form of mechanistic submodel, with empirical submodel devoted to the extraction of knowledge from operating data. The empirical submodel is a SVM model, which predicts cell voltage at different stack currents and temperatures under the reference hydrogen and oxygen partial pressure. The mechanistic submodel calculates the correction voltage by taking account of hydrogen and oxygen partial pressure changes.

The chapter is organized as follows: In section 2.1, the major concerns in the development of PEMFC models are summarized. In section 2.2, some of the most representative examples of PMEFC models in the literature are reviewed. In section 2.3, support vector machine is introduced for the modelling of PEMFC. In section 2.4, empirical

models of PEMFC are developed using SVM. In section 2.5, the combined empirical and mechanistic model of PEMFC is proposed.

2.1 General features of PEMFC models

Over the past decades, a great number of PEMFC models have been developed with different features and focuses. As the optimal model choice differs for each application and user, it is necessary to clarify what the key features of the desired model are before developing models. Although vital for the result, these initial criteria often tend to be overlooked [1]. Table 2.1 summarizes the key features of PEMFC models.

Table 2.1 Key features of PEMFC system model

Approach (mechanistic, empirical)
State (steady-state, transient)
Boundary (cell, stack, system)
Dimension (0D,1D,2D,3D)
Phenomena to Take into Account

- **Approach**

The first criterion in the table is modelling approach. A PEMFC model may fall into one of two categories: mechanistic or empirical. A mechanistic (or called ―theoretical") model is based on in-depth knowledge of the electrochemistry, heat transfer and mass transfer involved in the fuel cell, using basic, phenomenological equations such as the Butler-Volmer equation for cell voltage, the Stefan-Maxwell equation for gas-phase

transport, and the Nernst-Planck equation for species transport. Depending on its focus, the model explain the fundamental processes occurring in the fuel cell, such as cell flow pattern, current density distribution, voltage and pressure drops. However, these models usually require iterative methods to solve the underlying differential and partial differential equations, which makes them computationally intensive. Besides, given the highly reactive environment within the fuel cell, it is often impossible to measure critical parameters, such as temperature, pressure and potential gradients, or species concentration within the cell. Thus, the validation of these models is extremely difficult to achieve. In essence, the mechanistic models are suited for design and optimization of cell components, rather than for control purpose.

On the other hand, empirical models are based on experimental data specific to each application and operating condition. Empirical relationships are employed when the physical phenomena are difficult to model or the theory governing the phenomena is not well understood. As empirical models typically do not provide as many details as mechanistic models do and already, at least to some extent, are validated, they may provide a fast start into fuel cell modeling and a good basis for engineering applications. These models allow engineers to make quick prediction of the PEMFC‘s performance given operating conditions. This is of significant benefits for the control study. However, empirical models are limited to a specific application or a narrow corridor of operating conditions. They cannot be used to predict the performance of innovative designs, or the response of the fuel cell to parameter changes outside of the conditions under which the empirical relationships were developed. Empirical relationships also do not provide an adequate physical understanding of the phenomena inside the cell. They only correlate outputs with inputs.

However, it is worth pointing out that there is no sharp distinction between mechanistic and empirical models; for instance, a PEMFC system model may use a more mechanistic approach to model the fuel cell and empirical maps of compressors and other devices in the system.

- **State**

With respect to temporal changes, the system can be studied at steady-state or transient conditions. Steady-state models describe the behavior of PEMFC based on one operating point in each step. The main purposes of steady-state models are to design the fuel cell components and to choose the fuel cell operating points. However, unsteady-state behaviour is also an important issue, especially for the transportation application of PEMFC, where the operating conditions constantly change. Transient models are used to predict the performance of PEMFC as a function of time under varying operating conditions.

- **Boundary**

The system boundary defines the area of interest of the model. It could be on the fundamental cell level including the electrodes and the membrane, the high level with individual fuel cells assembled in a fuel cell stack or the higher level with fuel cell system consisting of a fuel cell stack and its auxiliary system of compressor, pumps, and so forth.

- **Dimension**

With respect to spatial changes, the problem can be zero-dimensional (lumped model), one-dimensional (D), two-D, or three-D, depending on the number of spatial independent variables of the resulting model (differential equations).

- **Phenomena to Take into Account**

PEMFC is a multidisciplinary area. Electrochemical, fluid/thermal dynamics and transport phenomena are all involved within a cell. Mass, momentum, species, charge, and energy conservation principles provide the fundamental governing equations. Depending on its focus, the PEMFC model usually accounts for specific phenomena.

2.2 Literature review of PEMFC models

This section presents a review of the most representative examples of PEMFC models, ranging from 0D to 3D models. A summary of the PEMFC models reviewed is given in Table 2.2.

- **0D models (lumped models)**

The simplest approach to dynamic modeling fuel cells is to ignore spatial changes and to consider changes with time only. A great number of studies considering lumped-parameter models for PEMFC can be found in the literature. Some influential lumped models are reviewed as follows.

Amphlett et al. [2] developed a steady-state model to study the transient behavior of PEMFC. This model accounted for activation and ohmic overvoltage. The power output of the PEMFC stack was calculated from the current, stack temperature, hydrogen and oxygen gas flow rates, and partial pressures. The model was used to predict transient response of the cell during start-up, load changes and shut-down.

Pukrushpan [3] developed a transient model of PEMFC for the control study. The transient phenomena captured in the model include the flow characteristics and inertia

dynamics of the compressor, the manifold filling dynamics, and consequently, the reactant partial pressures. Unlike other system models existing in the literature where a single polarization curve or a set of polarization curves for different cathode pressure was used, the fuel cell polarization curve used in this model was a function of oxygen and hydrogen partial pressures and membrane water content.

Yerramalla et al. [4] proposed a linear as well as a nonlinear dynamic model of PEMFC. The model accounted for energy and mass transfer, as well as electrochemical reactions and the inverter load. The voltage response predicted by the model was in the form of a ripple for varying loads, which implied that an effective controller was required when there were rapid fluctuations in the load.

Xue et al. [5] developed a system level lumped-parameter model of PEMFC for investigating the the mixed effects of temperature, gas flow, and capacitance, with particular emphasis focused on system transient behavior. The PEMFC system was divided into three control volumes and thus a lumped-parameter model for each control volume was derived. Simulation results revealed that complicated dynamic interactions existed among various components and mechanisms within the PEMFC system.

Pathapati et al. [6] developed a PEMFC dynamic model that incorporated the effects of charge double layer capacitance, the dynamics of flow and pressure in the anode and cathode channels, as well as mass/heat transfer transient features in the fuel cell body. The model was used to study the transient response of cell voltage, cell temperature, hydrogen /oxygen outlet flow rates, and anode and cathode channel temperatures and pressures to a

step change in the load. Simulation results were in good agreement with data from laboratory experiments.

Benziger et al. [7] introduced a new PEMFC design, which was based on coupled stirred tank reactors (STRs) and a membrane. This fuel cell can be regarded as a set of reactors connected through a set of flow regulators. The gas phase in each reactor compartment was assumed to be well mixed. The STR PEMFC was one-dimensional; spatial gradients were transverse to the membrane only. A lumped parameter model was then developed to examine start-up, and dynamic responses to changes in load, temperature, and reactant flow rates. Experimental data were used to estimate several parameters of the model and validate the model.

- **1D models**

Bernardi and Verbrugge [8] developed a model for an ion-exchange membrane attached to a gas-fed porous electrode. The model accounted for cell polarization characteristics, water transport, and catalyst utilization. In addition, the effect of electroosmotic convection was included in the model for the first time. It was assumed that the membrane was in a fully hydrated state at all times. Nernst-Planck equation was used to describe the flux of species in the membrane-free volume and Schlogl‘s velocity equation was used for the polyelectrolyte membrane. The simulation results matched well with experimental data. It was also found that the polarization resistance resulting from the oxygen reduction reaction was important at all current densities, and that water transport by pressure difference and electric potential forces was a strong function of the cell operating conditions.

Springer et al. [9] presented an isothermal, one-dimensional, steady-state model of PEMFC for investigating the water transport mechanisms and their effect on the cell performance. The model incorporated water diffusion coefficients, electro-osmotic drag coefficients, water sorption isotherms, and membrane conductivities. They applied equilibrium conditions between membrane water and electrode water vapor at the membrane/electrode interfaces and considered the electro-osmotic and diffusion driving forces for water in the membrane and diffusion for water vapor and reactant gases in the electrodes to obtain material balances throughout the cell. The data was obtained experimentally for 117 Nafion membrane. The results showed that the membrane resistance increased as the current density increased.

Baschuk and Li [10] presented a model for a single cell of PEMFC. This model incorporated all the essential fundamental physical and electrochemical processes occurring in the membrane electrolyte, cathode catalyst layer, electrode backing and flow channel. Specifically, the model considered the effect of the degree of water flooding in the cathode catalyst layer and/or cathode electrode backing region on the cell performance. The results showed that increasing the cell pressure increased significantly the extent of water flooding in the electrode and resulted in maximum flooding at low current densities.

Djilali and Lu [11] presented a model for PEMFC with a focus on the nonisothermal and nonisobaric effects. The model considered (a) diffusion through the porous electrodes of the humidified and oxidant gases, (b) the convective and electro-osmotic transport of liquid water in the electrodes and the membrane, (c) heat generation and transfer in the fuel cell, (d) non-uniform distribution of gas pressure in the porous gas diffusing electrodes, and (e) micro-hydrodynamics in very small pores (Knudsen diffusion). The model was solved

numerically to analyse fuel cell performance and water transport over a range of operating current densities. Non-uniform temperature and pressure distributions were found to have a strong influence on the predicted liquid water and vapor fluxes in the anode and cathode diffusion layers.

Weber et al. [12] developed a PEMFC model for investigating the effects of flooding. Specifically, the effects of the structural properties of the diffusion media, such as the bulk porosity, wettability, thickness, and pore-size distribution on the maximum power were studied.

Ziegler et al. [13] developed a dynamic isothermal PEMFC model with a membrane model that accounted for Schroeder‘s paradox. The model took into account: (a) mass transport in the gas phase and in the liquid phase as well as the phase transition between the two phases; (b) charges and the electrochemical transport. The dynamic effect of liquid water formation and transport on the current-voltage characteristics of the fuel cell was studied. A hysteresis effect was found in the measured time-dependent current-voltage relation.

- **2D models**

Fuller and Newman [14] developed a mathematical model of PEMFC for investigating the transport phenomena. A two-dimensional membrane electrode assembly was considered. Water management, thermal management, and utilization of fuel were examined in detail. The Stefan-Maxwell equation was used to describe the multi-component diffusion of gases. Condensation of water was not considered in this study, and the system was modeled as a single phase. The effect of operation conditions on transport in the fuel cell system was

investigated. It was found that the equilibrium sorption of water between the gas phase and the polymer-electrolyte depended strongly on temperature. The rate of heat removal was shown to be a critical parameter in the operation of the PEMFC.

Nguyen and White [15] presented a water and heat management model of PEMFC for evaluating the effectiveness of various humidification designs. The model accounted for water transport across the membrane by electro-osmosis and diffusion, heat transfer from the solid phase to the gas phase, and the latent heat associated with water evaporation and condensation in the flow channels. It was found that ohmic loss in the membrane had the greatest impact on the voltage loss and back diffusion of water from the cathode side of the membrane was insufficient to keep the membrane hydrated (i.e., conductive). It was concluded that the anode stream must be humidified to minimize the ohmic loss, and when air was used instead of pure oxygen the cathode stream must also be humidified.

Yi and Nguyen [16] developed an along-the-channel model for evaluating the effects of various designs and operating parameters on the performance of PEMFC. The model included the convective water transport across the membrane by a pressure gradient, temperature distribution in the solid phase along the flow channel, and heat removal by natural convection and concurrent and counter-current heat exchangers. Their results showed that the performance of PEMFC could be improved by anode humidification and positive differential pressure between the cathode and anode. It was also found that efficient heat removal was necessary to overcome excessive temperature rise, which led to local membrane dehydration.

Singh et al. [17] developed a 2-D isothermal model of PEMFC with a focus on transport phenomena within the cell. The model accounted for diffusion of the humidified fuel and oxidant gases through the porous electrodes, convective and electro-osmotic transport of liquid water in the electrodes and the membrane. A finite volume method was applied to solve the system of differential equations. The results indicated that the cathode potential loss, associated with the slow oxygen reaction rate, had the greatest impact on the current densities. It was also found that the anode and cathode water varied considerably along the oxidant and fuel flow channels.

Lee et al. [18] developed a model of PEMFC for investigating the processes, losses, and electrical characteristics in a membrane electrode assembly. The model employed a family of empirical equations that describe the electrochemical characteristics of the membrane electrode assembly in combination with methods for satisfying the electrical requirements of fuel cell stacks. Temperature, pressure, and oxygen partial pressure distributions were obtained in this study. The results indicated a strong relation between the distributions of oxygen partial pressure and the cell current. It was found that the distribution curves were very similar in shape, with the region of highest current production corresponding to the region of highest oxygen concentration.

Gurau et al. [19] developed a 2-D mathematical model of PEMFC. The self-consistent model for porous media was used for the equations describing transport phenomena in the membrane, catalyst layers, and gas diffusers, while standard equations of Navier-Stoka, energy transport, continuity, and species concentrations were solved in the gas channels. Polarization curves under various operating conditions were obtained by solving transport and charge conservation equations, as well as the equations for electrochemical reactions

and current density with the membrane phase potential. Effects of various parameters on the cell performance were also studied.

Um et al. [20] developed a transient, 2-D model of PEMFC. The model accounted for electrochemical kinetics, current distribution, hydrodynamics, and multi-component transport. The governing equations were solved using the finite volume method. The model was then used to analyze the effects of hydrogen dilution in the anode feed. The electrochemical and flow/transport simulations revealed that, in the presence of hydrogen dilution in the fuel stream, hydrogen was depleted at the reaction surface, resulting in substantial anode mass transport polarization and, hence, lower current density that was limited by hydrogen transport from the fuel stream to the reaction site.

Ge and Yi [21] developed a steady-state, 2-D model of PEMFC. The model included the flow mode (coflow and counterflow), operating conditions and membrane thickness on the water transport, ohmic resistance and water distribution in the membrane, current density distribution along the channel and performance of PEMFC. The results showed that counter-flow mode improved the current density distribution with dry or low humidity gases compared to the co-current flow (co-flow) mode. It was concluded that the cell performance can be improved by increasing the temperature.

Pasaogullari and Wang [22] introduced a new theory for liquid water transport in hydrophobic gas diffusion layers to simulate flooding in PEMFC. The model accounted for two-phase flow, transport of species, and electrochemical kinetics. The effects of operating conditions, such as inlet humidity and flow rates, on the two-phase transport and the performance of PEMFC were studied. The results showed that flooding of the porous

cathode reduced the rate of oxygen transport to the cathode catalyst layer and caused a substantial increase in the cathode polarization. It was also found that the humidity level and flow rates of reactant streams had significant influence on the cell performance.

Cao and Djilali [23] developed a 2-D, nonisothermal, nonisobaric model for PEMFC. In their research, conservation laws for water and current, together with an empirical relationship between electroosmotic drag and water content, were applied to obtain a transport equation for water molar concentration and to derive a new equation for the electric potential that strictly accounted for variable water content. The model was coupled with a computational fluid dynamics model that included the porous gas diffusion electrodes and the reactant flow channels. The resulting coupled model accounted for multi-species diffusion (Stefan-Maxwell equation), first-order reaction kinetics (Butler-Volmer equation), proton transport (Nernst-Planck equation), and water transport in the membrane (Schlogl equation). The results showed that water content distributions can be improved in the membrane when the cell was operated at a higher pressure on the cathode side than on the anode side.

Meng [24] developed a two-phase non-isothermal PEMFC model for evaluating condensation and evaporation rate coefficients. Effects of the inlet humidity and temperature variation on liquid water distribution with or without a condensation/evaporation interface were studied. In his later work [25], a transient PEMFC model was developed based on the previous one. Effects of liquid water transport and heat transfer phenomena on the transient responses of PEMFC to a step change in the cell voltage were studied. The results showed that under isothermal two-phase conditions, the presence of liquid water in the porous materials increased the current density over-shoot and under-shoot, while under the

non-isothermal two-phase conditions, the heat transfer process significantly increased the transient response time.

- **3D models**

Dutta et al. [26] developed a 3-D model of PEMFC to study current density distributions in the membrane. The control volume approach was used. It was found that the membrane thickness and cell voltage had a significant effect on the axial distribution of current density and net rate of water transport. The prediction of water transport between the cathode and anode sides showed the delicate balance of diffusion and electro-osmosis and their effect on the current distribution along channel. In their later study [27], the authors extended previous work by modeling a complete fuel cell including two flow channels (anode and cathode) separated by the membrane electrode assembly. The results indicated that flow distribution in both anode and cathode channels were significantly affected by the mass consumption patterns on the membrane electrode assembly. It was also found that the water transport was governed by both electro-osmosis and diffusion processes.

Berning and Djilali [28] developed a 3-D model for evaluating the impact of operating and geometric parameters on the performance of PEMFC. The model included heat, mass and electron transport, while phase change of water was neglected. Distributions of temperature, water fluxes, reactant concentrations and current densities were obtained. The results showed the existence of significant temperature gradients within the cell, the major impact of the 3-D nature on the current distribution, and the distinct three dimensional nature of the transport.

Mazumder and Cole [29] developed a 3-D model to study the formation and transport of liquid water in PEMFC. In this model, the phase change process was modelled as an equilibrium process, while the transport of liquid water was governed by pressure, surface tension, gravity and electro-osmotic drag. It was found that under the assumption of no liquid water formation, the model consistently overestimated the measured polarization behavior. Results also showed that the inclusion of liquid water transport greatly enhanced the predictive capability of the model and was necessary to match experimental data at high current density.

Meng and Wang [30] developed a 3-D, single-phase, isothermal model of PEMFC for studying the effects of electron transport through the gas diffusion layer. The electron transport equation was solved in the catalyst and gas diffusion layers, and in the current collector for investigating of the lateral electronic resistance in the gas diffusion layer for the first time. It was found that (a) the lateral electronic resistance of the gas diffusion layer was affected by the electronic conductivity, thickness of the diffusion layer and gas channel width (b) the lateral electronic resistance dominated the current distribution at high cell voltages, while the oxygen concentration played a more decisive role at low cell voltages.

Shimpalee et al. [31] developed a 3-D model of a large-scale PEMFC for studying the effects of operating conditions and geometry parameters on the distributions of current, temperature, and species mole. It was found that the humidified cathode condition gave higher overall performance than dry conditions.

Wang and Wang [32] derived a 3-D, transient model to study the dynamics of PEMFC. The model accounted for transient processes of membrane hydration and gas transport. Step

changes in the cell voltage and cathode inlet relative humidity were investigated. The results showed the time for PEMFC to reach steady state was in the order of 10s due to the effect of water accumulation in the membrane, consistent with theoretical estimation. In addition, overshoot and undershoot in the current densities were observed during the step changes in certain operating conditions.

Wang et al. [33] developed a 3-D model, two-phase PEMFC model to study the effects of structure on the performance of carbon paper and carbon cloth as gas diffusion media in the gas diffusion layers. Their study indicated that the carbon cloth was the better choice as a gas diffusion layer material at high-humidity operations due to the low tortuosity of its pore structure and its rough textural surface. However, under dry conditions, the carbon paper showed better performance because of its more tortuous structure, which prevented the loss of product water to dry gas streams, thus increasing the membrane hydration level and reducing the ohmic loss.

Gurau et al. [34] developed a 3-D multi-phase, multi-fluid, transient model for investigating the water transport in PEMFC. The model accounted for momentum and species transport in the cathode channel, gas diffusion layer, and catalyst layer for each phase. The liquid water produced by electrochemical reaction, phase change, and water transfer between the ionomer distributed in the catalyst layer and the catalyst layer pores, were taken into account. The model predicted liquid water accumulation at the channel-gas diffusion layer interface. It was found that liquid saturation increased in the catalyst layer as water approached a steady-state level.

Ye and Nguyen [35] developed a 3-D, two-phase transport model to predict liquid water saturation in the porous transport layer and the catalyst layer of PEMFC. It was found that (a) in the cathode catalyst layer, the liquid water saturation was higher under the channel than that under the ribs at high current densities (b) in the cathode porous transport layer, however, the liquid water saturation level was observed to be lower under the channel than that under the ribs.

Wang [36] developed a 3-D, two-phase model of PEMFC for investigating multiphase flows, species transport, and electrochemical processes. The model accounted for conservations of mass, momentum, and charge, as well as two-phase transports, in both the anode and cathode diffusion media. The results showed that (a) multiphase flows existed in both anode and cathode diffusion media at low-humidity conditions, (b) two-phase flow emerged near the outlet for a co-flow configuration, and (c) two-phase flow was presented in the middle of the fuel cell for a counter-flow configuration.

Table 2.2 Summary of PEMFC system models in the literature

nD	State	Account for	Ref
0D	transient	mass balance, heat transfer, and electrochemical kinetics	2
0D	transient	mass balance and electrochemical processes	3
0D	transient	mass balance, electrochemical processes, and voltage losses	4
0D	transient	mass and energy transfer and electrochemical processes	5
0D	transient	mass balance, heat transfer, electrochemical processes, and voltage losses	6
0D	transient	mass transfer, electrochemical processes, and fuel cell overpotential	7
1D	steady-state	mass transfer, charge conservation, electro-osmotic convection, and electrochemical processes	8
1D	steady-state	mass transfer, electro-osmotic convection, and electrochemical processes	9
1D	steady-state	oxygen transport, electrochemical processes, and water flooding	10
1D	steady-state	multicomponent mass, heat, and momentum transfer and charge conservation	11
1D	steady-state	two-phase transport, mass and momentum transfer, structural properties and water flooding	12
1D	steady-state/ transient	two-phase flow, water phase change, charge conservation, and mass transfer	13
2D	steady-state	multicomponent mass transfer and water and thermal management	14
2D	steady-state	heat transfer, mass balance, water management, and electrochemical processes	15
2D	steady-state	heat and mass transfer and electrochemical processes	16
2D	steady-state	multicomponent mass transfer and electrochemical processes	17
2D	steady-state	mass balance, temperature distribution, and electrochemical processes	18
2D	steady-state	momentum, heat and mass transfer, and electrochemical processes	19
2D	transient	momentum, heat and mass transfer, and charge conservation	20
2D	steady-state	mass transfer and electrochemical processes	21
2D	steady-state	mass and momentum transfer, two-phase flow, water flooding, charge conservation and electrochemical processes	22
2D	steady-state	mass, heat, and momentum transfer and charge conservation	23
2D	steady-state/ transient	mass, momentum, and energy transfer and charge conservation	24, 25
3D	steady-state	momentum and mass transfer and electrochemical processes	26, 27
3D	steady-state	momentum, heat, and mass transfer, charge conservation, and electrochemical processes	28
3D	steady-state	mass transfer and phase change	29
3D	steady-state	mass and momentum transfer and electron transport	30
3D	steady-state	mass, momentum and heat transfer, and water phase change	31
3D	transient	momentum and mass transfer and charge conservation	32
3D	steady-state	structural performance of gas diffusion layer, mass and momentum transfer, and charge conservation	33
3D	transient	mass and momentum transfer, water phase change, and charge conservation	34
3D	steady-state	mass and momentum transfer, charge conservation, and two-phase change	35
3D	steady-state	mass and momentum transfer, phase change, and charge conservation	36

2.3 Modelling by MATLAB/SIMULINK

MATLAB (matrix laboratory) is a numerical computing and programming language developed by MathWorks. MATLAB provides an interactive environment with hundreds of reliable and accurate built-in mathematical functions. These functions provide solutions to a broad range of mathematical problems including matrix algebra, complex arithmetic, linear systems, differential equations, signal processing, optimization, nonlinear systems, and many other types of scientific computations. The most important feature of MATLAB is its programming capability, which allows user-developed functions. It also allows access to Fortran algorithms and C codes by means of external interfaces. There are several optional toolboxes written for special applications such as signal processing, control systems design, system modelling, statistics, neural networks, fuzzy logic, symbolic computations, and others. Fox example, Libsvm 3.0, support vector machine toolbox developed by Chih-Jen Lin et al., will be used in the following section for system modelling.

MATLAB has been further enhanced by the very powerful SIMULINK program. SIMULINK is a graphical mouse-driven program, which provides a graphical editor, customizable block libraries, and solvers for modeling and simulating dynamic systems. It is integrated with MATLAB, enabling users to incorporate MATLAB functions into models and export simulation results to MATLAB for further analysis.

The procedures of system modelling using MATLAB/ SIMULINK comprise:

(1) Selecting blocks. The SIMULINK Library Browser contains a library of blocks commonly used to model a system, as shown in Figure 2.1. Generally, system model comprises at least a set of input block, output block and operator block.

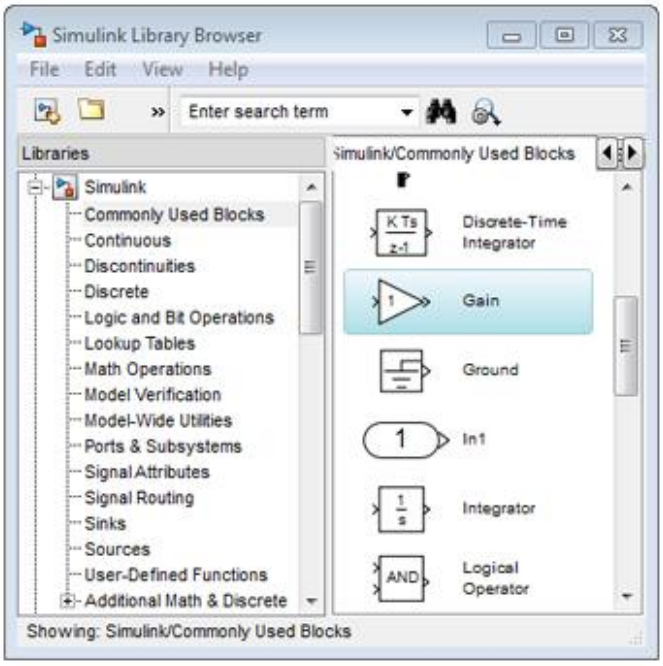

Figure 2.1 SIMULINK Library Browser

(2) Building the model. One can drag the desired blocks into an empty block diagram from the library and then connect these blocks with signal lines to establish mathematical relationships between system components (see Figure 2.2).

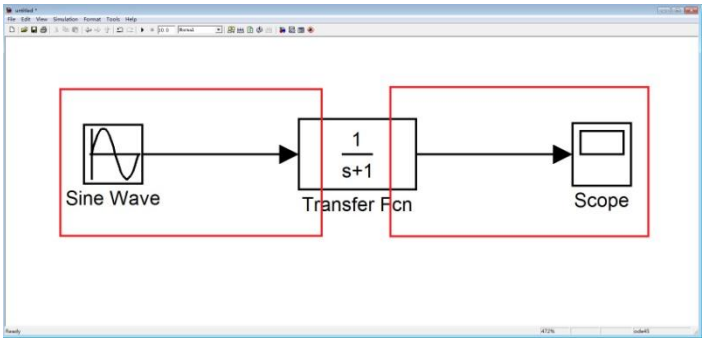

Figure 2.2 Connection of blocks

(3) Managing signals and parameters. SIMULINK models contain both signals and parameters. Signals are time-varying data represented by the lines connecting blocks. Parameters are coefficients that define system dynamics. (see Figure 2.3).

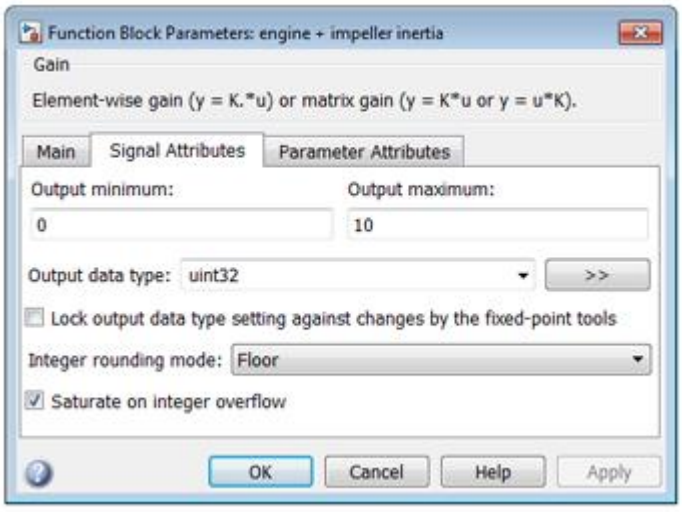

Figure 2.3 Configuration signal attribute dialogue box

(4) Simulating the model. One can simulate the dynamic behavior of the system model and view the results as the simulation runs. To ensure simulation speed and accuracy, one should carefully determine the solver parameters (see Figure 2.4).

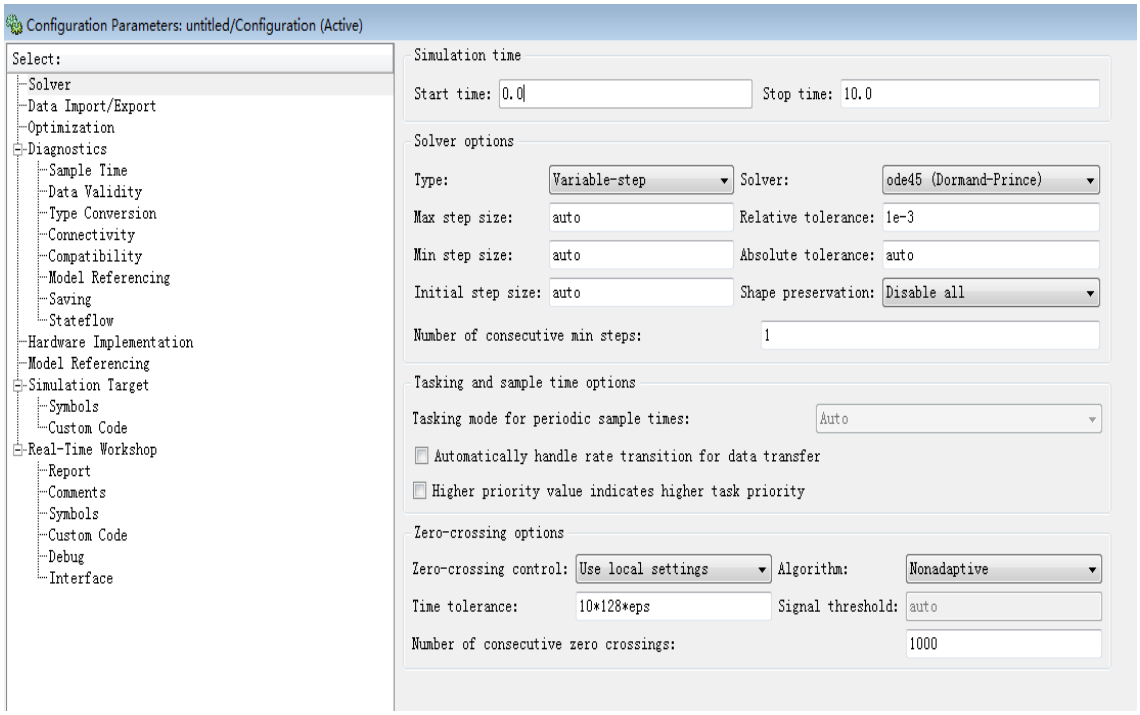

Figure 2.4 Configuration solver parameters dialogue box

2.4 Theory of support vector machine

The support vector machine (SVM) is a nonlinear generalization algorithm proposed by Vapnik and Lerner in the sixties [37]. It is firmly grounded in the framework of statistical learning theory, or *VC theory*, which has been developed over the last three decades by Chervonenkis and Vapnik [38]-[41]. This theory characterizes properties of learning machines which enable them to generalize well to unseen data.

The SVM has been largely developed at AT&T Bell Laboratories by Vapnik and co-workers since its creation. Due to this industrial context, a considerable number of researchers have already reported state-of-the-art performance in a variety of applications. Initial work focused on optical character recognition (OCR). Osuna et al. [42] applied SVM to digital image classification for human face detection. Within a short period of time, SVM classifiers became competitive with the best available systems for both OCR and pattern recognition tasks. A comprehensive tutorial on SVM classifiers has been published by Burges [43]. Later, excellent performances were also obtained in time series prediction and regression applications. For example, Muller et al. [44] used SVM for nonlinear time series predictions. Smola and Scholkopf [45] published an in-depth tutorial on support vector machine regression.

Due to its excellent performance in regression, SVM shows great potential for nonlinear system identification and system control. The major advantages of SVM are presented as follows [46]:

1) The traditional nonlinear identification methods, including artificial neural networks, fuzzy modelling, etc., are based on the empirical risk minimization principle (ERM), which

often causes the problem of over fitting, i.e. less training error may result in poorer generalization performance. In contrast, SVM employs structural risk minimization (SRM) principle, which enables it to pay attention to both expectation risk and generalization performance.

2) By introducing the kernel, SVM avoid difficulties of using linear functions in the high dimensional feature space and optimization problem is transformed into dual convex quadratic programs.

3) SVM delivers a unique solution, since the optimality problem is convex. This is an advantage compared to artificial neural networks, which have multiple solutions associated with local minima and for this reason may not be robust over different samples.

4) SVM provides a good out-of-sample generalization. By choosing appropriate parameters, SVM can be robust, even when the training sample has some bias.

For clarity and completeness, the following section present a brief introduction to the SVM theory, but the readers interested in the complete details of SVM regression should refer to the excellent tutorial by Smola and Scholkopf [45].

2.4.1 Linear regression

For a given training data set $\{(y_k\, x_k)|k=1,\ldots,n\} c\ \mathrm{R}^{\mathrm{n}}\mathrm{XR}$, $x_k \epsilon \mathrm{R}^{\mathrm{n}}$ are the input data and $y_k \epsilon \mathrm{R}$ are the output data, n is the number of samples. In ε-SV regression [40], the goal of SVM is to find a function $f(x)$ that has at most ε deviation from the actually obtained targets $\boldsymbol{y}_k$ for all the training data, and at the same time is as flat as possible. In other words, any errors will

be accepted as long as they are less than ε, any deviation that is larger than this will be rejected.

The case of linear function *f* has been described in the form as:

$$f(x) = \langle \omega, x \rangle + b \tag{2.1}$$

where $< , >$ denotes the dot product. Flatness in the case of (2.1) means that one seeks a small ω. One way to ensure this is to minimize the Euclidean norm, i.e. $||\omega||^2 = <\omega,\omega>$ Formally this can be written as a convex optimization problem:

$$\begin{aligned} &\text{minimize} \quad \frac{1}{2}\|\omega\|^2 \\ &\text{subject to} \begin{cases} y_i - \langle \omega, x_i \rangle - b \le \varepsilon \\ \langle \omega, x_i \rangle + b - y_i \le \varepsilon \end{cases} \end{aligned} \tag{2.2}$$

The tacit assumption in (2.2) was that such a function *f* actually exists that approximates all pairs (x_i, y_i) with ε precision, or in other words, that the convex optimization problem is feasible. Sometimes, however, this may not be the case, or some errors are allowed. Analogously to the ―soft margin" loss function [47] which was adapted to SVM by Cortes and Vapnik [48], one can introduce slack variables ξ_i, ξ_i^* to cope with otherwise infeasible constraints of the optimization problem (2.2). Hence, the formulation becomes [40]:

$$\begin{aligned} &\text{minimize} \quad \frac{1}{2}\|\omega\|^2 + C\sum_{i=1}^{l}\left(\xi_i + \xi_i^*\right) \\ &\text{subject to} \begin{cases} y_i - \langle \omega, x_i \rangle - b \le \varepsilon + \xi_i \\ \langle \omega, x_i \rangle + b - y_i \le \varepsilon + \xi_i^* \end{cases} \end{aligned} \tag{2.3}$$

where ξ_i, $\xi_i^* > 0$, $C > 0$. The preset constant *C* is weight factor. The larger *C* indicates the greater impact of the second term in the objective function, which represents the deviations that can be tolerated. Therefore, only small deviations can be tolerated in this case. In other

word, C determines the trade-off between the flatness of f and the amount up to which deviations larger than ε are tolerated. This corresponds to dealing with a so called ε –insensitive loss function $|\xi|_\varepsilon$ described by

$$|\xi|_\varepsilon = \begin{cases} 0 & \text{if } |\xi| < \varepsilon \\ |\xi| - \varepsilon & \text{otherwise} \end{cases} \tag{2.4}$$

Figure 2.5 depicts the situation graphically. Only the points outside the shaded region contribute to the cost, as the deviations are penalized in a linear fashion. They are named support vectors (SVs).

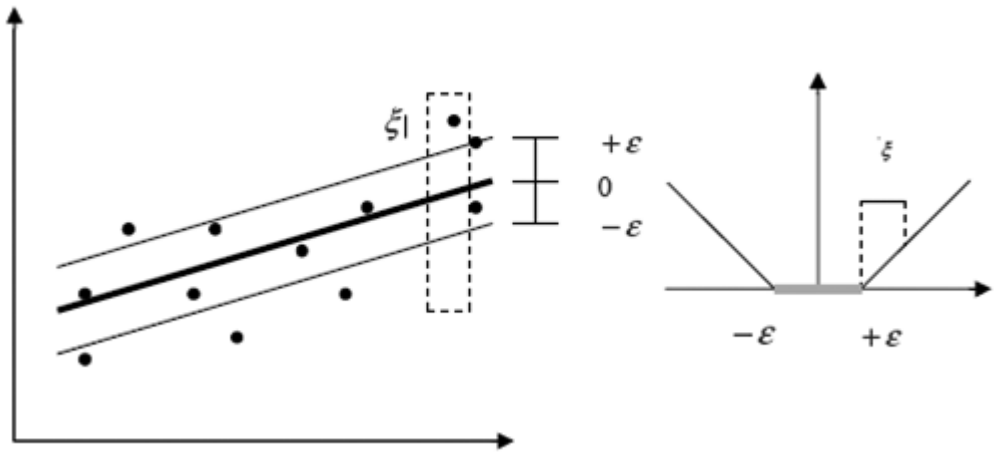

Figure 2.5 Linear SVM regression

It turns out that in most cases the optimization problem (2.3) can be solved more easily in its dual formulation. Moreover, as will be shown next, the dual formulation provides the key for extending SVM to nonlinear functions. The standard dualization method utilizing Lagrange multipliers is described as follows [49]:

$$
\begin{aligned}
L \coloneqq & \frac{1}{2}\|\omega\|^2 + C\sum_{i=1}^{l}\left(\xi_i + \xi_i^*\right) - C\sum_{i=1}^{l}\left(\eta_i\xi_i + \eta_i^*\xi_i^*\right) \\
& - \sum_{i=1}^{l}\alpha_i\left(\varepsilon + \xi_i - y_i + \langle\omega, x_i\rangle + b\right) \\
& - \sum_{i=1}^{l}\alpha_i^*\left(\varepsilon + \xi_i^* + y_i - \langle\omega, x_i\rangle - b\right)
\end{aligned} \tag{2.5}
$$

where L is the Lagrangian and η_i , η_i^* α_i , α_i^* are Lagrange multipliers. Hence the dual variables in (2.5) have to satisfy positivity constraints, i.e.

$$
\alpha_i^{(*)}, \eta_i^{(*)} \geq 0 \tag{2.6}
$$

where $\alpha_i^{(*)}$refers to α_i and α_i^*, $\eta_i^{(*)}$ refers to η_i and η_i^*.

It follows from the saddle point condition that the partial derivatives of L with respect to the primal variables (ω, b, ξ_i, ξ_i^*) have to vanish for optimality.

$$
\frac{\partial L}{\partial b} = \sum_{i=1}^{l}(\alpha_i^* - \alpha_i) \qquad = 0 \tag{2.7}
$$

$$
\frac{\partial L}{\partial \omega} = \omega - \sum_{i=1}^{l}(\alpha_i - \alpha_i^*)x_i \;\; = 0 \tag{2.8}
$$

$$
\frac{\partial L}{\partial \xi_i^{(*)}} = C - \alpha_i^{(*)} - \eta_i^{(*)} \qquad = 0 \tag{2.9}
$$

Substituting (2.7), (2.8), and (2.9) into (2.5) yields the dual optimization problem:

$$
\begin{aligned}
&\text{minimize}\begin{cases} -\frac{1}{2}\sum_{i,j=1}^{i}\left(\alpha_i - \alpha_i^*\right)\left(\alpha_j - \alpha_j^*\right)\left\langle x_i, x_j\right\rangle \\ -\varepsilon\sum_{i=1}^{l}\left(\alpha_i + \alpha_i^*\right) + \sum_{i=1}^{l} y_1(\alpha_i - \alpha_i^*) \end{cases} \\
&\text{subject to } \sum_{i=1}^{l}(\alpha_i - \alpha_i^*) = 0 \text{ and } \alpha_i, \alpha_i^* \in [0, C]
\end{aligned} \tag{2.10}
$$

Dual variables η_i and η_i^* through condition (2.8) have been eliminated for deriving (2.10). (2.8) can be rewritten as follows:

$$\omega = \sum_{i=1}^{l} (\alpha_i - \alpha_i^*) x_i \text{ and therefore, } f(x) = \sum_{i=1}^{l} (\alpha_i - \alpha_i^*) \langle x_i, x \rangle + b \tag{2.11}$$

This is the so-called support vector expansion, i.e. ω can be completely described as a linear combination of the training patterns x_i. In a sense, the complexity of a function's representation by support vectors is independent of the dimensionality of the input space, and depends only on the number of support vectors. Moreover, note that the complete algorithm can be described in terms of dot products between the data. Even when evaluating $f(x)$ it is not needed to compute ω explicitly (although this may be computationally more efficient in the linear setting). These observations will come in handy for the formulation of a nonlinear extension.

Computation of b is done by exploiting Karush-Kuhn-Tucker (KKT) conditions which states that at the optimal solution the product between dual variables and constraints has to vanish [50], [51]. In the SVM case, this means

$$\begin{aligned} \alpha_i \left(\varepsilon + \xi_i - y_i + \langle \omega, x_i \rangle + b \right) &= 0 \\ \alpha_i^* \left(\varepsilon + \xi_i^* + y_i - \langle \omega, x_i \rangle - b \right) &= 0 \end{aligned} \tag{2.12}$$

and

$$\begin{aligned} (C - \alpha_i) \xi_i &= 0 \\ (C - \alpha_i^*) \xi_i^* &= 0 \end{aligned} \tag{2.13}$$

Following conclusions can be made: (i) only samples (x_i, y_i) with corresponding $\alpha_i^* = C$ lie outside the ε - insensitive tube around f, (ii) $\alpha_i^* \alpha_i = 0$, i.e. there can never be a set of dual variables α_i, α_i^* which are both simultaneously nonzero as this would require nonzero slacks in both directions. Finally for $\alpha_i^* \in (0, C)$, $\xi_i^* = 0$ and moreover the second factor in (2.12) has to vanish. Hence b can be computed as follows:

$$b = y_i - \langle \omega, x_i \rangle - \varepsilon \quad \text{for } \alpha_i \in (0, C)$$
$$b = y_i - \langle \omega, x_i \rangle + \varepsilon \quad \text{for } \alpha_i^* \in (0, C) \tag{2.14}$$

From (2.12), it follows that only for $|f(x_i) - y_i| \geq \varepsilon$ the Lagrange multipliers may be nonzero, or in other words, for all samples inside the ε -tube, the α_i, α_i^* vanish: for $|f(x_i) - y_i| < \varepsilon$ the second factor in (2.12) is nonzero, hence α_i, α_i^* has to be zero such that the KKT conditions are satisfied. Therefore, a sparse expansion of ω exists in terms of x_i (i.e., all x_i are not needed to describe ω). The examples that come with non-vanishing coefficients are called support vectors (SVs).

2.4.2 Nonlinear regression

The basic idea of SVM nonlinear regression is to set into a high dimensional feature space F via a nonlinear function Φ mapping and to do linear regression in this space. Figure 2.6 shows the basic idea of SVM for nonlinear case.

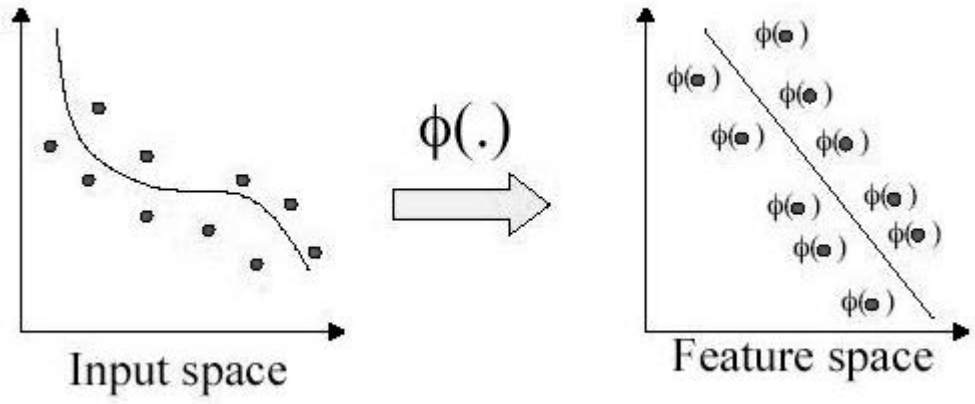

Figure 2.6 Nonlinear SVM regression

The expansion in (2.10) becomes:

$$\omega = \sum_{i=1}^{l} (\alpha_i - \alpha_i^*)\phi(x_i) \text{ and therefore, } f(x) = \sum_{i=1}^{l} (\alpha_i - \alpha_i^*)\langle \phi(x), \phi(x_i) \rangle + b \tag{2.15}$$

The difference with the linear case is that ω is no longer explicitly given. In the nonlinear setting, the optimization problem corresponds to finding the flattest function in feature space, not in input space.

In (2.15) the kernel function is introduced to address the problem of dimensionality. It is defined as a function that corresponds to the dot product of two vectors in feature space:

$$K(x, x_i) = \langle \phi(x), \phi(x_i) \rangle \tag{2.16}$$

The standard SVM to solve the approximation problem is as follows:

$$f(x) = \sum_{i=1}^{l} (\alpha_i - \alpha_i^*) K(x, x_i) + b \tag{2.17}$$

The coefficients α_i and α_i^* of (2.17) have been obtained by minimizing the following regularized risk functional

$$R_{\text{reg}}[f] = \frac{1}{2}\|\omega\|^2 + C\sum_{i=1}^{l} L_\varepsilon(y) \tag{2.18}$$

The term $||\omega||^2$ has been characterized as model complexity, C as a constant determining the trade-off and the ε - insensitive loss function $L_\varepsilon(y)$ has been given by

$$L_\varepsilon = \begin{cases} 0 & \text{if } |f(x) - y| < \varepsilon \\ |f(x) - y| - \varepsilon & \text{otherwise} \end{cases} \tag{2.19}$$

2.5 Modelling PEMFC by support vector machine

2.5.1 Problem formulation

Assume PEMFC can be described by nonlinear auto regressive moving average (NARMA) model:

$$y(k+1) = f[y(k), y(k-1), ..., y(k-n_y), x(k), x(k-1), ..., x(k-n_x)] \tag{2.20}$$

where x and y are the input vectors and output vectors of the system. n_x and n_y denote the lags of input and output, respectively. f is an unknown nonlinear mapping.

Set the input vector as:

$$u(i) = (y(i), y(i-1), ..., y(i-n_y), x(i), x(i-1), ..., x(i-n_x)) \tag{2.21}$$

Substitute the input vector (2.21) into (2.20):

$$y(i+1) = f[u(i)] \tag{2.22}$$

Therefore the training data is $\{y(i+1), u(i)\}$. The output can be obtained by using SVM to map the data set to high dimensional space:

$$y(k+1) = \sum_{i=1}^{l} (\alpha_i - \alpha_i^*) K(u(i), u(k)) + b \tag{2.23}$$

Thus, the PEMFC modeling problem can be stated as: developing an SVM model in the form of (2.23) based on a training set $\{y(i+1), u(i)\}$ to approximate the nonlinear mapping f.

2.5.2 Data preparation

Constructing a data set containing sufficient representative data points is a critical step in developing an SVM model that approximates PEMFC dynamics over a wide operating

range. The basic guidelines of constructing data set are provided as follows: (1) the samples should cover the entire expected operational range of the SVM model. (2) to prevent some elements that have larger original absolute values from dominating the final kernel value, it is necessary to carry out some pre-processing of the raw data before feeding them into the SVM model. In this research, all the data are scaled linearly to the range of [0,1]. Scaling can increase the training speed and assist in selecting optimal SVM hyper parameters.

In this study, for the sake of comparison with traditional modelling approach, data used for SVM modelling are obtained from the PEMFC model developed, presented and validated by Pukrushpan et al. [3]. This model is widely accepted nowadays as a good representation of the behaviour of an actual PEMFC for control purposes. Most parameters used in this model are based on the 75 kW stacks used in the FORD P2000 fuel cell prototype vehicle [52]. Figure 2.7 shows schematic of the PEMFC system and Table 2.3 gives its specifications. However, it is worth pointing out that one can also obtain the data from practical experiments. In this way, the SVM model achieves better performance and enhances its practical value.

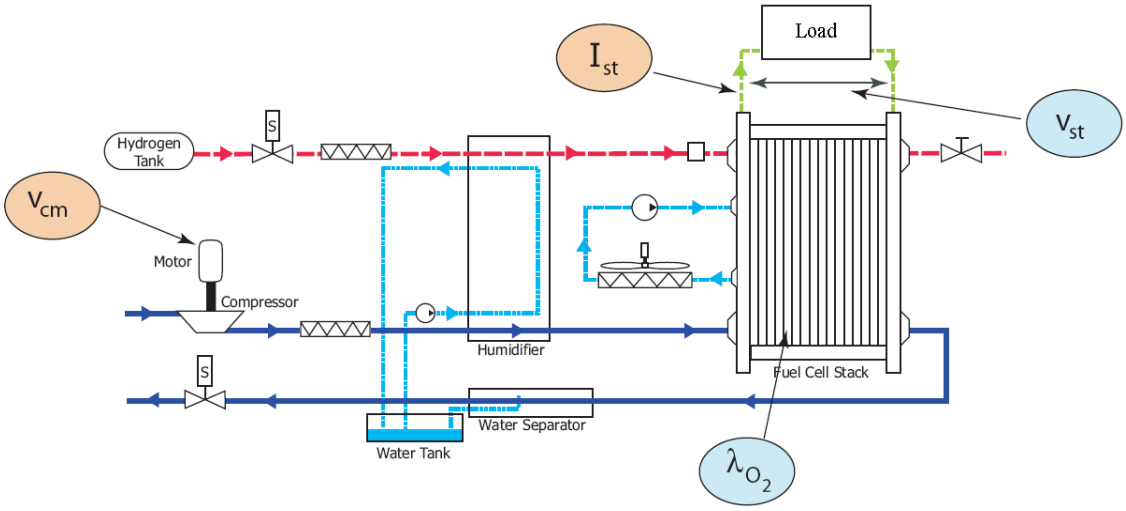

Figure 2.7 PEMFC system showing inputs and outputs [3]

Table 2.3 PEMFC system model specifications

Fuel Cell Stack	Mode	3 × Ballard Mark 700
	Membrane Type	Proton Electrolyte
	Maximum Power	75kW
	No. of Cells (n)	381
	Cell Active Area	280cm2
Air Compressor	Manufacturer	Allied Signals
	Type	Centrifugal
	Maximum Power	12.5kw

The classical SVM modelling algorithm is only a multi-input but single-output modelling method. However, the PEMFC modelling is a multi-input/multi-output (MIMO) modelling problem. As shown in Figure 2.7, the PEMFC has two inputs the stack current I_{st} and the compressor motor voltage V_{cm} and two outputs, the stack voltage V_{st} and the oxygen excess ratio λ_{O2}. In the original study by Pukrushpan, the stack current is considered as the disturbance input, which corresponds to uncontrollable load demand. The compressor motor voltage is modelled as control input to adjust the air flowrate supplied. The oxygen excess ratio is a performance output that indicates the oxygen level status in the cathode. The stack voltage is also a performance output that directly associates with the load. For the sake of comparison, the same inputs and outputs are considered for developing the SVM model in this thesis. Therefore, a set of two SVM models have to be generated and each model represents one performance output of PEMFC. Figure 2.8 shows the framework of MIMO SVM modelling.

To facilitate the model validation, the input-output data required for developing SVM model are obtained by exciting Pukrushpan's model with the designed signals $100+20\sin(0.3t)\sin(0.4t)$ and $150+50\sin t\sin(0.5t)$ for the stack current and the compressor motor voltage, respectively. Figure 2.9 shows the input signals and the corresponding

outputs. A set of 1000 data is collected from the simulation. The first 500 data are used for the identification of SVM models, while the remaining 500 data are used for validation purposes.

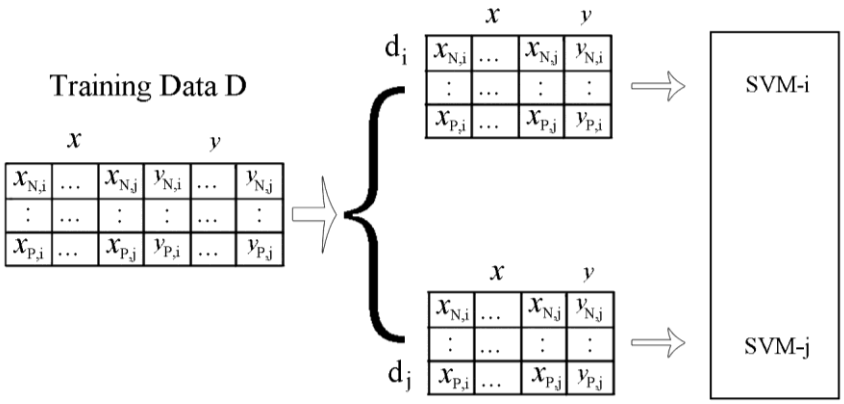

Figure 2.8 MIMO SVM modelling framework (reproduced from[55])

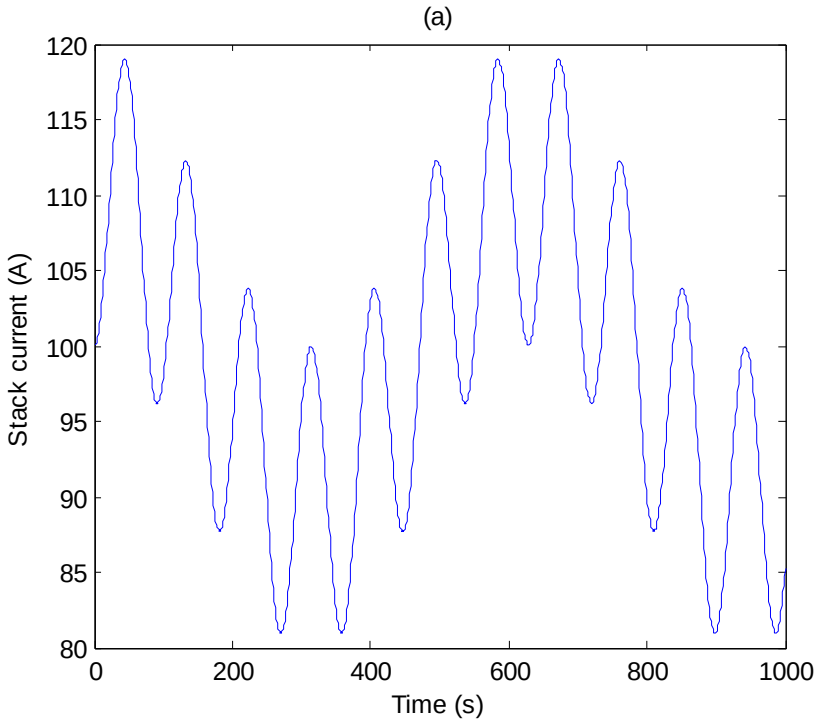

Figure 2.9 Input excitation and output response signals: (a) Stack current

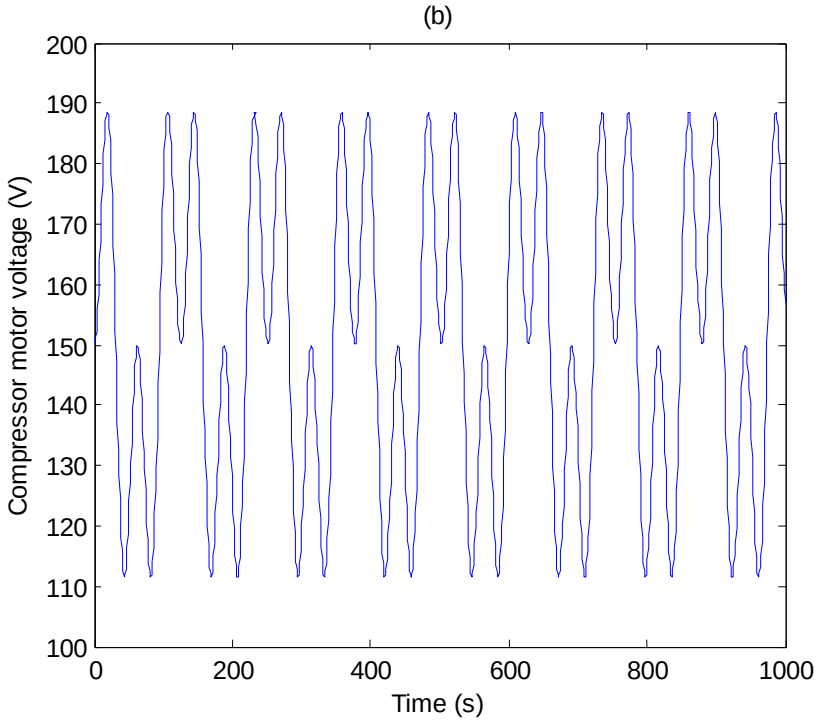

Figure 2.9 Input excitation and output response signals: (b) Compressor motor voltage

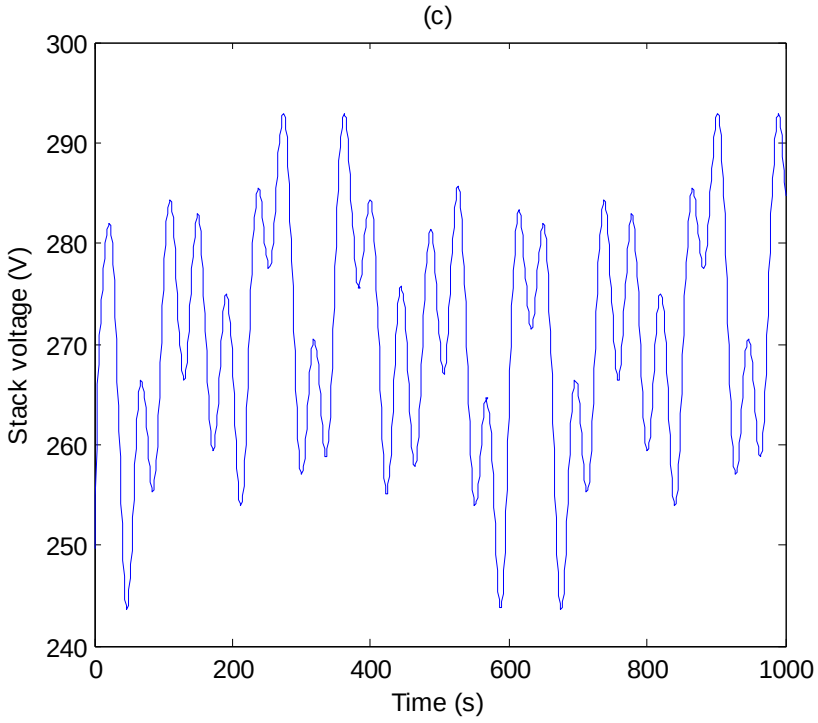

Figure 2.9 Input excitation and output response signals: (c) Stack voltage

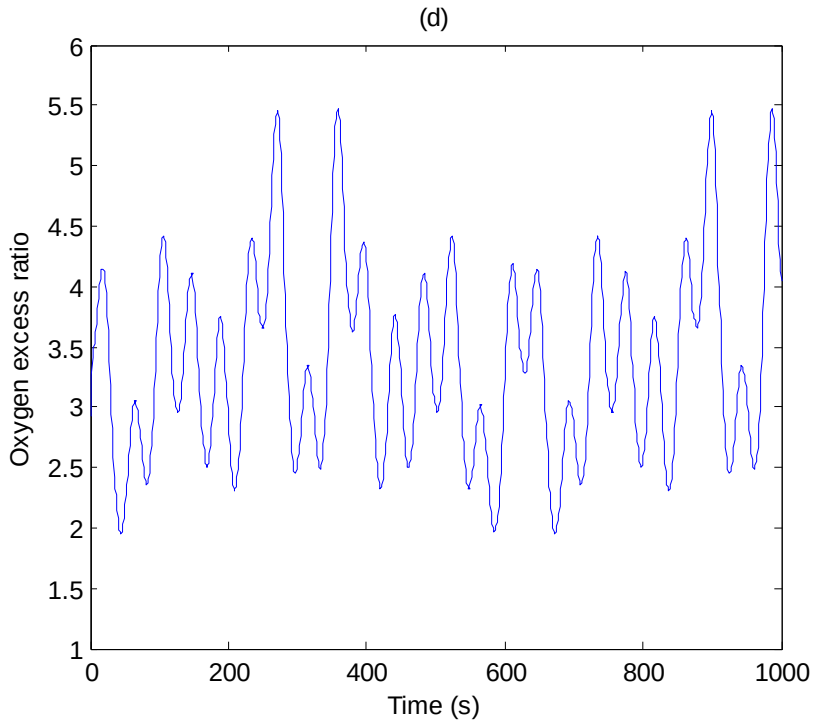

Figure 2.9 Input excitation and output response signals: (d) Oxygen excess ratio

2.5.3 Hyperparameter selection

Another key step in developing SVM model is the selection of a proper set of parameters C, ε and kernel parameters, which significantly affect the performance of SVM model. However, these parameters cannot be determined mathematically. Fortunately, some basic guidelines are provided in the literature [53].

The constant ε is used to find the target function that not only lies as close as possible to the border of the ε-tube but also is as flat as possible. The larger ε is, the flatter the function will be, and thus the fewer support vectors (SVs) exist. However, increasing ε causes larger estimation errors. Therefore, the value of ε ought to be determined in a way that it is proportional to the input noise level ζ.

C is the parameter that represents a trade-off between the model complexity and the tolerance to an error larger than ε. Since both C and ε can affect the complexity of the function, they should be tuned simultaneously. The principle for deciding the value of C is that it is equal to the output range.

It is also important to choose an appropriate kernel function and assign proper values to its parameters. There are many types of kernels: Radial Base Gaussian Function (RBGF) kernel, polynomial kernel, hyperbolic tangent kernel, two-layer neural networks kernel, B-splines kernel, etc. Among all the kernels, RBGF kernel function is the most popular one that ought to be tried first [54], and thusly is used in this study.

RBGF kernels are given by:

$$K(x, x_i) = \exp(-\frac{\|x - x_i\|^2}{2\sigma^2}) \tag{2.24}$$

Polynomial kernels are given by:

$$K(x, x_i) = (\langle x_i, x \rangle + c)^P, \quad p \in N,\ c > 0 \tag{2.25}$$

Hyperbolic tangent kernels are given by:

$$K(x, x_i) = \tanh(\theta + \langle x_i, x \rangle) \tag{2.26}$$

Generally, proper selection of SVM parameters is a tuning process. Thus, the SVM model is first identified with different parameter settings, giving the results shown in Table 2.4 and Table 2.5. The quality of the approximation is assessed using the root-mean-square error (RMSE) between the samples and the SVM model:

$$\text{RSME} = \sqrt{\frac{1}{n}\sum_{k=1}^{n}(y_{\text{p}} - y_{\text{a}})^2} \tag{2.27}$$

where n is the number of samples, y_p is the predicted value obtained by SVM model and y_a is the actual value from PEMFC. In this research, the actual value is generated by Pukrushpan's model.

Table 2.4 SVM model of stack voltage with different parameters

ζ	ε	C	Training (RMSE)	Testing (RMSE)	Number of support vector
20	0.01	10000	0.00412	0.00459	500
40	0.01	10000	0.00412	0.00434	499
60	0.01	10000	0.00417	0.00424	500
40	0.02	10000	0.00948	0.00856	499
40	0.01	1000	0.00412	0.00432	499

Table 2.5 SVM model of oxygen excess ratio with different parameters

ζ	ε	C	Training (RMSE)	Testing (RMSE)	Number of support vector
20	0.01	10000	0.00455	0.00406	499
40	0.01	10000	0.00422	0.00413	498
60	0.01	10000	0.00440	0.00417	499
40	0.02	10000	0.00722	0.00748	498
40	0.01	1000	0.00422	0.00413	498

As can be seen from both tables, ζ has significant impacts on the number of support vectors, while ε greatly affects the accuracy. The influence of C is not obvious in this case. In order to make a trade-off between the accuracy and the complexity of the SVM, the parameters are tuned thusly, $\zeta = 40$, $\varepsilon = 0.01$, and $C = 10000$.

2.5.4 Model Validation

The SVM models developed are validated by comparing with the traditional SIMULINK model in the literature, which was developed, presented and validated by Pukrushpan et al. [3]. In the stage of data preparation, the input-output data used for SVM modelling are

generated by exciting Pukrushpan's model with designed signals. A set of 1000 I/O data is collected from the simulation. The first 500 data are used for the identification of SVM model, while the remaining 500 data are used for validation purposes. In the stage of model validation, the results of SVM model are compared with those of Pukrushpan's model. The corresponding training and test results are plotted in Figure 2.10 and Figure 2.11. The outputs of Pukrushpan's model are recorded as the actual outputs in the figure, while the outputs of SVM models are depicted as the predicted outputs. The error is defined as the difference between the actual value and the predicted value. As can be seen from the both figures, the predicted results of SVM model are in good agreement with the actual values.

In order to quantify the validation of SVM models, the performance index of accuracy is calculated using the following equation:

$$\mathrm{ACC} = \left(1 - \sqrt{\frac{1}{n}\sum_{k=1}^{n}[(y_{\mathrm{p}} - y_{\mathrm{a}})/y_{\mathrm{a}}]^2}\right) \times 100\% \tag{2.28}$$

The results are presented in Table 2.6, including both indexes of RMSE and accuracy. The quantified results demonstrate that the SVM models are able to compete with traditional SIMULINK models in terms of accuracy. The accuracy is maintained above 99% in both training and testing experiment, which lays solid foundation for the development of control strategy.

Table 2.6 Quantified performance of SVM models

Model	Training		Testing	
	RMSE	ACC	RMSE	ACC
V_{st}	0.0041	99.99%	0.0043	99.99%
λ_{O2}	0.0042	99.87%	0.0041	99.87%

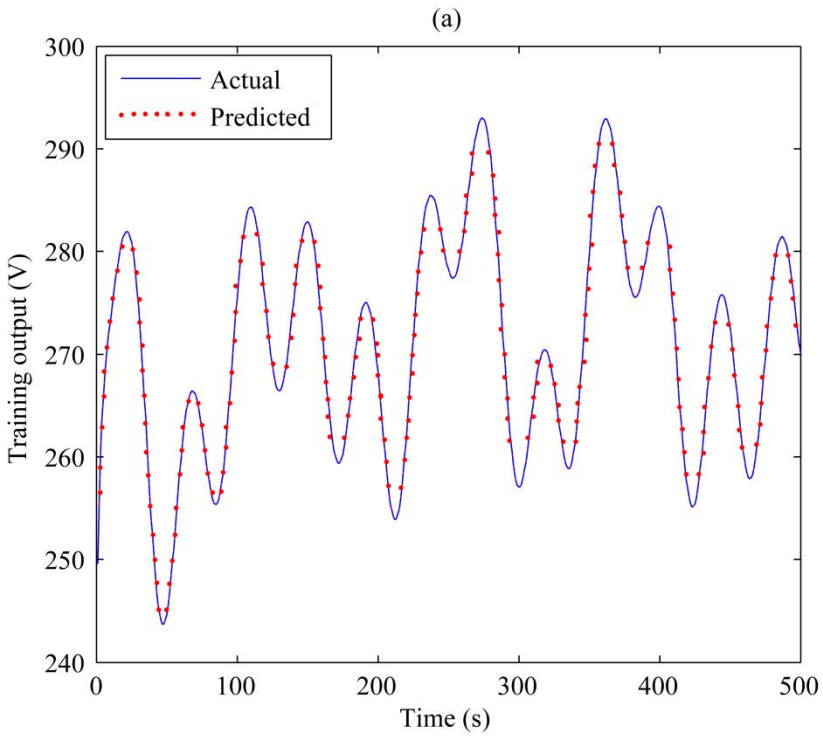

Figure 2.10 Performance of the SVM model for stack voltage: (a) Training output

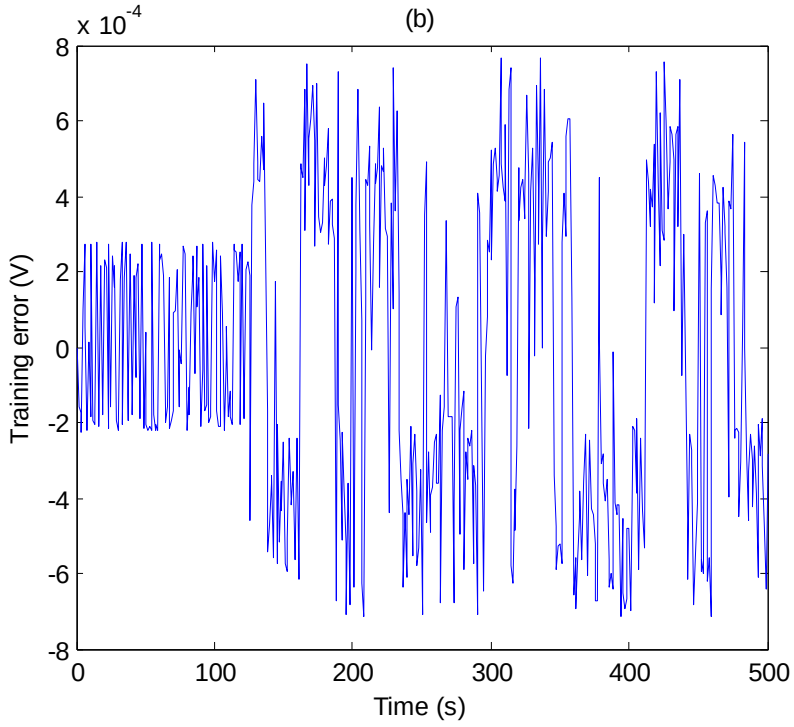

Figure 2.10 Performance of the SVM model for stack voltage: (b) Training error

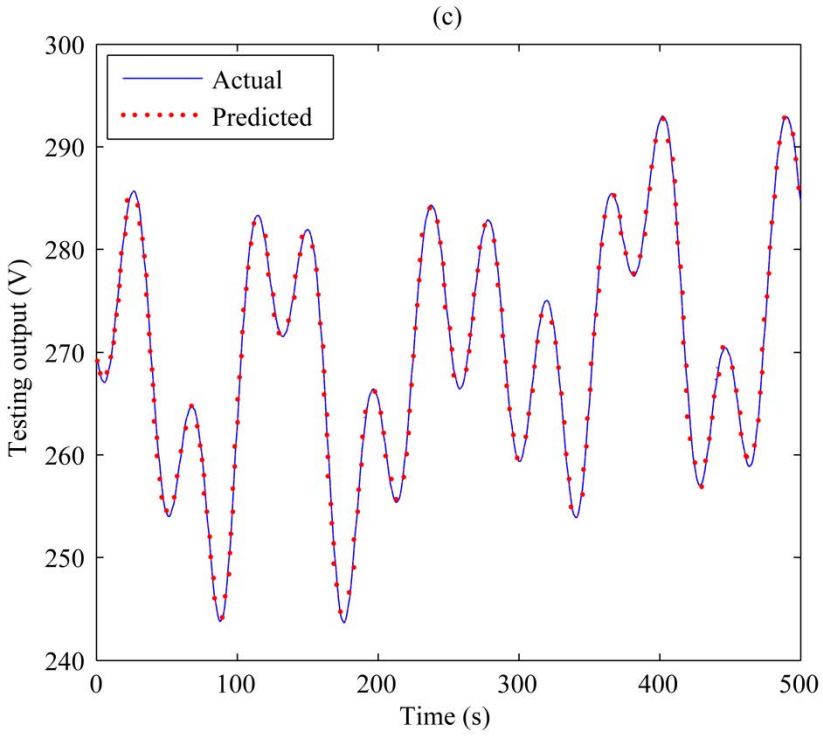

Figure 2.10 Performance of the SVM model for stack voltage: (c) Testing output

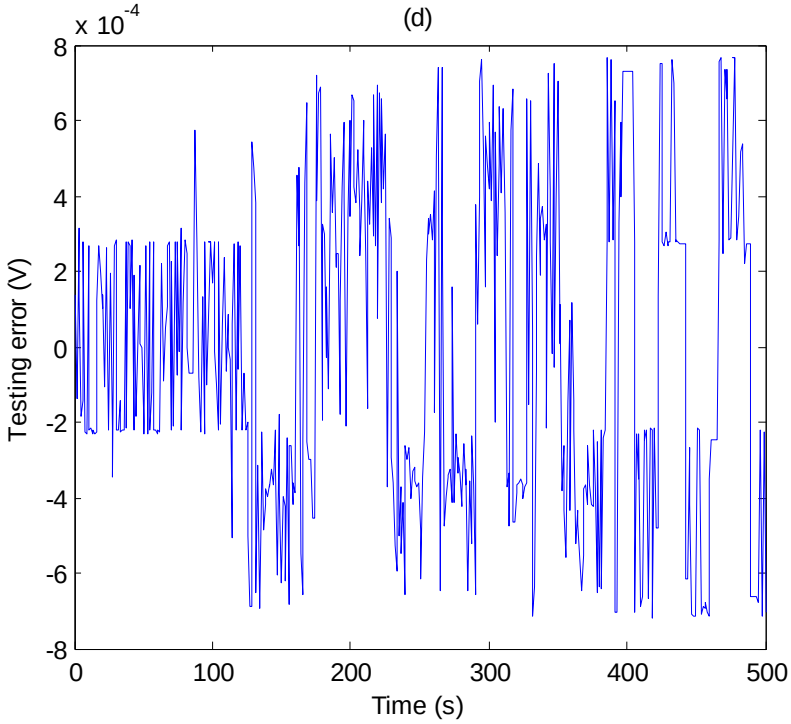

Figure 2.10 Performance of the SVM model for stack voltage: (d) Testing error

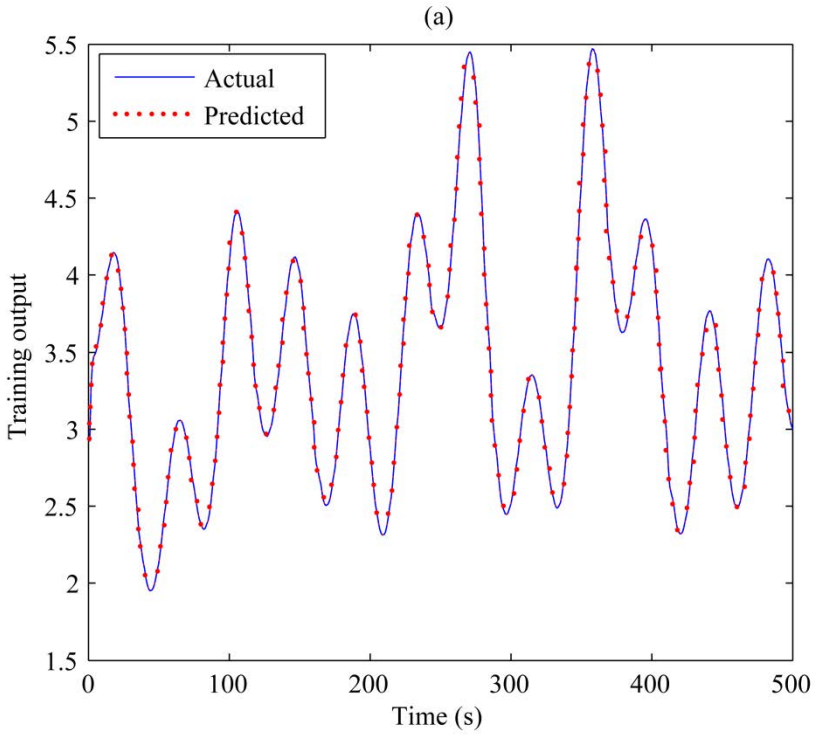

Figure 2.11 Performance of the SVM model for oxygen excess ratio: (a) Training output

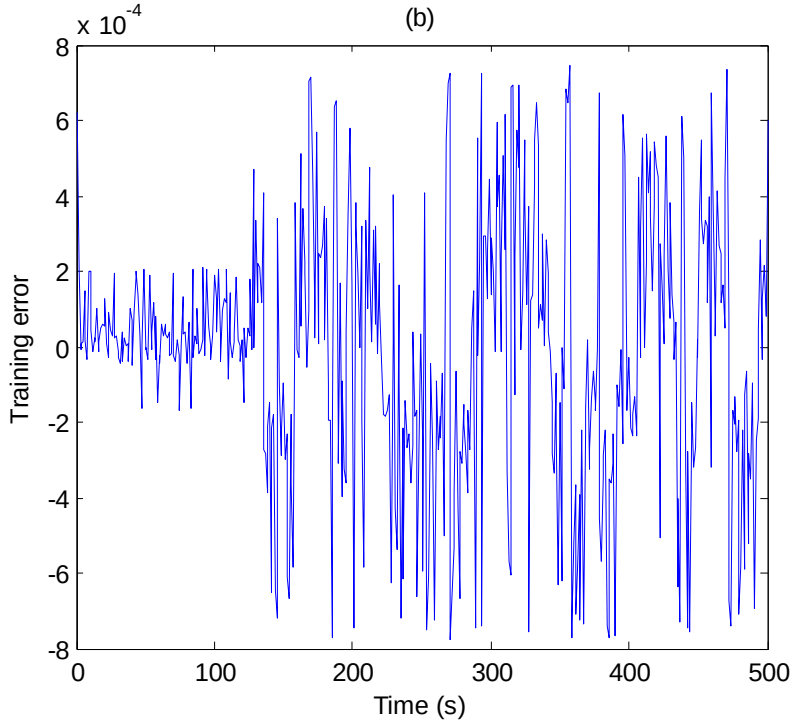

Figure 2.11 Performance of the SVM model for oxygen excess ratio: (b) Training error

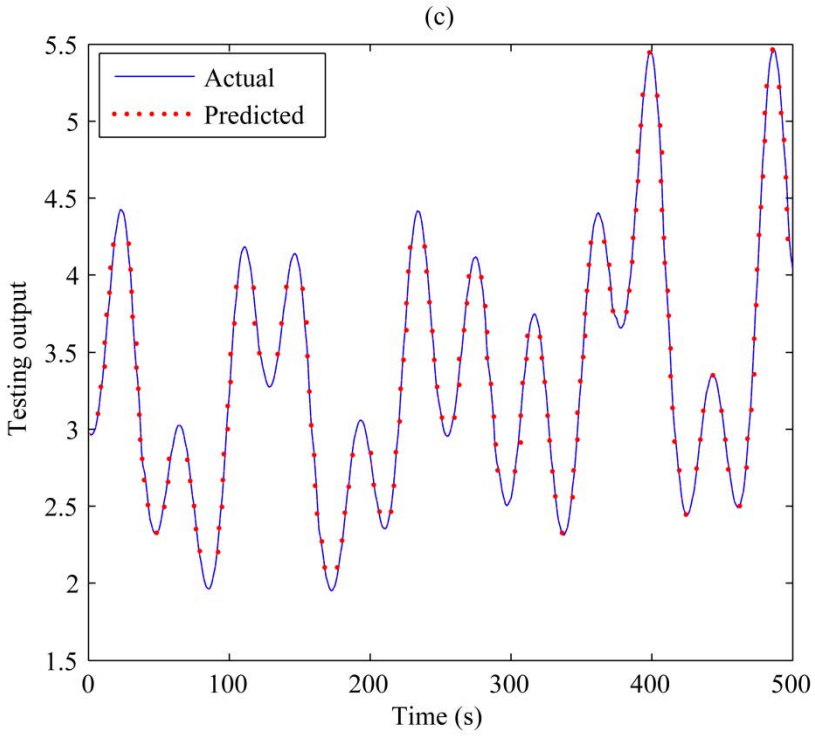

Figure 2.11 Performance of the SVM model for oxygen excess ratio: (c) Testing output

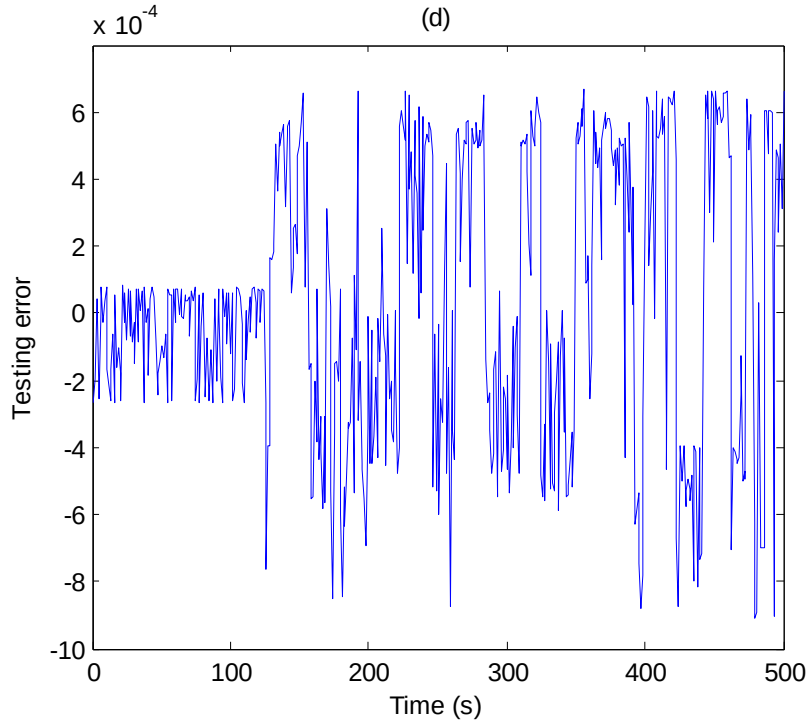

Figure 2.11 Performance of the SVM model for oxygen excess ratio: (d) Testing error

2.6 Combined empirical and mechanistic model of PEMFC

As discussed in the previous section, there are two types of PEMFC models: mechanistic or empirical. Each type has its own merits as well as limitations. One the one hand, the mechanistic model is based on phenomenological equations and provides adequate physical understanding of the phenomena inside the cell. Nevertheless, some sorts of numerical methods are required to solve the governing equations, thus making mechanistic models computational extensive. One the other hand, empirical models only focus on input and output relationship. Therefore, they usually have simple expression and thus provide low computational burden. This feature greatly facilitates the development of control strategy. However, empirical models are limited to a specific application or a narrow corridor of operating conditions. Moreover, the development of empirical models often requires a large number of experimental data to cover the entire expected operational range. Particularly, the amount of the data needed increases dramatically as the dimensions of inputs increase, and some data may not even be available. Therefore, few empirical models can address all important variables of PEMFC, such as stack current, temperature, hydrogen and oxygen partial pressure.

It is more desirable to develop a PEMFC model that combines the advantages of both two types of models. Motivated by this need, the hybrid modelling approach is employed to build the combine empirical and mechanistic model. The proposed model consists of two parts: empirical submodel and mechanistic submodel. The empirical submodel is a SVM model that concerns about stack current and temperature. The mechanistic submodel takes hydrogen and oxygen partial pressure changes into account. In this way, the input dimensions of the empirical submodel are reduced to two from four. Therefore, only limited

number of experimental data is needed to develop the empirical submodel. Besides, the combined model provides low computational burden, which lays a solid foundation for the development of the control strategy. Moreover, as the influence of the pressure is studied in a mechanistic way, the combined model has generalization ability and can predict PEMFC behaviour under any operational pressure.

2.6.1 Background of the combined model

In this section, an influential mechanistic PEMFC model is briefly reviewed. It is then modified for the combined model in the next section. The parameters used in this model are listed in Table 2.7.

Table 2.7 Summary of model parameters

Parameters	Description	Unit	Value
F	Faraday's constant	C $kmol^{-1}$	96484600
R	Universal gas constant	J $kmol^{-1}$ K	8314.47
N	Number of cells	-	35
k_r	Constant=$N/4F$	$kmols^{-1}$ A	$9.07x10^{-8}$
k_{H_2}	Hydrogen valve constant	$kmols^{-1}$ atm	$4.22x10^{-5}$
k_{O_2}	Oxygen valve constant	$kmols^{-1}$ atm	$2.11x10^{-5}$
τ_{H_2}	Hydrogen time constant	s	3.37
τ_{O_2}	Oxygen time constant	s	6.47
ξ_1	Constant	-	-0.9514
ξ_2	Constant	-	$3.12x10^{-3}$
ξ_3	Constant	-	$7.4x10^{-5}$
ξ_4	Constant	-	$-1.87x10^{-4}$
ξ_5	Constant	-	$1.605x10^{-2}$
ξ_6	Constant	-	$3.5x10^{-5}$
ξ_7	Constant	-	$8x10^{-5}$

The proportional relationship between the flow of gas through a valve and the partial pressure can be stated as [56]:

$$\frac{q_{H_2}}{p_{H_2}} = \frac{k_{an}}{\sqrt{M_{H_2}}} = k_{H_2} \tag{2.29}$$

$$\frac{q_{O_2}}{p_{O_2}} = \frac{k_{ca}}{\sqrt{M_{O_2}}} = k_{O_2} \tag{2.30}$$

where q_{H_2} is molar flow of hydrogen (kmol s^{-1}), q_{O_2} is molar flow of oxygen (kmol s^{-1}), p_{H_2} hydrogen partial pressure (atm), p_{O_2} oxygen partial pressure (atm), k_{H_2} hydrogen valve molar constant (kmol(atm $s)^{-1}$), k_{O_2} oxygen valve molar constant (kmol(atm $s)^{-1}$), k_{an} anode valve constant ($\sqrt{\text{K mol kg}}(\text{atm s})^{-1}$), k_{ca} cathode valve constant ($\sqrt{\text{K mol kg}}(\text{atm s})^{-1}$), M_{H_2} molar mass of hydrogen (kg $kmol^{-1}$), M_{O_2} molar mass of oxygen (kg $kmol^{-1}$).

For hydrogen, the derivative of the partial pressure can be calculated using the perfect gas equation as follows [56]:

$$\frac{d}{dt} p_{H_2} = \frac{RT}{V_{an}} (q_{H_2}^{in} - q_{H_2}^{out} - q_{H_2}^{r}) \tag{2.31}$$

where R is the universal gas constant (J $kmol^{-1}K^{-1}$), T absolute temperature (K), V_{an} volume of the anode (l), $q_{H_2}^{in}$ hydrogen input flow (kmol s^{-1}), $q_{H_2}^{out}$ hydrogen output flow (kmol s^{-1}), $q_{H_2}^{r}$ hydrogen flow that reacts (kmol s^{-1}).

The relationship between the hydrogen flow and the stack current can be written as [56]:

$$q_{H_2}^{r} = \frac{NI}{2F} = 2k_r I \tag{2.32}$$

where N is the number of the series-wound fuel cells in the stack, I the stack current (A), F Faraday‘s constant (C kmol) $^{-1}$, k_r modeling constant (kmol(sA)$^{-1}$).

In (2.31), replacing the output flow by (2.29) and the reacted flow by (2.32), taking the Laplace transform of both sides of (2.31) and isolating the hydrogen partial pressure, yields the following expression [56]:

$$p_{H_2} = \frac{1/k_{H_2}}{1+\tau_{H_2} s}(q_{H_2}^{in} - 2k_r I) \tag{2.33}$$

where s is the Laplace variable, τ_{H_2} is the value of system pole associated with hydrogen flow,

$$\tau_{H_2} = \frac{V_{an}}{k_{H_2} RT} \tag{2.34}$$

In the same way, the equations for the partial pressures of oxygen p_{O_2} can also be derived as [56]:

$$p_{O_2} = \frac{1/k_{O_2}}{1+\tau_{O_2} s}(q_{O_2}^{in} - k_r I) \tag{2.35}$$

where

$$\tau_{O_2} = \frac{V_{ca}}{k_{O_2} RT} \tag{2.36}$$

In [57], the authors introduce an influential model that describes the polarization curves of PEMFC where the fuel cell voltage is the sum of three terms: the open circuit voltage E_{nernst}, the activation loss η_{act} and the ohmic loss η_{ohmic}. The concentration loss cause rapid voltage drop only at extremely high current density [58]. Therefore, it is ignored under normal operating conditions. In mathematical form, polarization curves can be expressed as:

$$V_{cell} = E_{nernst} + \eta_{act} + \eta_{ohmic} \tag{2.37}$$

The open circuit voltage (reversible thermodynamic potential) E_{nernst} is described by the Nernst equation. Using thermodynamic values of the standard state entropy change, the expression is:

$$E_{nernst} = 1.299 - (8.5\times10^{-4})\cdot(T - 298.15) + (4.308\times10^{-5})\cdot T\cdot(\ln p_{H_2} + 0.5\ln p_{O_2}) \tag{2.38}$$

where T is the cell temperature (K).

The activation loss η_{act} is a result of the need to cause electron transfer and to break and form chemical bonds in the anode and cathode. It can be expressed as:

$$\eta_{act} = \xi_1 + \xi_2 T + \xi_3 T\ln C_{O_2} + \xi_4 T\ln I \tag{2.39}$$

where C_{O_2} is the concentration of dissolved oxygen at the gas/liquid interface, I is the stack current (A), and those four ξ_{i} (i = 1–4) are coefficients.

The oxygen concentration C_{O_2} can be expressed as:

$$C_{O_2} = \frac{p_{O_2}}{(5.08\times10^6)\cdot\exp(-498/T)} \tag{2.40}$$

The ohmic loss η_{ohmic} is due to the resistance of the polymer membrane to the transfer of protons and the resistance of the electrode and the collector plate to the transfer of electrons. It can be expressed as:

$$\eta_{ohmic} = -IR^{\text{internal}} = -I(\xi_5 + \xi_6 T + \xi_7 I) \tag{2.41}$$

where ξ_{i} (i = 5–7) are coefficients. It can be concluded from (2.41) that the η_{ohmic} is independent of the oxygen and hydrogen partial pressure.

The output voltage of the fuel cell stack can be calculated by the expression:

$$V_{st} = NV_{cell} \tag{2.42}$$

2.6.2 Combined empirical and mechanistic model

Mechanistic models are computationally intensive while empirical models needs excessive amount of data in the case of multiple inputs. To overcome these problems, the combined empirical and mechanistic model of PEMFC is proposed. The empirical submodel V^0 is a SVM model, which predicts cell voltage at different stack currents and temperatures under the reference hydrogen and oxygen partial pressure. The mechanistic submodel ΔV calculates the correction voltage by taking account of hydrogen and oxygen partial pressure changes. The structure of the model is illustrated in Figure 2.12.

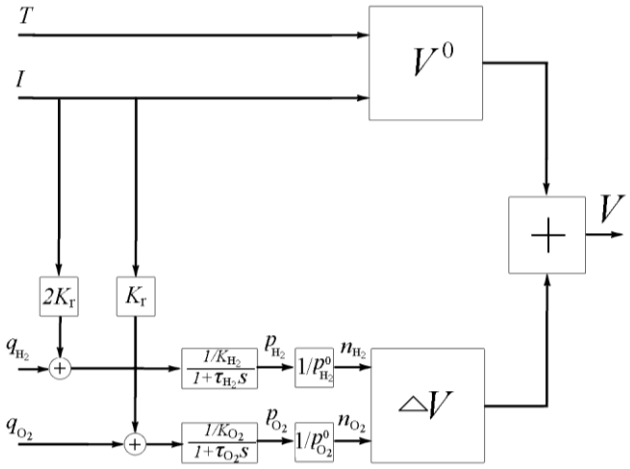

Figure 2.12 Schematic of the combined empirical and mechanistic model [59]

2.6.2.1 Mechanistic submodel

It is known that the continuous-time system can be discretized using zero-order holder. For instance, given a first-order inertial element in the form of Laplace transfer function:

$$G(s)=\frac{k}{s+a} \tag{2.43}$$

its discrete-time state equations can be obtained as,

$$\begin{cases} x(k+1)=e^{-aT_s}x(k)+\dfrac{k}{a}(1-e^{-aT_s})u(k) \\ y(k+1)=x(k+1) \end{cases} \tag{2.44}$$

where $u(k)$ is the input, $x(k)$ is the state, $y(k)$ is the output, T_s is the sample time.

(2.33) and (2.35) can be regarded as first-order inertial elements with $a = 1/\tau_{H_2}$, $k = 1/k_{H_2}\tau_{H_2}$ and $a = 1/\tau_{O_2}$, $k = 1/k_{O_2}\tau_{O_2}$, respectively. As such, in the case of sample time T_s =1s, (2.33) and (2.35) can be converted to discrete-time state equations,

$$P_{H_2}(k+1)=0.7432P_{H_2}(k)+6085[q_{H_2}(k)-2K_rI(k)] \tag{2.45}$$

$$P_{O_2}(k+1)=0.8568P_{O_2}(k)+6787[q_{O_2}(k)-K_rI(k)] \tag{2.46}$$

As shown in (2.38) and (2.39), the hydrogen and oxygen partial pressures influence the cell voltage through the terms E_{nernst} and η_{act}. Let $p_{O_2}^0$ and $p_{H_2}^0$ stand for the reference partial pressures of oxygen and hydrogen, respectively. The changes of oxygen and hydrogen partial pressure are defined as the proportional form:

$$p_{H_2} = n_{H_2}p_{H_2}^0, \qquad p_{O_2} = n_{O_2}p_{O_2}^0 \tag{2.47}$$

where n_{O_2} and n_{H_2} are ratios that represent the pressure changes to $p_{O_2}^0$ and $p_{H_2}^0$

Substituting (2.47) into (2.38), the thermodynamic potential can be rewritten as:

$$
\begin{aligned}
E_{nernst} &= 1.299 - (8.5\times10^{-4})\cdot(T - 298.15) + (4.308\times10^{-5})\cdot T\cdot(\ln n_{H_2} p^0_{H_2} + 0.5\ln n_{O_2} p^0_{O_2}) \\
&= E^0_{nernst} + (4.308\times10^{-5})\cdot T\cdot(\ln n_{H_2} + 0.5\ln n_{O_2})
\end{aligned}
$$

with

$$
E^0_{nernst} = 1.299 - (8.5\times10^{-4})\cdot(T - 298.15) + (4.308\times10^{-5})\cdot T\cdot(\ln p^0_{H_2} + 0.5\ln p^0_{O_2}) \tag{2.48}
$$

where E^0_{nernst} is the thermodynamic potential under the reference pressures $p^0_{O_2}$ and $p^0_{H_2}$.

Substituting (2.40) and (2.47) into (2.39), the total overvoltage can be rewritten as:

$$
\begin{aligned}
\eta_{act} &= \xi_1 + \xi_2 T + \xi_3 T\ln n_{O_2} C^0_{O_2} + \xi_4 T\ln I \\
&= \xi_1 + \xi_2 T + \xi_3 T\ln C_{O_2} + \xi_4 T\ln I + \xi_3 T\ln n_{O_2} \\
&= \eta^0_{act} + \xi_3 T\ln n_{O_2}
\end{aligned}
$$

with

$$
\eta^0_{act} = \xi_1 + \xi_2 T + \xi_3 T\ln C^0_{O_2} + \xi_4 T\ln I \tag{2.49}
$$

where η^0_{act} is the activation loss under the reference pressure $p^0_{O_2}$.

Substituting (2.48) and (2.49) into (2.37), the fuel cell voltage can be rewritten as:

$$
V_{cell} = V^0 + \Delta V
$$

with

$$
\begin{aligned}
V^0 &= E^0_{nernst}(T, p^0_{H_2}, p^0_{O_2}) + \eta^0_{act}(I, T, p^0_{O_2}) + \eta_{ohmic}(I, T) \\
\Delta V &= (4.308\times10^{-5})\cdot T\cdot(\ln n_{H_2} + 0.5\ln n_{O_2}) + \xi_3 T\ln n_{O_2}
\end{aligned} \tag{2.50}
$$

where V^0 is the reference voltage obtained under the reference hydrogen and oxygen partial pressure, ΔV is the correction voltage calculated by hydrogen and oxygen partial pressure changes. As reference hydrogen and oxygen partial pressure are predetermined constants, V^0 can be mapped as a function of the stack currents I and temperatures T by SVM model, which will be discussed in the next section. Therefore, (2.50) is the proposed combined model, which consists of empirical module V^0 and mechanistic module ΔV.

2.6.2.2 Empirical submodel

The empirical module V^0 is indentified using SVM modelling method. First, V^0 described previously is implemented under reference partial pressures $p^0_{H_2}$ = 2.5atm and $p^0_{O_2}$ = 1.4atm. Figure 2.13 shows the block diagram of V^0 developed in the MATLAB/SIMULINK environment. Using this simulation model, the input-output data needed for SVM training and testing are generated. The input-output data used for SVM modelling are generated by exciting the SIMULINK model with the designed signals 10+10sin(0.3t)sin(0.4t) and 343+15sin$t$sin(0.5t) for the stack current and the temperature, respectively. Figure 2.14 shows the input signals and the corresponding outputs. A set of 1000 data is collected from the simulation. The first 500 data are used for the identification of SVM model, while the remaining 500 data are used for validation purposes. Once again, the same steps used in previous section are employed for SVM modelling.

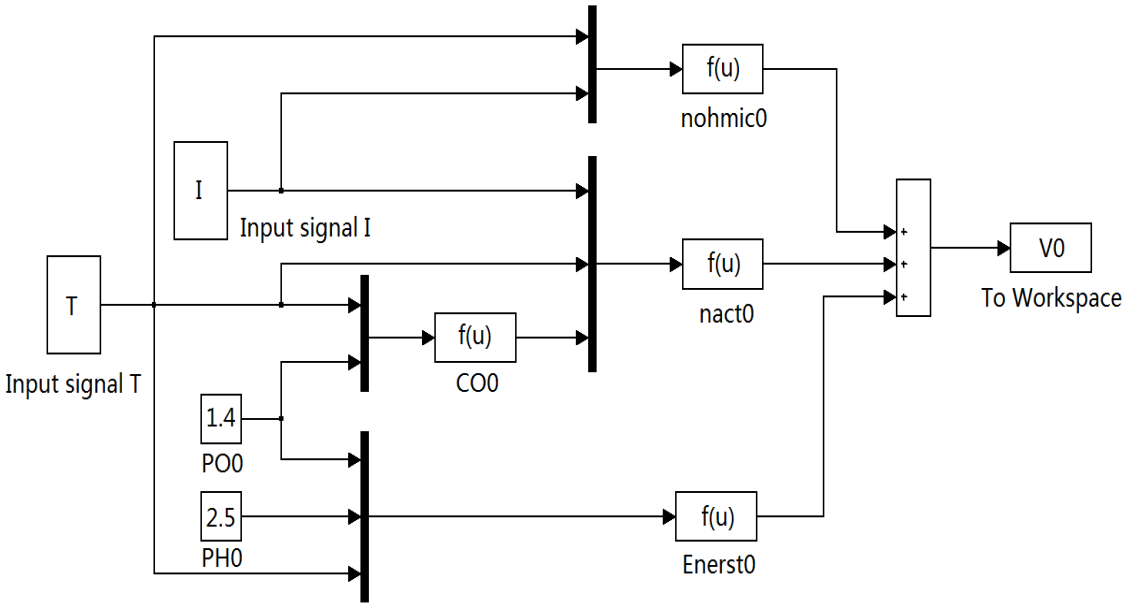

Figure 2.13 Block diagram of V^0 implemented in SIMULINK [59]

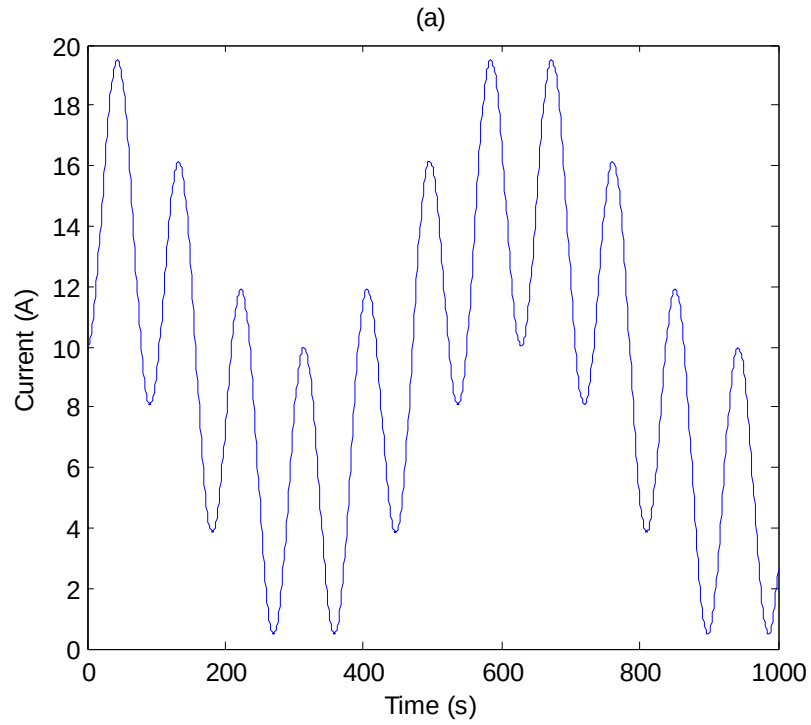

Figure 2.14 Input excitation and output response signals of V^0: (a) Current

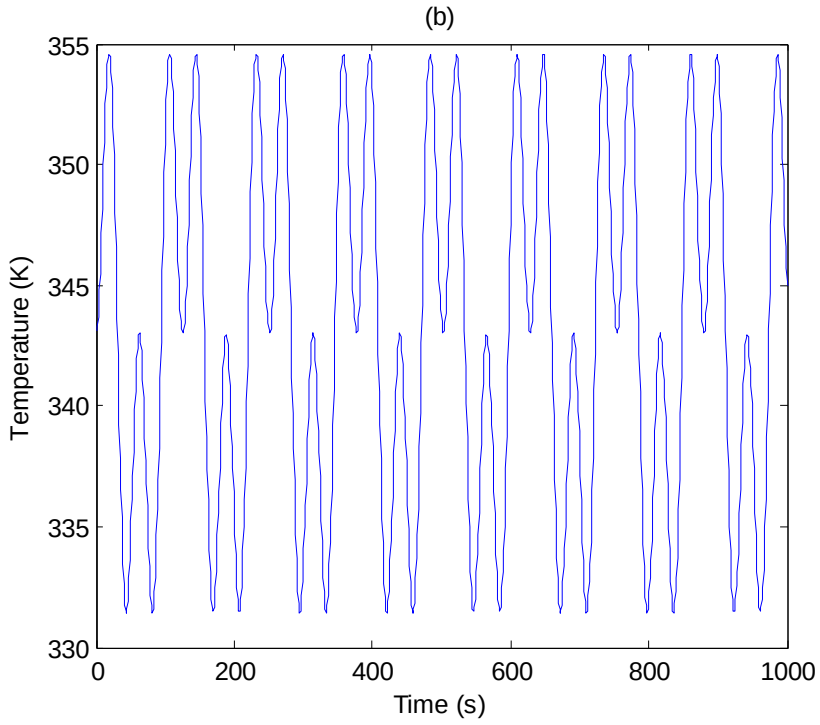

Figure 2.14 Input excitation and output response signals of V^0: (b) Temperature

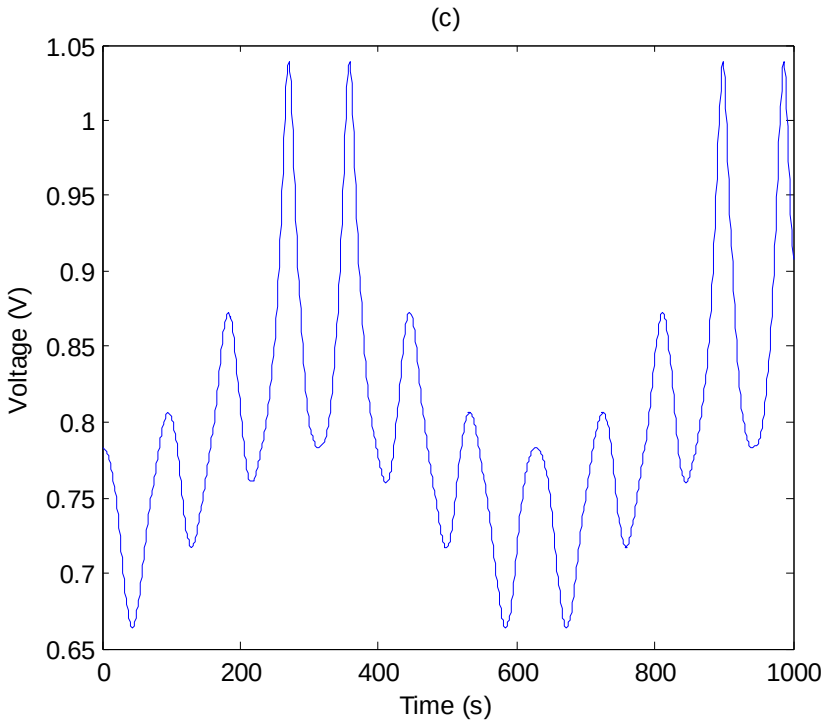

Figure 2.14 Input excitation and output response signals of V^0: (c) Voltage

2.6.3 Model validation

To validate the mechanistic submodel, the predicted values calculated by the mechanistic submodel are compared with the experimental data reported by Amphlett et al. [56], which are listed in Table 2.8. The experimental data were obtained with temperature of 343K and current of 6.66A. The first group is used as the reference value. Therefore, the reference voltage V^0 = 0.824V, the reference hydrogen partial pressure $p_{H_2}^0$ = 2.5atm and the reference oxygen partial pressure $p_{O_2}^0$ =1.4atm. Using (2.50), the correction voltages ΔV and the predicted voltage can be calculated for the other four groups. The results demonstrate the good performance of the mechanistic submodel, with the maximum error less than 1.5%.

Table 2.8 Mechanistic submodel validation

No	q_{H_2} (kmol/s)	p_{H_2} (atm)	n_{H_2}	q_{O_2} (kmol/s)	p_{O_2} (atm)	n_{O_2}	Actual voltage (V)	Predicted voltage (V)	Error (%)
1	4.121×10^{-4}	2.5	-	2.069×10^{-4}	1.4	-	0.824	-	-
2	5.107×10^{-4}	3.1	1.240	1.244×10^{-4}	0.6	0.429	0.792	0.799	0.838
3	5.107×10^{-4}	3.1	1.240	4.573×10^{-4}	3.1	2.214	0.851	0.854	0.353
4	3.315×10^{-4}	2.0	0.800	1.244×10^{-4}	0.6	0.429	0.781	0.792	1.408
5	3.315×10^{-4}	2.0	0.800	4.573×10^{-4}	3.1	2.214	0.847	0.847	0

The validation of empirical submodel employs similar method used in the previous section. The results of empirical submodel model are compared with those of the SIMULINK model. The corresponding training and testing results are plotted in Figure 2.15. The outputs of SIMULINK model are recorded as the actual outputs in the figure, while the outputs of empirical submodel are depicted as the predicted outputs. The error is defined as the difference between the actual value and the predicted value. As expected, the predicted results of the empirical submodel are in good agreement with the actual values, as shown in Figure 2.15. The quantified performance of the empirical submodel is presented in Table 2.9. It can be concluded that the empirical submodel achieves good performance, with accuracy above 99.9% in both training and testing phrase.

Table 2.9 Quantified performance of empirical submodel

	Training	Testing
RMSE	0.000275	0.000271
ACC	99.967%	99.969%

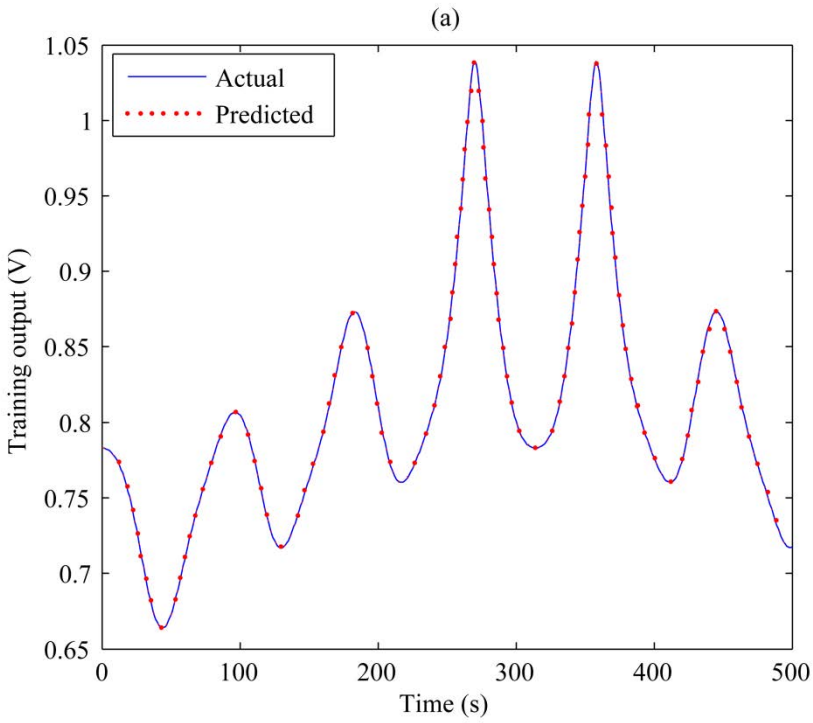

Figure 2.15 Training and testing results of the SVM model for V^0: (a) Training output

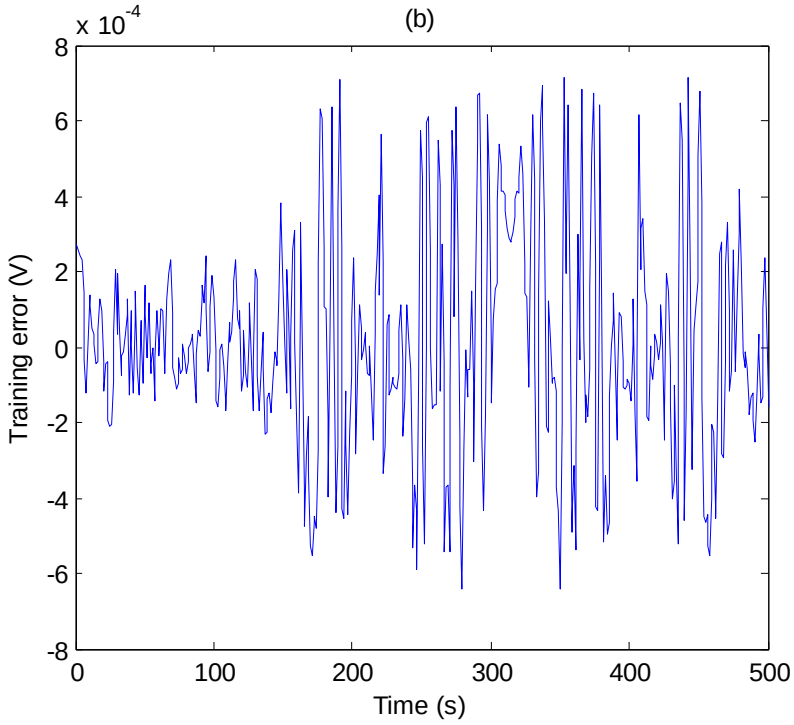

Figure 2.15 Training and testing results of the SVM model for V^0: (b) Training error

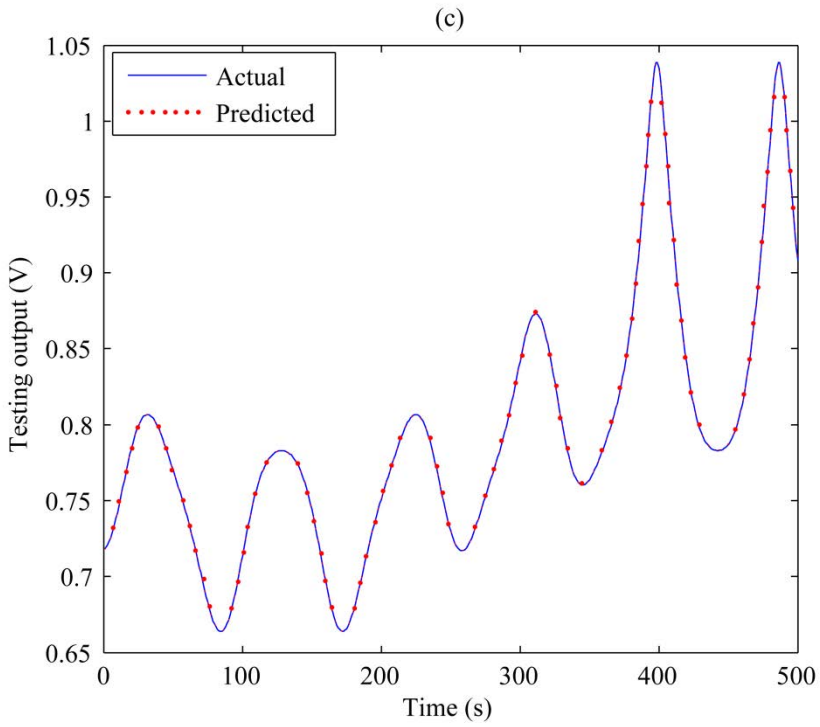

Figure 2.15 Training and testing results of the SVM model for V^0: (c) Testing output

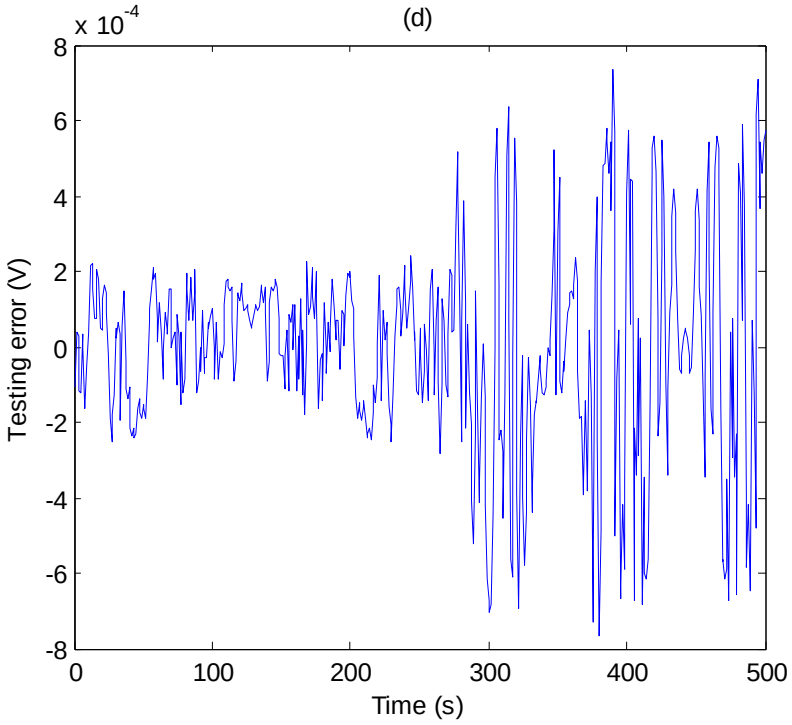

Figure 2.15 Training and testing results of the SVM model for V^0: (d) Testing error

To increase its credibility, the empirical submodel is further tested with the experimental data reported by Laurencelle et al. [60], as shown in Figure 2.16. They performed the practical experiments on Ballard MK5-E PEMFC stack with rated power of 5kW. The stack composed of 36 cells; each cell has a 232 cm^2 active area, graphite electrodes, and a Dow membrane. In their experiment, the hydrogen partial pressure and oxygen partial pressure are both regulated to 3 atm. The data set of cell voltage and current density were obtained at temperature levels of 24°C, 31°C, 39°C, 56°C and 72°C, respectively.

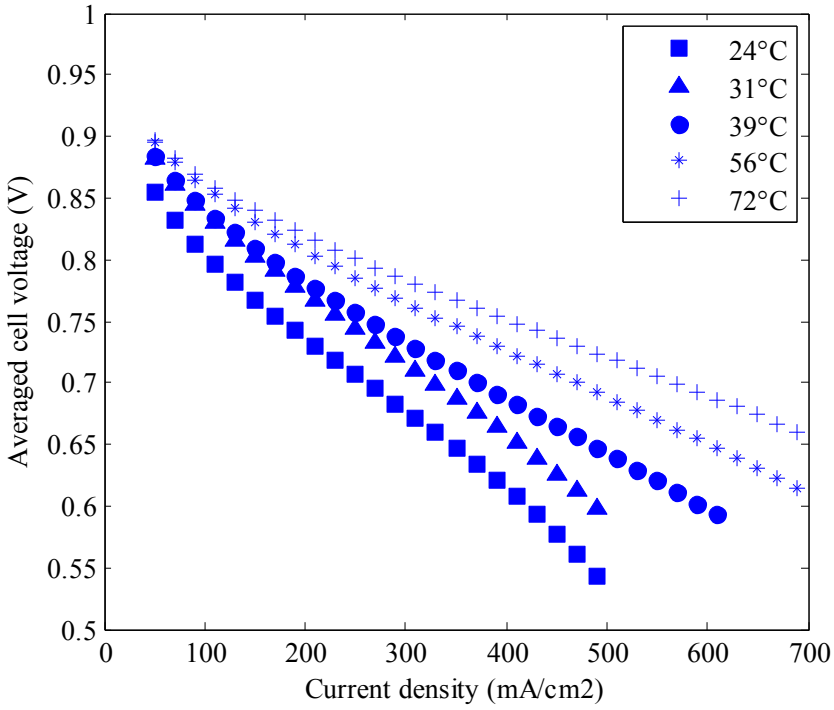

Figure 2.16 Characterization of Ballard MK5-E PEMFC stack [60]

The performance of the empirical submodel developed with the experimental data is shown in Figure 2.17. As can be seen, the empirical submodel fits very well with the experimental data. The performance is further quantified, giving the results shown in Table 2.10. As expected, the accuracy of the empirical submodel remains above 99.9%.

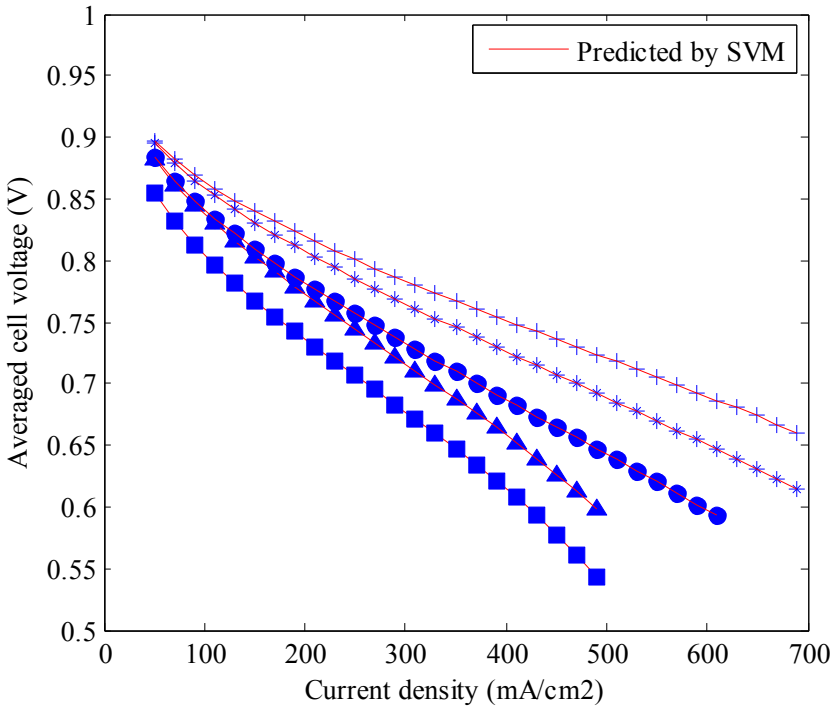

Figure 2.17 Experimental data and empirical submodel

Table 2.10 Quantified performance of empirical submodel

Model	RMSE	ACC
24°C	0.00042	99.936%
31°C	0.00039	99.945%
39°C	0.00034	99.952%
56°C	0.00035	99.953%
72°C	0.00039	99.947%

2.7 Conclusion

The objective of this chapter is to investigate new methods for PEMFC modelling. First, a new empirical model of PEMFC is developed by mapping stack voltage and oxygen excess ratio as a function of stack current and compressor motor voltage through regression

analysis of SVM. Simulation results demonstrate that the model achieves good performance with accuracy above 99% in both training and testing experiment. Further, the empirical modelling approach is integrated with the mechanistic modelling method to develop a combined model of PEMFC, which consists of an empirical submodel for the reference voltage and a mechanistic submodel for the correction voltage. The combined model overcomes the disadvantages of both the empirical model and the mechanistic model. Compared with the pure empirical model, the combined model can be built with less operational data due to the reduction of input dimensions from four to two. In addition, unlike the pure empirical model, the combined model has generalization ability as the influence of the pressure is studied in a mechanistic way. On the other hand, unlike the pure mechanistic model, the combine model has simple expressions and provides low computational burden due to the introduction of empirical submodel.

In the next chapter, various control strategies are developed based on the models built in this chapter. Specifically, a model predictive control strategy is developed based on the SVM model built in section 2.4 and a constrained predictive control strategy is developed based on the combined model built in section 2.5. The control strategies serve to regulate PEMFC performance outputs to desired values. Without these control strategies, PEMFC would not be able to work safely and efficiently.

Reference

[1] K. Haraldsson, K. Wipke, "Evaluating PEM fuel cell system models," *J. Power Sources*, vol. 126, pp. 88-97, 2004.

[2] J. C. Amphlett, R. F. Mann, B. A. Peppley, P. R. Roberge, A. Rodrigues, "A model predicting transient responses of proton exchange membrane fuel cells," *J. Power Sources*, vol. 61, pp. 183-188, 1996.

[3] J. T. Pukrushpan, "Modeling and Control of Fuel Cell Systems and Fuel Processors," Ph.D. dissertation, Dept. of Mech. Eng., University of Michigan, Ann Arbor, 2003.

[4] S. Yerramalla, A. Davari, A. Feliachi, T. Biswas, "Modeling and simulation of the dynamic behavior of a polymer electrolyte membrane fuel cell," *J. Power Sources*, vol. 124, pp. 104-113, 2003.

[5] X. Xue, J. Tang, A. Smirnova, R. England, N. Sammes, "System level lumped-parameter dynamic modeling of PEM fuel cell," *J. Power Sources*, vol. 133, pp. 188-204, 2004.

[6] P. R. Pathapati, X. Xue, J. Tang, "A new dynamic model for predicting transient phenomena in a PEM fuel cell system," *Renewable Energy*, vol. 30, pp. 1-22, 2005.

[7] J. Benziger, E. Chia, E. Karnas, J. Moxley, C. Teuscher, I. G. Kevrekidis, "The stirred tank reactor polymer electrolyte membrane fuel cell," *AIChE J.*, vol. 50, pp. 1889-1900, 2004.

[8] D. M. Bernardi, M. W. Verbrugge, "Mathematical-model of a gasdiffusion electrode bonded to a polymer electrolyte," *AIChE J.*, vol. 37, pp. 1151-1163, 1991.

[9] T. E. Springer, T. A. Zawodzinski, S. Gottesfeld, "Polymer electrolyte fuel cell model," *J. Electrochem. Soc.*, vol. 138, pp. 2334-2342. 1991.

[10] J. J. Baschuk, X. H. Li, "Modelling of polymer electrolyte membrane fuel cells with variable degrees of water flooding," *J. Power Sources*, vol. 86, pp. 181-196, 2000.

[11] N. Djilali, D. M. Lu, "Influence of heat transfer on gas and water transport in fuel cells," *Int. J. Therm. Sci.*, vol. 41, pp. 29-40, 2002.

[12] A. Z. Weber, R. M. Darling, J. Newman, "Modeling two-phase behaviour in PEFCs," *J. Electrochem. Soc.*, vol. 151, pp. A1715-A1727, 2004.

[13] C. Ziegler, H. M. Yu, J. O. Schumacher, "Two-phase dynamic modeling of PEMFCs and simulation of cyclo-voltammograms," *J. Electrochem. Soc.*, vol. 152, pp. A1555-A1567, 2005.

[14] T. F. Fuller, J. Newman, "Water and thermal management in solidpolymer-electrolyte fuel-cells," *J. Electrochem. Soc.*, vol. 140, pp. 1218-1225, 1993.

[15] T. V. Nguyen, R. E. White, "A water and heat management model for proton-exchange-membrane fuel-cells," *J. Electrochem. Soc.*, vol. 140, pp. 2178-2186, 1993.

[16] J. S. Yi, T. V. Nguyen, "An along-the-channel model for proton exchange membrane fuel cells," *J. Electrochem. Soc.*, vol. 145, pp. 1149-1159, 1998.

[17] D. Singh, D. M. Lu, N. Djilali, "A two-dimensional analysis of mass transport in proton exchange membrane fuel cells," *Int. J. Eng. Sci.*, vol. 37, pp. 431-452, 1999.

[18] J. H. Lee, T. R. Lalk, A. J. Appleby, "Modeling electrochemical performance in large scale proton exchange membrane fuel cell stacks," *J. Power Sources*, vol. 70, pp. 258-268, 1998.

[19] V. Gurau, H. T. Liu, S. Kakac, "Two-dimensional model for proton exchange membrane fuel cells," *AIChE J.*, vol. 44, pp. 2410-2422, 1998.

[20] S. Um, C. Y. Wang, K. S. Chen, –Computational fluid dynamics modeling of proton exchange membrane fuel cells," *J. Electrochem. Soc.*, vol. 147, pp. 4485-4493, 2000.

[21] S. H. Ge, B. L. Yi, –A mathematical model for PEMFC in different flow modes," *J. Power Sources*, vol. 124, pp. 1-11, 2003.

[22] U. Pasaogullari, C. Y. Wang, –Two-phase modeling and flooding prediction of polymer electrolyte fuel cells," *J. Electrochem. Soc.*, vol. 152, pp. A380–A390, 2005

[23] J. Cao, N. Djilali, –Numerical modeling of PEM fuel cells under partially hydrated membrane," *J. Energy Resour. Technol.*, vol. 127, pp. 26-36, 2005.

[24] H. Meng, –A two-phase non-isothermal mixed-domain PEM fuel cell model and its application to two-dimensional simulations," *J. Power Sources*, vol. 168, pp. 218-228, 2007.

[25] H. Meng, –Numerical investigation of transient responses of a PEM fuel cell using a two-phase non-isothermal mixed-domain model," *J. Power Sources*, vol. 171, pp. 738-746, 2007.

[26] S. Dutta, S. Shimpalee, J. W. Van Zee, –Three-dimensional numerical simulation of straight channel PEM fuel cells," *J. Appl. Electrochem.*, vol. 30, pp. 135-146, 2000.

[27] S. Dutta, S. Shimpalee, J. Van Zee, –Numerical prediction of massexchange between cathode and anode channels in a PEM fuel cell," *Int. J. Heat Mass Transfer*, vol. 44, pp. 2029–2042, 2001.

[28] T. Berning, N. Djilali, –Three-dimensional computational analysis of transport phenomena in a PEM fuel cellsA parametric study," *J. Power Sources*, vol. 124, pp. 440-452, 2003.

[29] S. Mazumder, J. V. Cole, "Rigorous 3-D mathematical modelling of PEM fuel cells II. Model predictions with liquid water transport," *J. Electrochem. Soc.*, vol. 150, pp. A1510–A1517, 2003.

[30] H. Meng, C. Y. Wang, "Electron transport in PEFCs," *J. Electrochem.Soc.*, vol. 151, pp. A358–A367, 2004.

[31] S. Shimpalee, S. Greenway, D. Spuckler, J. Van Zee, "Predicting water and current distributions in a commercial-size PEMFC," *J. Power Sources*, vol. 135, pp. 79-87, 2004.

[32] Y. Wang, C. Y. Wang, "Transient analysis of polymer electrolyte fuel cells," *Electrochim. Acta*, vol. 50, pp. 1307-1315, 2005.

[33] Y. Wang, C. Y. Wang, K. S. Chen, "Elucidating differences between carbon paper and carbon cloth in polymer electrolyte fuel cells," *Electrochim. Acta*, vol. 52, pp. 3965-3975, 2007.

[34] V. Gurau, T. Zawodzinski, J. Mann, "Numerical investigation of water transport in the PEMFC components," *ECS Trans.*, vol. 3, pp. 1095-1104, 2006.

[35] Q. Ye, T. V. Nguyen, "Three-dimensional simulation of liquid water distribution in a PEMFC with experimentally measured capillary functions," *J. Electrochem. Soc.*, vol. 154, pp. B1242–B1251, 2007.

[36] Y. Wang, "Modeling of two-phase transport in the diffusion media of polymer electrolyte fuel cells," *J. Power Sources*, vol. 185, pp. 261-271, 2008.

[37] V. Vapnik, A. Lerner, "Pattern recognition using generalized portrait method," *Autom. Remote Control*, vol. 24, pp. 774-780, 1963.

[38] V. Vapnik, A. Chervonenkis, "A note on one class of perceptrons," *Autom. Remote Control*, vol. 25, 1964.

[39] V. Vapnik, A. Chervonenkis, *Theory of Pattern Recognition [in Russian]*, Nauka Moscow, 1974.

[40] V. Vapnik, *Estimation of Dependences Based on Empirical Data*, Springer Berlin, 1982.

[41] V. Vapnik, *The Nature of Statistical Learning Theory*, Springer New York, 1995.

[42] E. Osuna, R. Freund, F. Girosi, ―An improved training algorithm for support vector machines," *in Proceedings of the 1997 IEEE Workshop on Neural Networks for Signal Processing VII*, pp. 276-285, 1997.

[43] C. J. C. Burges, ―Simplified support vector decision rules," *in Proceedings of the International Conference on Machine Learning*, pp. 71-77, 1996.

[44] K. R. Muller, J. A. Smola, G. Ratsch, B. Schölkopf, J. Kohlmorgen, V.N. Vapnik, "Predicting time series with support vector machines," *in Proceedings of 7th International Conference on Artificial Neural Networks*, pp. 999-1004, 1997.

[45] A. J. Smola, and B. Scholkopf, "A tutorial on support vector regression," *Stat. Comput.*, vol. 14, pp. 199-222, 2004.

[46] J. Lu, A. Zahedi, ―Modelling and control of PEMFC based on support vector machine," in *Proceedings of 2011 Australasian Universities Power Engineering Conference*, pp. 1-6, 2011.

[47] K. P. Bennett, O. L. Mangasarian, ―Robust linear programming discrimination of two linearly inseparable sets," *Optimization Methods and Software*, vol. 1, pp. 23–34, 1992.

[48] C. Cortes, V. Vapnik, ―Support vector networks," *Machine Learning*, vol. 20, pp. 273-297, 1995.

[49] R. Fletcher, *Practical Methods of Optimization,* John Wiley & Sons New York, 1989.

[50] W. Karush, "Minima of functions of several variables with inequalities as side constraints," Master's thesis, Dept. of Mathematics, Univ. of Chicago, 1939.

[51] H. W. Kuhn, A. W. Tucker, "Nonlinear programming," *in Proceedings of* 2*nd Berkeley Symposium on Mathematical Statistics and Probabilistics*, pp. 481-492, 1951.

[52] J. A. Adams, W-C.Yang, K. A. Oglesby, and K. D. Osborne, "The development of Ford's P2000 fuel cell vehicle," *in Proceedings of SAE 2000 World* Congress, paper no. 2000-01-1061.

[53] V. Cherkassky, Y.Q. Ma, "Practical selection of SVM parameters and noise estimation for SVM regression," *Neural Networks*, vol. 17, pp. 113-126, 2004.

[54] R. Debnath, H. Takahashi, "Kernel selection for the support vector machine," IEICE Trans. Inf. Syst., vol. E87-D, pp. 2903-2904, 2004.

[55] J. Lu, A. Zahedi, "Model predictive control for PEMFC based on least square support vector machine," *in Proceedings of 2012 Asia-Pacific Power and Energy Engineering Conference*, in press.

[56] M. Y. El-Sharkh, A. Rahman, M. S. Alam, P. C. Byrne, A. A. Sakla, T. Thomas, "A dynamic model for a stand-alone PEM fuel cell power plant for residential applications," *J. Power Sources*, vol. 138, pp. 199-204, 2004.

[57] J. C. Amphlett, R. M. Baumert, R. F. Mann, B. A. Peppley, P. R. Roberge, T. J. Harris, "Performance modelling of the Ballard-Mark-IV solid polymer electrolyte fuel cell. 2. Empirical model development," *J. Electrochem. Soc.*, vol. 142, pp. 9–15, 1995.

[58] M. V. Williams, H. R. Kunz, J. M. Fenton, "Analysis of Polarization Curves to Evaluate Polarization Sources in Hydrogen/Air PEM Fuel Cells," *J. Electrochem. Soc.*, vol. 152, pp. A635–A644, 2005.

[59] J. Lu, A. Zahedi, –Constrained model predictive control of PEMFC based on a combined empirical and mechanistic model," *J. Renewable Sustainable Energy*, vol. 4, paper no. 53116, pp. 1-15, 2012.

[60] F. Laurencelle, R.Chahine, J. Hamelin, K. Agbossou,M. Fournier, T. K. Bose, A. Laperriere, –Characterization of a Ballard MK5-E proton exchange membrane fuel cell stack," *Fuel Cells*, vol. 1, pp. 66-71, 2002.

Chapter 3 Control

The efficient and stable operation of PEMFC depends on the efficient control of the generated voltage/power in the presence of varying operating conditions and disturbances. However, PEMFC system‘s inherent nonlinearities, time-varying properties and tight operating constraints give rise to great challenges for system modelling and control [1]. The traditional modelling and control method is usually based on approximate linearization theory, which imposes serious restrictions on the structure of nonlinear systems [2]. Therefore, it is difficult to identify an accurate mathematical model of nonlinear systems, such as PEMFC. But when investigated in real time, time-dependent parameter can be more readily tracked and a model structure can be more accurately estimated [3]. Therefore, using this strategy, the controller can serve to achieve the control objectives. Model predictive control (MPC), characterized by its receding strategy, is such a methodology.

The major contributions of chapter 3 include: (1) The model predictive control (MPC) strategy is developed using MPC Toolbox of the MATLAB program. The core MPC Toolbox algorithm is based on a model of the system to be controlled, a performance index driving the selection of the decision variables. Based on the SVM models developed previously, the MPC controller performs quite well with respect to maintaining the performance outputs at the nominal value during the transient following abrupt changes in the disturbance input. (2) The novel MPC strategy is designed using the particle swarm optimization (PSO) algorithm. PSO is a population based stochastic optimization algorithm that has significant advantages, including, simple, fast and robust. Following the principle of MPC, the PSO is implemented in the MPC context for receding horizon optimization. The proposed MPC strategy shows satisfactory performance in both static and dynamic test. (3) The constrained MPC strategy

is designed and the standard PSO algorithm is modified to hand constraints. A key advantage of MPC over other control schemes is its ability of handling constraints in a systematic and straightforward manner. To prevent PEMFC from reactant starvation and excessive pressure difference across the membrane, dynamic constraints are designed and integrated with the MPC strategy. To handle the dynamic constrained optimization problem formulated by MPC, the standard PSO algorithm is modified by introducing the constraint checking procedure and improving the initialization process of each evolution. The constrained MPC stategy can successfully deal with the constraints and achieve good performance in tracking reference trajectory.

The chapter is organized as follows: In section 3.1, a literature review on PEMFC control strategy is conducted. In section 3.2, theory of MPC is introduced. In section 3.3, MPC strategy for PEMFC control is designed using the Model Predictive Control Toolbox of the MATLAB program. In section 3.4, theory of particle swarm optimization (PSO) is introduced and the new MPC strategy is designed based on the PSO optimizer. It section 3.5, the constrained MPC strategy is designed based on the combine model developed in the previous chapter, and the standard PSO algorithm is modified to hand the constraints .

3.1 Literature review of PEMFC control methods

Generally, the control strategies of PEMFC concern: (a) the power output in the presence of sudden variations in the uncontrollable load; (b) maximum power and efficiency of the system; (c) heat and water management; (d) fuel and air supply. There have been many studies focused on the controller design for PEMFC. This section presents a review of some representative examples, including proportional-integral-derivative (PID), model predictive

control (MPC), fuzzy control and etc. A summary of the controllers reviewed is given in Table 3.1.

- **PID**

Serra et al. [4] developed a nonlinear model and linearized it at several operating points to use the resulting linear models for control studies. The purposes of the control strategy were to regulate the output voltage and to maintain the pressure difference between the anode and cathode close to zero to prevent membrane damage. Four different control structures were considered, and PI controllers were implemented.

Zenith and Skogestad [5] presented a method to control the output voltage of a buck-boost converter connected to PEMFC. Their strategy was to have the fuel cell connected to the external circuit only part of the time, by setting a switch to ON and OFF in the converter. The results showed fast response of the system, with transients settling after about 5 milliseconds.

El-Sharkh et al. [6] studied active and reactive power control of a stand-alone PEMFC. A PI controller was implemented to control the stack current by manipulating the inlet flow rates of methane and hydrogen. A feedforward controller was used to regulate the inlet oxygen flow rate to maintain hydrogen-oxygen flow ratio at a desired level. The output voltage of an inverter (overall system power output) was controlled using a PI controller that adjusted the inverter modulation index. The results showed the fast response of the fuel cell power plant to load changes and the effectiveness of the proposed method for active and reactive power output control.

Methekar et al. [7] proposed a multi-input multi-output (MIMO) control strategy for PEMFC. The objective was to control the power density and average solid temperature. Transfer function models obtained from step tests on the distributed parameter PEMFC model were used to design controllers. Manipulated variables were selected and paired with the controlled variables using the relative gain array (RGA) analysis; the inlet molar flow rate of hydrogen was paired with the power density, and the inlet molar coolant flow rate with the average solid temperature. The power density was controlled using a PI controller that manipulated the hydrogen inlet flow rate. A linear ratio control strategy was proposed, where the inlet molar flow rate of oxygen was used as a dependent manipulated variable and changed in a constant ratio with respect to the hydrogen inlet molar flow rate. The average solid temperature was controlled using a cascade control system. The integral (slave) controller regulated the average coolant temperature by manipulating the inlet coolant flow rate. The PI (master) controller regulated the average solid temperature by manipulating the average coolant temperature set-point. The results showed that the inclusion of the ratio controller could improve the performance.

Woo and Benziger [8] proposed a PID controller to regulate output power of PEMFC by limiting the hydrogen feed rate, which was achieved by varying the internal resistance of the membrane electrode assembly in a self-draining fuel cell with the effluents connected to water reservoirs. The hydrogen feed rate affected the water level in the fuel cell, which in turn changed the internal resistance and the current of the fuel cell. The results showed that the current responded rapidly to load changes. It was recommended that this type of regulation could be applied to small fuel cell systems where recycling unreacted hydrogen may be impractical.

Lauzze and Chmielewski [9] developed a feedback control structure for the power control of PEMFC. A cascade control structure with two loops was proposed. In the inner loop, a PI (slave) controller was used to control the current density by manipulating the cell outlet voltage. In the outer loop, a PI (master) controller regulated the cell power density by manipulating the current density setpoint. The results showed oscillatory behaviour, as well as slow response speed of the output power. It was concluded that the use of a multivariable nonlinear control system was necessary to obtain better closed-loop responses.

Zenith and Skogestad [10] developed three dynamic lumped-parameter equations describing hydrogen pressure in the anode, oxygen fraction in the cathode, and stack temperature of a high-temperature PEMFC. For each model, a controller was developed. Hydrogen pressure in the anode was controlled by a PI feedback controller with a feedforward component. The controller used hydrogen pressure and cell current as measurements and manipulated the hydrogen inlet flow rate. Oxygen fraction in the cathode was controlled by a feedforward controller. The controller measured cell current and manipulated the air inlet flow rate. Temperature was controlled by a proportional (P) feedback controller with a feedforward component. The P controller used the cell current and outlet voltage as measurements and manipulated the air inlet flow rate. The actual inlet air flow rate was selected to be the maximum of the two flow rates calculated by the oxygen and temperature controllers.

Purkrushpan et al. [11] explored the use of model-based control strategies for the air supply control problem in PEMFC. In their research, the stack current was considered as disturbance input, which corresponded to uncontrollable load. The manipulated input was the compressor motor voltage. The performance (controlled) variables were the net power output and the

excess oxygen ratio, which was indicative of oxygen starvation. Three different control configurations were designed and evaluated. The first configuration was a static feedforward controller that calculated the compressor voltage corresponding to the air flow rate needed to replenish the oxygen depleted during a current command. The second configuration was a dynamic feedforward controller combined with a dynamic feedback (PI) controller to improve the robustness of the control system. The third configuration was a high-order (observer-based integral-augmented) feedback controller combined with a static feedforward controller. The results showed that the oxygen level in the cathode can be successfully maintained. However, the net power provided by the fuel cell system is compromised during the transients following abrupt changes in the stack current, suggesting a need for power management via the use of a secondary power source such as a battery.

- **MPC**

Golbert and Lewin [12] proposed a nonlinear model predictive controller based on a reduced-order model of PEMFC. Two control methods, adaptive control and nonlinear model predictive control, were proposed by the authors. The adaptive control was realized using a standard PI controller with an adaptive gain inversely proportional to the variable process steady-state gain. The results showed the performance obtained with the adaptive controller was better than that obtained with a conventional PI controller (which had a fixed gain). It was further found that the ability of nonlinear model predictive control to track power demands was better than that of the adaptive controller. In their later study [13], model predictive control was implemented to track the power demand fluctuations, while at the same time, minimizing fuel consumption to achieve the maximum efficiency. The manipulated variables were dry hydrogen flow rate, the coolant temperature, and the average current density. The

results showed the controller satisfied power demands while providing optimal fuel efficiency.

Arce et al. [14] proposed a predictive controller for power management in a hybrid PEMFC vehicle. The objective of the controller was to track power demand and to keep batteries close to a desired battery state of charge which was appropriately chosen to minimize hydrogen consumption. The controller variables included fuel cell on and off modes, battery charge and discharging states, fuel cell power demand and battery power demand. The simulation results demonstrated the effectiveness of the proposed controller.

Vahidi et al. [15] proposed a hybrid configuration, in which ultracapacitors supplemented the slow dynamics of PEMFC during fast current transients. A model predictive controller was designed for optimal distribution of current demand between the two power sources. The controller regulated oxygen level (oxygen excess ratio) and the ultracapacitor‘s state of charge by manipulating the compressor motor voltage and the current split proportion. The total current demand was considered as a measured disturbance. Simulation results demonstrated the good performance of the controller in splitting the demand between the fuel cell and the ultracapacitor; the controller achieved smooth transitions from the ultacapacitor to the fuel cell and vice versa, in the presence of unmeasured external loads.

Bordons et al. [16] presented three generalized predictive control (GPC) strategies to achieve three different operational objectives for PEMFC: starvation prevention, maximum efficiency, and voltage control. The structures of the three control strategies were the same, while the difference existed for the measurements and control outputs used by each controller. For both starvation prevention and maximum efficiency, their proposed GPC strategies used

the oxygen excess ratio and the current as measurements to regulate the controlled output (oxygen excess ratio). The only difference between the two strategies lied in the set point of the controlled output. To prevent the starvation, the oxygen excess ratio set point was a constant value of 2. To maximize the efficiency, however, it was not constant and was set by a reference generator, which at every sampling instant calculated the excess ratio set point on the basis of the current demand. Their GPC control strategy proposed for tracking the desired output voltage, used measurements of the cell output voltage and the current to regulate the output voltage. Closed-loop responses of the three GPC strategies were studied. Power delivered by the cell under the three control strategies was almost identical with the best performance, as it was expected, obtained by the strategy for maximum efficiency. The oxygen excess ratio responses showed that the first and second control strategies provided safe conditions for starvation prevention, while under the third control strategy (output voltage control) dangerous conditions occurred. In summary, each of the predictive control strategies achieved the control objective that it was supposed to accomplish.

- **Fuzzy control**

Fuzzy control of PEMFC has received much attention in the past years. Wu and Pai [17] developed a fuzzy PID controller to regulate the stack temperature by manipulating water flow rate. Results demonstrated that the proposed controller can effectively reduce the temperature variation of a reforming integrated fuel cell unit. Zhijun et al. [18] used a fuzzy control method to regulate the output voltage by manipulating the anode gas pressure. Results showed that the controller could achieve good performance at different levels of the external load.

- **Others**

Kolavennu et al. [19] developed a model reference adaptive controller using the Lyapunov method for tracking a time varying power profile in an automobile powered by PEMFC. The power required by automobile was calculated based roads with varying slopes. The calculated power was used as the controller set-point. The results showed that the adaptive controller had superior performance than that of a conventional PID controller.

Danzer et al. [20] proposed a model-based control structure that comprised a multivariable control of the cathode pressure and the oxygen excess ratio for PEMFC. Since the partial pressure of oxygen in the cathode flow field was a state variable that is hardly accessible by measurement, a tracking observer was employed to estimate this pressure using the measured air pressure at the outlet throttle. The controller used the throttle and the oxygen mass flow resistance as manipulated variables to regulate the oxygen excess ratio and cathode pressure. The effectiveness of the proposed control strategy was demonstrated by a comparison with a commonly used combination of feedforward control of the mass flow and PI control of the outlet pressure. The results showed that the proposed strategy had superior performance.

Table 3.1 Summary of PEMFC controllers in the literature

Controller	Control objectives	Manipulate inputs	Performance output	Disturbance	Model	Ref
PI	to regulate output stack voltage and to maintain the pressure difference between the anode and the cathode to 0	air compressor motor voltage and inlet flow rate of hydrogen/oxygen molar fraction and the inlet flow rate of hydrogen	output stack voltage-pressure difference	current	0D	4
PI	to control the converter output voltage	converter switch	output voltage	current	0D	5
PI	active and reactive power	methane flow rate/modulation index	current/output voltage of inverter	load	0D	6
PI	to satisfy high power density demand and control average solid temperature	hydrogen and coolant inlet flow rate	power density and temperature	load	1D	7
PID	to regulate current	hydrogen feed rate	current	load resistance	0D	8
cascade-PI	power control/temperature control/ humidity control/oxygen starvation prevention	cell outlet voltage, coolant flow rate, cathode temperature set point, cathode air flow rate	current density; temperature; relative humidity of the air inside the cell; oxygen mole fraction	load	0D	9
PI feedback /FF/P-FF	hydrogen pressure control/ air-composition control/ stack temperature	hydrogen inlet flow rate, air inflow, air inlet flow rate	hydrogen pressure; oxygen concentration; temperature	load	0D	10
FF-PI feedback	to prevent oxygen starvation	compressor motor voltage	oxygen excess ratio	current	0D	11
MPC/PI adaptive	to ensure acceptable response time for the power demand, while achieving high efficiencies over the operating range	current density and coolant inlet temperature	power density	load	0D	12
MPC	to regulate the power output of the fuel cell and to maximize efficiency	current density, fuel flow rate and coolant channels temperature	power density	load	0D	13
MPC	to improve battery performance and to avoid fuel cell and battery degradation	DC-DC converter gain, oxygen and hydrogen flow rates	motor power demand	road slope	0D	14
MPC	to prevent oxygen starvation	air compressor voltage and current split proportion	oxygen excess ratio and the ultra capacitor state of charge	load	0D	15
GPC	to prevent oxygen starvation	air compressor voltage	oxygen excess ratio	current	0D	16
fuzzy PID	to control the stack temperature	water flow rate	stack temperature	current		17
fuzzy	to regulate the output voltage	anode gas pressure	voltage	load		18
MRAC	to track a time-varying power profile	current	output power	road slope	0D	19
model-based multivariable	to prevent oxygen starvation	mass flow of oxygen and throttle resistance	oxygen excess ratio and cathode pressure	current	0D	20

3.2 Theory of model predictive control

In many control problems it is desired to design a stabilizing feedback such that a performance criterion is minimized while satisfying constraints on the controls and the states. Ideally one would look for a closed solution for the feedback satisfying the constraints while minimizing the performance. However, often the closed solution cannot be found analytically, even in the unconstrained case since it involves the solution of the corresponding Hamilton Jacobi- Bellmann equations. One approach to circumvent this problem is the repeated solution of an open-loop optimal control problem for a given state. The first part of the resulting open-loop input signal is implemented and the whole process is repeated. Control approaches using this strategy are referred to as model predictive control (MPC), moving horizon control or receding horizon control [21].

The thought of ideas for MPC can be traced back to the 1960s. Propoi had suggested the core of all MPC algorithms, the moving horizon approach in 1963 [22]. The current industrial and academic interest in MPC was started to surge after the first successfully implementation of MPC reported by Richalet et al. in 1978 [23]. Over the past decades, a wide variety of MPC algorithms have been developed, such as the Dynamic Matrix Control (DMC) by Cutler and Ramaker [24], the Generalized Predictive Control (GPC) by Clarke et al. [25] and Internal Model Control (IMC) reported by Garcia and Morari [26]. The main differences for all these MPC algorithms lie in types of models employed and the cost functions to be minimized. After 30 years since the first implementation of MPC in industry had been reported, the MPC has now become a standard advanced control technique in many process industries. The application area for MPC now covers not only the

petrochemicals and refining fields but also in food processing, automotive, metallurgy, pulp and paper, aerospace and defense industries [27].

MPC is now considered to be a mature technique for linear and rather slow systems. In these cases, MPC employs linear models to predict the system dynamics and considers linear constraints on the states and inputs. There are two major reasons for the use of linear models: (1) the identification of a linear model is easy; (2) linear models provide good results when the system is operating in the neighborhood of the operation point. Besides, the use of a linear model together with a quadratic objective function gives rise to a convex problem whose solution is well studied with many commercial products available.

On the other hand, nonlinear systems were considered beyond the realm of MPC. However, in many situations the operation of the system requires frequent changes from one operation point to another within large operation regimes and, therefore, a nonlinear model must be employed. In addition, from a theoretical point of view, the use of a nonlinear model changes the control problem from a convex QP to a non-convex Non-Linear Program, the solution of which is much more difficult. There is no guarantee, for example, that the global optimum can be found. To summarize, the barriers for nonlinear MPC are: (1) the difficulty of developing an accurate nonlinear model; (2) the computational problem associated with the Non-Linear Program.

During the last few years some impressive results have been produced in these fields. Applications of nonlinear MPC have also appeared in the literature. The majority of applications are in the area of refining, one of the original application fields of MPC, where it has a solid background. Other important applications can be found in petrochemicals and

chemicals. Although the number of applications is still limited, nonlinear MPC has shown great potential for high performance control.

For clarity and completeness, a brief introduction to MPC is provided in the following section. But readers interested in the complete details should refer to an excellent review by Allgöwer et al. [21].

3.2.1 Principle

Model predictive control is formulated as the repeated solution of a (finite) horizon open-loop optimal control problem subject to system dynamics and input and state constraints. The principle of model predictive control is illustrated in Figure 3.1. Based on measurements obtained at time t, the controller predicts the dynamic behaviour of the system over a prediction horizon T_p in the future and determines (over a control horizon $T_c \leq T_p$) the input such that a predetermined open-loop performance objective is minimized. If there were no disturbances and no model-plant mismatch, and if the optimization problem could be solved over an infinite horizon, then the input signal found at $t = 0$ could be applied open loop to the system for all $t \geq 0$. However, due to disturbances and model-plant mismatch the actual system behaviour is different from the predicted one. To incorporate feedback, the optimal open-loop input is implemented only until the next sampling instant. The sampling time between the new optimization can vary in principle. Typically, it is, however, fixed, *i.e.*, the optimal control problem is re-evaluated after the sampling time, δ. Using the new system state at time $t + \delta$, the whole procedure—prediction and optimization—is repeated, moving the control and prediction horizon forward.

Summarizing, a standard MPC scheme works as follows:

(1) Obtain estimates of the states of the system.

(2) Calculate an optimal input minimizing the desired cost function over the prediction horizon using the system model for prediction.

(3) Implement the first part of the optimal input until the next sampling instant.

(4) Continue with (2).

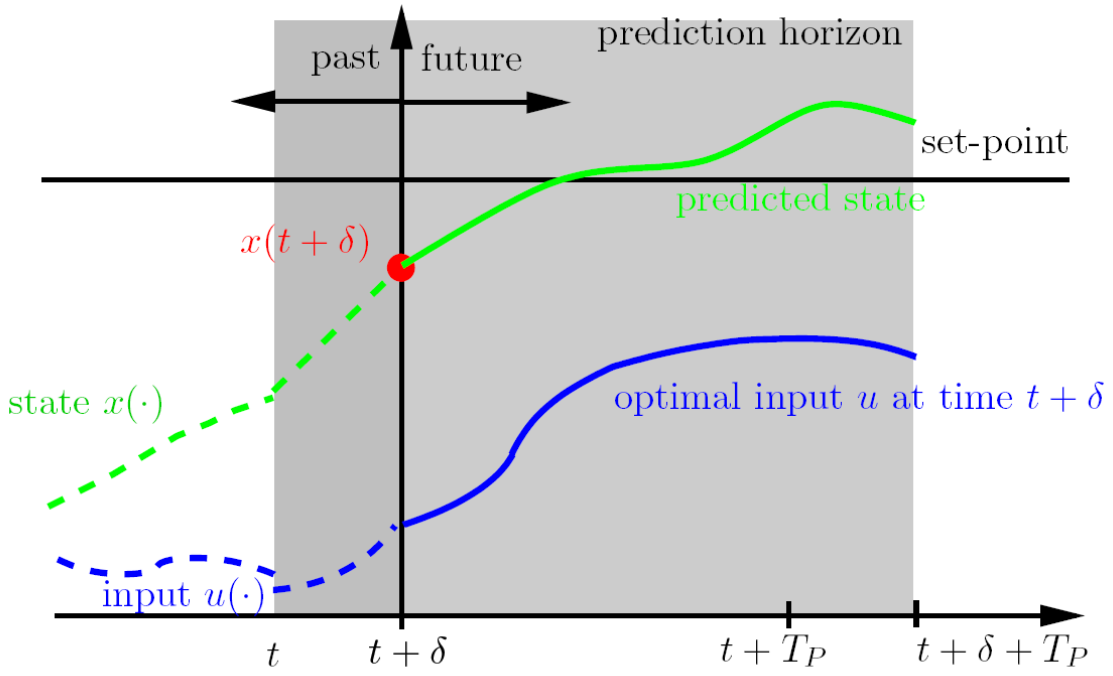

Figure 3.1 Principle of model predictive control [21]

3.2.2 Mathematical formulation

Consider a system described by the following nonlinear differential equation

$$\dot{x}(t) = f(x(t), u(t)), \quad x(0) = x_0, \tag{3.1}$$

subjects to input and state constraints of the form:

$$u(t) \in U, \quad \forall t \geq 0, \tag{3.2}$$

$$x(t) \in X, \quad \forall t \geq 0, \tag{3.3}$$

Here $x(t) \in \mathbf{R}^n$ and $u(t) \in \mathbf{R}^m$ denote the vector of states and inputs, respectively. Furthermore, the input constraint set U is assumed to be compact and X is connected. For example U and X are often given by box constraints of the form:

$$U := \{u \in R^m \mid u_{\min} \leq u \leq u_{\max}\}, \tag{3.4}$$

$$X := \{x \in R^n \mid x_{\min} \leq x \leq x_{\max}\}, \tag{3.5}$$

with the constant vectors $u_{\min}$, $u_{\max}$ and $x_{\min}$, $x_{\max}$.

In MPC the input applied to the system is determined by the solution of the following finite horizon open-loop optimal control problem, which is solved at every sampling instant:

Find $\min_{\bar{u}(\square)} J(x(t), \bar{u}(\cdot))$

subject to: $\dot{\bar{x}}(\tau) = f(\bar{x}(\tau), \bar{u}(\tau)), \quad \bar{x}(t) = x(t),$ (3.6)

$$\bar{u}(\tau) \in U, \quad \forall \tau \in [t, t+T_c], \tag{3.7}$$

$$\bar{u}(\tau) \in \bar{u}(t+T_c), \quad \forall \tau \in [t+T_c, t+T_p], \tag{3.8}$$

$$\bar{x}(\tau) \in X, \quad \forall \tau \in [t, t+T_p], \tag{3.9}$$

with cost function: $J(x(t)\bar{u}(\cdot)) := \int_t^{t+T_p} F(\bar{x}(\tau), \bar{u}(\tau))d\tau$

Here T_p and T_c are the prediction and the control horizon with $T_c \leqslant T_p$. The bar denotes internal controller variables and $\bar{x}(\cdot)$ is the solution of (3.6) driven by the input signal $\bar{u}(\cdot) : [t, t + T_p] \rightarrow U$ under the initial condition $x(t)$. The distinction between the real system variables and the variables in the controller is necessary, since even in the nominal case the predicted values will not be the same as the actual closed-loop values. The difference in the

predicted and the real values is due to determination of the applied input via a re-optimization (over a moving finite horizon T_c) at every sampling instant.

The cost functional J is defined in terms of the stage cost F, which specifies the performance. Often, a quadratic form for F is used:

$$F(x,u) = (x - x_s)^T \mathrm{Q}(x - x_s) + (u - u_s)^T \mathrm{R}(u - u_s) \tag{3.10}$$

Here x_s and u_s denote a desired reference trajectory, that can be constant or time-varying. The deviation from the desired values is weighted by the positive definite matrices Q and R. In the case of a stabilization problem (no tracking), i.e., $x_s = u_s$ = constant.

The state measurement enters the system via the initial condition in (3.6) at the sampling instants, *i.e.*, the system model used to predict the future system behavior is initialized by the actual system state. Since all state information is required for the prediction, the full state must be either measured or estimated. (3.8) fixes the input beyond the control horizon to $u(t + T_c)$.

3.3 Model predictive controller design

The objective of the proposed MPC strategy is to ensure that the performance outputs of PEMFC maintain the set point when sudden change in the load demand occurs. For the sake of comparison, the PEMFC system used in this section is the same one studied by Pukrsphan, which is reviewed in Chapter 2. The performance outputs of the PEMFC are the stack voltage and the oxygen excess ratio. The manipulated input is the compressor motor voltage. The disturbance input is the stack current, which corresponds to the uncontrollable load demand. Figure 3.2 shows the schematic of the whole control system.

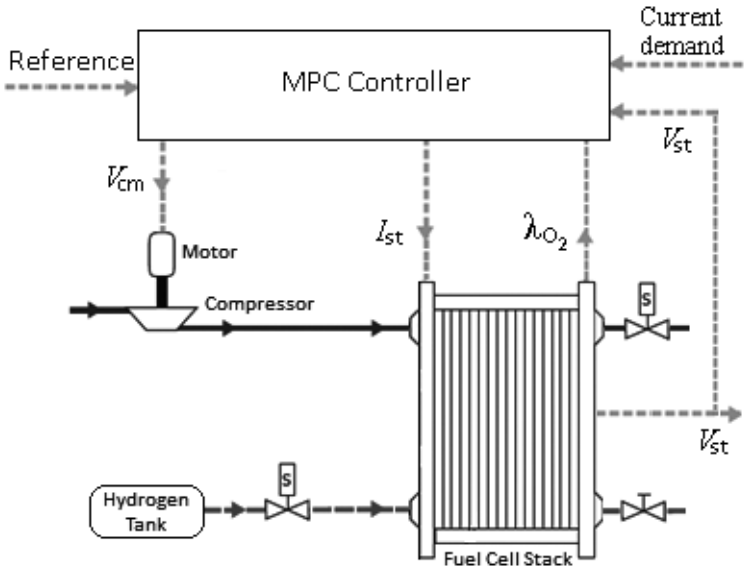

Figure 3.2 Schematic of the PEMFC system and the controller [28]

Based on the SVM models developed in Chapter 2, the model predictive controller is designed using the Model Predictive Control Toolbox of the MATLAB program [29]. The Model Predictive Control Toolbox is a powerful tool for the design, analysis, and implementation of the model predictive control algorithm. It provides a convenient graphical user interface (GUI) for the model predictive controller design. The core MPC Toolbox algorithm is based on a model of the system to be controlled, a performance index driving the selection of the decision variables.

The schematic of the proposed model predictive controller and the SVM models implemented in the MATLAB/SIMULINK environment is shown in Figure 3.3. When there is an MPC block, the natural choice is to associate the manipulated input, i.e. the compressor motor voltage, with the MPC block output port (―mv" port) and PEMFC outputs, i.e. the stack voltage and the oxygen excess ratio, with the MPC block's input port (―mo" port). The stack current is considered as disturbance input, which is connected to the MPC block's

–measured disturbance (md)" port. The desired outputs are two constants, which are set as references and associated with the MPC block's –ref" port.

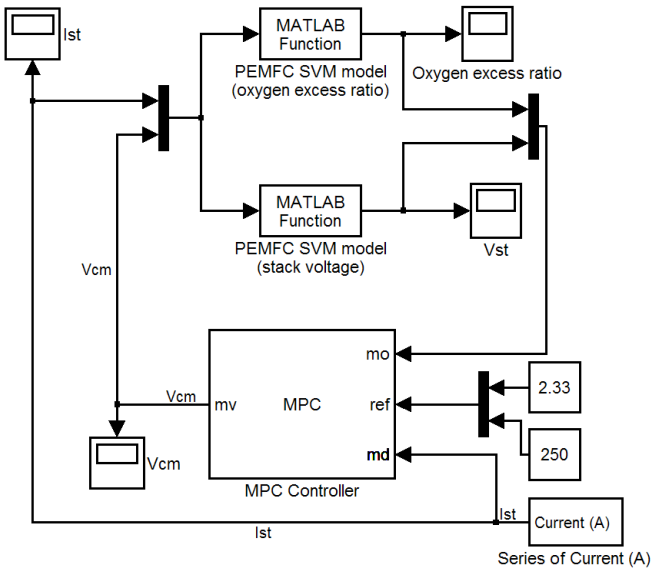

Figure 3.3 PEMFC control system implemented in SIMULINK (reproduced from [30])

The model predictive controller comprises an internal model for the prediction of system behaviour and computation of the control movements. The MPC toolbox requires the model used in controller design to be affine, i.e., a linear, time-invariant (LTI) system describing deviations from a nominal condition. One can define such a model by creating a state space model or linearizing a SIMULINK model. In this study, a state space model is created by using linearized system matrices, as provided in [31].

Once the internal plant model has been defined, the remaining design decisions comprise [30]:

(1) Specifying signal properties and assigning their nominal values. In this study, the manipulated variable is the compressor voltage V_{cm}, the measured disturbance is the stack

current I_{st}, the outputs are the stack voltage V_{st} and the oxygen excess ratio λ_{O2}. The nominal value for V_{st} and λ_{O2} are 250 and 2.33.

(2) Specifying controller properties. The selection of prediction horizon P and control horizon M is a tuning process. The designers usually choose P and M such that controller performance is insensitive to small adjustments in these horizons [29]. Here, the prediction horizon and the control horizon are both set to 3 samples. The control interval is set as 0.1 time unit.

(3) Specifying constraints. The oxygen excess ratio and the compressor motor voltage have lower bound, 1 and 0, respectively.

(4) Weight tuning. The weights specify the trade-off between robustness and response speed. The weight for output is set to 1.0, and the weight for manipulated variable is set to 0.1.

For the purpose of comparison, the objective of the proposed model predictive controller is the same one adopted in [31], that is to maintain the oxygen excess ratio $\lambda_{O2} = 2.33$ and the stack voltage $V_{st} = 250$ during the transient following abrupt changes in I_{st}. Besides, the time evolution of the stack current that acts as an input disturbance to the system is shown in Figure 3.4(a). Once again, the time evolution of the stack current is set as the same one adopted in [31]. The corresponding variation in the compressor motor voltage, the manipulated input, is shown in Figure 3.4(b). The time evolution of the performance outputs, the oxygen excess ratio and the stack voltage are shown in Figure 3.4(c) and Figure 3.4(d), respectively.

The results displayed in Figure 3.4(c) and Figure 3.4(d) show that the proposed controller performs quite well with respect to maintaining the performance outputs at the nominal value consistent with a given input level of the stack current. Besides, no overshoot is observed in Figure 3.4(c) and Figure 3.4(d). This is favorable as no redundant power is used to produce the unnecessary overshoot. However, the proposed controller suffers from some deficiencies. Its response speed is relatively slow, which leads to long settling times as shown in Figure 3.4(c) and Figure 3.4(d).

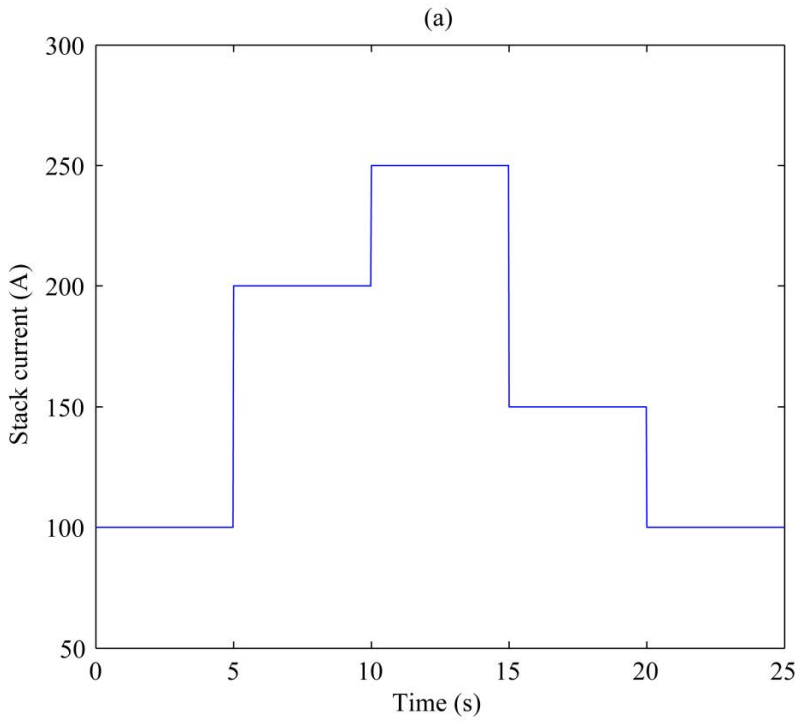

Figure 3.4 Performance of the MPC: (a) Stack current

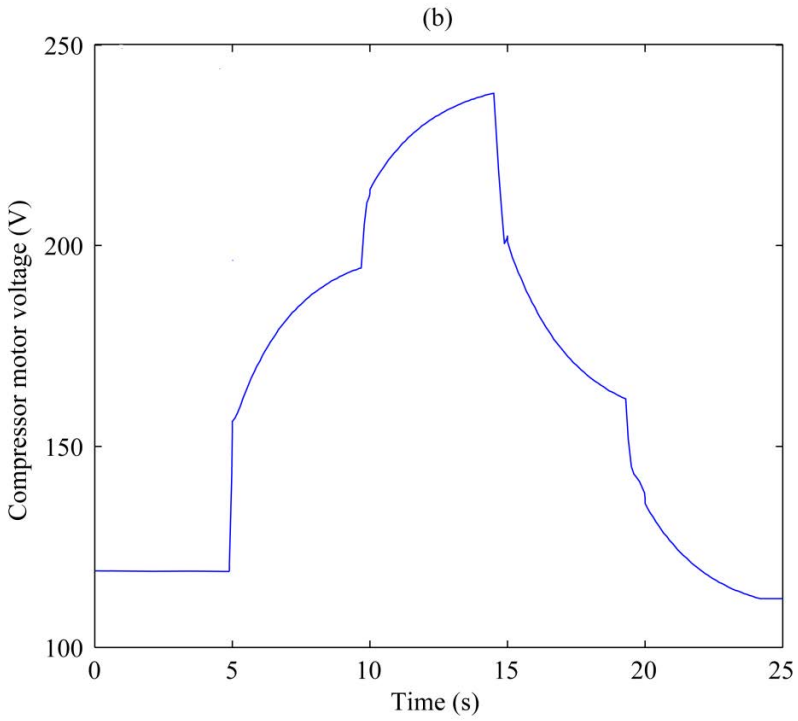

Figure 3.4 Performance of the MPC: (b) Compressor motor voltage

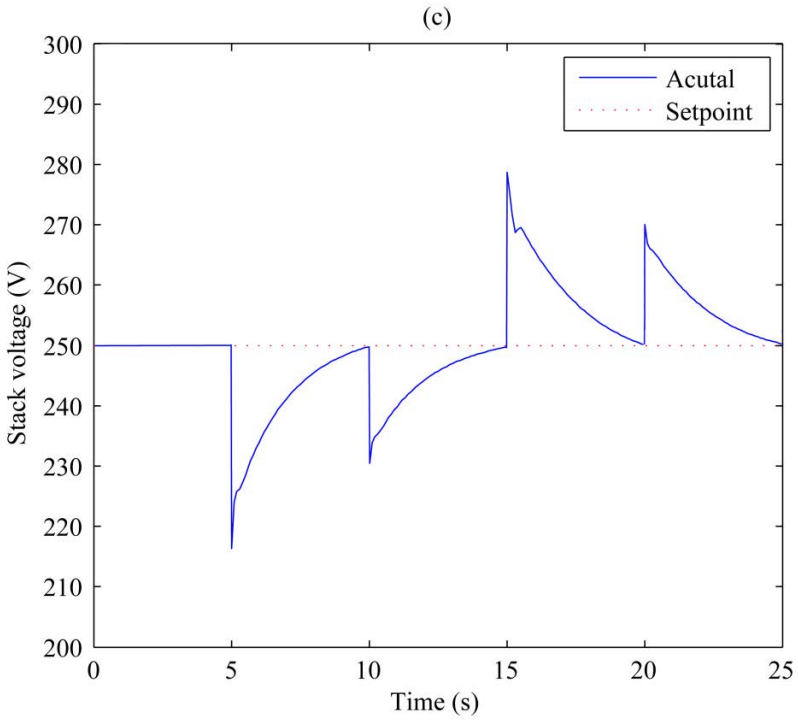

Figure 3.4 Performance of the MPC: (c) Stack voltage

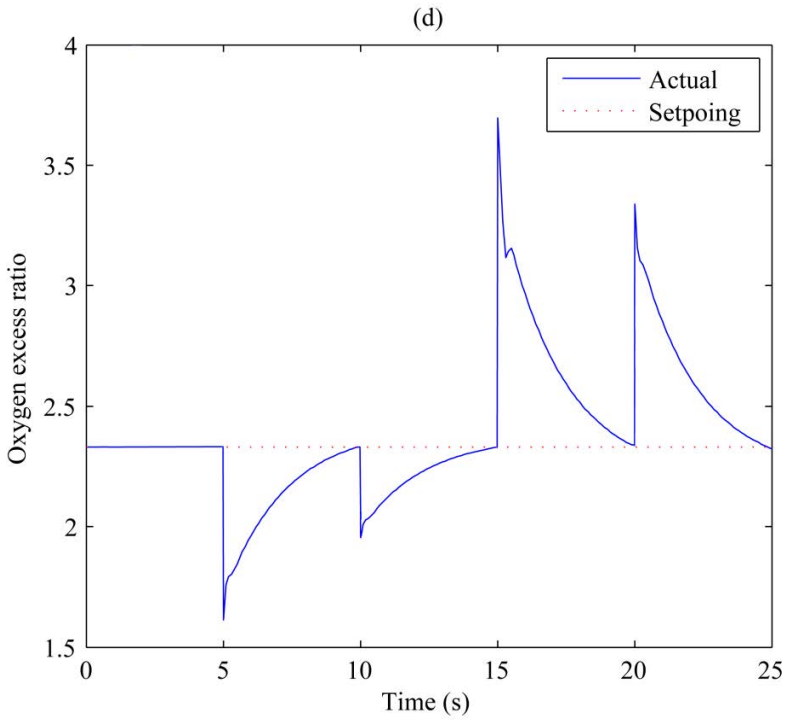

Figure 3.4 Performance of the MPC: (d) Oxygen excess ratio

3.4 MPC strategy integrated with particle swarm optimization

3.4.1 Theory of particle swarm optimization

Particle swarm optimization (PSO) is a population based stochastic optimization method first introduced by Kennedy and Eberhart in 1995 [32]. Since then, PSO has become one of the most promising global optimizing techniques. Its mechanism is inspired by the social behaviour displayed by various species like bird flocking or fish schooling. The PSO system consists of a population (swarm) of potential solutions called particles. These particles move through the search domain with a specified velocity in search of optimal solution. Each particle updates its velocity according to its previous best position. The best positions are distinguished as personal best and global best.

It has been demonstrated that PSO achieves better results in comparison to other evolutionary algorithms, such as genetic algorithm (GA). The difference between PSO and GA lies in how to change the population/swarm from one iteration to the next. In GA, genetic operators like selection, mutation and crossover are used whereas in PSO, the particles are modified according to two formulas after each iteration. Conceptually, in PSO, the particles stay alive and inhibit the search space during the whole run, whereas in GA, the individuals are replaced in each generation. PSO is a more robust and fast algorithm compared to GA and it can solve nonlinear, non-differentiable, and multi-modal problems, generating a high-quality solution within shorter calculation time and more stable convergence characteristic.

For clarity and completeness, a brief introduction to PSO is provided in the following section. But readers interested in the complete details should refer to reference [33].

A fixed number of solutions (called particles in a PSO context) are randomly initialized in a d-dimensional solution space. A particle *i* at time step *t* has a position vector:

$$X_i^t = (x_{i1}^t, x_{i2}^t, ..., x_{id}^t)$$

and a velocity vector:

$$V_i^t = (v_{i1}^t, v_{i2}^t, ..., v_{id}^t)$$

The maximum velocity is represented as:

$$V_{i\max}^t = (v_{i\max 1}^t, v_{i\max 2}^t, ..., v_{i\max d}^t)$$

The velocity V_i^t of each particle is clamped to a maximum velocity $V_{imax}{}^t$ which is specified by the user. $V_{imax}{}^t$ determines the resolution with which regions between the present position

and the target position are searched. Large values of $V_{imax}{}^{t}$ facilitate global exploration, while smaller values encourage local exploitation. If $V_{imax}{}^{t}$ is too small, the swarm may not explore sufficiently beyond locally good regions. On the other hand, too large values of $V_{imax}{}^{t}$ risk the possibility of missing a good region [34].

The best previous position (the position giving the best fitness value) of the *i*th particle is recorded and represented as:

$$p_i = (p_{i1}, p_{i2}, ..., p_{id})$$

The best particle among all the particles in the population is represented as:

$$p_g = (p_{g1}, p_{g2}, ..., p_{gd})$$

The PSO algorithm iterates updating the velocities and positions of the particles until a stopping criterion is met (usually a number of times or until a minimum error is achieved). The update rules are:

$$v_{id}^{t+1} = wv_{id}^{t} + c_1 r_1 (p_{id}^{t} - x_{id}^{t}) + c_2 r_2 (p_{gd}^{t} - x_{id}^{t}) \tag{3.11}$$

$$x_{id}^{t+1} = x_{id}^{t} + v_{id}^{t+1} \tag{3.12}$$

where w is inertia weight. r_1 and r_2 are two random numbers between (0,1). c_1 and c_2 are two constants called cognitive and social acceleration coefficients respectively.

The velocity update of a PSO particle given in (3.11) consists of three parts, as shown in Figure 3.5. The first part represents particle‘s previous velocity, which serves as a memory of the previous flight direction. This memory term can be visualized as a momentum, which prevents the particle from drastically changing its direction and biases it towards the current direction. The second part is called the cognition part and it indicates the personal

experience of the particle. This cognition part resembles individual memory of the position that was best for the particle. The effect of this term is that particles are drawn back to their own best positions, resembling the tendency of individuals to return to situations or places that were most satisfying in the past. The third part represents the cooperation among particles and is therefore named as the social component [35]. This term resembles a group norm or standard which individuals seek to attain. The effect of this term is that each particle is also drawn towards the best position found by its neighbor. The balance among these three parts determines the balance of the global and local search ability and therefore the performance of a PSO [36].

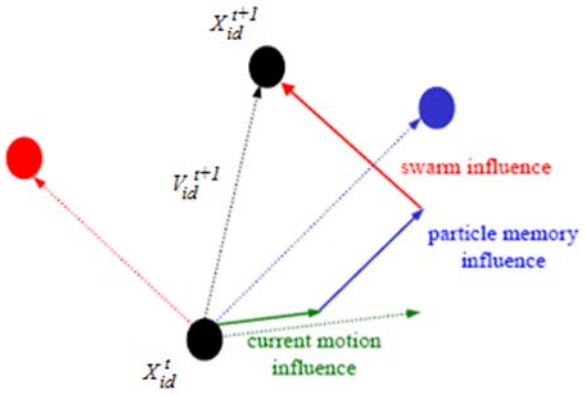

Figure 3.5 Schematic of velocity updating in PSO

The inertia weight *w* is employed to control the impact of the previous history of velocities on the current velocity, thereby influencing the trade-off between global and local exploration abilities of the particles. It can be a positive constant or even a positive linear or nonlinear function of time. A larger inertia weight encourages global exploration while a smaller inertia weight tends to facilitate local exploration to fine-tune the current search area. Suitable selection of the inertia weight provides a balance between global and local

exploration abilities and thus requires less iteration on an average to find the optimum [37]. Generally, for initial stages of the search process, large inertia weight to enhance the global exploration (searching new area) is recommended while, for last stages, the inertia weight is reduced for local exploration (fine tuning the current search area). Time-varying inertia weight was introduced in [38].

c_1 and c_2 represent the weighting of the stochastic acceleration terms that pull each particle towards personal best and global best positions. Therefore, adjustment of these constants changes the amount of tension in the system. Small values of these constants allow particles to roam far from the target regions before tugged back, while high values result in abrupt movement toward, or past, target regions [39]. The constants r_1, r_2 are the uniformly generated random numbers in the range of [0, 1].

Implementing PSO algorithm by mathematical programming is a highly skilful job. Fortunately, some software packages have already been developed. This study employs a MATLAB PSO toolbox developed by Birge [40].

3.4.2 Particle swarm optimization in the MPC context

The objective of the new MPC strategy is to regulate the output voltage of PEMFC to the reference trajectory by manipulating the stack current and the compressor motor voltage. The MPC strategy employs the SVM models developed in Chapter 2 as the predictive model. PSO is applied to solve the optimization problem formulated by MPC. The schematic of proposed MPC algorithm is shown in Figure 3.6.

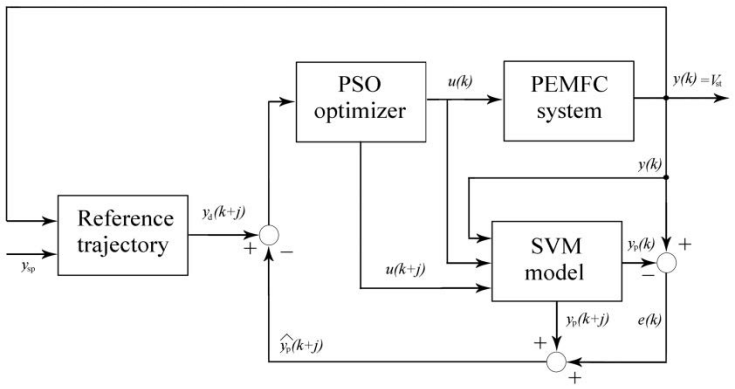

Figure 3.6 Schematic of the proposed MPC integrated with PSO [41]

The predictive output voltage for *p* steps ahead is obtained by the SVM model:

$$y_{\mathrm{p}}(k+j)=\sum_{i=1}^{l}(\alpha_i-\alpha_i^*)K(\mathbf{U}(i),\mathbf{U}(k+j))+b \qquad 1\le j\le p \tag{3.13}$$

Due to model-plant mismatch and external disturbance, there exist difference between the predictive output and the actual output, which is called predictive error. Assuming the actual output voltage at *k* instance is $y(k)$, the predictive error at *k* instance is:

$$\mathrm{e}(k)=y(k)-y_{\mathrm{p}}(k) \tag{3.14}$$

The predictive output voltage of feedback system for *p* steps can be defined as:

$$\hat{y}(k+j)=y_{\mathrm{p}}(k+j)+\mathrm{e}(k) \tag{3.15}$$

Reference trajectory of output voltage is introduced to avoid excessive movement of control input, which is defined as:

$$y_{\mathrm{d}}(k+j)=\mathrm{c}^j y(k)+(1-\mathrm{c}^j)y_{\mathrm{sp}}, \qquad 1\le j\le p,\ 0\le \mathrm{c}\le 1 \tag{3.16}$$

where y_{sp} is the set point of output voltage. *c* is an adjustable parameter, called softness coefficient.

The optimization problem for the model predictive controller is the minimization of the sum of squared errors between the referenced trajectory and the predictive output, with an additional penalty imposed on excessive changes in the manipulated variables:

$$J(k)=\sum_{j=1}^{p} q_j\left[\hat{y}(k+j)-y_{\mathrm{d}}(k+j)\right]^2+\sum_{i=1}^{l} r_i\left[u(k+i)-u(k+i-1)\right]^2 \quad 1\le j\le p, 1\le i\le l, q_j\ge 0, r_i\ge 0 \tag{3.17}$$

where $\hat{y}_{\mathrm{p}}(k+j)$ is the predicted output voltage of PEMFC, p is predictive horizon, $u(k+i)$ is the manipulated variable at time $k+i$, l is control horizon, and q_j and r_i are weight factor.

Then PSO algorithm is employed to solve the optimization problem. Define the position vector of a particle as follows:

$$X_i^t=[u(k),u(k+1),\ldots,u(k+P-1)] \tag{3.18}$$

The PSO algorithm can be summarized by Figure 3.7:

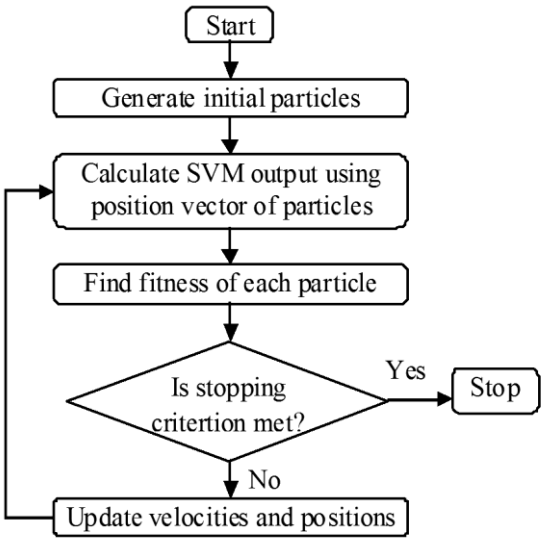

Figure 3.7 Flowchart of the PSO algorithm [41]

The proposed MPC algorithm is simulated in the MATLAB/SIMULINK environment. To demonstrate the effectiveness of proposed MPC strategy, both static scenario and dynamic scenario are considered. For static scenario, PEMFC is considered to work at rated power and the set point of the output voltage is a constant. For dynamic scenario, the reference trajectory contains two step changes. The sample time is set as 1 second for both scenarios.

Figure 3.8 shows the tracking curves of PEMFC voltage in static test. In addition, various values of softness coefficient are also tested to investigate its impact to system performance. The results demonstrate that the proposed MPC strategy is able to control PEMFC to reach the steady state. The results also indicate that, as c decreases, the system reaches the rated voltage with fewer steps and thus less time. However, decreasing c will also weaken the robustness of the system. In other word, there exists a trade-off between convergence speed and robustness of the control system.

The result of dynamic test is depicted in Figure 3.9. One can observe that the controller forces PEMFC voltage to track the reference trajectory to reach new steady state. The result reveals that the proposed MPC strategy has strong robustness.

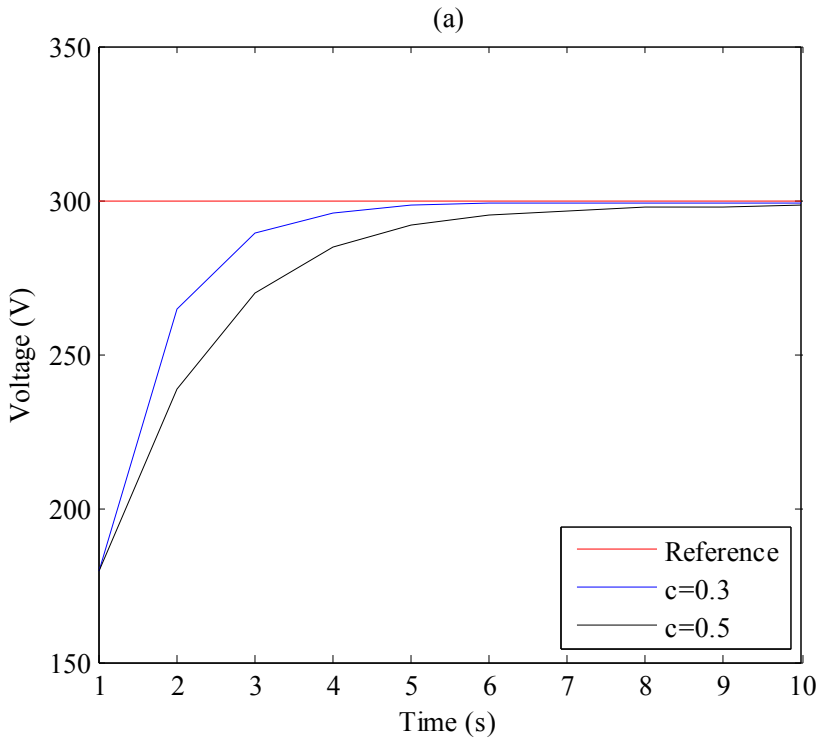

Figure 3.8 Performance of the proposed MPC: (a) static scenario

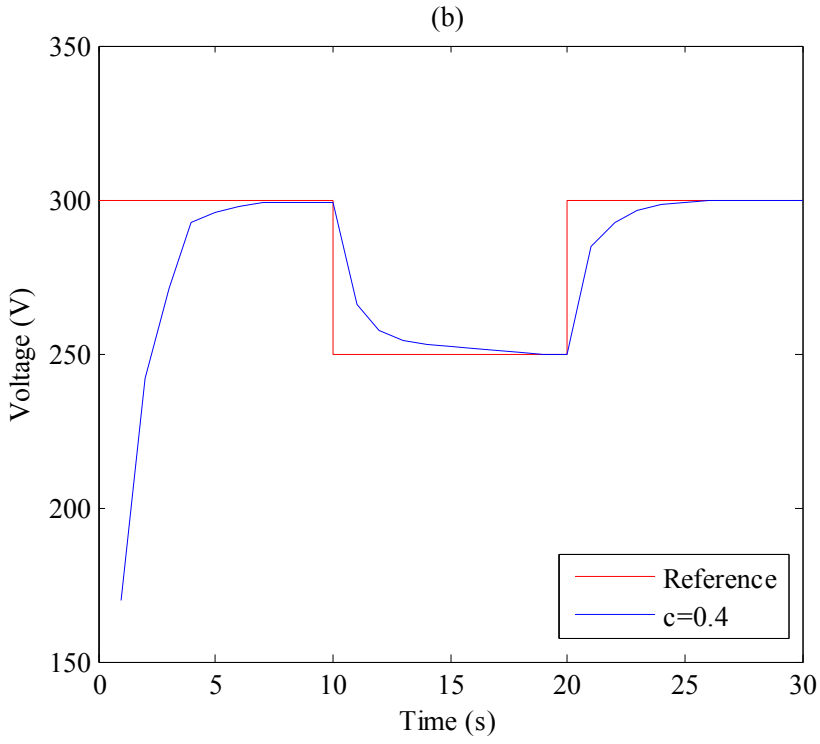

Figure 3.8 Performance of the proposed MPC: (b) dynamic scenario

3.5 Constrained MPC with modified particle swarm optimization

Based on the combined empirical and mechanistic model developed in Chapter 2, the constrained MPC strategy is designed in this section. A key advantage of MPC over other control schemes is its ability of handling constraints in a systematic and straightforward manner [42]. In this section, dynamic constraints are designed and the standard particle PSO algorithm is modified for constraint handling. In addition, the modified PSO is accelerated by improving the initialization process based on the optimal control sequence obtained at the previous sampling period.

The schematic of the constrained MPC is depicted in Fig. 3.9. The objective of the controller is to track the reference trajectory of the output voltage V_r. Meanwhile, the controller prevents PEMFC from reactant starvation and excessive pressure difference across the membrane. To achieve this, dynamic constraints are designed and standard PSO algorithm is modified to solve the resulting constrained MPC problem.

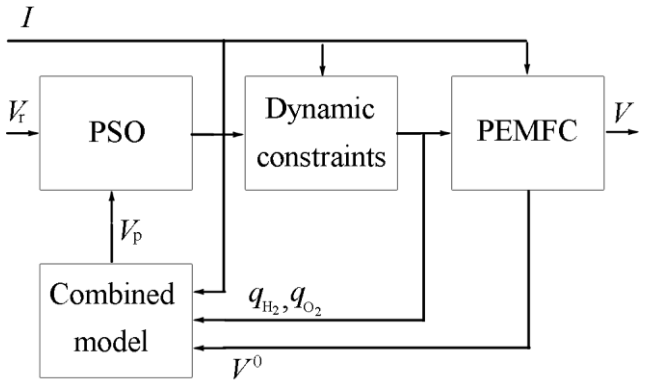

Figure 3.9 Framework of the constrained MPC [43]

3.5.1 Formulation of constrained MPC for PEMFC

MPC is formulated as the repeated solution of a finite horizon open-loop optimal control problem subject to system dynamics and input and state constraints. The optimal current and future control input are calculated by minimizing the objective function. Typically, the objective function is defined as the difference between set points and predicted outputs. Only the optimal current input is applied to the plant, and this procedure is repeated at the next sampling instance (called receding horizon principle). In this study, the objective function of the MPC for PEMFC is defined by:

$$J = \sum_{i=1}^{N} \left[(V_p(k+i) - V_r(k+i))^T Q (V_p(k+i) - V_r(k+i)) + \Delta u(k+i)^T R \Delta u(k+i) \right] \tag{3.19}$$

where N is the predictive horizon; $V_p(k + i)$ is the predicted output of the system at instant $k + i$ through models based on information available at instant k; $V_r(k + i)$ is the desired output at instant $k + i$; $\Delta u(k + i) = u(k + i) - u(k + i - 1)$ is the predicted change in the control input; $Q > 0$, $\boldsymbol{R}=\boldsymbol{R}^T \geq 0$. The control horizon is set to be equal to the predictive horizon.

Reference trajectory of output voltage is introduced to avoid excessive movement of the control input, which are defined as:

$$V_r(k+i) = c^i V(k) + (1 - c^i) V_{sp} \tag{3.20}$$

where $V_r(k + i)$ is the reference trajectory of the output voltage at time $k + i$, $V(k)$ is the actual output voltage at time k, V_{sp} is the set point of the output voltage and c is an adjustable parameter ($0 < c < 1$).

One of the most important advantages of the MPC over other control schemes is its ability to deal with constraints in a systematic and straightforward manner. In the PEMFC system, several constraints must be respected.

In Chapter 2, (2.45) describes the relationship between stack current and hydrogen partial pressure, and (2.46) describes the relationship between stack current and oxygen partial pressure. As shown in both equations, one of the most important challenges for the PEMFC controller is to ensure sufficient amount of reactants – hydrogen and oxygen – provided when fuel cell stack current abruptly changes due to the uncontrollable load. When a large load is applied to the fuel cell, the sudden increase in the stack current can cause the reactants starvation if the reactants cannot be replenished immediately and sufficiently. This catastrophic event permanently damages cells and limits the power response of the system. Therefore, excessive amounts of hydrogen and oxygen should be ensured at all times:

$$q_{H_2}(k) - 2K_r I(k) > 0 \tag{3.21}$$

$$q_{O_2}(k) - K_r I(k) > 0 \tag{3.22}$$

In addition, the hydrogen and air supply must be coordinated in a way that the pressure difference across the fuel cell membrane is small to avoid membrane damage [44]. Therefore, the partial pressure difference between oxygen and hydrogen should be maintained in a safe range. It is mentioned in some documents that the biggest pressure difference should be 0.02 MPa to 0.05 MPa [45]. Besides, membrane dehydration in anode affects pressure more than that in cathode. Thus, for the sake of membrane humidity, hydrogen partial pressure must be maintained lower than oxygen partial pressure [45]. In this study, the pressure difference between oxygen and hydrogen is maintained in the following range:

$$0 \le P_{O_2}(k) - P_{H_2}(k) \le \delta p \tag{3.23}$$

where δp is the maximum allowable pressure difference, which is assumed to be 0.3atm (approximately 0.03MPa). $P_{H_2}(k)$ and $P_{O_2}(k)$ can be determined by (2.45) and (2.46).

3.5.2 Modified particle swarm optimization for constraint handling

The proposed constrained MPC method formulates a dynamic nonlinear optimization problem, to which the conventional optimization techniques cannot be easily applied. Therefore, in this research, the real-time optimization problem is solved using PSO.

In the literature, several studies, which proposed to extend PSO to constrained optimization problems, are reported, and different constraint handling techniques were used. Parsopoulus and Vrahatis converted the constrained optimization problem into a non-constrained optimization problem by adopting a non-stationary multi-stage assignment penalty function and then applying PSO to the converted problems [46]. Ray and Liew employed a Pareto ranking scheme to handle constraints, which is a concept of multi-objective optimization [47].

In this section, a simple but efficient method is introduced to solve constrained optimization problems by modifying the standard PSO algorithm. Figure 3.10 shows the flowcharts of the modified PSO algorithm. As shown in the dashed area of Figure 3.10, a constraint checking procedure is introduced to check constraint violation after updating. If not satisfied, the position of this particle X_i is set to the current global best (p_g). Here, p_g serves as a backup for all particles. As the fitness function is a convex function, p_g must be

the currently found nearest one to the optimum. Therefore, it is reasonable to use p_g as the backup.

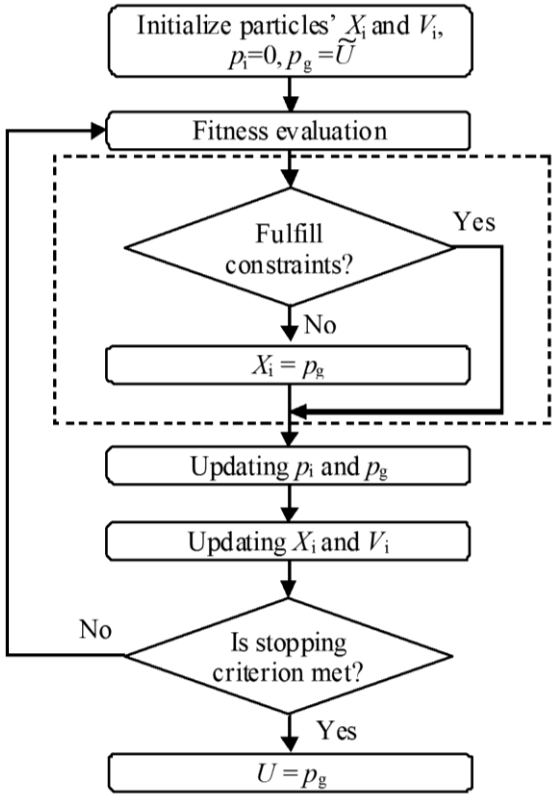

Figure 3.10 Flow chart of the modified PSO for the constrained MPC [43]

The initialization of p_g is critical to the proposed method as it is the backup of all particles. Searching for a feasible solution at the initialization of each time step is time consuming and difficult to implement. Fortunately, the constrained optimization problem is solved in the context of MPC. As required by the receding horizon principle, the MPC calculates an evolution at each time step. Therefore, the past evolutions contain useful information that can help improve the initialization of the current evolution.

The optimal input sequence at k is assumed to be $U^*(k)=[u^*(k),u^*(k+1),...,u^*(k+N)]$. As required by receding horizon principle, the first control move $u^*(k)$ is implemented and the rest control moves are discared. These discarded moves are the predicted optimal inputs in the succeeding $k+N-1$ steps, assuming that the system parameters remain constant across the period. Using the last $k+N-1$moves, a new input sequence $\tilde{U}(k+1)$ is created to initialize p_g of the next sampling step. This vector is not only anticipated to be feasible, but also a very good guess for the solution of the next optimization problem.

$$U^*(k) = [u^*(k), \quad u^*(k+1), \ ...,u^*(k+N-1),u^*(k+N)]$$

$$\tilde{U}(k+1)=[u^*(k+1),u^*(k+2), \ ...,u^*(k+N), \qquad 0 \quad]$$

Compared to other techniques, this approach has the following advantages:

(1) It is quite simple. There is no pre-processing of the constraints and there is neither complicated manipulation. Fitness function and constraints are handled separately, thus there are no limitations concerning the constraints.

(2) It is faster. The only part of the algorithm dealing with constraints is to check if a solution satisfies all the constraints. This will reduce the computation time when handling multiple or complicated constraints.

To verify its performance, the proposed constrained MPC strategy is emplemented in the MATLAB/SIMULINK environment. A load disturbance is assumed, which causes step changes of the stack current I at t = 5 s and t = 15 s, respectively. Figure 3.11(a) shows the step changes of the stack current. In real world application, the temperature of PEMFC is usually regulated to the optimal value. Therefore, the temperature T is considered as a

constant of 343K. The hydrogen and oxygen reference partial pressures are $p_{H_2}^0$ = 2.5atm and $p_{O_2}^0$ = 1.4atm. The sampling rate of the MPC was chosen as T_s = 1 s. Other parameters are: N=10, Q=10, $\boldsymbol{R}$=diag(0.1 0.1), c=0.5.

The results displayed in Figure 3.11(b) show that the proposed MPC strategy performs quite well with respect to regulating the voltage to the set point. The corresponding control moves, oxygen and hydrogen flowrates, are also shown in Figure 3.11(c) and Figure 3.11(d). Figure 3.11(g) provides information concerning the constraints on pressure difference. As expected, the pressure difference between oxygen and hydrogen is maintained below 0.3atm at all times. Besides, as can be seen from Figure 3.11(h) and Figure 3.11(i), excessive amounts of oxygen and hydrogen are guaranteed at all times and reactants starvation is effectively avoided.

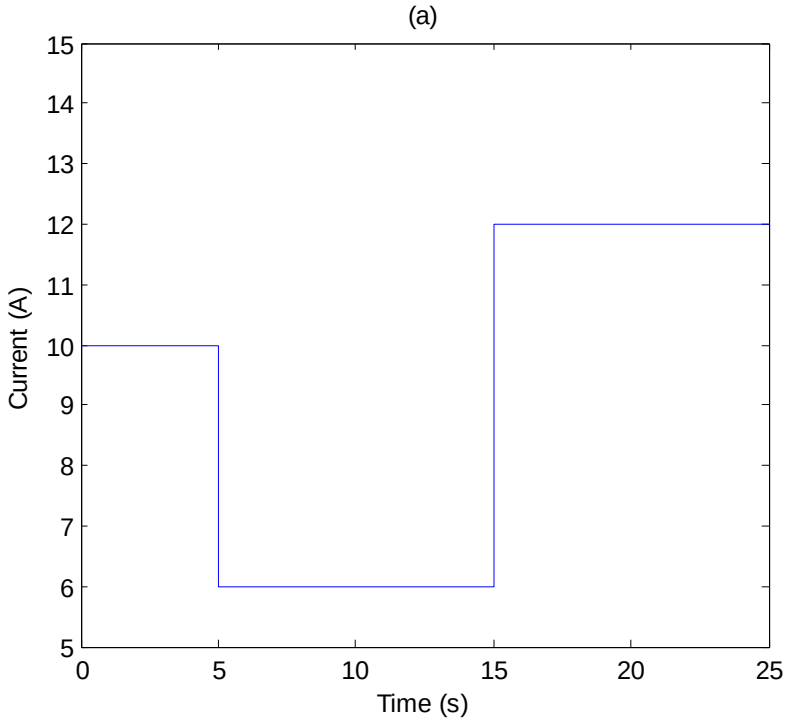

Figure 3.11 Performance of the constrained MPC: (a) Current

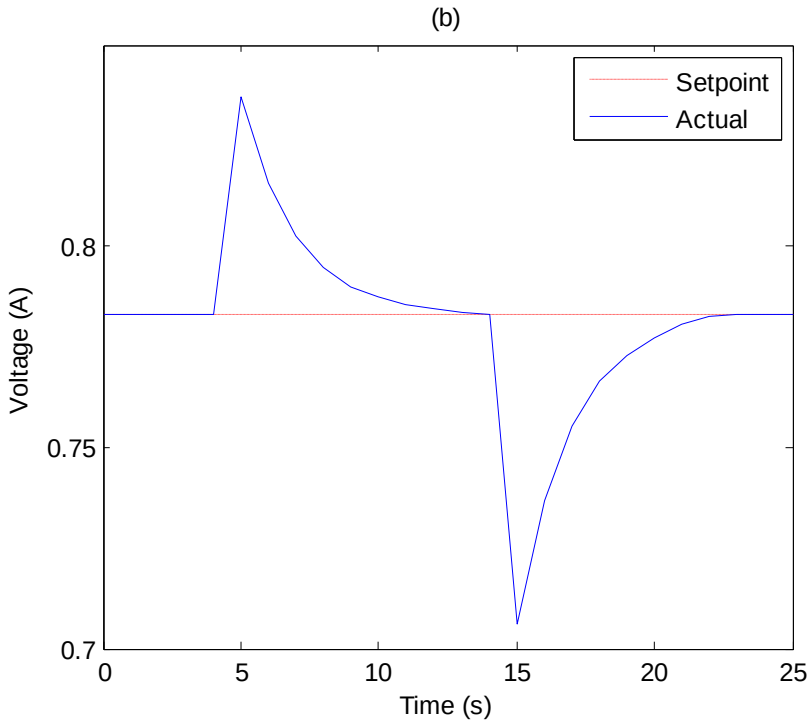

Figure 3.11 Performance of the constrained MPC: (b) Voltage

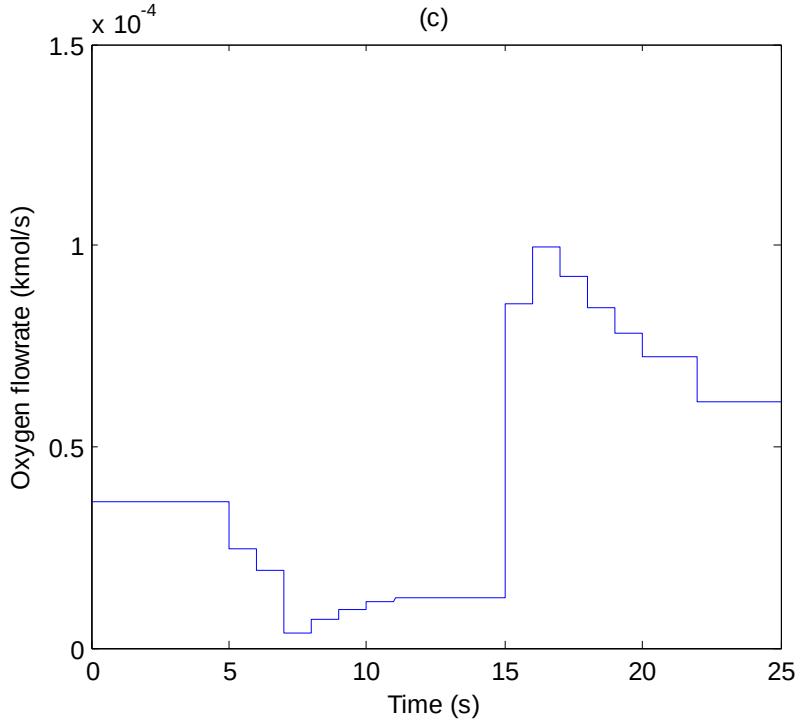

Figure 3.11 Performance of the constrained MPC: (c) Oxygen flowrate

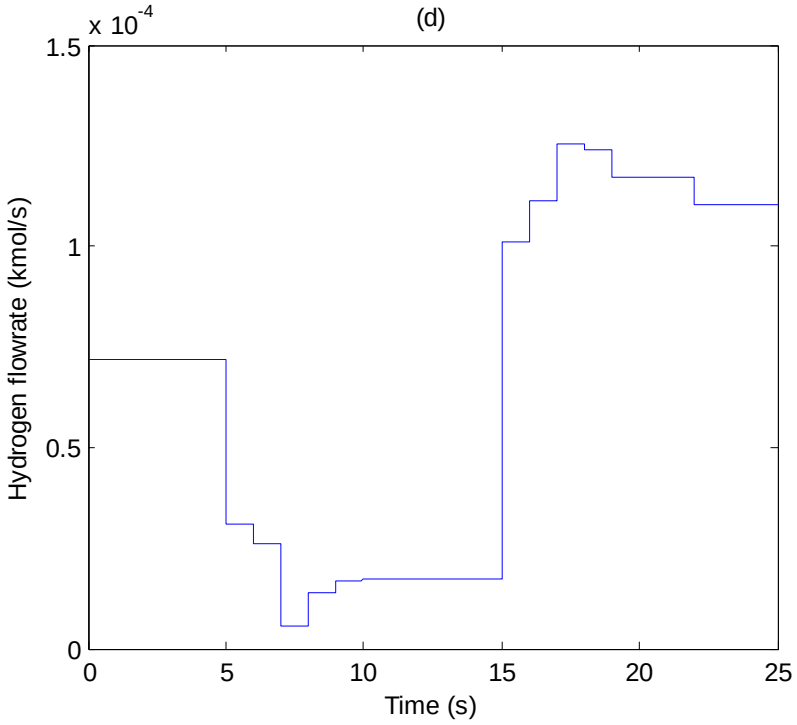

Figure 3.11 Performance of the constrained MPC: (d) Hydrogen flowrate

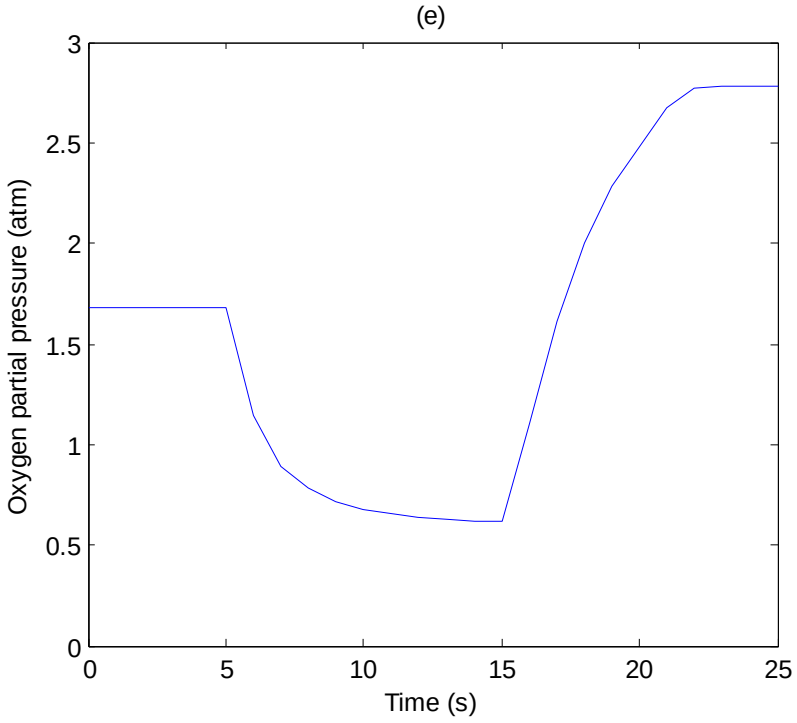

Figure 3.11 Performance of the constrained MPC: (e) Oxygen partial pressure

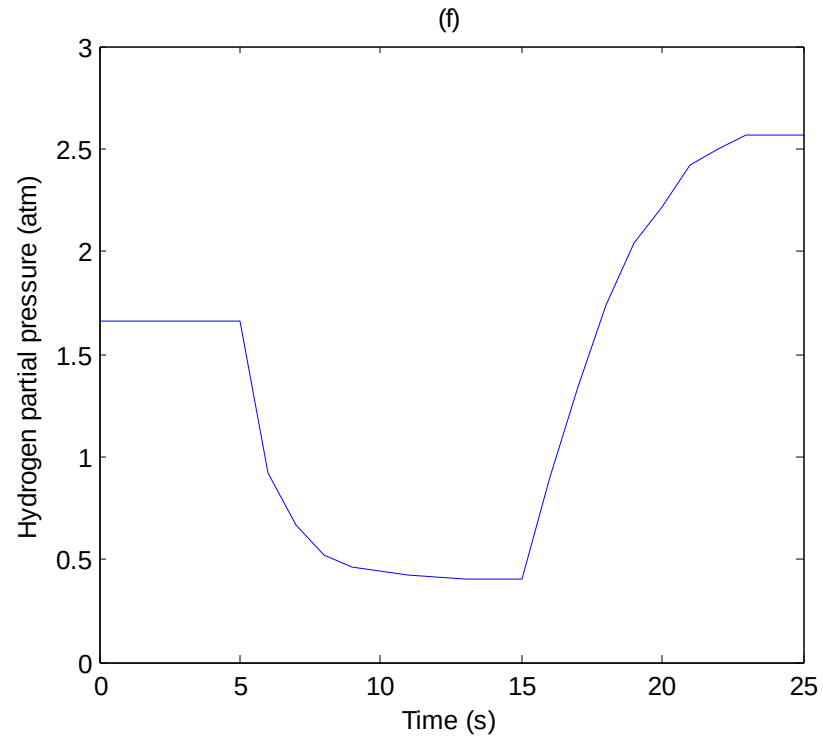

Figure 3.11 Performance of the constrained MPC: (f) Hydrogen partial pressure

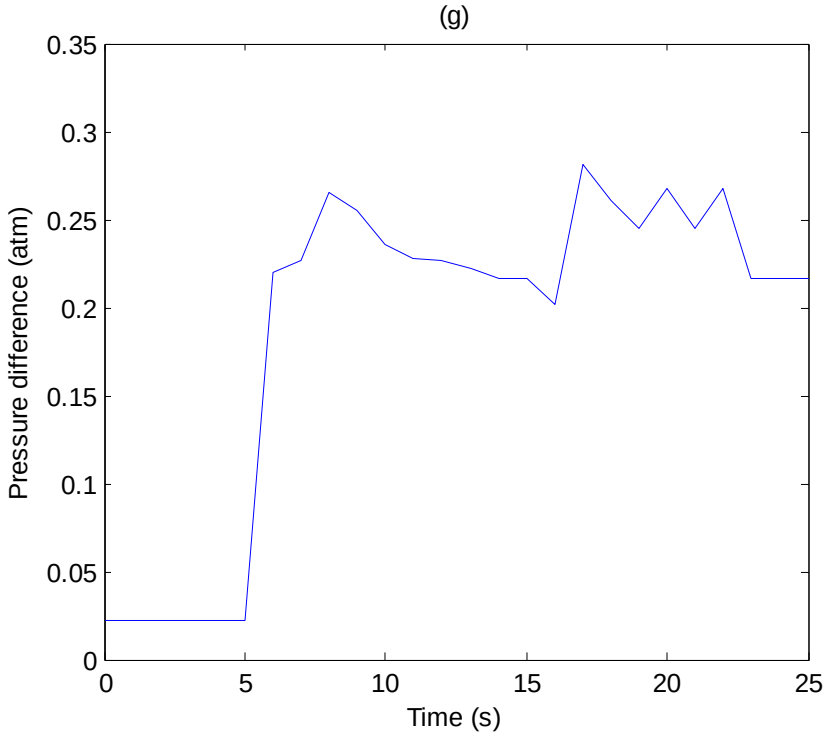

Figure 3.11 Performance of the constrained MPC: (g) Pressure difference

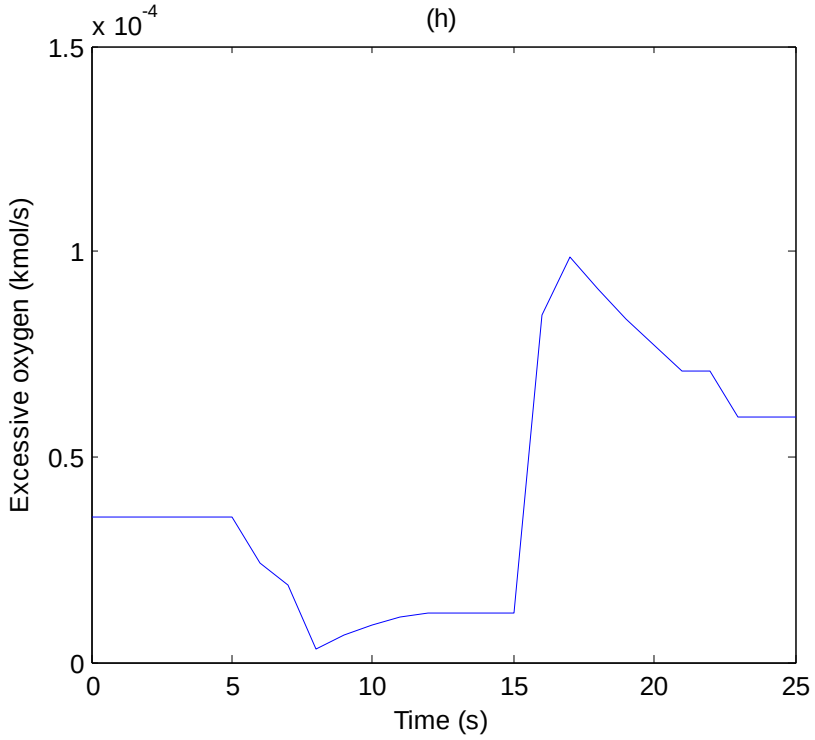

Figure 3.11 Performance of the constrained MPC: (h) Excessive oxygen

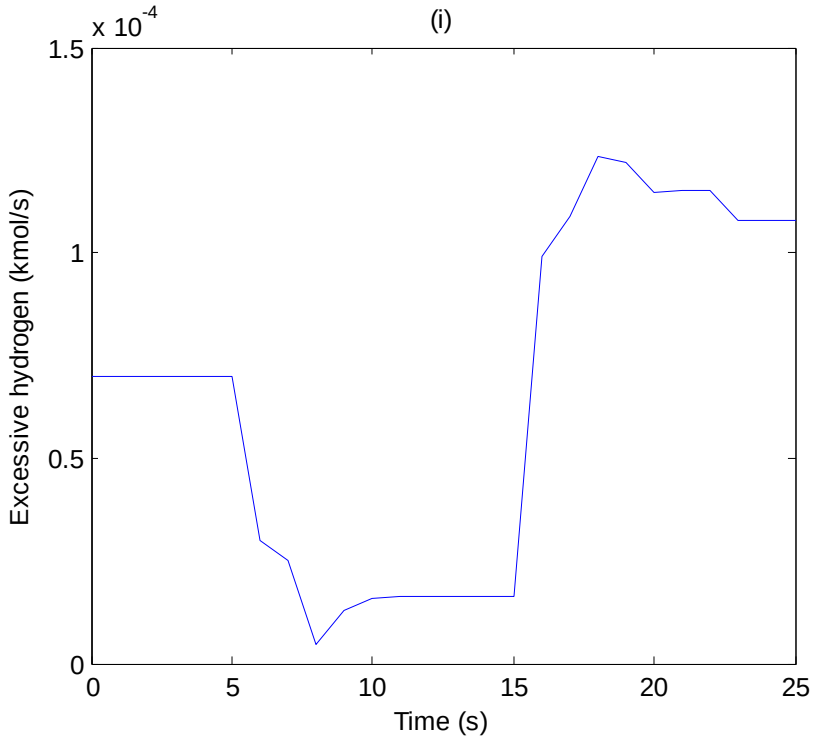

Figure 3.11 Performance of the constrained MPC: (i) Excessive hydrogen

3.6 Conclusion

The objective of this chapter is to investigate various control strategies of PEMFC. First, a basic MPC strategy is developed based on the SVM model using MPC Toolbox of the MATLAB program. The controller serves to regulate stack voltage and oxygen excess ratio to the desired values. Then, a novel MPC strategy is proposed by integrating SVM model with PSO algorithm. The controller serves to track constant and changing target value of stack voltage. Finally, a constrained MPC strategy is formulated and solved by modifying the standard PSO algorithm. The controller serves to track the reference trajectory of stack voltage. Meanwhile, the controller prevents PEMFC from reactant starvation and excessive pressure difference across the membrane. Simulation results demonstrate that each of the control strategies achieves the control objective that it is supposed to accomplish.

In the next chapter, an optimal control strategy is proposed for the tracking of time-varying maximum efficiency point of PEMFC. The maximum efficiency point tracking controller is developed based on extremum seeking control theory. With the proposed controller, PEMFC is able to operates at the maximum efficiency even when operating conditions are changing. Therefore, it is crucial for the design of a cost-effective fuel cell system.

Reference

[1] J. G. Williams, G. Liu, S. Chai, D. Rees, "Intelligent control for improvements in PEM fuel cell flow performance," *Int. J. Autom. Comput.*, vol. 5, pp. 145-151, 2008.

[2] T. Van Den Boom, M. A. Botto, J. S´a Da Costa, "Robust control of dynamical systems using neural networks with input-output feedback linearization," *Int. J. Control*, vol. 76, pp. 1783-1789, 2003.

[3] L. C. Iwan, R. F. Stengel, "The application of neural networks to fuel processors for fuel cell vehicles", in *Proceedings of the 37th IEEE Conference on Decision and Control*, vol. 2, pp. 1585-1590, 1998.

[4] M. Serra, J. Aguado, X. Ansede, J. Riera, –Controllability analysis of decentralised linear controllers for polymeric fuel cells," *J. Power Sources*, vol. 151, pp. 93-102, 2005.

[5] F. Zenith, S. Skogestad, –Control of fuel cell power output," *J. Power Sources*, vol. 17, pp. 333-347, 2007.

[6] M. El-Sharkh, A. Rahman, M. Alam, A. Sakla, P. Byrne, T. Thomas, –Analysis of active and reactive power control of a stand-alone PEM fuel cell power plant," *IEEE Trans. Power Systems*, vol. 19, pp. 2022-2028, 2004.

[7] R. N. Methekar, V. Prasad, R. D. Gudi, –Dynamic analysis and linear control strategies for proton exchange membrane fuel cell using a distributed parameter model," *J. Power Sources*, vol. 165, pp. 152-170, 2007.

[8] C. Woo, J. Benziger, –PEM fuel cell current regulation by fuel feed control," *Chem. Eng. Sci.*, vol. 62, pp. 957-968, 2007.

[9] K. C. Lauzze, D. J. Chmielewski, –Power control of a polymer electrolyte membrane fuel cell," *Ind. Eng. Chem. Res.*, vol. 45, pp. 4661-4670, 2006.

[10] F. Zenith, S. Skogestad, –Control of the mass and energy dynamics of polybenzimidazole-membrane fuel cells," *J. Power Sources*, vol. 19, pp. 415-432, 2009.

[11] J. T. Pukrushpan, A. G. Stefanopoulou, H. Peng, "Control of fuel cell breathing," *IEEE Control Syst. Mag.,* vol. 24, pp. 30-46, 2004.

[12] J. Golbert, D. R. Lewin, –Model-based control of fuel cells: (1) Regulatory control," *J. Power Sources*, vol. 135, pp. 135-151, 2004.

[13] J. Golbert, D. R. Lewin, –Model-based control of fuel cells: (2) Optimal efficiency," *J. Power Sources*, vol. 173, pp. 298-309, 2007.

[14] A. Arce, A. J. del Real, C. Bordons, –MPC for battery/fuel cell hybrid vehicles including fuel cell dynamics and battery performance improvement," *J. Process Control*, vol. 19, pp. 1289-1304, 2009.

[15] A. Vahidi, H. Peng, –Current management in a hybrid fuel cell power system: A model-predictive control approach," *IEEE Trans. Control Syst. Technol.*, vol. 14, pp. 1047-1057, 2006.

[16] C. Bordons, A. Arce, A. del Real, –Constrained predictive control strategies for PEM fuel cells," in *Proceedings of American Control Conference*, pp. 2486-2491, 2006.

[17] W. Wu, C. Pai, –Modeling and control of a proton exchange membrane fuel cell system with alternative fuel sources," *Ind. Eng. Chem. Res.*, vol. 48, pp. 8999-9005, 2009.

[18] M. Zhijun, Z. Xinjian, C. Guangyi, –Design and simulation of fuzzy controller for PEMFCs," in *Proceedings of IEEE International Conference on Industrial Technology*, pp. 220-224, 2005.

[19] P. K. Kolavennu, S. Palanki, D. A. Cartes, J. C. Telotte, –Adaptive controller for tracking power profile in a fuel cell powered automobile," *J. Process Control*, vol. 18, pp. 558-567, 2008.

[20] M. A. Danzer, J. Wilhelm, H. Aschemann, E. P. Hofer, "Model-based control of cathode pressure and oxygen excess ratio of a PEM fuel cell system. *J. Power Sources*, vol. 176, pp. 515-522, 2008.

[21] F. Allgöwer, R. Findeisen, Z. K. Nagy, "Nonlinear model predictive control: from theory to application," *J. Chin. Inst. Chem. Engrs.*, vol. 35, pp. 299-315, 2004.

[22] A. I. Propoi, "Use of linear programming methods for synthesizing sampled-data automatic systems," *Autom. Remote Control*, vol. 24, pp. 837-844, 1963.

[23] J. Richalet, "Model predictive heuristic control: applications to industrial processes," *Automatica*, vol. 29, pp. 413-428, 1978.

[24] C. R. Cutler, B. L. Ramaker, "Dynamic matrix control: a computer control algorithm," in *Proceedings of the Joint Automatic Control Conference*, Paper No: WP5-B, 1979.

[25] D.W. Clarke, C. Mohtadi, P.S. Tuffs, "Generalized predictive control: Part I. The basic algorithm," *Automatica*, vol. 23, pp. 137-148, 1987

[26] C. E. Garcia, M. Morari, "Internal Model Control 1: A unifying review and some new results," *Ind. Eng. Chem. Process Des. Dev.*, vol. 21, pp. 308-323, 1982.

[27] S. J. Qin, T. A. Bagwell, "An overview of nonlinear model predictive control applications," in F. Allogower, A. Zheng, editors, *Nonlinear model predictive control*, pp. 369-393, Birkhauser, 2000.

[28] J. Lu, A. Zahedi, "Modelling and control of PEMFC based on support vector machine," in *Proceedings of 2011 Australasian Universities Power Engineering Conference*, pp. 1-6, 2011.

[29] A. Bemporad, N. L. Ricker, M. Morari, *Model Predictive Control Toolbox for Matlab*, The Mathworks, Inc., 2004.

[30] J. Lu, A. Zahedi, –Model predictive control for PEMFC based on least square support vector machine," *in Proceedings of 2012 Asia-Pacific Power and Energy Engineering Conference*, in press.

[31] M. Grujicic, K. Chittajallu, J. T. Pukrushpan, "Control of the transient behaviour of polymer electrolyte membrane fuel cell systems," *in Proceedings of Institution of Mechanical Engineers, Part D: Journal of Automobile Engineering*, vol. 218, pp. 1239-1250, 2004.

[32] J. Kennedy, R. C. Eberhart, "Particle swarm optimization," *in Proceedings of International Conference on Neural Networks*, pp. 1942-1948, 1995.

[33] R. Thangaraj, M. Pant, A. Abraham, P. Bouvry, –Particle swarm optimization: Hybridization perspectives and experimental illustrations," *Appl. Math. Comput.*, vol. 217, pp. 5208-5226, 2011.

[34] P. Engelbrecht, *Fundamentals of Computational Swarm Intelligence*, John Wiley & Sons New York, 2005.

[35] J. Kennedy, –The particle swarm: social adaptation of knowledge," *in Proceedings of the IEEE International Conference on Evolutionary Computation*, pp. 303-308, 1997.

[36] Y. Shi, R. C. Eberhart, –Parameter selection in particle swarm optimization," *in Proceedings Annual Conference on Evolutionary Programming*, pp. 591-600, 1998.

[37] Y. T. Kao, E. Zahara, –A hybrid genetic algorithm and particle swarm optimization for multimodal functions," *Appl. Soft Comput.*, vol. 8, pp. 849-857, 2008.

[38] M. A. Abido, "Multiobjective particle swarm optimization technique for environmental/economic dispatch problem," *Electr. Power Syst. Res.*, vol. 79, pp. 1105–1113, 2009.

[39] R. C. Eberhart, Y. Shi, "Particle swarm optimization: developments, applications and resources," *in Proceedings of the IEEE Congress on Evolutionary Computation*, vol. 1, pp. 81-86, 2001.

[40] B. Birge, "PSOt-a Particle Swarm Optimization Toolbox for Use with Matlab," in *Proceedings of Swarm Intelligence Symposium*, pp. 182-186, 2003.

[41] J. Lu, A. Zahedi, "Support vector machine based predictive controller with swarm intelligence for PEMFC," in *Proceedings of 2012 Australasian Universities Power Engineering Conference*, in press.

[42] L. X. Wang, F. Wan, "Structured neural networks for constrained model predictive control," *Automatica*, vol. 37, pp. 1235-1243, 2001.

[43] J. Lu, A. Zahedi, "Constrained model predictive control of PEMFC based on a combined empirical and mechanistic model," *J. Renewable Sustainable Energy*, vol. 4, paper no. 53116, pp. 1-15, 2012.

[44] A. G. Stefanopoulou, K-W. Suh, "Mechatronics in fuel cell systems," *Control. Eng. Pract.,* vol. 15, pp. 277-289, 2004.

[45] Y. Y. Zhang, G. Y. Cao, X. J. Zhu, "Pressure control of PEMFC distributed power generator," *J Shanghai University*, vol. 10, pp.262–267, 2006.

[46] K. E. Parsopoulus, M. N. Vrahatis. "Particle swarm optimization method for constrained optimization problems," *in Proceedings of the 2nd Euro-International Symposium on Computational Intelligence*, pp. 214-220, 2002.

[47] T. Ray, K. M. Liew, "A swarm with an effective information sharing mechanism for unconstrained and constrained single objective optimisation problems," *in Proceedings of IEEE Congress on Evolutionary Computation*, pp. 75-80, 2001.

Chapter 4 Maximum Efficiency Point Tracking

The core factor that affects commercialization potential of PEMFC is the cost of electricity provided by PEMFC system. The cost of electricity is determined by the capital cost of the fuel cell system, the cost of fuel and the efficiency of the whole system. The fuel cell system that always operates at the maximum efficiency produces the least expensive electricity. Therefore, the ability to increase the operational efficiency is a crucial issue for the design of a cost-effective fuel cell system with high market competitiveness [1]. The efficiency of the fuel cell system nonlinearly depends on various operating conditions. Among them, the air flow supplied to the fuel cell system is one of the most significant factors in determining the efficiency. The conventional method of controlling the air flow is to stabilize the oxygen supply at a predetermined constant rate for the optimal efficiency. In practice, however, the optimal point can deviate from the pre-set value due to the varying operating conditions, such as the uncontrollable load. Therefore, the maximum efficiency point tracking (MEPT) controller is necessary to maintain the optimal efficiency over a broad range of operating conditions.

The major contributions of chapter 4 include: (1) The efficiency curves of PEMFC under different operating conditions are obtained and analyzed. The efficiency curves are unimodal with the peak determined by the combination of the stack current and the oxygen excess ratio. (2) The MEPT controller is designed based on the extremum seeking control (ESC) theory. The ESC controller feeds a probe signal into the control input to search for the optimal performance output in real time. As indicated by the efficiency curves, the MEPT controller is designed for searching the optimal oxygen excess ratio in real time to maximize the efficiency of PEMFC.

The chapter is organized as follows: In section 4.1, the maximum efficiency point tacking problem is formulated and analyzed. In section 4.2, the theory of extremum seeking control is briefly introduced. In section 4.3, the MPET controller is designed based on extremum seeking control algorithm. It section 4.4, the system is simulated and results are discussed.

4.1 Problem statement

The economics of PEMFC depends heavily on the efficiency of the system. One of the major advantages of PEMFC is that it can attain high efficiency since it is not limited by the Carnot cycle. On average, the combustion efficiency of the PEMFC is about 20–30% higher than that of fossil fuels such as oil, natural gas and coal [2]. The efficiency of PEMFC system is a product of efficiencies of its components, such as fuel cell stack and other auxiliary systems [3].

Auxiliary systems (also known as the balance of plant) are necessary for the correct operation of fuel cell systems. The most important auxiliary systems are the air supply system, namely the air compressor, to pressurize the air to the correct operating pressure; the humidifier to guarantee that the fuel cell is properly humidified for optimal performance; and the cooling system to maintain the temperature. However, these auxiliary devices will draw power produced by the fuel cell, thereby reducing the net power output and the overall efficiency. Among them, the air compressor consumes the most part of the total parasitic power, thereby producing the greatest impact on the system efficiency [4].

At the same time, one of the most important challenges for the PEMFC system is to ensure sufficient amount of oxygen is provided in the cathode when the fuel cell stack current abruptly changes. When a large load is applied to the fuel cell, the sudden increase in

the fuel cell stack current can cause the oxygen starvation if the depleted oxygen cannot be replenished immediately and sufficiently [5]. This catastrophic event permanently damages cells and limits the power response of the system. This problem arises from the fact that oxygen reacts instantaneously as current is drawn from the stack, while the air supply rate is limited by the manifold dynamics and compressor operational constraints [6].

The control and management of air supply has been the focus of many studies. The main objectives of the air supply control are to improve system performance and to prevent oxygen starvation. In terms of system performance improvement, Blunier et al. optimized the inlet air pressure and stoichiometry with the constraint of relative air humidity to maximize the output voltage [7]. Feroldi et al. proposed a predictive control strategy using dynamic matrix control (DMC) to manipulate compressor motor voltage and cathode air flow valve area for better system efficiency [8]. For oxygen starvation prevention, Danzer et al. proposed a multivariable model-based control scheme to control the oxygen excess ratio and the cathode pressure [9].

These control strategies stabilize a predetermined air stoichiometry which may or may not be the optimal operating condition for the maximum efficiency. Another disadvantage of these methods is that they require knowledge of system parameters, which must be either measured offline or estimated. However, in practice, parameters vary over time as the fuel cell system frequently moves from one operational point to another. Therefore, it is more desirable to develop an air supply control strategy with respect to time-varying parameters and model uncertainty.

4.1.1 Review of PEMFC system model

The dynamic model of the PEMFC system that we used to investigate the impact of air supply on system efficiency in this work was developed and validated by Pukrushpan et al. [10]-[13]. Figure 4.1 shows the schematic of the PEMFC system analysed. However, it is worth pointing out that our MEPT control approach is a non-model based method and accepts various kinds of fuel cell models, such as support vector machine model [14].

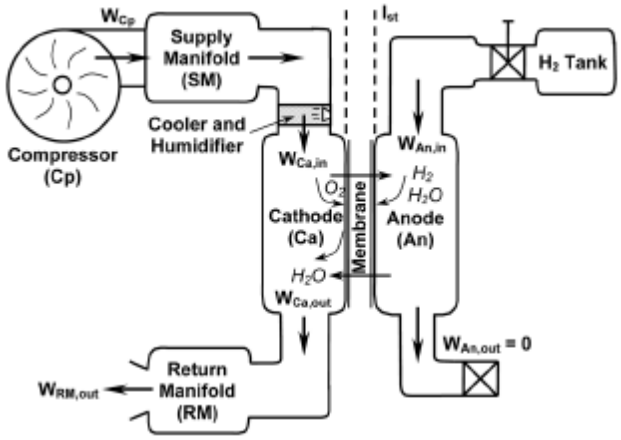

Figure 4.1 Components and volumes in PEMFC reactant supply system [14]

The model under consideration comprises the fuel cell stack and the auxiliary systems and contains nine state variables. The fuel cell stack model is composed of four interacting sub-models, namely stack voltage, cathode flow, anode flow, and membrane hydration models. The stack voltage is calculated as a function of stack current, cell temperature, air pressure, oxygen and hydrogen partial pressures, and membrane humidity. Models of auxiliary components, namely a compressor, manifolds, an air cooler, and a humidifier, are developed based on physical-chemical knowledge of the process involved. Most parameters used in this model are based on the 75 kW stacks used in the FORD P2000 fuel cell prototype vehicle [15].

For clarity and completeness, a brief review of the model equations is conducted, but readers interested in the complete details should refer to the literature [10]-[13].

4.1.1.1 State equations

This section describes the state equations corresponding to the reactant supply subsystem. The governing equations for the mass of air in the supply manifold, for the mass of oxygen, nitrogen and water in the cathode and for the mass of hydrogen and water in the anode are respectively defined using the principle of mass conservation as [13]:

$$\frac{dm_{SM}}{dt} = W_{Cp} - W_{SM,out} \tag{4.1}$$

$$\frac{dm_{O_2}}{dt} = W_{O_2,in} - W_{O_2,out} - W_{O_2,react} \tag{4.2}$$

$$\frac{dm_{N_2}}{dt} = W_{N_2,in} - W_{N_2,out} \tag{4.3}$$

$$\frac{dm_{w,Ca}}{dt} = W_{v,Ca,in} - W_{v,Ca,out} + W_{v,Ca,gen} + W_{v,m} \tag{4.4}$$

$$\frac{dm_{H_2}}{dt} = W_{H_2,in} - W_{H_2,out} - W_{H_2,react} \tag{4.5}$$

$$\frac{dm_{w,An}}{dt} = W_{v,An,in} - W_{v,An,out} - W_{v,m} \tag{4.6}$$

where m, W denote mass and mass flow rate. The subscripts SM, Cp, Ca, An denote the location of the variable, e.g., m_{sm} is the mass of air in the supply manifold and W_{Cp} is the mass flow rate of air in the compressor. The subscripts m, v and w denote membrane related quantity, water vapour related quantity and liquid water related quantity, respectively.

The governing equation for the rotational speed of the compressor is defined by the power conservation principle as [13]:

$$J_{Cp}\frac{d\omega_{Cp}}{dt}=(\tau_{CM}-\tau_{Cp}) \tag{4.7}$$

where J_{Cp}, ω_{Cp}, η_{CM} , η_{Cp} , denote the compressor inertia, the compressor motor rotation speed, the compressor motor torque, and the compressor torque, respectively.

The governing equations for the supply manifold pressure and for the return manifold pressure are respectively defined using the energy conservation principle and standard thermodynamic relationships as [13]:

$$\frac{dp_{SM}}{dt}=\frac{\gamma R_a}{V_{SM}}(W_{Cp}T_{Cp}-W_{SM,out}T_{SM}) \tag{4.8}$$

$$\frac{dp_{RM}}{dt}=\frac{R_aT_{RM}}{V_{RM}}(W_{Ca,out}-W_{RM,out}) \tag{4.9}$$

where p, V and T denote pressure, volume and temperature, respectively. The subscripts RM denotes the return manifold. γ is the air-specific heat ratio and R_α is the universal gas constant.

Finally, the model states are accumulated in the state vector:

$$x=[m_{O_2}\ m_{N_2}\ m_{H_2}\ \omega_{Cp}\ m_{w,An}\ m_{w,Ca}\ m_{SM}\ p_{RM}\ p_{SM}]^T \tag{4.10}$$

4.1.1.2 Oxygen Excess Ratio

The air supply system has significant influence on the fuel cell system performance. On the one hand, insufficient air supply may cause oxygen starvation in the cathode, which

causes voltage reduction and permanent damage to cells. On the other hand, the compressor operation implies a power consumption that diminishes the system efficiency.

Oxygen excess ratio is indicative of oxygen starvation and can be considered as a good performance index. It describes the excess oxygen supplied to the cathode as follows:

$$\lambda_{O_2} = \frac{W_{O_2,in}}{W_{O_2,react}} \tag{4.11}$$

where $W_{O_2,in}$ and $W_{O_2,react}$ are the mass flow rates of oxygen entering the cathode and consumed by the chemical reaction, respectively. A value of $\lambda_{O2} = 1$ indicates the amount of oxygen supplied to the cathode is equal to the amount required by the stoichiometric chemical reaction $2H_2 + O_2 \rightarrow 2H_2O$.

$W_{O_2,react}$ is directly proportional to the current drawn from the fuel cell stack I_{st} according to [13]:

$$W_{O_2,react} = M_{O_2} \frac{nI_{st}}{4F} \tag{4.12}$$

where M_{O_2}, n, and F are the oxygen molar mass, the number of cells in the stack and the Faraday number, respectively.

$W_{O_2,in}$ depends on the oxygen mass fraction x_{O_2}, the atmospheric humidity ratio ω_{atm} and the flow out of supply manifold into the cathode $W_{SM,out}$ [16]:

$$W_{O_2,in} = (x_{O_2} / 1 + \omega_{atm}) W_{SM,out} \tag{4.13}$$

(4.11) and (4.12) explicitly denote the dependency of λ_{O2} on the stack current I_{st}, which directly affects $W_{O_2,react}$. If a constant amount of oxygen is supplied to the cathode, λ_{O2} decreases as I_{st} increases, which potentially causes oxygen starvation.

One the other hand, the compressor motor voltage V_{cm} affects λ_{O2} indirectly through $W_{O_2,in}$ [9]. Specifically, V_{cm} controls the compressor motor torque η_{cm} through the static motor equation [14]:

$$\tau_{CM} = \eta_{CM} \frac{k_t}{R_{CM}} (V_{CM} - k_v \omega_{Cp}) \tag{4.14}$$

where η_{cm} is the compressor motor mechanical efficiency. k_t, k_v and R_{cm} are the motor constants.

η_{cm} then determines the compressor motor rotational speed ω_{Cp} through the first-order nonlinear dynamics shown in (4.7). The compressor flow rate W_{Cp} is then modelled by applying the Jensen and Kristensen nonlinear fitting method as functions of the rotational speed ω_{Cp} [10]. Finally, W_{Cp} through (4.8) affects the supply manifold pressure, p_{SM}, which together with the cathode pressure, p_{Ca}, determines the outlet flow of supply manifold [16]:

$$W_{SM,out} = k_{SM,out} (p_{SM} - p_{Ca}) \tag{4.15}$$

where $k_{SM,out}$ is the supply manifold outlet flow constant.

For controller design, I_{st} is considered as disturbance input corresponding to the uncontrollable load and V_{cm} is the controlled input to manipulate λ_{O2}.

4.1.2 Steady-state analysis of PEMFC system's efficiency

The efficiency of the fuel cell system can be defined as the ratio of the net power output P_{net} to the power that is supplied to the system P_{fuel}:

$$\eta = \frac{P_{\text{net}}}{P_{\text{fuel}}} \tag{4.16}$$

The chemical power contained in fuel flow is related to the fuel cell stack current [17]:

$$P_{\text{fuel}} = \frac{Hn_{\text{cells}}}{2F} I_{\text{st}} \tag{4.17}$$

where H is the low heating value of hydrogen, F refers to the Faraday constant, I_{st} is the fuel cell stack current and n_{cells} denotes the number of cells in the fuel cell stack.

The net power output is defined as the power produced by the fuel cell stack from which the parasitic power consumed by the air compressor is deducted:

$$P_{\text{net}} = P_{\text{st}} - P_{CM} \tag{4.18}$$

The stack power is the product of the stack current and voltage:

$$P_{\text{st}} = I_{\text{st}} V_{\text{st}} \tag{4.19}$$

The stack voltage V_{st} is calculated by subtracting the voltage losses from the fuel cell open circuit voltage E. Generally, these losses are nonlinear functions of the states x and the stack current I_{st} [10]:

$$V_{\text{st}} = E - V_{\text{act}} - V_{\text{ohm}} - V_{\text{con}} \tag{4.20}$$

where V_{act} , V_{ohm} and V_{con} are activation loss, ohmic loss and concentration loss, respectively.

P_{CM} is given by [16]:

$$P_{CM} = \frac{V_{CM}(V_{\mathrm{CM}} - K_{\mathrm{v}}\omega_{\mathrm{Cp}})}{R_{\mathrm{CM}}} \tag{4.21}$$

Take all these equations into account, the system efficiency η can be described as a function of the fuel cell stack current I_{st} and the compressor motor voltage V_{cm}:

$$\eta(I_{st}, V_{\mathrm{CM}}) = \frac{P_{st} - P_{CM}}{P_{fuel}} = \frac{2F\left[I_{st}V_{st}R_{CM} - V_{\mathrm{CM}}(V_{\mathrm{CM}} - K_{\mathrm{v}}\omega_{\mathrm{Cp}})\right]}{Hn_{\mathrm{cells}}R_{\mathrm{CM}}I_{st}} \tag{4.22}$$

As V_{cm} is considered as the controlled input to manipulate λ_{O2}, η is plotted as a function of λ_{O2} at different I_{st} level in Figure 4.2. The result indicates that for a certain stack current level high oxygen excess ratio enhances the system efficiency. This is because high oxygen excess ratio corresponds to more oxygen supplied to the cathode, which improves P_{st} and P_{net} and thereby increases the system efficiency. However, further increase of λ_{O2} will cause P_{net} decrease due to the excessive increase of parasitic power P_{cm} consumed by the air compressor and thus deteriorative effects on system efficiency. However, the stack current also has significant impact on the system efficiency through P_{fuel} and λ_{O2} as shown by (4.12) and (4.17). When all these effects are taken into account, the efficiency curves are unimodal with the peak determined by the combination of I_{st} and λ_{O2}.

When PEMFC works in the normal operating range, the optimal value of λ_{O2} which maximizes the system efficiency for certain stack current is always above 1. The reason is due to that low oxygen excess ratio means insufficient oxygen supply, which deteriorates P_{net} and thus prevents the system reaching the maximum efficiency. This implies that improved performance may be achieved by identifying the maximum efficiency point and regulating the system about this point. As the maximum efficiency point always corresponds to a safe oxygen excess ratio value, the oxygen starvation can be avoided simultaneously.

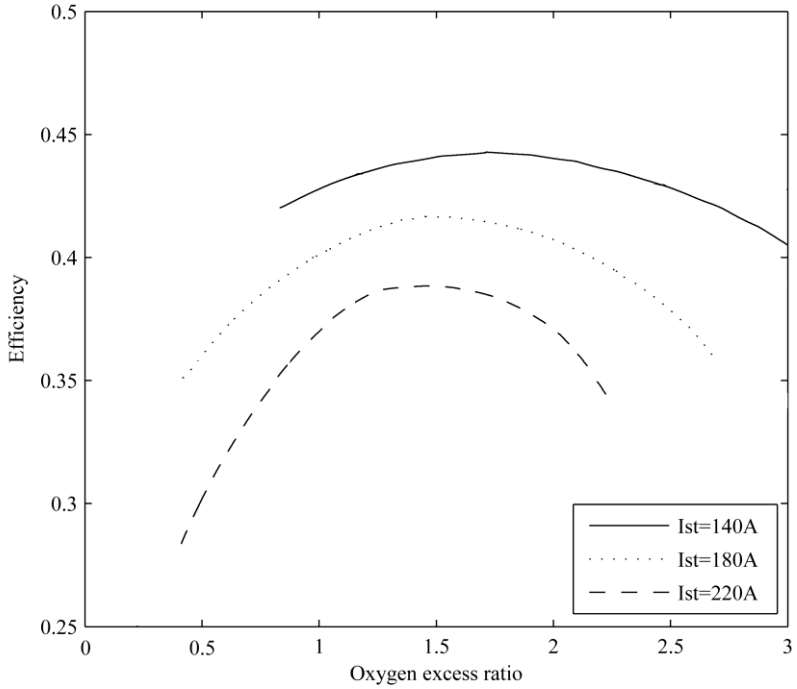

Figure 4.2 Efficiency curves of PEMFC under different operating conditions

4.2 Theory of extremum seeking control

The mainstream methods of adaptive control for linear and nonlinear systems are applicable only for regulation to known set points or reference trajectories. In some applications, the reference-to-output map has an extremum and the control objective is the optimization of an objective function which may depend on unknown model parameters, or the selection of the desired inputs to keep a performance function at its extremum value. Maximum efficiency point tracking for the PEMFC system is such a case because its parameters, such as the stack current, are changing continuously in its operation and real-time estimation of maximum efficiency point is a difficult task. The uncertainty in the reference-to-output map makes it necessary to use some sort of adaptation to track the varying set point which extremizes the performance function, for fuel cell system efficiency

in this case. This problem is called extremum seeking control (ESC) or self-optimizing control.

The early application of extremum seeking control can date back to 1920s [18]. However, a solid theoretical foundation has not yet been established for the extremum seeking control until very recently [19]. In 2000, Krstic and Wang presented the first stability analysis for an extremum seeking system applied to a general nonlinear dynamic system [20]. Applications of these approaches have been reported for combustion instability [21], electromechanical valve actuator [22], automotive application [23], source seeking [24], chemical engineering [25], etc.

The theory of extreme seeking control is briefly reviewed as follows. Consider a dynamic system with state $x \epsilon R^n$ and input $u \epsilon R^m$ that has to be operated so as to maximize a convex function $J(x,u)$. The problem is shown below:

$$\max_u J(x,u) \tag{4.23}$$

$$\text{Subject to } \dot{x} = F(x,u) \tag{4.24}$$

where $F(x,u)$ is the function describing the dynamics of the system.

The necessary conditions of optimality are given by [26]:

$$\frac{dJ}{du} = \frac{\partial J}{\partial u} - \frac{\partial J}{\partial x}\left[\frac{\partial F}{\partial x}\right]^{-1}\frac{\partial F}{\partial u} = 0 \tag{4.25}$$

The extremum seeking control law is an integral controller that forces the gradient to zero:

$$\dot{u} = k\left[\frac{dJ}{du}\right] \tag{4.26}$$

where k is the controller gain.

The key problem is the estimation of the gradient. In this research, a perturbation based extremum seeking feedback scheme is employed [20]. As will be shown next, it is a gradient search method which perturbs the input parameters with sinusoidal signal, and to make a real-time estimation of the gradient of the output relative to these inputs. Therefore, it allows us to track time-varying extremum.

4.3 Maximum efficiency point tracking controller design

This section proposes an air supply control strategy based on the extremum seeking control algorithm for searching the optimal oxygen excess ratio in real time to maximize the efficiency of fuel cell systems. This closed-loop, real-time and non-model based control method is able to guarantee the maximum efficiency point is achieved under changing operating conditions.

The extremum seeking control problem for the PEMFC efficiency optimization can be defined as:

Maximize:	$\eta = J(x,u,w)$	objective function
Subject to:	$\dot{x} = F(x,u,w)$	state equations
$x = [m_{O_2}, m_{N_2}, m_{w,Ca}, m_{sm}, p_{sm}, p_{rm}, m_{H_2}, m_{w,An}, \omega_{Cp}]^T$		states
$u = V_{cm}$		controlled input
$w = I_{st}$		disturbance input

The optimization is subject to the fuel cell system dynamics $f(x,u,w)$ briefly reviewed in Section 4.1.1. The air compressor motor voltage V_{cm} is the controlled input, the fuel cell stack current I_{st} is modelled as the disturbance input, while the performance output variables are the efficiency η and the oxygen excess ratio λ_{O2}. The goal of the extremum seeking control is to design a controller to manipulate the compressor motor voltage to an unknown set point for the optimal oxygen excess ratio, therefore maximizing the system efficiency. The explicit form of $J(x,u,w)$ is unknown and hence not available for the design.

Figure 4.3 shows the scheme of the fuel cell MEPT control system. Before engaging in extensive efforts to prove the scheme mathematically, an intuitive explanation of its basic idea is given as follows. The MEPT controller feeds a small sinusoidal perturbation signal into the compressor motor voltage $\hat{V}_{cm}$, which is the estimate of unknown optimal voltage V_{cm}^{*}. This process is also known as modulation. The perturbation frequency must be chosen large enough to avoid the PEMFC dynamics to influence the performances of the MEPT controller. This perturbation causes a response of the system efficiency. The efficiency signal is then high-pass filtered and demodulated to eliminate the static component and to estimate the derivative. Finally, the maximum efficiency η^{*} is determined through gradient method. a and ω are the amplitude and frequency of the sinusoidal perturbation signal. k is the adaptive gain of the integrator. ω_{h} is the cut-off frequency of the high-pass filter. A more detailed mathematical explanation is given below:

The efficiency function η can be approximated in the neighborhood of MEP by Taylor series:

$$\eta = \eta^{*} + \frac{\eta''}{2}(V_{cm} - V_{cm}^{*})^{2} \tag{4.27}$$

$\hat{V}_{cm}$ denotes the estimation of the unknown optimal compressor motor voltage V_{cm}^{*}. Let $\bar{V}_{cm}$ denotes the estimation error:

$$\bar{V}_{cm} = V_{cm}^{*} - \hat{V}_{cm} \tag{4.28}$$

According to Figure 4.3, we can get:

$$V_{cm} = \hat{V}_{cm} + a\sin\omega t \tag{4.29}$$

With (4.28) and (4.29), (4.27) can be rewritten as:

$$\eta = \eta^{*} + \frac{\eta''}{2}(a\sin\omega t - \bar{V}_{cm})^2 = \eta^{*} + \frac{a^2\eta''}{4} + \frac{\eta''}{2}\bar{V}_{cm}^2 - a\eta''\bar{V}_{cm}\sin\omega t - \frac{a^2\eta''}{4}\cos 2\omega t \tag{4.30}$$

Estimation error $\bar{V}_{cm}$ is a small value, thus its quadratic term $\bar{V}_{cm}^{\,2}$ can be neglected:

$$\eta = \eta^{*} + \frac{a^2\eta''}{4} - a\eta''\bar{V}_{cm}\sin\omega t - \frac{a^2\eta''}{4}\cos 2\omega t \tag{4.31}$$

The high-pass filter applied to the efficiency signal η, serves to remove the DC component, namely:

$$\frac{s}{s+\omega_h}[\eta] \approx - a\eta''\bar{V}_{cm}\sin\omega t - \frac{a^2\eta''}{4}\cos 2\omega t \tag{4.32}$$

This signal is then demodulated by multiplication with $\sin\omega t$, giving:

$$\begin{aligned}\zeta &\approx - a\eta''\bar{V}_{cm}\sin^2\omega t - \frac{a^2\eta''}{4}\cos 2\omega t\sin\omega t \\ &= -\frac{a\eta''}{2}\bar{V}_{cm} + \frac{a\eta''}{2}\bar{V}_{cm}\cos 2\omega t - \frac{a^2\eta''}{8}(\sin 3\omega t - \sin\omega t)\end{aligned} \tag{4.33}$$

The estimated compressor motor voltage is:

$$\hat{V}_{cm} \approx \frac{k}{s}[-\frac{a\eta''}{2}\bar{V}_{cm} + \frac{a\eta''}{2}\bar{V}_{cm}\cos 2\omega t - \frac{a^2\eta''}{8}(\sin 3\omega t - \sin\omega t)] \tag{4.34}$$

The last two high frequency terms can be attenuated by the integrator, thus:

$$\hat{\bar{V}}_{cm} \approx \frac{k}{s}[-\frac{a\eta''}{2}\bar{V}_{cm}] \tag{4.35}$$

Noting V_{cm}^* is constant, from (4.28) we can get:

$$\dot{\bar{V}}_{cm} = -\dot{\hat{V}}_{cm} \tag{4.36}$$

Finally we get:

$$\dot{\bar{V}}_{cm} = \frac{ka\eta''}{2}\bar{V}_{cm} \tag{4.37}$$

Since η has a maximum, its second order derivative η'' should be negative, and $ka\eta''<0$. Therefore, the estimation error $\bar{V}_{cm}$ converges to 0, which means that the compressor motor voltage converges to V_{cm}^* and the fuel cell system reaches the maximum efficiency point η^*.

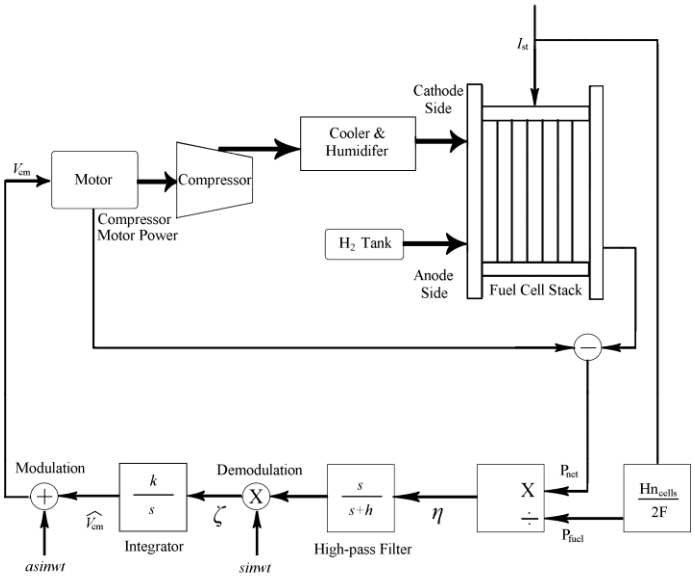

Figure 4.3 Schematic of the MEPT control system [27]

The synthesis process for extremum seeking controller requires proper selection of the perturbation amplitude a and frequency ω, adaptive gain k, and high-pass filter cut-off frequencies ω_h. The extremum seeking control theory does not provide mathematical methods to determine these values. Generally, proper selection of these parameters is a tuning process [28]. However, some valuable guidelines are provided for effective calibration.

According to (4.37), the value of k and a have a significant effect on the system convergence speed. Large values for a and k allow faster convergence rates. However, larger a and k also respectively increase the oscillation amplitude and sensitivity to disturbances. In other words, the selection of these parameters involves a trade-off between convergence speed and stability [29]. One usually increases the adaptive gain k to obtain maximum convergence rate for a desirable amount of sensitivity. Meanwhile, a small value of a is able to be kept so as to avoid the control parameters fluctuating dramatically. High perturbation frequency ω is selected to ensure significant time scale separation between the extremum seeking feedback loop and fuel cell dynamics. However, an over high value of ω will decrease the convergence speed. The cut-off frequency of high-pass filter must be designed in coordination with the perturbation frequency. Specifically, the high-pass filter must not attenuate the perturbation frequency.

4.4 Simulation results and discussion

The capability of the proposed control method is analyzed by means of simulation experiment in the MATLAB/SIMULINK environment. In order to understand the performance of the MEPT controller under varying operating conditions, a series of step

changes in the stack current I_{st} is applied in the simulation, which is shown in Figure 4.4(a). For the sake of comparison with results found by the steady-state analysis in section 2, the step changes in the stack current are set as the same values used in steady-state analysis. The controller has been tuned thusly: the amplitude a=2, the adaptive gain k=10, the perturbation frequency ω=2π, the high-pass filter frequency ω_h=π.

In Figure 4.4(b), one can observe that, as expected, the MEPT controller is able to trace the MEPs from 37% to 45%, and finally to 41%, which correspond to the optimal values found by the steady-state analysis in section 4.1.2. The seeking process of the controlled input, i.e. the compressor motor voltage, is given in Figure 4.4(c). Figure 4.4(d) shows corresponding changes in the oxygen excess ratio. Notice that the oxygen excess ratio is in a safe position, so the oxygen starvation phenomenon is effectively prevented.

To evaluate the performance of the proposed controller, it is necessary to understand the tracking behavior of efficiency as a function of oxygen excess ratio. Figure 4.4(e) shows the maximum efficiency point tracking process in the phase plane. One can observe a fast tracking that drive the system‘s operational point close to the maximum efficiency point when changes in the stack current occur. Then the system oscillates around the maximum efficiency point rather than converging to it exactly.

In order to have a comprehensive understanding of the proposed MEPT controller, two controlled simulation experiments are conducted. The scenario of PEMFC system with the MPET controller is considered as the base case. In the other two controlled experiment, the air supply system is not controlled by the MEPT controller. Therefore, one can clearly observe the benefits of the MEPT controller.

In the first scenario, the PEMFC system is tested without the MPET controller under the changing stack current condition. The compressor motor voltage V_{cm} is set as a constant of 150V in this scenario. The other parameters remain the same as those of the previous experiment. The results are given in Figure 4.5.

Compared with the results displayed in Figure 4.4, Figure 4.5(a) clearly indicates that the fuel cell system without the MEPT controller shows lower efficiency. This is because the constant compressor motor voltage cannot ensure that the optimal oxygen excess ratio is achieved under the changing stack current. As a result, excessive parasitic power is consumed by the compressor to maintain the unnecessary high level of oxygen excess ratio and thus deteriorates the system efficiency. The above explanation is proved by Figure 4.5(b), which clearly shows that the oxygen excess ratio is higher than that of the previous experiment.

In the second scenario, the PEMFC system is tested with the air supply controller proposed by Grujicic et al. [30]. The aim of their controller is to maintain a preset optimal oxygen excess ratio value of 2.33 by regulating the compressor motor voltage V_{cm} under changing stack current. In this scenario, all parameters remain the same, except that a control law of the compressor motor voltage provided by Grujicic et al. in [30] is applied. The results are show in Figure 4.6.

Figure 4.6(c) shows the oxygen excess ratio is effectively regulated to the pre-set value of 2.33 after the abrupt changes in the stack current. However, as can be seen from Figure 4.6(a), the efficiency of the system is still lower than that of the base case. This reveals that the pre-set optimal oxygen excess value may not be the true optimal one under changing

operational conditions. Therefore, an extremum seeking control strategy is essential for tracking the varying optimal value.

In summary, the simulation results indicate that the fuel cell MEPT controller converges to the maximum efficiency point and can account for time-varying parameters, such as the stack current, by searching for the optimal compressor motor voltage online. Compared with traditional methods, extremum seeking control approach has the following advantages [31]. First, the optimization problem is solved by feedback control law. Hence, extremum seeking control has a main advantage of strong robustness over other open-loop control methods. Second, it is a real-time control method. Therefore, it can be used for real-time optimization of time-varying systems. Third, it does not require prior knowledge of system model. In other words, it is a non-model based control method. Despite these desirable properties, it also comes with drawback. The periodic perturbation will bring oscillations into the system. Thus when the system reaches the MEPs, the system oscillates about this value rather than converging to it exactly. A perturbation signal with dynamic amplitude that converges to zero as the MEPT controller converges to optimal value may solve this problem. One simple way to do this is to make the periodic perturbation signal exponentially decaying in amplitude [32].

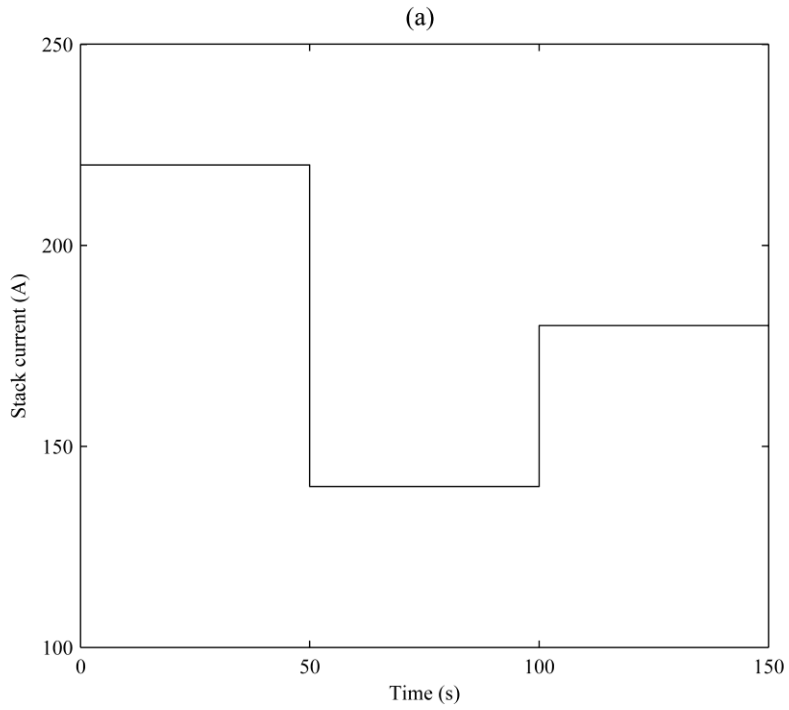

Figure 4.4 Performance of the MEPT controller: (a) Stack current

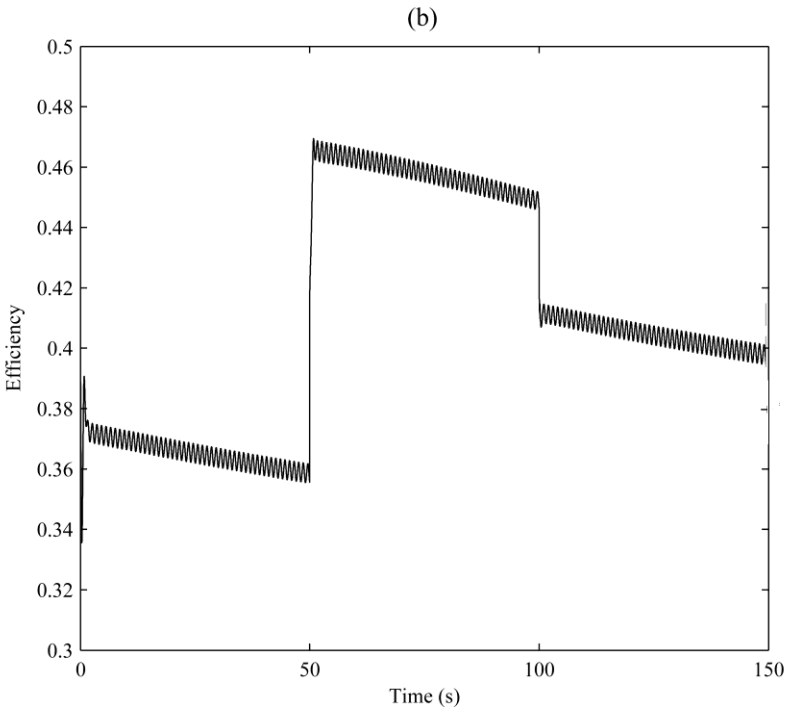

Figure 4.4 Performance of the MEPT controller: (b) Efficiency

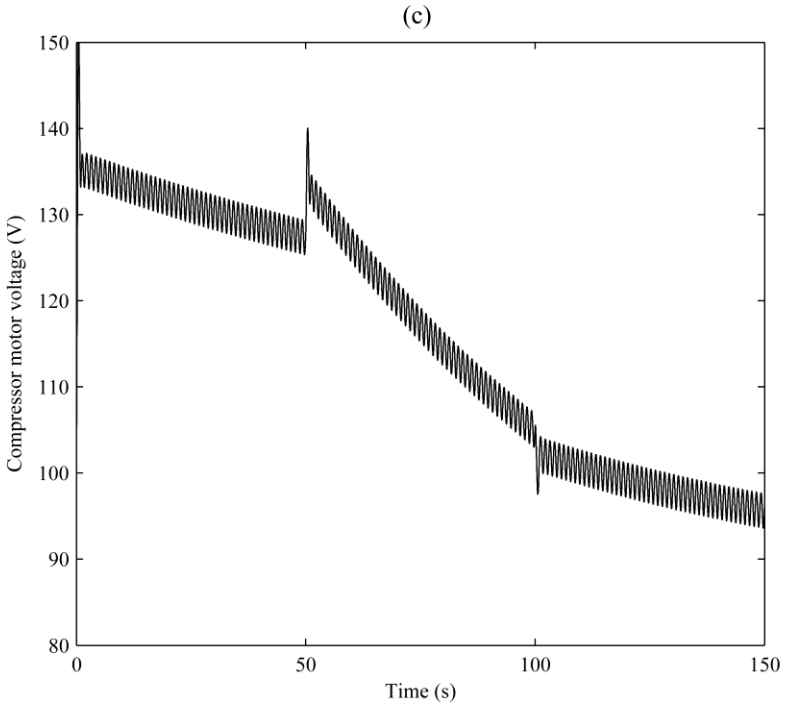

Figure 4.4 Performance of the MEPT controller: (c) Compressor motor voltage

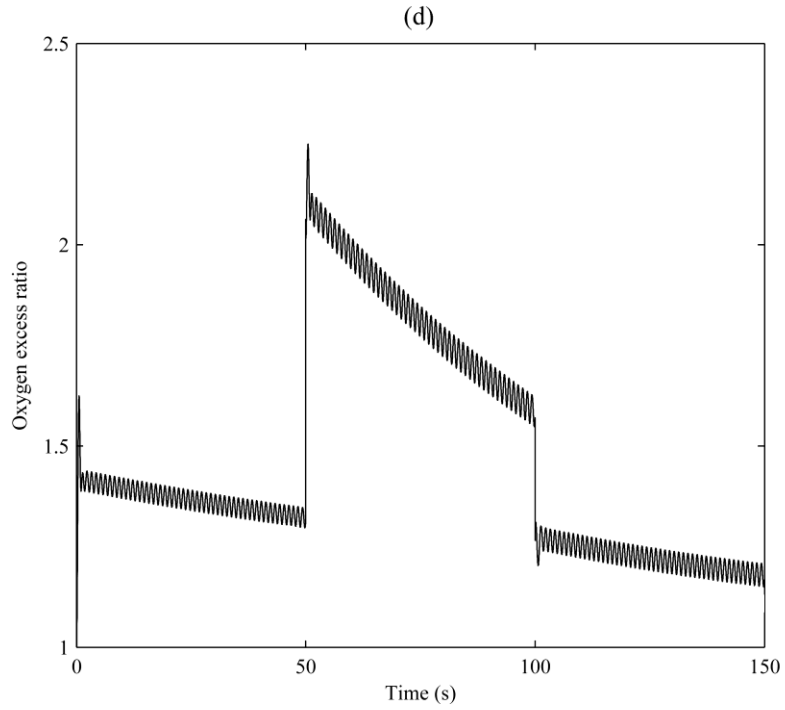

Figure 4.4 Performance of the MEPT controller: (d) Oxygen excess ratio

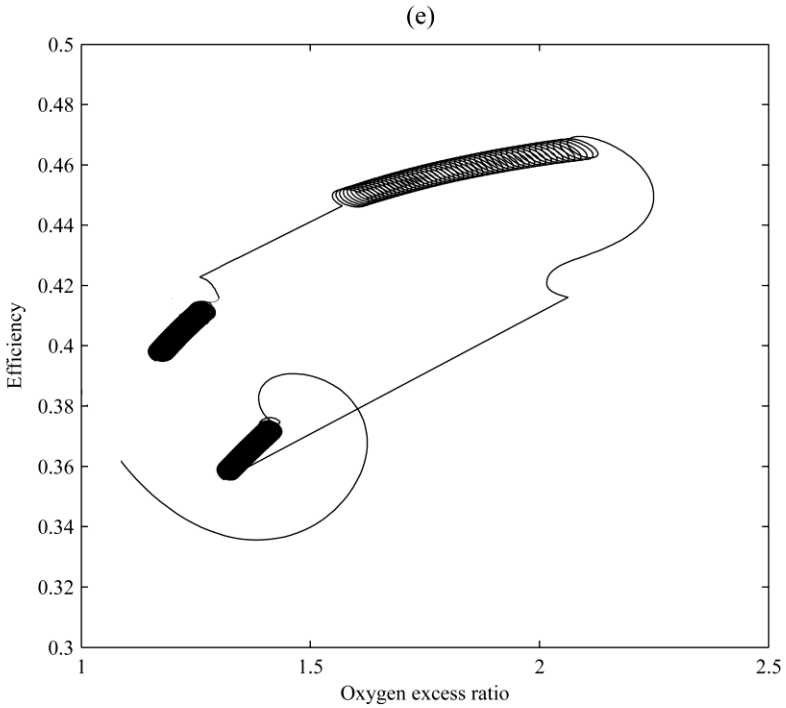

Figure 4.4 Performance of the MEPT controller: (e) Efficiency vs. oxygen excess ratio

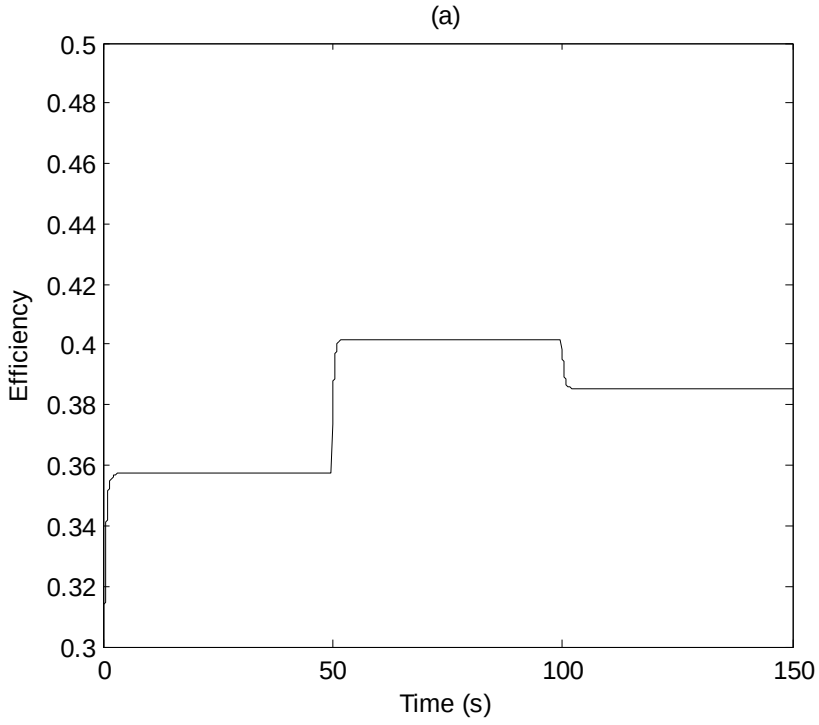

Figure 4.5 Response of PEMFC without controller: (a) Efficiency

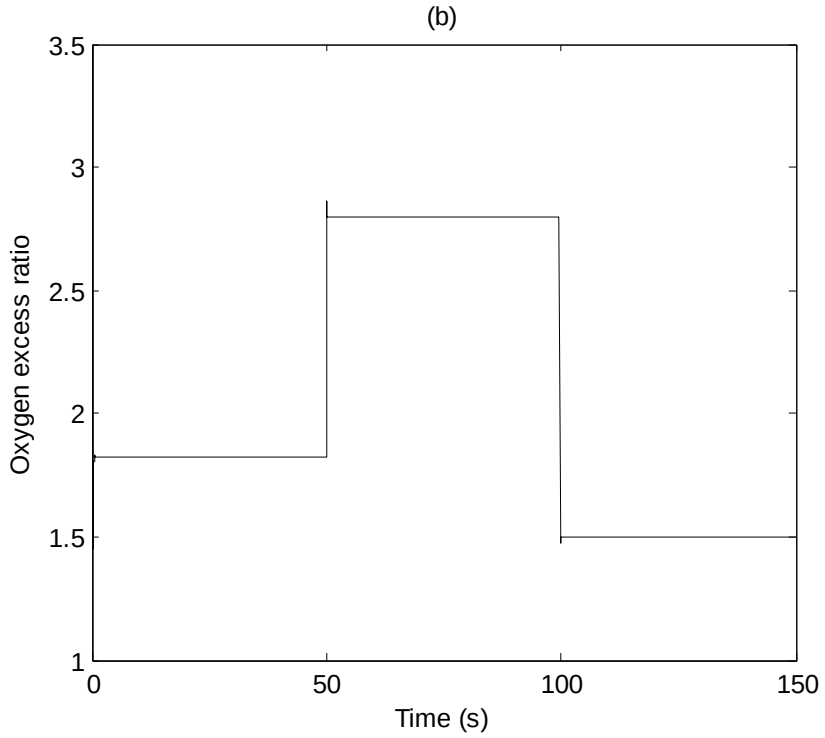

Figure 4.5 Response of PEMFC without controller: (b) Oxygen excess ratio

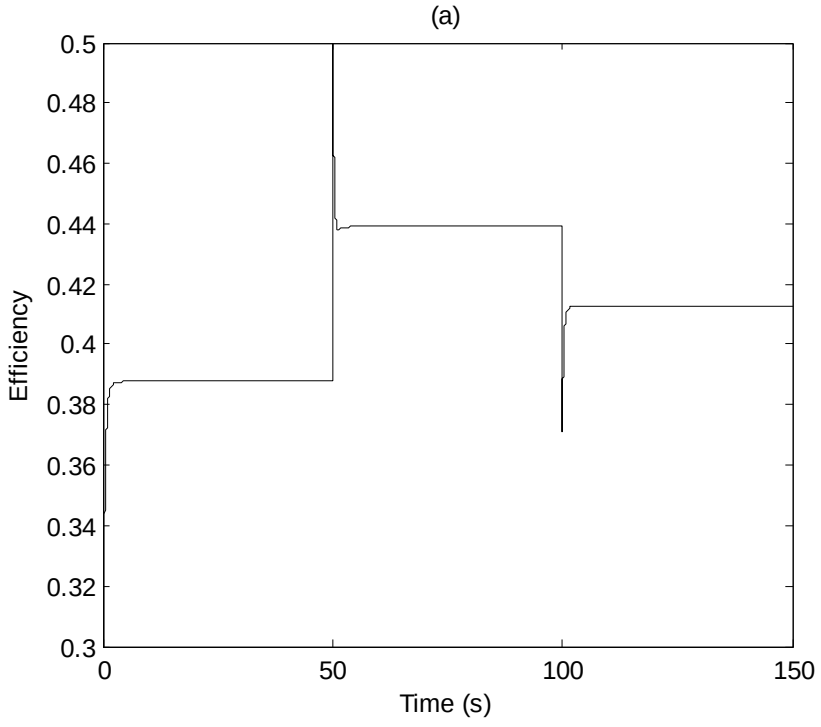

Figure 4.6 Response of PEMFC with Pukrusphan‘s controller: (a) Efficiency

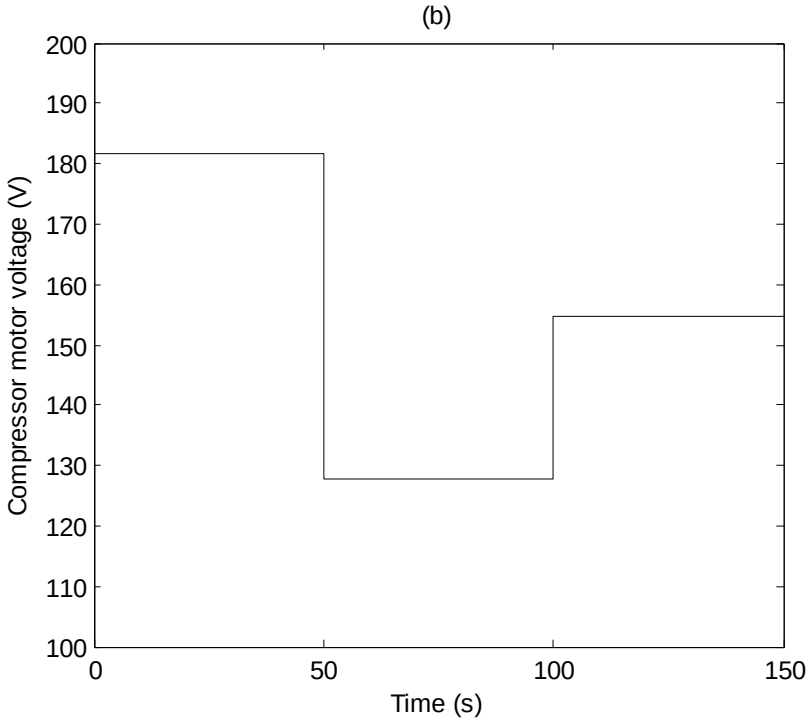

Figure 4.6 Response of PEMFC with Pukrusphan's controller: (b) Compressor motor voltage

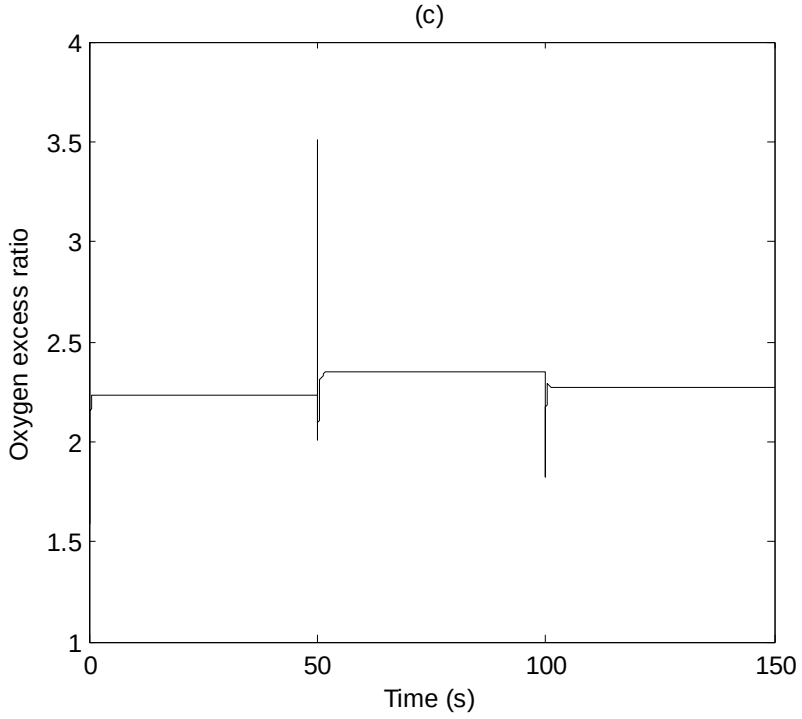

Figure 4.6 Response of PEMFC with Pukrusphan's controller: (c) Oxygen excess ratio

4.5 Conclusion

The objective of this chapter is to develop an optimal controller for the tracking of time-varying maximum efficiency point of PEMFC. First, the steady-state efficiency analysis is conducted. The result shows that the efficiency curves of PEMFC are unimodal with the peak determined by the combination of stack current and oxygen excess ratio. Then, the MPET controller is developed based on extremum seeking control theory. By searching for the optimal oxygen excess ratio in real-time, the proposed MPET controller is able to track the maximum efficiency point under changing stack current conditions. Simulations results show the operational efficiency achieved by the MEPT controller corresponds to the optimal values found by the steady-state analysis.

In the next chapter, a control-oriented thermal model is built and a linearized-model-based controller is developed for the thermal management of PEMFC. Current PEMFC operates in the temperature range of 60–80°C as required by the material of membrane electrolyte, most commonly Nafion®. Therefore, an efficient thermal management system is highly important for the safe operation of PEMFC.

Reference

[1] W. Na, B. Gou, "The efficient and economic design of pem fuel cell systems by multi-objective optimization," *J. Power Sources*, vol.166, pp. 411-418, 2007.

[2] A. C. Gillet, –From water to water. Hydrogen as a renewable energy vector for the future," in *Proceedings of World Renewable Energy Congress*, pp. 513–517, 1999.

[3] F. Barbir, –Recent progress and remaining technical issues in PEM fuel cell development," *in Proceedings of 13th World Hydrogen Energy Conference*, pp. 173–180, 2000.

[4] J. T. Pukrushpan, H. Peng, A. G. Stefanopoulou, "Simulation and analysis of transient fuel cell system performance based on a dynamic reactant flow model," in *Proceedings of ASME International Mechanical Engineering Congress and Exposition*, pp. 637-648, 2002.

[5] J. Sun, and I. Kolmanovsky, –Robust reference governor for fuel cell starvation protection," *IEEE Trans. Control Syst. Technol.*, vol. 13, pp. 911-920, 2005.

[6] A. Vahidi, A. G. Stefanopoulou, H. Peng, –Model predictive control for starvation prevention in a hybrid fuel cell system," in *Proceedings of American Control Conference*, pp. 834-839, 2004.

[7] B. Blunier, A. Miraoui, "Optimization and air supply management of a polymer electrolyte fuel cell," in *Proceedings of IEEE Conference on Vehicle Power and Propulsion*, pp. 273-279, 2005.

[8] D. Feroldi, M. Serra, J. Riera, "Performance improvement of a PEMFC system controlling the cathode outlet air flow," *J. Power Sources*, vol.169, pp. 205-212, 2007

[9] M. A. Danzer, J. Wilhelm, H. Aschemann, and E. P. Hofer, "Model-based control of cathode pressure and oxygen excess ratio of a PEM fuel cell system," *J. Power Sources*, vol.176, pp. 515-522, 2007.

[10] J. T. Pukrushpan, "Modeling and Control of Fuel Cell Systems and Fuel Processors," Ph.D. dissertation, University of Michigan, Ann Arbor, 2003.

[11] J. T. Pukrushpan, A. G. Stefanopoulou and H. Peng, *Control of fuel cell power systems: Principles, modeling, analysis, and feedback design*. Springer-Verlag London, 2004.

[12] J. T. Pukrushpan, A. G. Stefanopoulou and H. Peng, "Modeling and control for pem fuel cell stack system," *in Proceedings of American Control Conference*, vol. 4, pp. 3117-3122, 2002.

[13] M. Grujicic, K. M. Chittajallu, E. L. Law, J. T. Pukrushpan, "Model-based control strategies in the dynamic interaction of air supply and fuel cell," *in Proceedings of Institution of Mechanical Engineers, Part A: Journal of Power and Energy*, vol. 218, pp. 487-499, 2004.

[14] J. Lu, A. Zahedi, "Modelling and control of PEMFC based on support vector machine," in *Proceedings of Australiasian Universities Power Engineering Conference*, pp. 1-6, 2011.

[15] J. A. Adams, W. Yang, K. A. Oglesby, and K. D. Osborne, "The development of Ford's P2000 fuel cell vehicle," *SAE 2000 World Congress* 2000-01-1061.

[16] K. Suh, A. G. Stefanopoulou, "Performance limitations of air flow control in power-autonomous fuel cell systems," *IEEE Trans. Control Syst. Technol.*, vol. 15, pp. 465-473, 2007.

[17] F. Grasser, A. C. Rufer, "PEMFC system efficiency optimisation through model based control strategies," *in Proceedings of IEEE Conference on Vehicle Power and Propulsion*, pp. 1-6, 2006.

[18] M. Leblanc, "Sur la electrification des chemins de fer au moyen de coraunts alternatif de frequence elevee," *Revue Generale de l'Electricite*, vol. XII, pp. 275 – 277, 1922.

[19] M. Guay, T. Zhang, –Adaptive extremum seeking control of nonlinear dynamic systems with parametric uncertainties," *Automatica*, vol. 39, pp. 1283-1293, 2003.

[20] M. Krstic, H. Wang, "Stability of extremum seeking feedback for general nonlinear dynamic systems," *Automatica*, vol.36, pp. 595-601, 2000.

[21] A. Banaszuk, K. B. Ariyur, M. Krstic, C. A. Jacobson, "An adaptive algorithm for control of combustion instability and application to compressor instability control," *Automatica*, vol. 40, pp. 1965 – 1972, 2004

[22] K. S. Peterson, A. G. Stefanopoulou, "Extremum seeking control for soft landing of an electromechanical valve actuator," *Automatica*, vol. 40, pp. 1063 – 1069, 2004.

[23] C. Zhang, R. Ordonez, "Numerical optimization-based extremum seeking control with application to ABS design," *IEEE Trans. Autom. Control*, vol. 52, pp. 454 – 467, 2007.

[24] C. Zhang, D. Arnold, N. Ghods, A. Siranosian, and M. Krstic, "Source seeking with nonholonomic unicycle without position measurement and with tuning of forward velocity," *Syst. Control Lett.*, vol. 56, pp. 245 – 252, 2007.

[25] N. Hudon, M. Guay, M. Perrier, and D. Dochain, "Adaptive extremum-seeking control of convection – reaction distributed reactor with limited actuation," *Comput. Chem. Eng.*, vol. 32, pp. 2994 – 3001, 2008.

[26] J. Nocedal, S.Wright, *Numerical Optimization*, Springer New York, 1999.

[27] J. Lu, A. Zahedi, –Air Supply Control for Maximum Efficiency Point Tracking in Fuel Cell Systems," *J. Renewable Sustainable Energy*, vol. 4, paper no. 033106, pp. 1-15, 2012.

[28] S. J. Moura, "A Switched Extremum Seeking Approach to Maximum Power Point Tracking in Photovoltaic Systems," University of Michigan, Ann Arbor, Apr. 2009. [Online]. Available: www-personal.umich.edu/~sjmoura/files/EECS498.pdf

[29] Y. A. Chang, S. J. Moura, "Air flow control in fuel cell systems: An extremum seeking approach," in *Proceedings of American Control Conference*, pp. 1052-1059, *2009*.

[30] M. Grujicic, K. Chittajallu, J. T. Pukrushpan, "Control of the transient behaviour of polymer electrolyte membrane fuel cell systems," *in Proceedings of Institution of Mechanical Engineers, Part D: Journal of Automobile Engineering*, vol. 218, pp. 1239-1250, 2004.

[31] J. Lu, A. Zahedi, –Maximum efficiency point tracking control for fuel cell power systems," *in Proceedings of 2010 International Conference on Power system Technology*, pp. 1-6, 2010.

[32] D. DeHaan, M. Guay, "Extremum-seeking control of state-constrained nonlinear systems," *Automatica,* vol. 41, pp.1567-1574, 2005.

Chapter 5 Thermal Modelling and Management

The efficient thermal management has been considered as one of the most critical technical issues before PEMFC can be commercialized [1]. A PEMFC produces a similar amount of waste heat to its electric power output and tolerates only a small deviation in temperature from its design point. The balance between the heat production and its removal determines the operating temperature of a PEMFC. Since the heat generation changes continuously as the load current varies, it is extremely important to have thermal management system to control the heat removal and thus regulate the temperature to a safe range.

The major contributions of chapter 5 include: (1) The control-oriented thermal model of PEMFC is developed based on energy conservation principle. The model consists of two submodels: stack and coolant. (2) The model-based controller is designed based on the linearized thermal model. Since the thermal model is formulated in nonlinear affine form with disturbance, the input/output linearization method is employed by introuducing a dynamic feedforward/static state feedback law. The linearized model based controller is then designed for the temperature control.

The chapter is organized as follows: In section 5.1, the general issues of thermal management in PEMFC are discussed. Next in section 5.2, the existing thermal models and control methods are reviewed. In section 5.3, a control-oriented thermal model of PEMFC is developed. In section 5.4, a model-based controller is designed for the thermal management of PEMFC.

5.1 General issues of thermal management in PEMFC

5.1.1 Influence of temperature on PEMFC performance

Temperature is one of the key factors in determining the performance of PEMFC. A simple way to improve the performance is to operate PEMFC at its maximum allowed temperature. At higher temperature, electrochemical activities increase and reaction takes place at a higher rate, which in turn increases the efficiency [2].

Temperature in the cell also influences cell humidity, which significantly influences membrane ionic conductivity. In particular, PEMFC employs perfluorosulfonic acid polymers, most commonly Nafion®, as the membrane electrolyte. The requirement of good hydration of Nafion® (in order to have high proton conductivity) limits the maximum operating temperature to about 80°C [3].

The durability of the membrane electrolyte is another barrier for higher-temperature operation due to performance degradation during long-term operation. In particular, Nafion® membrane has the glass transition temperature ranging from 80 to 120°C, which leads to a serious break down of the MEA [4]. Furthermore, Endoh et al. [5] reported that the perfluorosulfonic acid polymer suffers from degradation under low-humidity operations even at 80°C. Therefore, the durability of the Nafion® membrane is another factor that limits the maximum operating temperature as 80°C.

On the other hand, low operating temperature deteriorates the performance of PEMFC. Cell temperature below 60°C may lead to water condensation and flooding of electrodes, with a resultant voltage loss caused by added resistance to reactant mass transport. A low operating

temperature is also undesirable as determined from consideration of proton conductivity and electrochemical reaction kinetics.

Summarizing, current PEMFC operates in the temperature range of 60 - 80°C and tolerates only a small temperature variation. This implies that an efficient thermal management system is required to regulate the temperature of PEMFC within this range when variations in operating conditions occur.

5.1.2 Overview of cooling methods

The cooling methods can be classified into two categories: passive cooling and active cooling. Passive cooling refers to design features used for cooling without power consumption. Typical passive cooling methods include heat spreaders, heat pipe and natural cooling with cathode air flow. In contrast, active cooling refers to the use of blowers or pumps to transport heat by circulating coolant. Generally, active cooling method can offer thermal capabilities that are superior to passive cooling. However, this is achieved at the cost of parasitic power and thus deteriorative effect on system efficiency. Typical active cooling methods include cooling with separate air flow, liquid cooling and phase change cooling. Several important factors should be considered when decide the proper cooling method, including the rated power of PEMFC, the working space and environment. Table 5.1 summarized the most commonly used cooling methods for PEMFC.

Table 5.1 Summary of cooling strategies for PEMFC [6]

Cooling strategy	Techniques	Advantages	Disadvantages/Challenges
Heat spreaders	Highly thermal conductive material	- Simple system - No internal coolant - Small parasitic power	- Limited heat transfer length - Highly thermal conductive material is expansive and poor in mechanical properties
Heat pipe	Heat pipes into cell	- Simple system - Small parasitic power - High thermal conductivity	- Integration of heat pipes with bipolar plates - Development of heat pipes with small thickness and low weight
Cooling with cathode air flow	Cathode air for cooling	- Simple system - Small parasitic power	- Drying out membrane
Cooling with separate air flow	Separate air channels for cooling	- Simple system - Small parasitic power	- Trade-off between cooling performance and parasitic power
Liquid cooling	Antifreeze coolant	- Strong cooling capacity - Flexible control	- Radiator size - Coolant degradation - Large parasitic power
Phase change cooling	Evaporative cooling	- Simultaneous cooling and internal humidification - Simplified system	- Dynamic control of water evaporation rate - Thermal mass of liquid water on cold start-up
	Cooling through boiling	- Elimination of coolant pump - Simplified system	- Development of suitable working media - Two-phase flow instability

5.2 Literature review of thermal models and control methods

5.2.1 Review of thermal models

Yu and Jung [7] developed a PEMFC system model with detailed cooling module to investigate of operating strategy of pump and fan. The models integrated model of fan, water pump, coolant passage, and electric motors. Their models were dynamic lump-parameters models. In another work proposed by the same group [8], a two-dimensional numerical thermal model of PEMFC is developed to simulate the temperature-sensitive electrochemical reaction and capture the thermal management effect on the performance. The model consists of three sub-models; a water transport model, an agglomerate structure electrochemistry model and a two-dimensional heat transfer model. Their heat transfer submodel was focused on heat rejection from the fuel cell into the cooling water and included the conduction heat

transfer inside the MEA and convective heat rejection from MEA to cooling water flow and gases. The thermal management system model included radiator, cooling pump and fan for investigating the trade-off between the temperature distribution effect and parasitic losses.

Bao et al. [9] modeled the key components in the water and thermal management system, namely the fuel cell stack, radiator, condenser and membrane humidifier. They are combined with a steady-state, one-dimensional, isothermal fuel cell model to analyze the effect of air stoichiometric ratio and the cathode outlet pressure on thermal loads of different components of PEMFC system.

Pharoah and Burheim [10] presented a two-dimensional thermal model to predict temperature distributions in PEMFC. It was found that the most significant factor in determining the temperature distribution was the gas channel geometry (width and channel type), followed by the thermal conductivity of the porous transport layer and state of the water in the cell.

Shimpalee and Dutta [11] proposed a numerical three-dimensional model that includes the energy equation to predict the temperature distribution inside a straight channel PEMFC and the effect of heat produced by the electrochemical reactions on fuel cell performance. This model gave details of current density, temperature contours, and velocity profiles in both cross-flow plane and axial-flow plane that cannot be obtained by simplistic one-dimensional and two-dimensional simulations.

Ju et al. [12] presented a three-dimensional thermal model coupled with electrochemical and mass transport models in order to study thermal and water management in PEMFC. It was

found by their numerical simulation that the thermal effect on PEMFC became more critical at higher current density and/or lower gas diffusion layer thermal conductivity.

5.2.2 Review of control methods

Lee et al. [13] designed a proportional integral derivative (PID) controller to regulate the coolant flow rate under various current density ($0.2A \cdot cm^{-2}$, $0.4A \cdot cm^{-2}$ and $0.6A \cdot cm^{-2}$). However, the control accuracy was fairly low. The minimum error of steady state was zero, the maximum error was $13^{o}C$, and the average error was $40^{o}C$ (the set point is $65^{o}C$) .

Lauzze and Chmielewski [14] proposed a proportional integral (PI) feedback structure for the power/temperature controller of PEMFC. The controller used jacket flow rate as the manipulated input to bring the temperature back to the temperature set-point when the output power of PEMFC increased. It was also found that the low power limit of PEMFC should be carefully considered. If the power limit was too low, the coolant flow may be saturated at a value of zero, which means the cell cannot maintain the desired operating temperature.

Ahn and Choe [15] proposed a state feedback control strategy with a feed-forward of the disturbance and a compensator for minimization of the temperature effect on the air flow rate. The output states were the coolant flow rate and the stack inlet coolant temperature. Classic PI controller was also tested for the sake of comparison. The state feedback controller showed better performance in terms of response speed and overshoot. Moreover, the state feedback controller consumed less parasitic power than that of PI controller.

Methekar et al. [16] proposed a linear ratio control strategy to control the average power density and average solid temperature. Their control strategy was based on the transfer

function model, which was obtained from step tests on the distributed parameter PEMFC model. The manipulated variables were selected using steady-state relative gain array (RGA) analysis to be the inlet molar flow rates of hydrogen and coolant. However, the performance of the linear controllers was slow due to the presence of nonlinearities in the dynamic response of the PEMFC.

Hua et al. [17] proposed an incremental fuzzy controller with integrator to regulate the coolant flow rate and bypass valve factor for the temperature control of PEMFC. The controller was able to overcome sudden disturbance, and the integrator eliminated temperature steady state error. The simulation results demonstrated that the fuzzy controllers were more robust than their conventional counterparts under the model parameters variation test.

5.3 Development of control-oriented thermal model of PEMFC

In this section, the dynamic thermal model of PEMFC is developed based on the energy conservation principle. The thermal model consists of two submodels: the stack and the coolant. Thus, the model has two state variables: the stack temperature and the coolant temperature. The stack current is considered as the disturbance input, which corresponds to uncontrollable load demand. The coolant flux is modeled as the manipulated input to regulate the temperature when variations in the stack current occur. For simplification, some necessary assumptions are given as follows: (1) All gases are ideal gases and fully saturated with water vapour. (2) The produced water is in the liquid phase. (3) The input gases are proportionally changing according to the consumed gases. The parameters used in the model are shown in Table 5.2.

Table 5.2 Summary of thermal model parameters

Parameters	Description	Unit	Value
C_{H_2}	The heat capacity of hydrogen	J/mol/K	28.944
$C^{g}_{H_2O}$	The heat capacity of vapour	J/mol/K	33.590
$C^{l}_{H_2O}$	The heat capacity of water	J/mol/K	75.370
C_{O_2}	The heat capacity of oxygen	J/mol/K	29.696
C_{N_2}	The heat capacity of nitrogen	J/mol/K	29.148
C_{st}	The heat capacity of stack	J/ K/ kg	4000
C_{rv}	The heat capacity of reservoir	J/ K/ kg	450
F	Faraday constant	C/mol	96485
H	Heating value of hydrogen	J/mol	285500
M_{st}	Stack mass	kg	17.5
M_{rv}	Reservoir mass	kg	20
n	Cell number		112
R_t	Thermal resistance	K/W	0.145
T_{amb}	Ambient temperature	K	298

5.3.1 Thermal model of PEMFC stack

The energy balance of the PEMFC stack is determined by the total heat produced by the electrochemical reaction Q_{tot}, the heat brought in by the input gas flow Q_{in}, the power consumed by the electrical load P_{st}, the heat brought out by the exhaust gas flow Q_{out}, and the heat loss at the stack surface Q_{amb}, the heat removed by convection between the stack and the coolant Q_{conv}. Considering the transient heat variation, the dynamic thermal model of the PEMFC stack can be described as follows:

$$M_{st} C_{st} \frac{dT_{st}}{dt} = \dot{Q}_{tot} + \dot{Q}_{in} - P_{st} - \dot{Q}_{out} - \dot{Q}_{amb} - \dot{Q}_{conv} \tag{5.1}$$

where M_{st} is the PEMFC stack mass, and C_{st} is the PEMFC heat capacity.

- Q_{tot}

The total energy produced by electrochemical reaction is calculated as the product of the heating value of hydrogen H and the reacted hydrogen molar flow rate $N_{an,H_2}^{reacted}$:

$$\dot{Q}_{tot} = H \times N_{an,H_2}^{reacted} \tag{5.2}$$

- Q_{in}

The reacted hydrogen molar flow rate $N_{an,H_2}^{reacted}$, the reacted oxygen molar flow rate $N_{ca,O_2}^{reacted}$, and the generated water molar flow rate N_{ca,H_2O}^{gen} can be expressed as the functions of the cells number n, the PEMFC stack current I_{st} and the Faraday constant F.

$$N_{an,H_2}^{reacted} = nI_{st} / (2F) \tag{5.3}$$

$$N_{ca,O_2}^{reacted} = nI_{st} / (4F) \tag{5.4}$$

$$N_{ca,H_2O}^{gen} = nI_{st} / (2F) \tag{5.5}$$

According to assumption (3), the anode input hydrogen molar flow rate N_{an,H_2}^{in} is set as λ_{H_2} times of the reacted hydrogen molar flow rate $N_{an,H_2}^{reacted}$. Similarly, the cathode input air molar flow rate $N_{ca,air}^{in}$ is set as the λ_{O_2} times of the reacted air molar flow rate $N_{ca,O_2}^{reacted} / 21\%$.

$$N_{an,H_2}^{in} = \lambda_{H_2} N_{an,H_2}^{reacted} \tag{5.6}$$

$$N_{ca,air}^{in} = \lambda_{O_2} N_{ca,O_2}^{reacted} / 21\% \tag{5.7}$$

Simultaneously, according to assumption (1), the anode input vapor molar flow rate N_{an,H_2O}^{in} and the cathode input vapor molar flow rate N_{ca,H_2O}^{in} are calculated as below:

$$N_{an,H_2O}^{in} = \frac{P_{sat}}{P_{an} - P_{sat}} N_{an,H_2}^{in} \tag{5.8}$$

$$N_{ca,H_2O}^{in} = \frac{P_{sat}}{P_{ca} - P_{sat}} N_{ca,air}^{in} \tag{5.9}$$

Therefore, the heat brought into the stack by the input gas flow is calculated as follows:

$$\dot{Q}_{in} = (N_{an,H_2}^{in} C_{H_2} + N_{an,H_2O}^{in} C_{H_2O}^{g})(T_{an}^{in} - T_{st}) + (N_{ca,air}^{in} C_{air} + N_{ca,H_2O}^{in} C_{H_2O}^{g})(T_{ca}^{in} - T_{st}) \tag{5.10}$$

- P_{st}

The electrical energy produced by PEMFC stack is calculated as the product of the PEMFC stack current I_{st} and voltage V_{st}:

$$P_{st} = V_{st} I_{st} \tag{5.11}$$

- Q_{out}

According to the molar conservation principles, the gases output molar flow rate are presented below:

$$N_{an,H_2}^{out} = N_{an,H_2}^{in} - N_{an,H_2}^{reacted} \tag{5.12}$$

$$N_{ca,o_2}^{out} = N_{ca,o_2}^{in} - N_{ca,o_2}^{reacted} \tag{5.13}$$

$$N_{ca,N_2}^{in} = 0.79 N_{ca,air}^{in} \tag{5.14}$$

The anode/cathode vapor outputs are shown as follows:

$$N_{an,H_2O}^{out} = N_{an,H_2O}^{in} - \frac{P_{sat}}{P_{an} - P_{sat}} N_{an,H_2}^{reacted} \tag{5.15}$$

$$N_{ca,H_2O}^{out} = N_{ca,H_2O}^{in} - \frac{P_{sat}}{P_{an} - P_{sat}} N_{ca,O_2}^{reacted} \tag{5.16}$$

According to assumption (2), the heat brought out by the exhaust gas and water is calculated as below:

$$\dot{Q}_{out} = (N^{out}_{an,H_2} C_{H_2} + N^{out}_{an,H_2O} C^{g}_{H_2O} + N^{out}_{ca,O_2} C_{O_2} + N^{out}_{ca,N_2} C_{N_2} + N^{out}_{ca,H_2O} C^{g}_{H_2O} + N^{gen}_{ca,H_2O} C^{l}_{H_2O})(T_{st} - T_{amb}) \quad (5.17)$$

- Q_{amb}

The heat loss at the PEMFC stack surface is calculated as below:

$$\dot{Q}_{amb} = (T_{st} - T_{amb}) / R_t \quad (5.18)$$

where T_{amb} is the ambient temperature, R_{t} is the PEMFC thermal resistance.

- Q_{conv}

According to the thermal convection principle [18], the convection between the stack and the coolant is calculated as:

$$\dot{Q}_{conv} = A_p h(T_{st} - \frac{T_{cl} + T_{amb}}{2}) \quad (5.19)$$

5.3.2 Thermal model of coolant

Similarly, the coolant temperature in the reservoir is expressed as below:

$$M_{rv} C_{rv} \frac{dT_{cl}}{dt} = \dot{Q}_{conv} - \dot{Q}_{cl} \quad (5.20)$$

where M_{rv} is the reservoir mass, and C_{rv} is the reservoir heat capacity.

The heat removed by the coolant is:

$$\dot{Q}_{cl} = C^{l}_{H_2O} M_{cl} (T_{cl} - T_{amb}) \quad (5.21)$$

where M_{cl} is the coolant flux.

Finally, we arrive at the following expression for the thermal model of PEMFC

$$\begin{cases} \dot{T} = f(T) + g(T)M_{cl} + w(T)I_{st} \\ y = h(T) \end{cases} \tag{5.22}$$

where $T = \begin{bmatrix} T_{st} \\ T_{cl} \end{bmatrix}$, $f(T) = \begin{bmatrix} a_1 T_{st} + a_2 T_{cl} + a_3 \\ b_1 T_{st} + b_2 T_{cl} + b_3 \end{bmatrix}$, $g(T) = \begin{bmatrix} 0 \\ b_4 T_{cl} + b_5 \end{bmatrix}$, $w(T) = \begin{bmatrix} a_4 T_{st} + a_5 \\ 0 \end{bmatrix}$, $h(T) = T_{st} - T_0$

As can be seen from the above expression, the state variables are the stack temperature T_{st} and the coolant temperature T_{cl}, the coolant flux M_{cl} is the manipulated input, and the stack current I_{st} is the disturbance input. $a_1 \sim a_5$, $b_1 \sim b_5$ are constant coefficients, T_0 is the predetermined set point.

This thermal model is nonlinear with disturbances and uncertainty. The main reasons are as follows: (1) the stack current I_{st} is considered as disturbance, which corresponds to uncontrollable load; (2) many physical parameters may vary to a large extent under different operating conditions.

5.3.3 Model validation

The thermal model is validated by comparing with the experimental data reported by Lebbal and Lecoeuche [19], as shown in Figure 5.1. The figure shows an example of how PEMFC reaches its operating temperature. As can be seen, the proposed thermal model fits very well with the experimental data and accurately presents the temperature dynamics of PEMFC. Indeed the error between the proposed model and experimental data is very small. The maximum relative error is less than 0.08%.

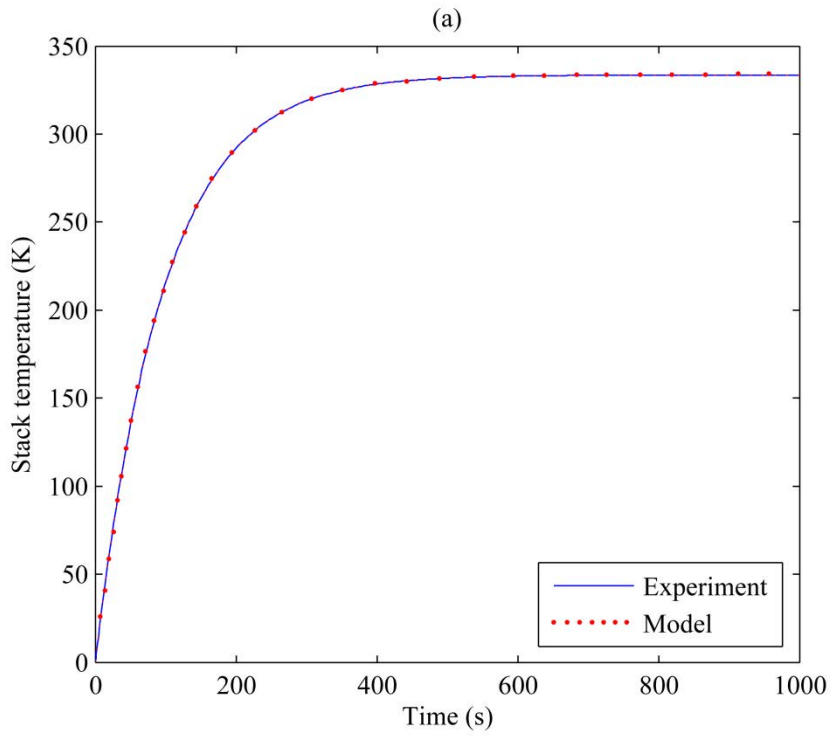

Figure 5.1 Thermal model validation: (a) Experimental data and thermal model

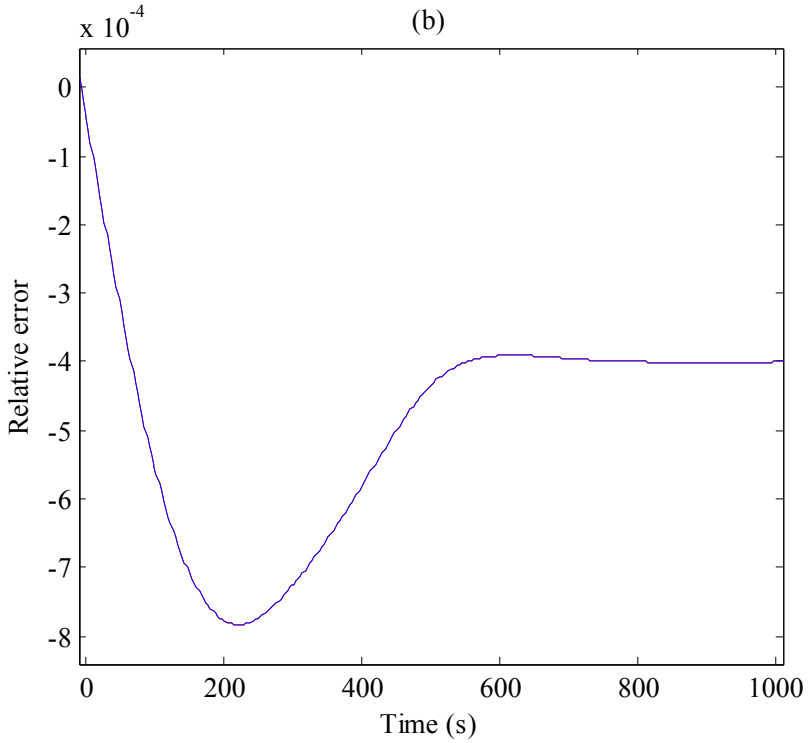

Figure 5.1 Thermal model validation: (b) Relative error

5.4 Thermal controller design

Since the thermal model described by (5.22) is formulated in nonlinear affine form with disturbance, the input/output linearization method is employed by introuducing a dynamic feedforward/static state feedback law. A model-based controller is then designed after linearization.

Given a nonlinear system with measured disturbance:

$$S_1 : \begin{cases} \dot{x} = f(x) + g(x)u + \sum_{k=1}^{p} w_k(x) d_k \\ y = h(x) \end{cases} \tag{5.23}$$

where $x \in R^n$ denotes the vector of state variables, $u \in R^1$ denotes a manipulated input, d_k denotes a measurable disturbance input, and $y \in R^1$ denotes an output (to be controlled). $f(x)$, $g(x)$, $w_k(x)$ denote analytic vector fields, and $h(x)$ denotes analytic scalar fields.

In the following discussion, standard Lie derivative notation will be using:

$$L_f h(x) = \sum_{l=1}^{n} \frac{\partial h(x)}{\partial x_l} f_l(x) \tag{5.24}$$

where $f_l(x)$ denotes the l-th row element of $f(x)$.

One can define higher order Lie derivatives as well as mixed Lie derivative in an obvious way:

$$L_f^0 h(x) = h(x) \tag{5.25}$$

$$L_f^k h(x) = L_f (L_f^{k-1} h(x)) \tag{5.26}$$

$$L_g L_f^{k-1} h(x) = L_g (L_f^{k-1} h(x)) \tag{5.27}$$

Then, the relative order of the output y with respect to the manipulated input vector u, r is defined as the smallest integer for which [20]:

$$L_g L_f^{r-1} h(x) \neq 0 \tag{5.28}$$

Similarly, the relative order of the output y with respect to the disturbance input d_k, ρ_k is defined as the smallest integer for which [20]:

$$L_{w_k} L_f^{\rho_k - 1} h(x) \neq 0 \tag{5.29}$$

Theorem: Consider a nonlinear system in the form of (5.23). Let r, ρ_k denote the relative orders of output y with respect to manipulated input u and disturbance input d_k, respectively. Then the dynamic feedforward/static state feedback law [21]:

$$u = \frac{v - \sum_{j=0}^{r} \alpha_j L_f^j h(x) - \sum_{d_k} \alpha_r L_{w_k} L_f^{r-1} h(x) d_k - \sum_{d_k} \sum_{l=0}^{r-\rho_k} \sum_{j=\rho_k+1}^{r} \alpha_j \frac{d^l}{dt^l} (L_{w_k} L_f^{j-l-1} h(x) d_k)}{\alpha_r L_g L_f^{r-1} h(x)} \tag{5.30}$$

induces to a disturbance-free linear input/output behaviour:

$$S_2 : \sum_j \alpha_j \frac{d^j y}{dt^j} = \mathrm{v} \tag{5.31}$$

where a_j are adjustable parameters, v is the input after linearization.

Form (5.22), it can be easily verified that: $L_g L_f^0 h(T) = 0;\ L_g L_f^1 h(T) \neq 0;\ L_w L_f^0 h(T) \neq 0.$ Consequently, the relative order of the output with respect to the manipulated input M_{cl} is r=2, the relative order of the output with respect to the disturbance input I_{st} is ρ=1. In order to stabilize the system after linearization, the poles of the corresponding linear system can be chosen as s_1=-1, s_2=-2. Since $a_0+a_1 s+a_2 s^2=(s+1)(s+2)$, then a_0=2, a_1=3, a_2=1. Therefore, one obtains the dynamic feedforward/static state feedback law:

$$M_{cl}=\frac{v-\sum_{j=0}^{2}\alpha_j L_f^j h(T)-\sum_{r=1}^{2}\alpha_r L_w L_f^{r-1}h(T)I_{st}-\alpha_2\frac{d}{dt}(L_w h(T)I_{st})}{\alpha_2 L_g L_f h(T)} \tag{5.32}$$

induce the linear input/output behaviour:

$$\frac{d^2y}{dt^2}+3\frac{dy}{dt}+2y=v \tag{5.33}$$

(5.33) can be rewritten as the state-space form:

$$\begin{cases}\dot{x}=Ax+Bv\\ y=Cx\end{cases} \tag{5.34}$$

where $A=\begin{bmatrix}0 & 1\\ -2 & -3\end{bmatrix}$, $B=\begin{bmatrix}0\\ 1\end{bmatrix}$, $C=\begin{bmatrix}1 & 0\end{bmatrix}$,

Following the standard procedure of LQR controller design with ***Q***=1, ***R***=1, one constructs the controller:

$$v=-0.236x_1(t)-0.0777x_2(t)+0.2448T_0 \tag{5.35}$$

where $x_1(t)=T_{st}$, $x_2(t)=T_{st}/dt$. T_0 is the set point. Figure 5.2 show the schematic of PEMFC thermal system implemented in the MATLAB/SIMULINK environment.

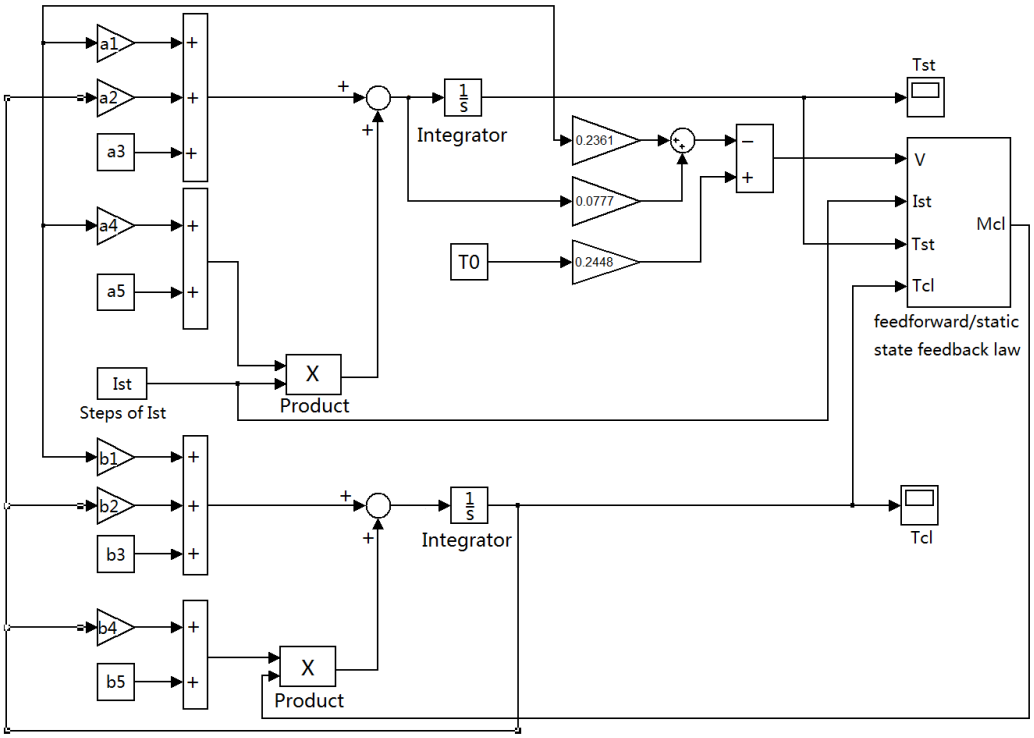

Figure 5.2 Schematic of PEMFC thermal system implemented in SIMULINK [22]

5.5 Simulation results and discussion

To demonstrate the effectiveness of the proposed controller, a load disturbance is assumed, which causes step changes of the stack current I at t = 1000 s and t = 2000 s, respectively. The corresponding operation parameters of PEMFC are demonstrated below. Hydrogen input flow rate factor λ_{H_2} = 1.5, air input flow rate factor λ_{O_2} = 2, anode/cathode input temperature $T_{an}^{in} = T_{ca}^{in}$ = 323 K, anode pressure P_{an} = 2.9 atm, cathode pressure P_{ca} = 3 atm. The target value of stack temperature T_0 here is taken as a constant and set to 353 K (80°C).

Simulation results are shown in Figure 5.3. Figure 5.3(a) shows the step changes of stack current that acts as the disturbance input, which arises from uncontrollable load demand. The corresponding movements of manipulated input, coolant flux, are shown in Figure 5.3(b). Figure 5.3(c) and Figure 5.3(d) show the variations in stack temperature and coolant temperature, respectively.

As shown in Figure 5.3(a), the stack current steps from 60 A to 100 A at the 1000 s, which leads to a sudden increase in the total energy produced by PEMFC. In order to maintain the operational temperature of PEMFC, the coolant flux increases accordingly, serving to remove the excessive heat generated, as shown in Figure 5.3(b). On the other hand, when the stack current steps from 100 A to 40 A at the 2000 s, coolant flux decreases as the energy produced by PEMFC decreases. The result displayed in Figure 5.3(c) shows that the proposed control algorithm can track the temperature set point well, with error less than 1K (measured at 353K), which is acceptable for engineering applications. Compared with PID control strategy in literature [13], the proposed method achieves better performance in terms of control accuracy.

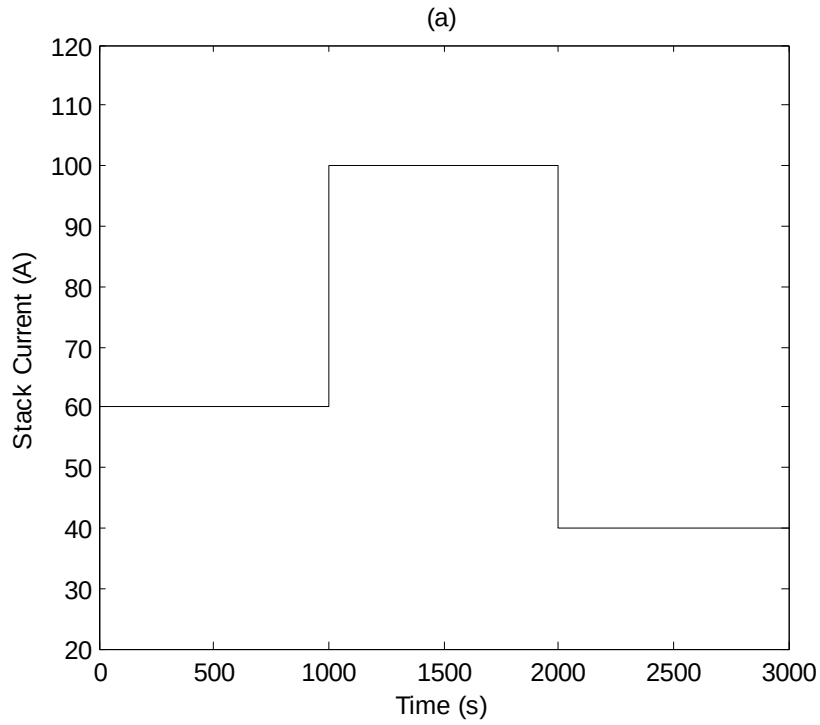

Figure 5.3 Performance of the proposed thermal controller: (a) Stack current

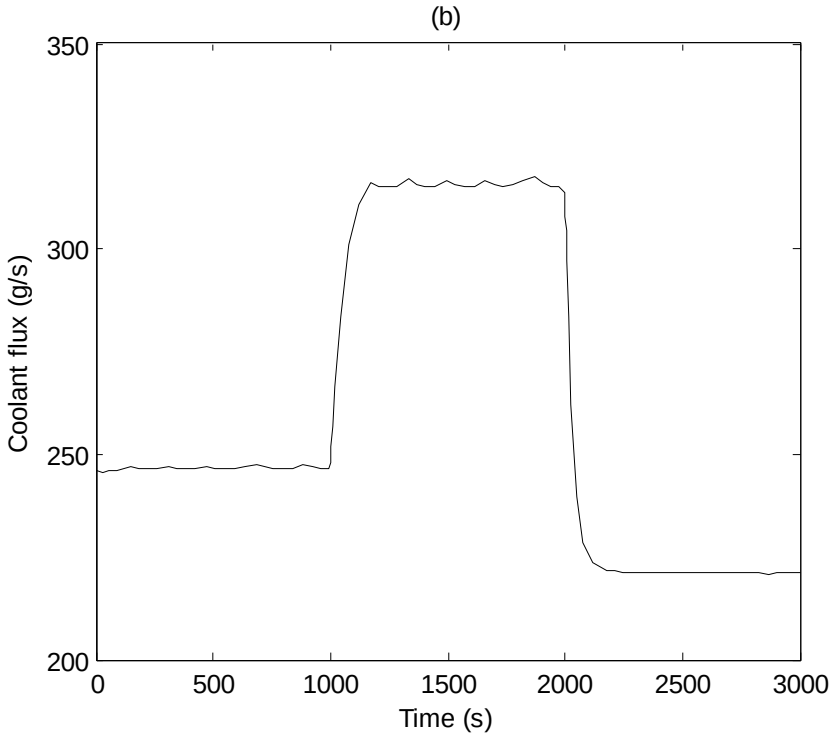

Figure 5.3 Performance of the proposed thermal controller: (b) Coolant flux

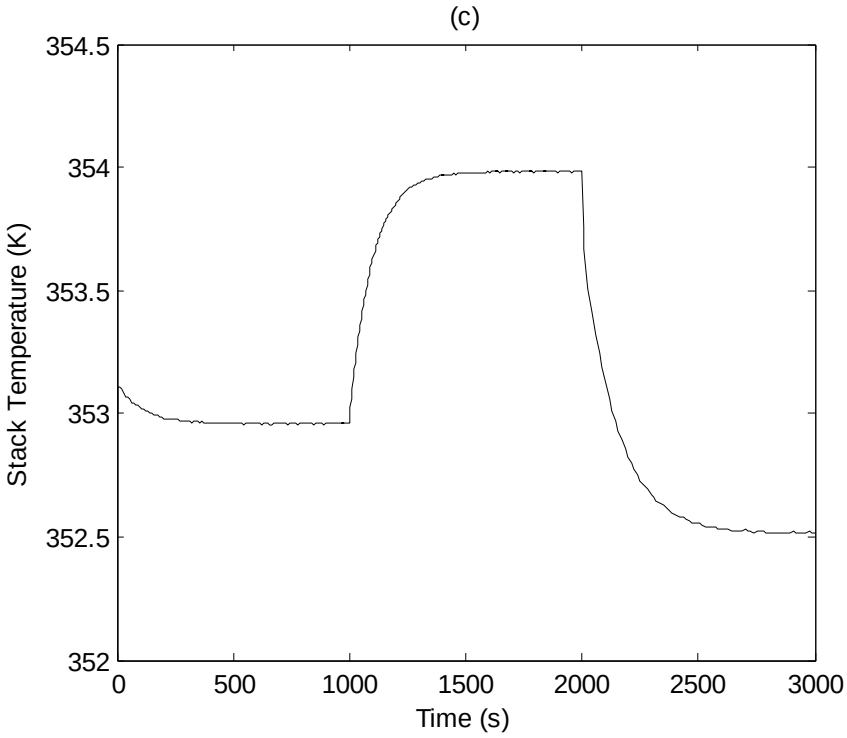

Figure 5.3 Performance of the proposed thermal controller: (c) Stack temperature

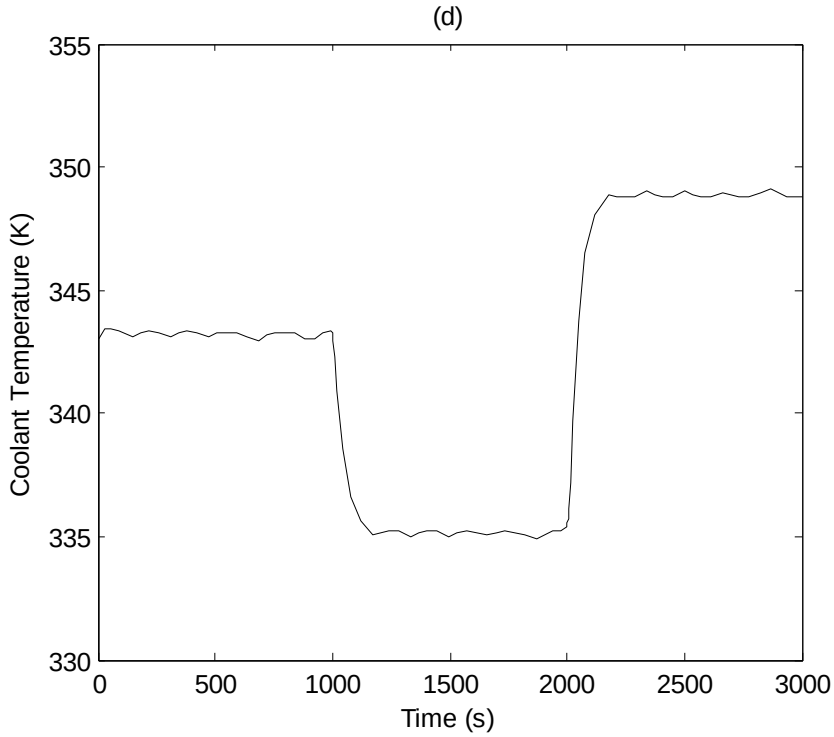

Figure 5.3 Performance of the proposed thermal controller: (d) Coolant temperature

5.6 Conclusion

The objective of this chapter is to propose a model-based controller for the thermal management of PEMFC. First, the control-oriented thermal model that considers both PEMFC stack and coolant is developed based on the energy conservation principle. Since the model is formulated in nonlinear affine form with disturbance, the input/output linearization method is employed by introuducing a dynamic feedforward/static state feedback law. The temperature controller is then designed based on the linearized model. The simulation results demonstrate that the proposed controller has superior performance than PID controller in terms of accuracy.

In the next chapter, several key issues concerning China‘s transition towards hydrogen economy are reviewed. As an emerging giant of the world economy and international energy markets, China is transforming the global energy system by dint of its sheer size and its growing weight in international energy trade. How rapidly China‘s energy needs develop and how they are met will have far-reaching consequences for the rest of the world. This chapter, for the first time, provides a full picture of future hydrogen economy in China, including drivers, resources and technologies.

Reference

[1] R. Shimoi, M. Masuda, K. Fushinobu, Y. Kozawa, K. Okazaki, "Visualization of the membrane temperature field of a polymer electrolyte fuel cell," *J. Energy Res. Technol.*, vol. 126, pp. 258 – 261, 2004.

[2] A. Faghri, Z. Guo, "Challenges and opportunities of thermal management issues related to fuel cell technology and modelling," *Int. J. Heat Mass Transfer*, vol. 48, pp. 3891-3920, 2005.

[3] T. J. P. Freire, E. R. Gonzalez, "Effect of membrane characteristics and humidification conditions on the impedance response of polymer electrolyte fuel cells," *J. Electroanal. Chem.*, vol. 503, pp.57-68, 2001.

[4] H. A. Gasteiger, M. F. Mathias, "Fundamental research and development challenges in polymer electrolyte fuel cell technology," *in Proceedings of 3rd International Symposium on Proton Conducting Membrane Fuel Cells*, pp.1-24, 2004.

[5] E. Endoh, S. Terazono, H. Widjaja, Y. Takimoto, "Degradation Study of MEA for PEMFCs under Low Humidity Conditions," *Electrochem. Solid-State Lett.*, vol. 7, pp. A209-A211, 2004.

[6] G. Zhang, S. G. Kandlikar, "A critical review of cooling techniques in proton exchange membrane fuel cell stacks," *Int. J. Hydrogen Energy*, vol. 37, pp. 2412-2429, 2011.

[7] S. Yu, D. Jung, "A study of operation strategy of cooling module with dynamic fuel cell system model for transportation application," *Renewable Energy,* vol. 35, pp.2525-2532, 2010.

[8] S. Yu, D. Jung, "Thermal management strategy for a proton exchange membrane fuel cell system with a large active cell area," *Renewable Energy,* vol. 33, pp.2540-2548, 2008.

[9] C. Bao, M. Ouyang, B. Yi, –Analysis of the water and thermal management in proton exchange membrane fuel cell systems," *Int. J. Hydrogen Energy*, vol. 31, pp. 1040-1057, 2006.

[10] J. G. Pharoah, O. S. Burheim, –On the temperature distribution in polymer electrolyte fuel cells," *J. Power Sources*, vol. 195, pp. 5235-5245, 2010.

[11] S. Shimpalee, S. Dutta, –Numerical prediction of temperature distribution in PEM fuel cells," *Numer. Heat Transfer, Part A*, vol. 38, pp. 111-128, 2000.

[12] H. Ju, H. Meng, C. Y. Wang, –A single-phase, non-isothermal model for PEM fuel cells," *Int. J. Heat Mass Transfer*, vol. 48, pp. 1303-1315, 2005.

[13] H. I. Lee, C. H. Lee, T. Y. Oh, S. G. Choi, I. W. Park, K. K. Baek, –Development of 1kW class polymer electrolyte membrane fuel cell power generation system," *J. Power Sources*, vol. 107, pp. 110–119, 2002.

[14] K. C. Lauzze, D. J. Chmielewski, –Power Control of a Polymer Electrolyte Membrane Fuel Cell," *Ind. Eng. Chem. Res.*, vol. 45, pp. 4661-4670, 2006.

[15] J. W. Ahn, S. Y. Choe, –Coolant controls of a PEM fuel cell system," *J. Power Sources*, vol. 179, pp. 152–164, 2008.

[16] R.N. Methekar, V. Prasad, R.D. Gudi, –Dynamic analysis and linear control strategies for proton exchange membrane fuel cell using a distributed parameter model," *J. Power Sources*, vol. 165, pp. 152–170, 2006.

[17] P. Hua, G. Y. Cao, X. J. Zhu, M. R. Hu, "Coolant circuit modeling and temperature fuzzy control of proton exchange membrane fuel cells," *Int. J. Hydrogen Energy*, vol. 35, pp. 9110-9123, 2010.

[18] F. P. Incropera, D. P. Dewitt, *Fundamentals of Heat Transfer*, John Wiley&Sons New York, 1985.

[19] M. E. Lebbal, S. Lecoeuche, –Identification and monitoring of a PEM electrolyser based on dynamical modelling," *Int. J. Hydrogen Energy*, vol. 34, pp. 5992-5999, 2009.

[20] D. Prodromos, K. Costas, –Dynamic compensation of measurable disturbances in non-linear multivariable systems," *Int. J. control*, vol. 58, pp.1279-1301, 1993.

[21] L. L. Li, C. A. Zhao, G. J. Yang, H. Yu, –Feedfoward/feedback linearization of nonlinear systems with measurable disturbances," *Electric Machines and Control*, vol. 4, pp. 31-34, 2000.

[22] J. Lu, A. Zahedi, –Thermal modelling and management of proton exchange membrane fuel cell," *Energy Sources, Part A Recovery, Utilization and Environmental Effects*, in press.

Chapter 6 Building the Hydrogen Economy in China

China is unique in terms of its vast area, huge population and rapid economic growth. These factors pose a great challenge to ensure a continuous and sufficient energy supply. This is especially true considering the fact that China has been the world‘s second largest net importer of oil since 2009. In addition, the structure of China‘s economy also has a major impact on its greenhouse-gas emissions profile and its consequent approach to addressing climate change. Currently, China relies heavily upon coal-fired power for electricity generation and is the leading emitter of greenhouse gases. Hydrogen shows the great potential in solving China‘s concerns for improving energy security and reducing greenhouse gas emissions. Besides its large coal reserve, China has abundant and widely distributed renewable energy resources. The use of hydrogen can facilitate the exploitation the renewable energy resources, thus diversifying the energy supply. Moreover, hydrogen is the cleanest fuel especially when coupled with fuel cell. Motivated by the enormous advantages, China is taking the first steps towards future hydrogen economy.

The major contributions of chapter 6 include: (1) China‘s main drivers for the transition towards the hydrogen economy are indentified, including energy security, climate change, urban air pollution and competiveness. (2) China‘s energy supply matrix is reviewed, including both fossil fuels (coal, oil and natural gas) and renewable resources (hydro, wind, solar, biomass). The potential role of different energy resources in future hydrogen economy is also analysed. At the current stage, coal appears to be the suitable source for hydrogen production due to its abundant reserves and mature infrastructure, while renewable resources are likely to play a more important role in the long term. (3) China‘s policy and government

support programs for the R&D of hydrogen and fuel cell technologies are reviewed. Research achievements are also summarized.

The Chapter is organized as follows: In section 6.1, the motivation of this study is explained. In section 6.2, a brief introduction to China‘s geographic and economic data, together with its energy consumption profile, is presented. In section 6.3, China‘s drivers for hydrogen economy are identified. In section 6.4, China‘s energy system and potential sources for hydrogen production are discussed. In section 6.5, the interests in hydrogen and fuel cell technologies within China are reviewed. Section 6.6 presents some comments on China‘s current status and future direction for hydrogen economy.

6.1 Why is China’s transition towards hydrogen economy important

China is the emerging giant of the world economy. Growth in China‘s real gross domestic product (GDP) averaged a phenomenal 10% per year since 1980. Such a high rate of growth is not unprecedented – double-digit rates have been recorded in some countries over other periods – but no large country has sustained such a rate for such a long period. High growth rates in the 1980s made little difference to the world economy, because China‘s economies were relatively small. Today, the size means that continuing high growth makes a much bigger difference to the world economy. For example, 10% growth in China is equivalent to almost 2% of US growth at market exchange rates.

Phenomenal rates of economic growth in the last three decades in China have been accompanied by a growing thirst for energy. A rising share of the energy needs has to be met by imports, as demand is outstripping indigenous supply. One example will suffice to illustrate this point. China was forced to end its oil self-sufficiency energy policy and import

oil from overseas in 1993. In 2009, China became the world‘s second largest consumer of oil behind the United States and the world‘s second largest net importer of oil. As such, China is increasingly exposed to changes in world energy markets. In turn, China is also transforming the global energy system by dint of its sheer size and its growing weight in international energy trade. How rapidly China‘s energy needs develop and how they are met will have far-reaching consequences for the rest of the world.

The major concern for improving energy security and reducing greenhouse gas emissions, together with the rapid development of hydrogen and fuel cell technologies in recent years, is focusing China‘s opinion on options for future hydrogen economy. Hydrogen can be produced from a variety of sources, both fossil fuel (coal, oil, natural gas) and renewable resources (hydro, wind, solar, biomass). This characteristic provides an opportunity for China to diversify its energy supply and alleviate its high dependence on oil imports from a hydrogen economy. Hydrogen can then be utilised in high-efficiency power generation systems, including fuel cells, for both vehicular transportation and distributed electricity generation. Overall, emissions in a hydrogen energy cycle are expected to be lower than for today‘s carbon energy cycle, but the centralized production of hydrogen offers the extra advantage of enabling large scale capture and sequestration of CO_2 emissions. Sequestration, along with the efficiency improvement due to fuel cell technology, could make a major difference in emissions from a hydrogen economy. Furthermore, China‘s participation in international trade amplifies the importance of its contribution to collective efforts to enhance global energy security to reduce global green gas emissions. The more effective are China‘s transition towards hydrogen economy, the more other countries stand to benefit.

China has already shown the ambition for future hydrogen economy. A workshop for China‘s Roadmap toward hydrogen economy was held in 2005 with participants from academia, industry and government. The workshop clarified a clear vision of future hydrogen economy in China: by 2020 – technology development phase; by 2050 – market penetration phase; and beyond 2050 – fully developed market and infrastructure phase. This roadmap has proven highly valuable in coordinating public and private sector research and development investments in hydrogen and fuel cell technologies. It is believed that China will have a secure and clean energy system at the end of the roadmap and the whole world will benefit from it.

6.2 Geography, economy and energy consumption

China is the world‘s second-largest country by land area, covering 9.6 million square kilometers; it also has the highest population in the world, with more than 1.3 billion citizens [1]. However, the population distribution of China conceals major regional variation. Most of the population is concentrated in the eastern part of China, especially the coastal region. These areas also tend to be more industrialized. In contrast, the west and northern part of the country are very sparsely populated and less developed. Figure 6.1 illustrates the distribution of population and major cities in China [2].

Since the initiation of its economic reforms in 1978, China has become one of the world‘s fastest-growing economies, with annual growth rates averaging 10% over the past 30 years. China became the world's second largest economy after the United States in 2010 [3]. It was reported by National Bureau of Statistics that China‘s GDP reached $7.26 trillion in 2011 [4]. Meanwhile, China is also the largest exporter and second largest importer of

goods in the world. According to the data released by General Administration of Customs, the total foreign trade volume of China totalled $3.64 trillion in 2011 [5].

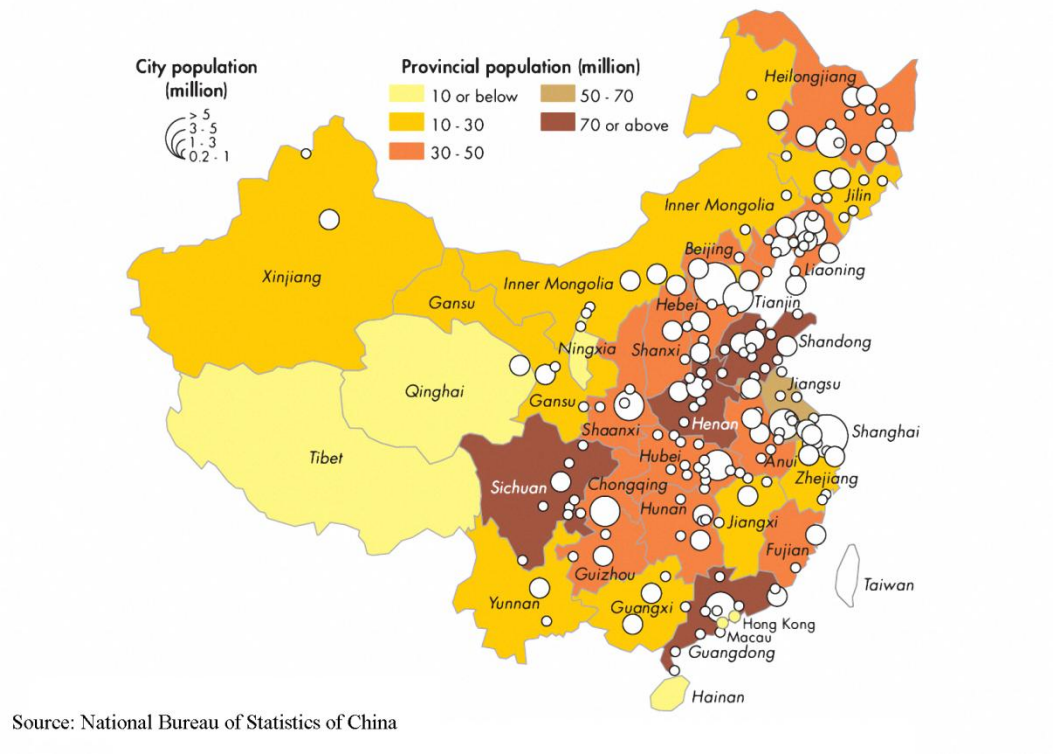

Figure 6.1 Distribution of population and major cities in China [2]

The energy consumption of China is soaring as its economy is expanding rapidly. China overtook the United States and became the world‘s largest energy user in 2010 [6]. Currently, China accounts for 21.3% of the world‘s energy demand but its rate of consumption is growing more than four times the world‘s rate [7]. Figure 6.2 shows China‘s energy consumption by fuel in 2000 and 2010 [7]. As can been seen from the figure, coal is the backbone of China‘s energy system. It meets over half of the country‘s primary energy needs, providing most of the fuel used by power stations and much of the final energy used by industry, commercial businesses and households. In fact, coal‘s importance in the overall

fuel mix has been growing in recent years, due to the booming demand for electricity, which is almost 80% coal-based. Oil demand has been growing quickly, with total oil consumption increasing from 230.1 million tons oil equivalent (toe) in 2000 to 437.7 million toe in 2010. However, its share of primary demand decreased from 28.6% to 18.2%, reflecting the huge increase in the total energy consumption during this period. While China has made an effort to diversify its energy supplies, hydroelectric sources, natural gas, nuclear power, and other renewables account for relatively small shares of China‘s energy consumption mix.

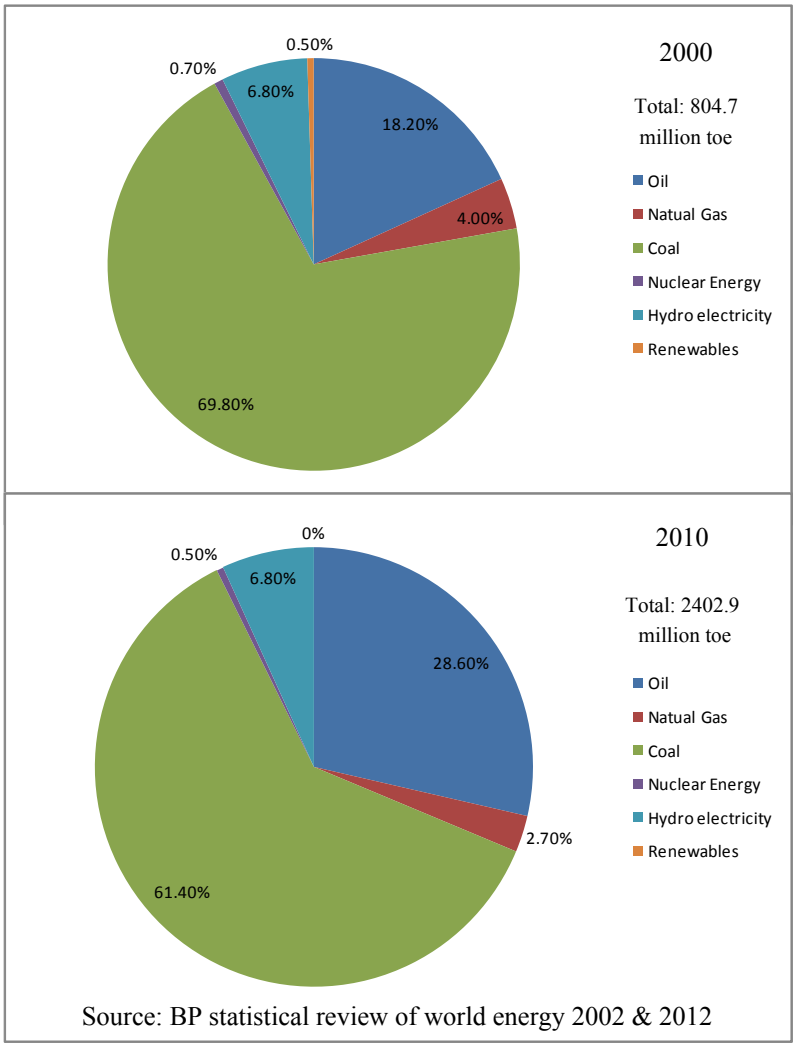

Figure 6.2 China‘s energy consumption by fuel in 2000 and 2010

Figure 6.3 shows the China‘s energy consumption by sector in 2009 [8]. In 2009, the industrial sector—including manufacturing, utilities, and mining— is China‘s largest energy user, accounting for about 72% of total energy use. The residential sector is next with about 11%, while transport, storage and post also contribute almost 8%. The agriculture, forestry, animal husbandry, fisheries, and water conservation sectors together consumed only account for about 2%, reflecting the low level of agricultural mechanization in China.

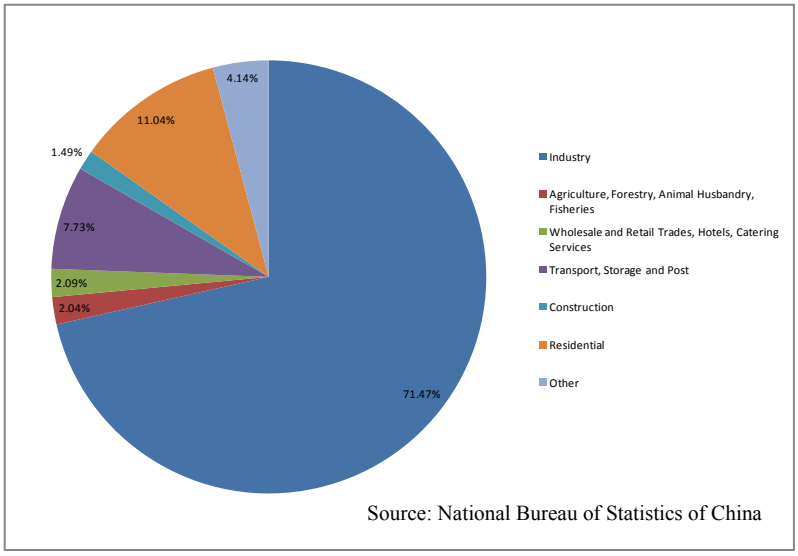

Figure 6.3 China‘s energy consumption by sector in 2009

6.3 Drivers of building the hydrogen economy in China

In a recent literature overview of hydrogen studies, four main drivers towards a hydrogen energy system were identified: (1) climate change, (2) energy security, (3) air pollution and (4) competitiveness [9].

6.3.1 Energy security

China did not realize the urgency and importance of energy security until the 1990s due to the weak economic development and relatively lower demand for energy resources before 1990s. For many years, China was able to meet its energy needs entirely from domestic resources. Therefore, energy security was not the China‘s priority as its dependence on global markets was minimal.

However, that has changed dramatically in the last decade and China‘s concerns about energy security have grown in parallel. China‘s energy consumption has been soaring due to the rapid economic growth, expanding middle class population and the largest-scale of urbanization. China was forced to end its oil self-sufficiency energy policy and import oil from overseas in 1993. In 2009, China became the world‘s second largest consumer of oil behind the United States and the world‘s second largest net importer of oil [10]. In less than a generation, China has moved from being a minor and largely self-sufficient energy consumer to become the one of world‘s fastest-growing energy consumers and largest energy importers. In such context, there is no doubt that China now considers energy security as its first priority.

China‘s energy security considerations today focus largely on guaranteeing a continuous and sufficient supply of oil from overseas. Currently, China depends on foreign imports for over 50% of the oil it consumes, and half of this imported oil is from the Middle East [11]. Figure 6.4 shows the China‘s crude oil imports by source in 2010 [10]. China has many reasons to worry about its oil supply: small oil reserves, high dependence on oil imports,

dramatic fluctuation of oil prices in international market, and political risk in oil-supplying countries.

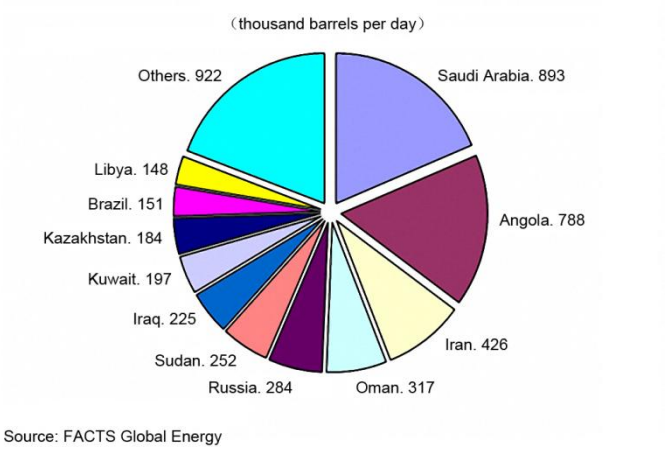

Figure 6.4 China‘s crude oil imports by source in 2010 [9]

On the other hand, China has abundant and widely distributed renewable energy resources that have the potential to gradually displace fossil fuel in the nation‘s energy mix. It is more desirable for China to draw its energy to a large extent from local and indigenous renewable energy resources, with much less dependence on energy imports from overseas. The use of hydrogen can facilitate the exploitation the renewable energy resources. Hydrogen can be produced from diverse resources, both renewable (solar, wind, hydro, biomass) and non-renewable (coal, oil, natural gas) [12]. It is important to stress that, unlike coal, oil or natural gas, hydrogen is not a primary energy source. Its role more closely mirrors that of electricity as an ‗energy carrier‘, which is produced using energy from another source and then transported for future use, where its stored chemical energy can be utilised. It is this key element of the energy storage capacity of hydrogen that provides a solution to one of the major issues of renewable energy resources, namely the vexing problem of intermittency of supply. For instance, many people have predicted the growth

of a solar/wind hydrogen economy in the future. Photovoltaic cells or wind turbines would convert sunlight or wind into electricity. This electricity would be used to split water (electrolysis) into hydrogen and oxygen, in order to store the energy as hydrogen fuel. Fuel cells consume the hydrogen to generate stable electrical power [13].

In sum, hydrogen opens up the possibility of (decentralised) production and utilization on the basis of a variety of energy sources, diversifying energy supply. This may greatly contribute to reduce the dependence on imported oil [14].

6.3.2 Climate change

China plays a critical role in the battle against world climate change caused by the greenhouse gas emissions. In fact, China overtook the United States in 2007 as the world‘s largest annual emitter of energy-related CO_2 [15]. Chinese CO_2 emissions tripled between 1990 and 2009, reaching almost 7 billion tons (Gt) of CO_2 in 2009 (24% of global emissions). Under the Kyoto Protocol, the State Council promised in 2009 that China was going to reduce the intensity of carbon dioxide emissions per unit of GDP in 2020 by 40% - 45% compared with the level of 2005.

To achieve this goal, a perfect fuel that is cheap, clean and efficient is required. Hydrogen is an ideal candidate for this fuel. Compared with other conventional fuels, hydrogen has a variety of good properties in terms of reducing CO_2 emission [16]:

- can be produced from fossil fuels by conversion, with CO_2 separation. This one can be considered as the cleanest way to continue using those fossil fuels
- can be produced from other sources (renewable, nuclear) without CO_2 emission;

- can be utilized in different applications (transportation, electricity production, etc.), without producing any pollutant but water steam.

These characteristics give hydrogen special significance in China's CO_2 emission reduction campaign. Actually, the development of technologies for distribution and utilization of hydrogen will be the basis for the introduction of those CO_2-free production technologies [16].

6.3.3 Urban air pollution

China is now facing serious urban air pollution problem. China is now home to 13 of the world's 20 most polluted cities [17]. The vehicle exhaust emissions have been blamed for the main contributor to the worsening air quality in big cities. Since 2009, China has been the largest automobile market in the world. Its annual vehicle production and sales reached 18.26 million and 18.06 million in 2010. By the end of 2010, the vehicle population in China has totalled 190 million. It was reported by the Ministry of Environmental Protection that the total volume of vehicle exhaust emissions reached more than 52.26 million tons in 2010, including 40.80 million tons of carbon monoxide (CO), 4.87 million tons of hydrocarbon (HC), 5.99 million tons of nitrogen oxide (NO_x) and 598,000 tons of particulate matter (PM) [18].

Fuel cells are considered the most promising power source for future generation vehicles and the only technology with the potential of competing with internal combustion engines [16]. Fuel cell vehicles offer efficiencies two to three times higher than those of conventional vehicles, maintaining similar performances in terms of range, top speed and acceleration. Moreover, by skipping the combustion process that occurs in traditional

internal combustion engines, the generation of pollutants during the combustion process is avoided. With pure hydrogen, a fuel cell vehicle is a true –zero emission" vehicle, producing only water as by-product. Even with other fuels, emissions from fuel cell vehicles will be very low with near-zero levels of NO_x, SO_x and particulates, therefore eliminates 20,000 kg of acid rain and smog-causing pollutants from the environment. In any case fuel cells generally provide the lowest emissions of any non-renewable power generation method, as shown in Table 6.1 [19].

Table 6.1 Pollutant emission factors for the total portion of the fuel cycle [18]

Source	SO_x (gSO_x/kWh)	NO_x gNO_x/kWh)	C in CO_2 (gC/kWh)	C in CO (gC/kWh)	Paritcles
Coal	3.400	1.8	322.8	40.0	0.00020
Oil	1.700	0.88	258.5	40.0	0.00015
Natural Gas	0.001	0.9	178.0	20.0	0.00002
Nuclear	0.030	0.003	7.8	7.8	0.00005
Photovoltaic	0.020	0.007	5.3	1.3	0
Fuel cells	0	0	1.3	0.3	0

6.3.4 Competitiveness

China's global competitiveness will be fostered if China companies are able to forge a lead in hydrogen and fuel cell technologies. This is especially true for China's automobile industry. China is currently the largest automobile market in the world. Although some indigenous automobile manufacturers are emerging, foreign companies still occupy the largest market share and take a leading position in many key technologies, especially the internal combustion engine [20]. As such, China's indigenous automobile manufacturers can hardly to compete with their foreign counterparts in the domestic market, let alone the global market. The emergence of fuel cell provides an opportunity for China to reverse the tide. Although fuel cell vehicle is still at a nascent stage, it shows great potential of competing with the internal combustion engine vehicle. China intends to develop fuel cell vehicles to

leapfrog internal combustion engine vehicles [21]. Using this strategy, China‘s indigenous manufacturers are able to stand on the same starting line with their foreign counterparts for the first time. If China companies are able to commercialize fuel cell vehicles, they may create new market space and greatly enhance their competitiveness.

6.4 Energy resources for hydrogen production in China

China is the world‘s largest hydrogen consumer with 22% of global hydrogen consumption share [22]. China‘s maximum demand comes from ammonia producers. On the other hand, fossil fuels play a dominant role in China‘s hydrogen production, accounting for 97% of total hydrogen production. Water electrolysis only contributes to 3% of total hydrogen production [23]. As such, China is eager to exploit its abundant renewable energy resources for hydrogen production in the future.

6.4.1 Coal

China held the third-largest coal reserves in the world behind the United States and Russia [10]. In 2003, the Ministry of Land and Resources of China, in accordance with international norms for coal resources reporting [24], stated that China‘s total coal reserves stood at 1021 Gt, comprising 334 Gt of ―basic reserves‖ and 687 Gt of ―prognostic reserves‖ [25]. ―Proven reserves‖ were reported to be 189 Gt, suggesting a reserve-to-production ratio of over 70 years. According to the norm [24], ―basic reserves‖ are defined as those resources that can be potentially exploited under current technoeconomic conditions. ―Prognostic reserves‖ include those amounts that are not economic to recover or for which economic significance is uncertain because data is insufficient. ―Proven reserves‖ are the economically recoverable fraction of basic reserves.

The distribution of coal resources shows imbalanced, as shown in Figure 6.5 [25]. Most resources are in the west and north. Shanxi, Shaanxi and Inner Mongolia together account for 65% of the nation‘s proven coal reserves, while just 13% lie in the southern part of the country, mainly in Guizhou and Yunnan. Over 90% of identified coal reserves are in less-developed, arid areas that are environmentally vulnerable.

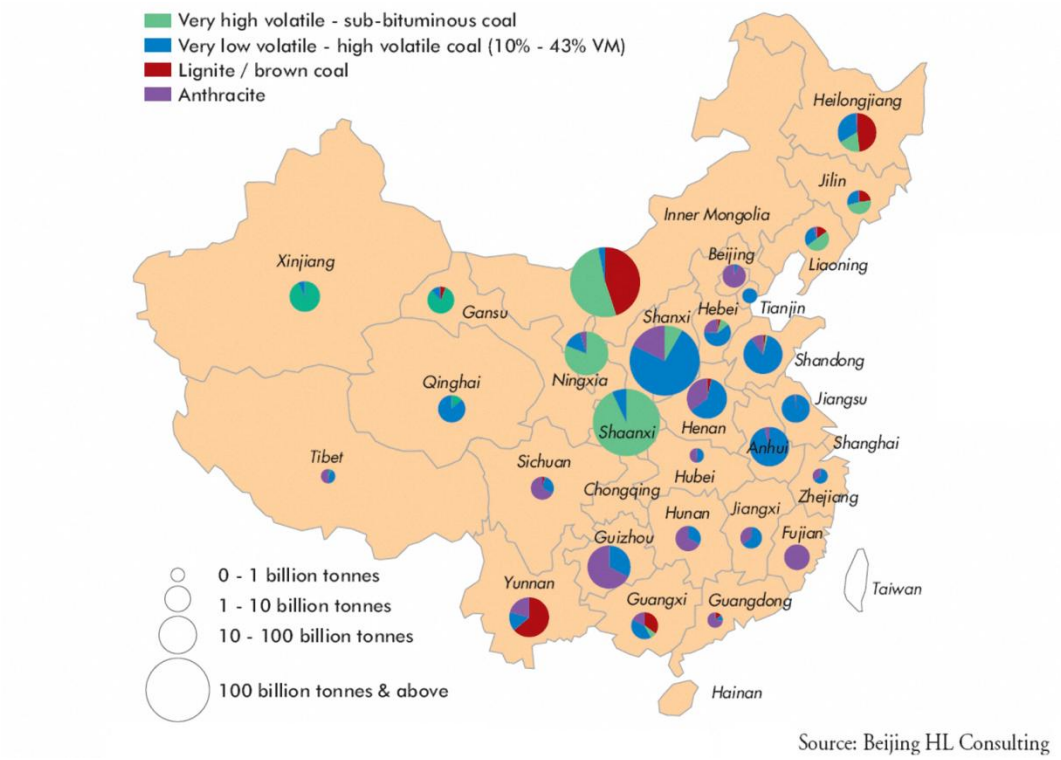

Figure 6.5 Location of major coal resources in China [20]

China is the largest producer and consumer of coal in the world [10]. Coal production rose to almost 3.1 Gt in 2009, making China overtake the United States and become the world‘s largest coal producer. Also in 2009, China consumed an estimated 3.2 Gt of coal, representing over 46% of the world total. Coal consumption has been on the rise in China

over the last ten years due to due to the booming demand for electricity, which is almost 80% coal-based.

Gasification is the primary method for converting coal into hydrogen [26]. It is also the core of current Integrated Gasification Combined Cycle (IGCC) technology for power generation. In a commonly used gasification process, coal is first ground to a fine powder and mixed with water before being gasified at high pressure using pure oxygen. The feedstock is heated to high temperature (about 1400°C), causing its decomposition and producing a mixture of hydrogen, carbon monoxide and some residues; the resultant synthesis gas stream is quenched and scrubbed. The syngas is then put through a CO shift reactor, and CO_2 is removed using a physical solvent. The acid gases contained in this solvent are desorbed by pressure reduction. The hydrogen can be further purified to remove any remaining impurities. In China, around 50 million tons coal is used for gasification each year [23].

6.4.2 Oil

According to *Oil & Gas Journal* (*OGJ*), China had 20.4 billion barrels of proven oil reserves as of January 2011 [10]. Figure 6.6 delineates the location of some of the major Chinese oil basins [10]. As can be seen, China‘s major oil fields are located in the northern region of the country. Particularly, the northwest‘s Xinjiang Province has received significant attention. Recently, China announced the plan to make Xinjiang into the country‘s largest oil production and storage base. It is also worth pointing out that about 15% of overall Chinese oil production is from offshore reserves, and most of China‘s oil production growth likely will come from offshore fields.

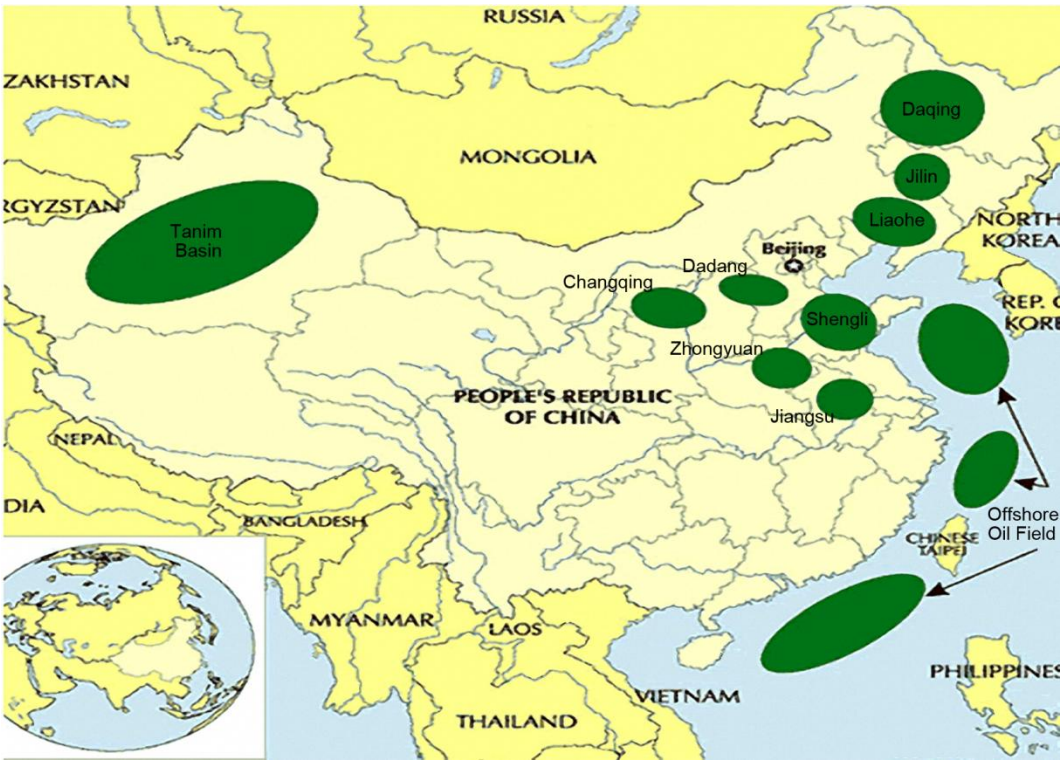

Figure 6.6 Location of major oil resources in China [9]

China is the second largest consumer of oil and the second largest net importer of oil in the world [10]. In 2010, China produced an estimated 4.3 million barrels per day of oil and consumed an estimated 9.2 million barrels per day of oil, making the net oil imports reach about 4.8 million barrels per day [10].

Oil, especially low quality fuels such as petroleum coke or residuals might be used as a fuel for gasification (as with coal) to supply hydrogen [26]. Combined with desulfurisation and sequestration, oil-produced hydrogen could be made with almost zero emissions. In addition, light fractions of petroleum can be converted to hydrogen in much the same way as natural gas. The limitations of this process are that it is less efficient overall, and less

hydrogen is produced due to the lower molar content of hydrogen in oil. In China, about 0.766 million tons of hydrogen is produced from oil each year [23].

6.4.3 Natural gas

Estimates of natural gas reserves in China vary dramatically depending on the source [27]. At the end of 2008, China National Petroleum Corporation (CNPC) announced that China‘s total proven reserves amounted to 5.94 trillion cubic metres, including 3.09 trillion cubic metres of technically and economically producible reserves. However, other estimations are also available. In 2007, Cedigaz estimated that China‘s proven reserves amounted to 3.7 trillion cubic metres, while the IEA estimated China‘s recoverable, proven and probable reserves from identified fields to amount to around 5.0 trillion cubic metres. As with coal resources, the distribution of natural gas is uneven. China‘s major gas fields are located inland, in the western and central parts of the country. Figure 6.7 illustrates the major natural gas field and infrastructure in China [27].

The consumption of natural gas has been limited in China until recently. This was mainly due to the lack of infrastructure, particularly long-distance pipelines connecting inland gas fields to major consumer cities, mostly in the coastal areas in China. Since the 1990s, the government has promoted the construction of natural gas transport infrastructure and improved inter-regional connections between regional networks. The total length of natural gas pipeline across the country amounted to 36,000 km by the end of 2010. China is ambitious to triple its current record to 100,000 km by the end of 2015 to meet the rising demand [28].

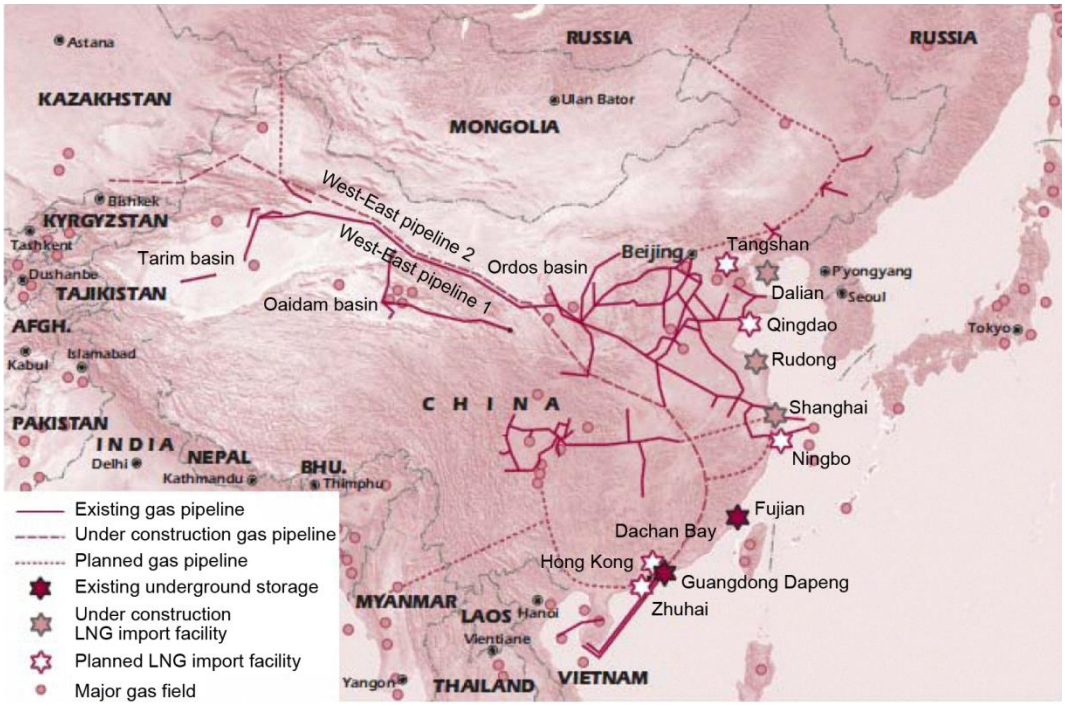

Sources: China National Petroleum Corporation, Petroleum Economist, IEA

Figure 6.7 Major natural gas field and infrastructure in China [22]

Although natural gas use is increasing in China, the fuel only comprises a small proportion of the country‘s total energy consumption. In 2007, China‘s natural gas production amounted 69.2 billion cubic metres and consumption attained 69.5 billion cubic metres, making China a net natural gas importer for the first time in almost two decades [27]. Also in 2007, China became one of the world‘s top 10 countries in terms of natural gas consumption.

Hydrogen can be produced from natural gas directly via various processes, including steam reforming, partial oxidation, auto-thermal reforming and thermal decomposition, as well as indirectly via electrolysis using electricity and/or heat from gas combined cycle processes [26]. Nearly 60% of global hydrogen production is generated from natural gas.

Hydrogen from natural gas for the ammonia and petroleum industries represents the largest portion of the current global production. In china, however, natural gas is mainly used as a raw material for chemicals production due to the high price [29]. About 1.18 million tons of hydrogen is produced from natural gas in China each year [23].

6.4.4 Renewable energy resources

China boasts its fairly abundant renewable energy resources. These renewable energy resources offer the opportunity of zero fuel-cycle emissions for hydrogen production via electrolysis. According to the Medium and Long-Term Development Plan for Renewable Energy, China has a goal to generate at least 15% of total energy output by 2020 using renewable energy resources [30]. In recent years, China has strengthened its legislation to promote renewable energy, including the Atmospheric Pollution Prevention and Control Law 2000, the Renewable Energy Law 2005 and the Energy Conservation Law 2007. Meanwhile, China is the world's top investor in renewable energy projects, having invested around $120 billion to $160 billion between 2007 and 2010 [10].

6.4.4.1 Hydropower

Hydropower is the most important renewable energy resource in China. According to the results of the 2003 Nationwide Hydropower Resource Assessment, China‘s technically exploitable hydropower totals 542 GW, with an annual power generation potential of 2470 TWh. China‘s economically feasible hydropower resource is estimated to be 400 GW, with an annual generation potential of 1750 TWh, of which small-scale hydropower accounts for 125 GW, widely distributed throughout the provinces, especially in the southwest [31].

China was the world‘s largest producer of hydroelectric power in 2010, generating 721 TWh of electricity from hydroelectric sources, representing around 17% of domestic electricity use [32]. China also had the highest installed hydropower capacity, with 213 GW at the end of 2010, accounting for one fifth of the world‘s total installed hydropower capacity.

Small hydropower plays a key role in the electrification of China, especially in remote rural areas. Small hydropower generally refers to plants below 50 MW. About one-third of China‘s countries rely on small-scale hydropower as their main source of electricity. With supportive policies and incentives, China had more than 55 GW of small-scale hydropower projects by the end of 2010, with a generating output of about 160 TWh [33].

6.4.4.2 Wind

Wind is the second leading renewable source for power generation in China. China‘s exploitable onshore wind resources are 253 GW, ranking first in the world, with a further offshore potential of 750 GW [34]. Figure 6.8 shows China's annual average wind power. As can be seen, areas rich in wind resources are located mainly along the southeast coast and the northern region. In addition, the ocean-based wind resources are also abundant. With current technology, wind turbines can be installed in the ocean up to 10 km away from the coast and at ocean depths of up to 20 m.

Wind power is the most cost-effective renewable energy today. Construction of wind power projects in China began in the 1980s. Since then, China‘s wind power projects have developed rapidly. In 2010, China installed 16 GW of new wind power capacity, bringing its accumulated installed capacity to 41.8 GW - thus making it the largest wind-installation

country in the world [35]. Despite the rapid growth, China‘s installed wind power capacity today is only a small part of the country‘s wind resource potential. One of main barriers to further development is the lack of transmission infrastructure.

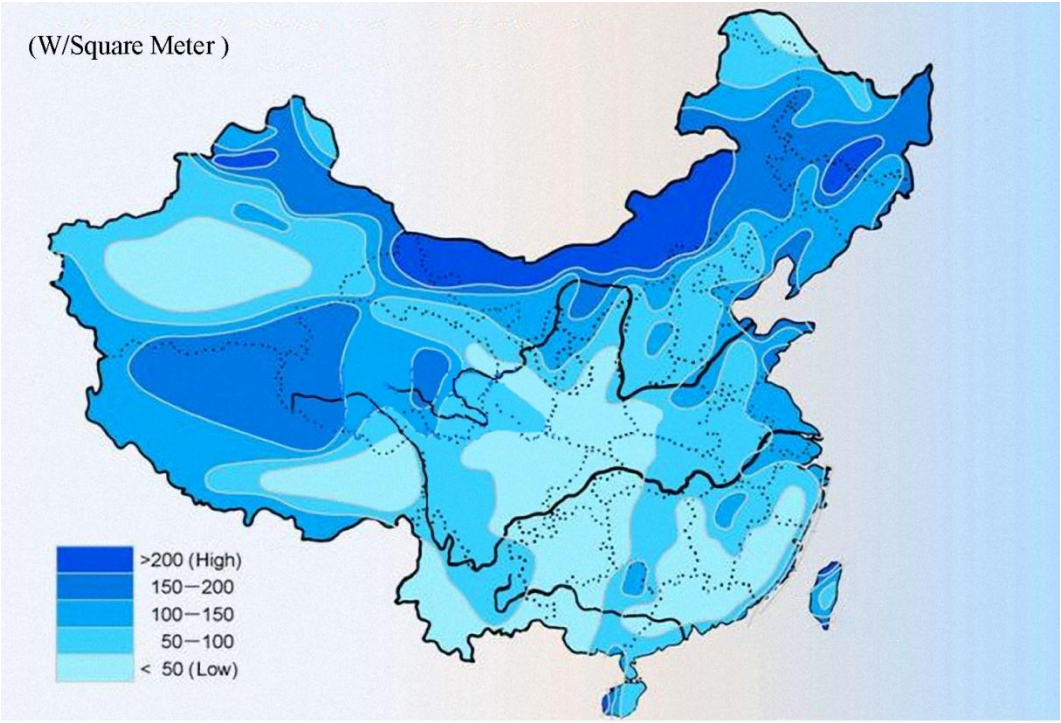

Figure 6.8 China's annual average winder power [29]

6.4.4.3 Solar

Solar resources are receiving increasing attention in China. It is estimated that the annual surface absorption of solar energy is equivalent to approximately 1300 billion tons of standard coal equivalent (tce) [36]. Figure 6.9 shows the distribution of China‘s solar resources. As can be seen, two-thirds of China‘s land area has abundant solar energy, particularly in the northwest, Tibet and Yunnan, with average annual radiation levels of over 6000 MJ/m^2.

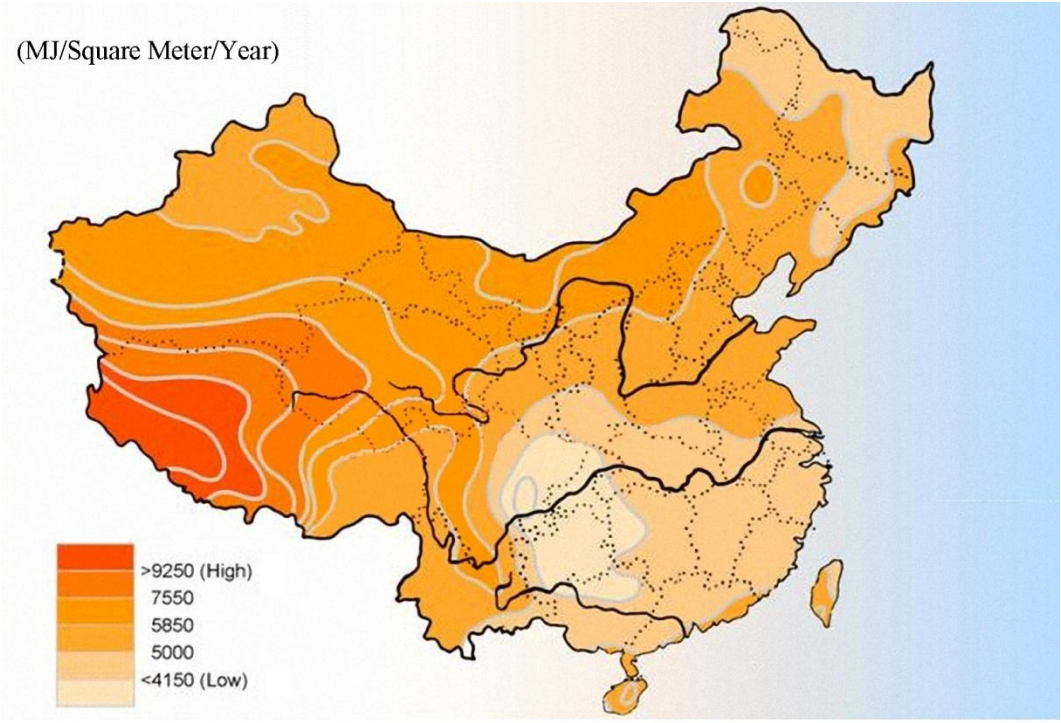

Source: Center for Wind and Solar Energy Resources Assessment, China Meteorological Administration

Figure 6.9 Distribution of China‘s solar resources [31]

The photovoltaic power generation is experiencing a rapid growth in China. In 2010, China‘s annual production of photovoltaic cell was 8.7GW, about half the world total. Meanwhile, China installed 500 MW of new photovoltaic capacity in 2010, bringing its accumulated installed capacity to 800 MW [37]. Previously, about half of installed capacity was used for supplying power to residents in remote rural areas and for special applications, such as communications and navigation [30]. Now, the grid-connected photovoltaic power plant is receiving the increasing attention. The biggest photovoltaic power plant in China, 20 MW Xuzhou Xiexin Photovoltaic Power Plant, was successfully combined to the East China Power Grid at the end of 2009 [37].

Solar water heaters are also widely used in China today. By the end of 2005, China‘s annual production of solar heaters was 15 million m^2 [30]. The accumulated heat-collecting area of installed solar water heaters reached 80 million m^2 in 2006, about half the world total.

6.4.4.4 Biomass

China‘s biomass energy resources include straw and other agricultural wastes such as rice husks, waste from forestry and forest product processing, animal manure, energy crops and plantations, organic effluents from industry, municipal wastewater and municipal solid waste (MSW). Of about 600 Mt of crop straw produced every year, nearly 300 Mt (around 150 million tce) can be used as fuel. Around 900 Mt of waste from forestry and forest product processing is available each year, and nearly 300 Mt of this (about 200 million tce) can be used for energy production [31]. Presently, the nation‘s biomass resource that can potentially be converted into energy is about 500 million tce per year, less than 20% of current total primary energy consumption.

Biomass is utilized mainly through direct combustion for heating or cooking in China. In addition, biomass is wildly used for biogas generation, which provide clean cooking energy for the vast rural areas. At the end of 2005, the total number of household biogas digesters reached 18 million, with an estimated total annual production of 7 billion cubic metres. About 1500 large-scale biogas plants for livestock waste and organic industrial effluent produced a further 1 billion cubic metres [30]. Biogas is now widely integrated with animal husbandry and has become an important means of waste treatment in the agricultural sector. On the contrast, only a small proportion of biomass is used for power generation. By the end

of 2005, the installed capacity of biomass power in China reached 2 GW. Bagasse (sugar cane residue) plants totalled 1.7 GW, while MSW incineration and land-fill gas power plants accounted for a further 200 MW; the remainder was agricultural or forestry waste gasification [30].

China has already begun to produce bio-ethanol for use as a transport fuel. In 2005, the production capacity for bio-ethanol using food grains as a feedstock was just over 1 Mtpa [30]. The technology for producing bio-ethanol from non-food-grain feedstock has reached the pre-commercial stage in China.

6.5 Hydrogen and fuel cell research in China

6.5.1 Policy and government supported program

The most recent, and arguably the most ambitious, of China‘s national science plans, is the National Medium to Long-term Plan for the Development of Science and Technology [38]. Introduced in January 2006, the product of two years of meetings and consultations with well over 2000 members of the technical community, the plan serves as the China‘s guiding document on innovation policy and involves government investments and incentives for key science and technology. Energy sector receives great attention with seven key energy technologies indentified in the plan. Hydrogen and fuel cell technology is one of them.

Presently, the majority of hydrogen and fuel cell researches in China are financially supported by the Ministry of Science and Technology (MOST) through two main programs: the National High Technology Research and Development Program (863 Program) and the

National Basic Research Program (973 Program). In 2011, 973 Program has $11.1 million of fuel cell funding available split equally into two projects: the first for solid oxide fuel cell (SOFC) research and the second for platinum-free fuel cells. In addition, 863 Program has an additional $15.8 million available for hydrogen and fuel cell projects. Table 6.2 shows the hydrogen and fuel cell researches supported by 973 Program and 863 Program in recent years.

Table 6.2 Hydrogen and fuel cell projects supported by 973 and 863 Program

Program	**2000**	**2001**	**2002**	**2003**	**2004**	**2005**	**2006**	**2007**	**2008**	**2009**	**2010**
973	Large-scale production, storage and transport of hydrogen and fuel cells										
973				Large-scale production of hydrogen using solar energy							
973						Highly efficient catalytic conversion of natural gas and syngas					
863		Post-fossil thematic program for hydrogen technology									
863		Post-fossil thematic program for high-temperature fuel cells									
863		Key program for electric vehicles									
863							Key program for energy-saving and new energy vehicles				
863								Key program for hydrogen production and high temperature polymer electrolyte fuel cells			
863							Annual thematic program for hydrogen and fuel cells				
863								Annual thematic program for hydrogen and fuel cells			

In addition to MOST, researchers can also obtain funding support from the National Natural Science Foundation of China (NSFC), which is a governmental organization directly affiliated with the State Council of China for the management of the National Natural Science Fund. As can been seen from Figure 6.10, the number of hydrogen and fuel cell related projects supported by NSFC has been increasing steadily since 2000.

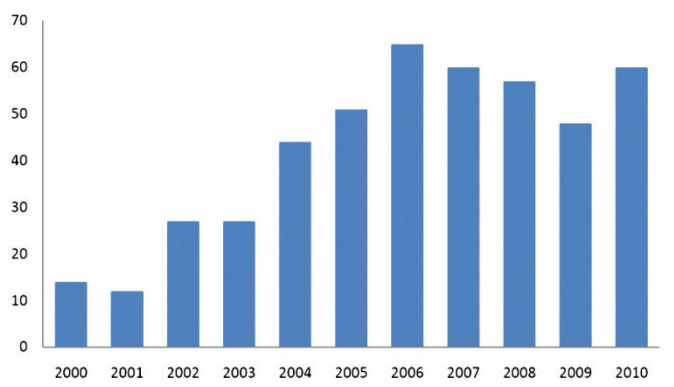

Figure 6.10 Number of projects on hydrogen and fuel cell supported by NSFC

6.5.2 Research and development

Research on fuel cells in China started at Dalian Institute of Chemical Physics (DICP), Chinese Academy of Science (CAS) in the mid-1950s. Since then, DICP has been at the forefront of fuel cell research in China. Two types of alkaline fuel cell (AFC) were first developed over the period of the 1960s and the 1970s, respectively. An alkaline free-electrolyte flow H_2-O_2 fuel cell and a large capacity oxidation-deoxidation electrolyte flow energy storage fuel cell were successfully developed in the 1980s. Consequently, the research and development of PEMFC, MCFC, SOFC, and DMFC have been carrying out since the 1990. The series productions of PEMFC engines developed in DICP ranges from 30kW to 100kW. In 2001, DICP established Dalian Sunrise Power Co. Ltd. to facilitate the commercialization of fuel cells. In addition to DICP, other universities or institutes have their own speciality: Shanghai Jiao Tong University sets up a 50 kW MCFC test system, while Shanghai Institute of Ceramics runs an 800W SOFC test system. Both projects are supported by 863 Program.

In terms of hydrogen production and storage, great progress has also been achieved [39]. A novel biological hydrogen production process from organic waste water via zymotechnics was developed with capacity of 368 Nm^3/d. High-performance magnesium-based composite material was invented with hydrogen storage capacity of 3.36 wt% at 150°C. A pioneering manufacturing process of lanthanon alloy was designed with hydrogen storage capacity of 48 kgH_2/m^3.

The commercial companies in China also showed great interest in the research and commercialization of hydrogen and fuel cell technologies. Some of them have strong connection with institutes and universities. Shanghai Fuel Cell Vehicle Powertrain Co., Ltd has particularly strong links with Tongji University in developing "Chaoyue" series of fuel cell cars. DICP also works closely with its spin-off company Sunrise Power Co., Ltd. In addition, patent application has attracted great attention. For instance, Sunrise Power Co., Ltd has one of the largest holdings with more than 200 patents.

Chinese institutes, universities and companies who are active in hydrogen and fuel cell research and development are summarized in Table 6.3 - 6.5, respectively.

Table 6.3 Summary of relevant Chinese institutes

Institute	Research Interests and Progress	Selected Reference
Dalian Institute of Chemical Physics (DICP)	DICP has broad research interests in fuel cells, including AFC, MCFC, SOFC, PEMFC, DMFC and etc.	[40-44]
Changchun Institute of Applied Chemistry (CIAC)	CIAC has special interest in PEMFC, DMFC and MCFC. CIAC has been studying PEMFC since 1990s with emphasis on methanol reformer, catalyst and electrode manufacturing. CIAC also made great progress in studying intermetallic compound used for the anode and $LiAlO_2$ micro-powder used for the electrolyte of MCFC.	[45-47]
Guangzhou Institute of Energy Conversion (GIEC)	GIEC's research interests include microbio fuel cell (MFC) and hydrogen production.	[48-49]
Shanghai Institute of Ceramics (SIC)	SIC puts its emphasis on SOFC, specially the material used for electrode and electrolyte in SOFC. Excellent research has been done in processing ceramic and zirconia nano powder used for the electrolyte.	[50-53]
Shanghai Institute of Organic Chemistry (SIOC)	SIOC focuses its research on key material and component in PEMFC, including proton exchange membrane, membrane electrode assembly and flow field plate.	[54]
General Research Institute for Nonferrous Metals (GRINM)	GRINM's research interest focuses on hydrogen storage techniques. Great progress has been made in studying metal hydride for hydrogen storage.	[55-58]

Table 6.4 Summary of relevant Chinese universities

University	Research Interests and Progress	Selected Reference
Tsinghua University	Tsinghua University's research interests include fuel cell engine and fuel cell bus, production, storage and transport of hydrogen.	[59-62]
Tongji University	Tongji University's research interests include fuel cell car and hydrogen infrastructure. Tongji University successfully developed "Chaoyue" serious of fuel cell cars and established the first hydrogen fuelling station in Shanghai.	[63-66]
University of Science and Technology of China (USTC)	USTC focuses its research on SOFC. Current research areas include mid-temperature SOFC, new material for electrode and electrolyte of SOFC.	[67-70]
Shanghai Jiao Tong University (SJTU)	SJTU's research interests include PEMFC, SOFC, and MCFC. Excellent research has been done in modelling and control of fuel cell systems.	[71-74]
Beijing Institute of Technology (BIT)	BIT's research interests include PEMFC, fuel cell vehicle, as well as hydrogen production and storage.	[75-78]
Tianjin University	Tianjin University has wide research interest, including SOFC, PEMFC as well as hydrogen production and storage.	[79-82]
Huazhong University of Science and Technology (HUST)	HUST's put its emphasis on SOFC. Current research areas include new material for electrode and electrolyte of SOFC, intermediate temperature SOFC.	[83-86]
South China University of Technology (SCUT)	SCUT's research interests include PEMFC, DMFC, SOFC, microbio fuel cell as well as hydrogen production and storage.	[87-92]
Wuhan University of Technology (WUT)	WUT puts its emphasis on PEMFC and fuel cell vehicle.	[93-96]
University of Science and Technology Beijing (USTB)	USTB has wide research interests in PEMFC.	[97-101]

Table 6.5 Summary of relevant Chinese companies

Company	Research Interests and Products
Dalian Sunrise Power Co., Ltd	Established by DICP in 2001. Full spectrum of research from catalysts to fuel cell systems. Offers technical support and owns 200-300 fuel cell patents.
Shanghai Shen-Li High Tech Co., Ltd	PEMFC development and transport fuel cell demonstration are main focuses. Also has 10 kW hydrogen fuelled stationary products and 100-300W portable systems.
Shanghai Fuel Cell Vehicle Powertrain Co., Ltd	Focuses on research and development of fuel cell vehicle. Has close cooperation with Tongji University and Shanghai Automotive Industry Corporation (SAIC).
Shanghai Zhongke Tongli Chemical Material Co., Ltd.	Established by SIOC in 2002. Focuses on research of key material and components of PEMFC. Has fluorine-containing polymer membrane products.
Shanghai Everpower Power Technology Co., Ltd	Develops small PEMFC systems up to 5 kW for backup power and small vehicles. Staffs have 15-20 years fuel cell experience gained at fuel cell companies such as Ballard.
Pearl Hydrogen Technology Co., Ltd.	Focuses on commercialization of PEMFC for telecoms backup and light vehicles targeting greater lifetime and lower cost. Manufacturing capacity: 2 MW / year.
Shanghai Sunwise New Energy Systems Co., Ltd	Develops hydrogen refueling stations, including the permanent installation at Anting and a number of mobile units. Also develops on-board storage of hydrogen for FCEV.
Beijing Fuyuan Century Fuel Cell Power Co., Ltd	PEMFC development and commercialization. Has broad spectrum of products, ranging from fuel cells used in mobile phones to 40kW fuel cell for vehicles.
Beijing Ln-Power Sources Co., Ltd	Current research areas are hydrogen production and PMEFC. Full spectrum of products, include hydrogen refueling station and various PEMFC system.

6.5.3 International networking

In 1978, the Chinese government started to implement open policy. Based on reciprocity and mutual interest, China began international research cooperation through intergovernmental and non-governmental channels. Initially, the international research cooperation programs were mainly participated in by academia. Currently, however, the industry leaders also express great interest in the international cooperation of certain research fields.

Among all the partners, the European Union is the most active one who has been involved in outstanding research cooperation with China. Under the Sixth and Seventh Framework Programme (FP6 & FP7) proposed by the European Commission, China participated in 8 projects in the field of hydrogen and fuel cell research, as shown in Table 6.6 [102].

Table 6.6 China's participants in FP6 and FP7's hydrogen and fuel cell projects [102]

Title	Acronym	Chinese participants
New Methods for Superior Integrated Hydrogen Generation System	NEMESIS	Nanjing Univ. of Tech
Carbon Dioxide Capture and Hydrogen Production from Gaseous Fuels	CACHET	Dalian Inst. of Chem. Phy, CAS.
International Partnership for a Hydrogen Economy for generation of New Ionomer membranes	IPHE-GENIE	Shanghai Jiaotong Univ.
Demonstration of SOFC stack technology for operation at 600°C	SOFC600	Dalian Inst. of Chem. Phy, CAS. and Shanghai Jiaotong Univ.
Handbook for Approval of Hydrogen Refuelling Stations	HYAPPROVAL	Tech. Inst. of Phy and Chem, CAS
Hydrogen for clean urban transport in Europe	HYFLEET:CUTE	China FCB Demonstration Project Management Office
Fuel Cell Testing, Safety, Quality Assurance	FCTESQA	Dalian Inst. of Chem. Phy., CAS,
Carbon dioxide capture and hydrogen production with membranes	CACHET II	Dalian Inst. of Chem. Phy., CAS, and Inst. of Metal res., CAS.

One the other hand, Canada showed special interest in cooperation with China for the commercialization of fuel cells. Palcan Fuel Cell Co. Ltd. of Canada supplied fuel cell stacks to its Chinese partners for the assembly of several prototypes of fuel cell two-wheelers (bicycles, scooters). Recently, Palcan is involved in a joint program with Shanghai Mingliang Plastic Co. Ltd. to manufacture about 20,000 PEM fuel cell stacks each year. Ballard Power Systems Inc. of Canada, the fuel cell industry leader, also has its ambitious plan for Chinese market. With the help of Ballard, the Shanghai Fuel Cell Vehicle Powertrain Co., Ltd is planned to manufacture 10,000 fuel cell vehicles in Shanghai by 2012.

6.5.4 Demonstration programs

6.5.4.1 Tianjin IGCC power plant demonstration project

Due to China‘s coal-based energy system, the clean utilization of coal has always been attached the highest priority. Motivated by this need, China launched its __Green Coal-Based Power Generation Plan”. As the first part of the plan, Huaneng Group, the largest power company in China, started the construction of Tianjin Integrated Gasification Combined Cycle (IGCC) power plant in 2009. Strongly supported by 863 Program, the pioneer project has ambition to achieve near-zero emissions with the help of carbon capture and storage (CCS) technology. The first carbon storage site locates in Tianjin Dagang Oil Field. The first phase of the project has been completed by the end of 2011, including 2000 t/d coal gasifier and 250 MW coal-based poly-generation system.

6.5.4.2 Fuel cell bus demonstration program

The fuel cell bus demonstration project was launched by the Chinese government in March 2003 in collaboration with the Global Environmental Facility (GEF) and the United Nations Development Programme (UNDP). The first phase took place between June 2006 and October 2007, with three Daimler-Chrysler fuel cell buses in operation for use by the Beijing public. These buses travelled a total distance of more than 92,116 km during their service with average hydrogen consumption rate 1kg/100km. The second phase took place in Shanghai and was launched in November 2007. The three fuel cell buses trialed in second phase were jointly developed by Shanghai Fuel Cell Vehicle Powertrain Co., Ltd and Tongji University, powered by Ballard stacks.

6.5.4.3 Bejing Olympics 2008

A total of 20 Passat fuel cell cars were operated during the 2008 Beijing Olympic Games, with total operation mileage over 76,000 km. These cars were designed by Shanghai Volkswagen Passat and co-manufactured by Shanghai Fuel Cell Vehicle Powertrain Co., Ltd, Tongji University and Shanghai Automotive Industry Corporation. After the Olympics, sixteen of them were sent to California for fleet demonstrations at the California Fuel Cell Partnership (CAFCP). Here, the fleet covered an additional 37,000 km between February and June 2009.

6.5.4.4 Shanghai World EXPO 2010

During the 2010 World Expo, a total of 1,017 clean energy vehicles were in use transporting visitors, including 90 fuel cell cars, 6 fuel cell buses. The fuel cell vehicles were manufactured by SAIC, Shanghai Volkswagen Automotive Co., Ltd, FAW-Volkswagen Automotive Co., Ltd, Chang‘an Automobile Co. Ltd and Chery Automobile Co. Ltd. Hydrogen was brought to the Expo refuelling station and the Anting hydrogen station on tube trailers from a by-product hydrogen purification plant; two mobile hydrogen refuelling stations were also in use.

6.6 Conclusion

In this Chapter, several key issues concerning China‘s future hydrogen economy are reviewed, including drivers for transition towards the hydrogen economy, energy resources and their potential role in future hydrogen production, government‘s policy and support for the research of hydrogen and fuel cell technology.

Among the four drivers identified, energy security seems to be the most important one for China. Need for alternative fuel is especially urgent in the transport sector. The growing oil price in China, as well as the tightening financial belts caused by the economy crisis, has evoked widespread public's interests in renewable energy vehicles. In 2010, China government established the renewable energy vehicle union, which consisted of 16 state-owned powerful companies. The objective of the union is to facilitate the research and commercialization of renewable energy vehicles. With strong government incentives, renewable energy vehicles are likely to expand their market share in near future. As a result, the dependence on oil import can be greatly alleviated by then.

The brief analysis of energy supply shows that China currently faces a dilemma in terms of hydrogen production. China‘s coal-based energy system is both beneficial and detrimental to the transition towards hydrogen-based economy. In favour of hydrogen economy is the availability of so much potential hydrogen fuel, while the current reliance on coal, the low price of ―dirty" energy delivery and the established infrastructure of the coal power industry may make it difficult to increase industrial momentum towards the hydrogen economy. On the other hand, the oil and natural gas are not the ideal sources for hydrogen production due to their high price and limited reserve. In the long term, renewable energy resources are likely to play a more important role in hydrogen production due to their abundance in China. The major barrier to the commercialization of renewable energy is the high cost of infrastructures, which results in the expensive electricity tariff and the low market acceptance. Under such circumstances, government incentive is an effective way to encourage renewable energy production.

Chinese government has made ambitious policy and provides strong financial support for hydrogen and related technology development. All of China‘s top-tier institutes and universities are conducting hydrogen and fuel cell research. Of the various fuel cell types, the high temperature variants—SOFC and MCFC—are most suitable for hydrogen that is derived from hydrocarbon sources. Unlike low temperature cells such as the PEMFC, both the SOFC and MCFC can tolerate carbon oxides in the fuel and indeed are able to oxidise CO directly. Studies have shown that fuel produced from coal gasifiers can be used in the SOFC and MCFC. Considering China‘s coal-based energy system, this may be an important application in the future.

Reference

[1] Central Intelligence Agency. The world factbook. Available from: https://www.cia.gov/library/publications/the-world-factbook/geos/ch.html [accessed July 2012].

[2] National Bureau of Statistics of China. Census. Available from: http://www.stats.gov.cn/ [accessed July 2012].

[3] World Bank. China overview. Available from: http://www.worldbank.org/en/country/china/overview [accessed July 2012].

[4] National Bureau of Statistics of China. China‘s 2011 GDP. Available from: http://www.stats.gov.cn/ [accessed January 2012].

[5] General Administration of Customs of China. China's total foreign trade volume in 2011. Available from: http://www.customs.gov.cn [accessed January 2012].

[6] International Energy Agency. China overtakes the United States to become world‘s largest energy consumer. Available from: http://www.iea.org/index_info.asp?id=1479 [accessed July 2012].

[7] British Petroleum. BP statistical review of world energy 2002 and 2012. Available from: http:// www.bp.com/ [accessed July 2012].

[8] National Bureau of Statistics of China. China statistical yearbook 2011. Available from: http://www.stats.gov.cn/ [accessed July 2012].

[9] M. McDowall, M. Eames, –Forecasts, scenarios, visions, backcasts and roadmaps to the hydrogen economy: a review of the hydrogen futures literature,” *Energy Policy*, vol. 34, pp.1236–1250, 2006.

[10] International Energy Agency. Country analysis briefs – China. Available from: http://www.eia.gov/cabs/china/Full.html [accessed July 2012].

[11] J. Zhang, "China's energy security: prospects, challenges and opportunities," Center for Northeast Asian Policy Studies, the Brookings Institution. Available from: http://www.brookings.edu/~/media/research/files/papers/2011/7/china%20energy%20zhang/07_china_energy_zhang_paper [accessed July 2012].

[12] P. P. Edwards, V. L. Kuznetsov, W. I. F. David, N. P. Brandon, "Hydrogen and fuel cells: Towards a sustainable energy future," *Energy Policy*, vol. 36, pp. 4356–4362, 2008.

[13] A. Boudghene Stambouli, "Fuel Cells for Large Scale Applications," *in First International Workshop on Hydrogen*, 2005.

[14] S. Dunn, "Hydrogen Futures: Toward a Sustainable Energy System," Worldwatch Institue. Available from: www.worldwatch.org/system/files/EWP157.pdf [accessed July 2012].

[15] International Energy Agency. CO_2 emissions from fuel combustion – 2011 highlights. Available from: www.iea.org/co2highlights/co2highlights.pdf [accessed July 2012].

[16] M. Conte, A. Iacobazzi, M. Ronchetti, R. Vellone, "Hydrogen economy for a sustainable development: state-of-the-art and technological perspectives," *J. Power Sources*, vol. 100, pp. 171–187, 2001.

[17] World Bank. Mid-term evaluation of China's 11th Five Year Plan. Available from: http://siteresources.worldbank.org/CHINAEXTN/Resources/318949-1121421890573/China_11th_Five_Year_Plan_main_report_en.pdf [accessed July 2012].

[18] Ministry of Environmental Protection of China. China vehicle emission control annual report 2011. Available from: www.mep.gov.cn/ [accessed July 2012].

[19] A. Boudghene Stambouli, ―Fuel cells: The expectations for an environmental-friendly and sustainable source of energy,‖ *Renewable Sustainable Energy Rev.*, vol. 15, pp. 4507–4520, 2011.

[20] J. Zhao, M. Melaina, ―Transition to hydrogen-based transportation in China: Lessons learned from alternative fuel vehicle programs in the United States and China,‖ *Energy Policy*, vol. 34, pp. 1299–1309, 2006.

[21] F. Z. Zhang, Philip C. ―Hydrogen and fuel cell development in China: a review,‖ *European Planning Studies*, vol. 18, pp. 1153-1568, 2010.

[22] Markets and Markets consulting firm. Hydrogen generation market. Available from: http://www.marketsandmarkets.com/Market-Reports/hydrogen-generation-market-494.html [accessed July 2012].

[23] Z. Q. Mao, ―Strategies of developing hydrogen infrastructure in China,‖ Available from:http://www.iphe.net/docs/Meetings/Japan_9-05/Strategies_of_Developing_Hydrogen_Infrastructure_in_China.pdf [accessed July 2012].

[24] United Nations Economic Commission for Europe. United Nations International Framework Classification for Reserves/Resources – Solid Fuels and Mineral Commodities. Available from: http://www.unece.org/energy/se/unfc_fc_sf.html [accessed July 2012].

[25] International Energy Agency. Clean coal in China. Available from: www.iea.org/textbase/nppdf/free/2009/coal_china2009.pdf [accessed July 2012].

[26] B. McLellan, J. C. Diniz da Costa, A. L. Dicks, V. Rudolph, R. J. Pagan, C. Sheng, et al, ―Hydrogen Economy Options for Australia,‖ *Dev. Chem. Eng. Mineral Process*, vol. 12, pp. 447–460, 2004.

[27] International Energy Agency. Natural gas in China market evolution and strategy. Available from: www.iea.org/papers/2009/nat_gas_china.pdf [accessed July 2012].

[28] China Daily. China to boost natural gas pipelines network. Available from: http://www.chinadaily.com.cn/business/2010-10/20/content_11435212.htm [accessed July 2012].

[29] X. Deng, H. W. Wang, H. Y. Huang, M. G. Ouyang, ―Hydrogen flow chart in China," *Int. J. Hydrogen Energy*, vol. 35, pp. 6475–6481, 2010.

[30] National Development and Reform Commission of China. Medium and Long-Term Development Plan for Renewable Energy in China. Available from: http://www.chinaenvironmentallaw.com/wp-content/uploads/2008/04/medium-and-long-term-development-plan-for-renewable-energy.pdf [accessed July 2012].

[31] National Development and Reform Commission and Energy Research Institute. Report on China's Renewable Energy Industry Development 2006. Available from: http://www.doc88.com/p-5520229581.html [accessed July 2012].

[32] Worldwatch Institute. Use and capacity of global hydropower increases. Available from: http://www.worldwatch.org/node/9527 [accessed July 2012].

[33] China News. China's small-scale hydropower installed capacity reaches 55.12 million kW. Available from: http://www.chinanews.com/ny/news/2010/04-23/2245014.shtml [accessed July 2012].

[34] Center for Wind and Solar Energy Resources Assessment, China Meteorological Administration. China's wind resources. Available from: http://cwera.weather.com.cn/ [accessed July 2012].

[35] Green Peace. China becomes world‘s number 1 in wind installation. Available from: http://www.greenpeace.org/eastasia/press/releases/climate-energy/2011/china-world-leader-wind-energy/ [accessed July 2012].

[36] Center for Wind and Solar Energy Resources Assessment, China Meteorological Administration. China‘s solar resources. Available from: http://cwera.weather.com.cn/ [accessed July 2012].

[37] H. H. Xu, ―Status and trends of PV industry and technology in China,” Available from: http://apps1.eere.energy.gov/solar/newsletter/pdfs/01_statusandtrendsofpvinchina_xuhonghua_s.pdf [accessed July 2012].

[38] State Council of China. National Medium to Long-term Plan for the Development of Science and Technology. Available from: http://www.gov.cn/ [accessed July 2012].

[39] J. Xu, J. C. Chen, ―Achievements and prospects of China‘s energy science and technology in the Tenth Five-Year Plan,” *Sci. Technol. Ind. China*, vol. 2, pp. 14–19, 2006.

[40] L. M. Zhang, W. S. Yang, ―High-performance low-temperature solid oxide fuel cells using thin proton-conducting electrolyte with novel cathode,” *Int. J. Hydrogen Energy*, vol. 37, pp. 8635–8640, 2012.

[41] M. Zhang, G. Q. Lin, B. Wu, Z. G. Shao, ―Composition optimization of arc ion plated CrNx films on 316L stainless steel as bipolar plates for polymer electrolyte membrane fuel cells,” *J. Power Sources*, vol. 205, pp. 318–323, 2012.

[42] P. J. Wang, L. Zhou, G. L. Li, H. X. Lin, Z. G. Shao, X. F. Zhang, et al, ―Direct internal reforming molten carbonate fuel cell with core-shell catalyst,” *Int. J. Hydrogen Energy*, vol. 37, pp. 2588–2595, 2012.

[43] C. Qu, H. M. Zhang, F. X. Zhang, B. Liu, ―A high-performance anion exchange membrane based on bi-guanidinium bridged polysilsesquioxane for alkaline fuel cell application," *J. Mater. Chem.*, vol. 22, pp. 8203–8207, 2012.

[44] L. L. Sun, S. L. Wang, W. Jin, H. Y. Hou, L. H. Jiang, G. Q. Sun, ―Nano-sized Fe_2O_3-SO_4^{2-} solid superacid composite Nafion (R) membranes for direct methanol fuel cells," *Int. J. Hydrogen Energy*, vol. 35, pp. 12461–12468, 2012.

[45] L. G. Feng, W. W. Cai, C. Y. Li, J. Zhang, C. P. Liu, W. Xing, ―Fabrication and performance evaluation for a novel small planar passive direct methanol fuel cell stack," *Fuel*, vol. 94, pp. 401–408, 2012.

[46] Z. L. Chai, C. Wang, H. J. Zhang, C. M. Doherty, B. P. Ladewig, A. J. Hill, et al., ―Nafion-carbon nanocomposite membranes prepared using hydrothermal carbonization for proton-exchange-membrane fuel cells," *Adv. Funct. Mater.*, vol. 20, pp. 4394–4399, 2010.

[47] M. S. Zhao, C. Y. Sun, ―A novel anode material for molten carbonate fuel cell," in *Proceedings of 6th International Symposium on Molten Salt Chemistry and Technology*, pp. 402–408, 2001.

[48] X. Y. Kong, Y. M. Sun, Z. H. Yuan, D. Li, L. H. Li, Y. Li, ―Effect of cathode electron-receiver on the performance of microbial fuel cells," *Int. J. Hydrogen Energy*, vol. 35, pp. 7224–7227, 2010.

[49] J. J. Xie, D. R. Su, X. L. Yin, C. Z. Wu, J. X. Zhu, ―Thermodynamic analysis of aqueous phase reforming of three model compounds in bio-oil for hydrogen production," *Int. J. Hydrogen Energy*, vol. 36, pp. 15561–15572, 2010.

[50] X. J. Liu, Z. L. Zhan, X. Meng, W. H. Huang, S. R. Wang, T. L. Wen, "Enabling catalysis of Ru-CeO2 for propane oxidation in low temperature solid oxide fuel cells," *J. Power Sources*, vol. 199, pp. 138–141, 2012.

[51] X. F. Ye, J. Zhou, S. R. Wang, F. R. Zeng, T. L. Wen, Z. L. Zhan, "Research of carbon deposition formation and judgment in Cu-CeO_2-ScSZ anodes for direct ethanol solid oxide fuel cells," *Int. J. Hydrogen Energy*, vol. 37, pp. 505–510, 2012.

[52] X. Meng, Z. L. Zhan, X. J. Liu, H. Wu, S. R. Wang, T. L. Wen, "Low-temperature ceria-electrolyte solid oxide fuel cells for efficient methanol oxidation," *J. Power Sources*, vol. 196, pp. 9961–9964, 2011.

[53] R. Zheng, S. R. Wang, H. W. Nie, T. L. Wen, "SiO_2-CaO-B_2O_3-Al_2O_3 ceramic glaze as sealant for planar ITSOFC," *J. Power Sources*, vol. 128, pp. 165–172, 2004.

[54] Y. Q. Zhu, P. Q. Zhao, X. D. Cai, W. D. Meng, F. L. Qing, "Synthesis and characterization of novel fluorinated polyimides derived from bis[4-(4'-aminophenoxy)phenyl]-3,5-bis(trifluoromethyl)phenyl phosphine oxide," *Polymer*, vol. 48, pp. 3116–3124, 2007.

[55] H. P. Yuan, X. G. Zhang, Z. N. Li, J. H. Ye, X. M. Guo, S. M. Wang, et al., "Influence of metal xide on $LiBH_4$/2$LiNH_2$/MgH_2 system for hydrogen storage properties," *Int. J. Hydrogen Energy*, vol. 37, pp. 3292–3297, 2012.

[56] X. G. Zhang, Z. N. Li, F. Lv, H. L. Li, J. L. Mi, S. M. Wang, et al., "Improved hydrogen storage performance of the $LiNH_2$-MgH_2-$LiBH_4$ system by addition of ZrCo hydride," *Int. J. Hydrogen Energy*, vol. 35, pp. 7809–7814, 2010.

[57] Z. Huang, F. Cuevas, X. P. Liu, L. J. Jiang, S. M. Wang, M. Latroche, et al., "Effects of Si addition on the microstructure and the hydrogen storage properties of

$Ti_{26.5}V_{45}Fe_{8.5}Cr_{20}Ce_{0.5}$ BCC solid solution alloys," *Int. J. Hydrogen Energy*, vol. 34, pp. 9385–9392, 2009.

[58] C. B. Wan, X. Ju, Y. Qi, C. Fan, S. M. Wang, X. P. Liu, et al., "A study on crystal structure and chemical state of TiCrVMn hydrogen storage alloys during hydrogen absorption-desorption cycling," *Int. J. Hydrogen Energy*, vol. 34, pp. 8944–8950, 2009.

[59] Y. Lu, C. Zhang, H. X. Zhao, X. H. Xing, "Improvement of Hydrogen Productivity by Introduction of NADH Regeneration Pathway in Clostridium paraputrificum," *Appl. Biochem. Biotechnol.*, vol. 167, pp. 732–742, 2012.

[60] C. C. Pan, B. Yang, J. Iqbal, R. H. Yu, "Effects of annealing treatment on microstructure and properties of $Nd_{0.75}Mg_{0.25}(Ni_{0.8}Co_{0.2})_{3.5}$ hydrogen storage alloys," *Rare Met. Mater. Eng.*, vol. 40, pp. 367–371, 2011.

[61] X. N. Feng, J. Q. Li, L. G. Lu, J. F. Hua, L. F. Xu, M. G. Ouyang, "Research on a battery test profile based on road test data from hybrid fuel cell buses," *J. Power Sources*, vol. 209, pp. 30–39, 2012.

[62] J. F. Hua, J. Q. Li, M. G. Ouyang, L. G. Lu, L. F. Xu, "Proton exchange membrane fuel cell system diagnosis based on the multivariate statistical method," *Int. J. Hydrogen Energy*, vol. 36, pp. 9896–9905, 2011.

[63] Y. P. Hou, C. Y. Shen, Z. H. Yang, Y. T. He, "A dynamic voltage model of a fuel cell stack considering the effects of hydrogen purge operation," *Renewable Energy*, vol. 44, pp. 246–251, 2012.

[64] Y. P. Hou, B. W. Wang, G. B. Ouyang, H. L. Shen, Y. T. He, "An Analytic Hierarchy Process to evaluate PEM fuel cell engine performance," *Int. J. Hydrogen Energy*, vol. 36, pp. 6780–6787, 2011.

[65] R. Lin, B. Li, Y. P. Hou, J. M. Ma, "Investigation of dynamic driving cycle effect on performance degradation and micro-structure change of PEM fuel cell," *Int. J. Hydrogen Energy*, vol. 34, pp. 2369–2376, 2009.

[66] G. Luo, L. Xie, Q. Zhou, I. Angelidaki, "Enhancement of bioenergy production from organic wastes by two-stage anaerobic hydrogen and methane production process," *Bioresour. Technol.*, vol. 102, pp. 8700–8706, 2011.

[67] Y. X. Zhang, C. R. Xia, M. Ni, "Simulation of sintering kinetics and microstructure evolution of composite solid oxide fuel cells electrodes," *Int. J. Hydrogen Energy*, vol. 37, pp. 3392–3402, 2012.

[68] L. Zhao, B. B. He, J. Q. Gu, F. Liu, X. F. Chu, C. R. Xia, "Reaction model for cathodes cooperated with oxygen-ion conductors for solid oxide fuel cells using proton-conducting electrolytes," *Int. J. Hydrogen Energy*, vol. 37, pp. 548–554, 2012.

[69] Z. B. Liu, B. B. Liu, D. Ding, Z. Y. Jiang, C. R. Xia, "Development of three-layer intermediate temperature solid oxide fuel cells with direct stainless steel based anodes," *Int. J. Hydrogen Energy*, vol. 37, pp. 4401–4405, 2012.

[70] W. Kong, H. Y. Zhu, Z. Y. Fei, Z. J. Lin, "A modified dusty gas model in the form of a Fick's model for the prediction of multicomponent mass transport in a solid oxide fuel cell anode," *J. Power Sources*, vol. 206, pp. 171–178, 2012.

[71] B. Huang, X. J. Zhu, Y. Lv, H. Liu, "High-performance $Gd_{0.2}Ce_{0.8}O_2$-impregnated $LaNi_{0.6}Fe_{0.4}O_3$-delta cathodes for intermediate temperature solid oxide fuel cell," *J. Power Sources*, vol. 209, pp. 209–219, 2012.

[72] K. Feng, T. Hu, X. Cai, Z. G. Li, P. K. Chu, "Ex situ and in situ evaluation of carbon ion-implanted stainless steel bipolar plates in polymer electrolyte membrane fuel cells," *J. Power Sources*, vol. 199, pp. 207–213, 2012.

[73] P. Hu, G. Y. Cao, X. J. Zhu, M. R. Hu, –Coolant circuit modeling and temperature fuzzy control of proton exchange membrane fuel cells," *Int. J. Hydrogen Energy*, vol. 35, pp. 9110–9123, 2010.

[74] A. G. Liu, Y. W. Weng, –Modeling of molten carbonate fuel cell based on the volume-resistance characteristics and experimental analysis," *J. Power Sources*, vol. 195, pp. 1872–1829, 2010.

[75] H. W. He, H. P. Gao, Y. M. Zhang, –Fuel cell output power-oriented control for a fuel cell hybrid electric vehicle," *in Proceedings of American Control Conference*, pp. 605-610, 2008.

[76] S. Wang, L. X. Sun, F. Xu, C. L. Jiao, J. Zhang, H. Y. Zhou, et al., –Hydrolysis reaction of ball-milled Mg-metal chlorides composite for hydrogen generation for fuel cells," *Int. J. Hydrogen Energy*, vol. 37, pp. 6771–6775, 2012.

[77] N. A. Niaz, I. Ahmad, W. S. Khan, S. T. Hussain, –Synthesis of nanostructured Mg-Ni alloy and its hydrogen storage properties," *J. Mat. Sci. Technol.*, vol. 28, pp. 401–406, 2012.

[78] J. Sun, X. P. Qiu, F. Wu, W. T. Zhu, –H_2 from steam reforming of ethanol at low temperature over Ni/Y_2O_3, Ni/La_2O3 and Ni/Al_2O_3 catalysts for fuel-cell application," *Int. J. Hydrogen Energy*, vol. 30, pp. 437–445, 2005.

[79] L. D. Fan, C. Y. Wang, M. M. Chen, J. Di, J. M. Zheng, B. Zhu, –Potential low-temperature application and hybrid-ionic conducting property of ceria-carbonate composite electrolytes for solid oxide fuel cells," *Int. J. Hydrogen Energy*, vol. 36, pp. 9987–9993, 2011.

[80] Z. L. Wu, Y. Y. Zhou, G. S. Lin, S. X. Wang, S. J. Hu, –An improved model for predicting electrical contact resistance between bipolar plate and gas diffusion layer in proton exchange membrane fuel cells," *J. Power Sources*, vol. 182, pp. 265–269, 2008.

[81] J. H. Wang, H. Chen, Y. Tian, M. F. Yao, Y. D. Li, –Thermodynamic analysis of hydrogen production for fuel cells from oxidative steam reforming of methanol," *Fuel*, vol. 97, pp. 805–811, 2012.

[82] Y. M. Yu, N. Q. Zhao, C. S. Shi, C. N. He, E. Z. Liu, J. J. Li, –Electrochemical hydrogen storage of expanded graphite decorated with TiO_2 nanoparticles," *Int. J. Hydrogen Energy*, vol. 37, pp. 5762–5768, 2012.

[83] Y. N. Ye, D. Yan, X. P. Wang, J. Pu, B. Chi, L. Jian, –Development of novel glass-based composite seals for planar intermediate temperature solid oxide fuel cells," *Int. J. Hydrogen Energy*, vol. 37, pp. 1710–1716, 2012.

[84] Q. Zhang, T. Wei, Y. H. Huang, –Electrochemical performance of double-perovskite Ba_2MMoO_6 (M = Fe, Co, Mn, Ni) anode materials for solid oxide fuel cells," *J. Power Sources*, vol. 198, pp. 59–65, 2012.

[85] X. B. Chen, Y. D. Zhen, J. Li, S. P. Jiang, –Chromium deposition and poisoning in dry and humidified air at $(La_{0.8}Sr_{0.2})_{(0.9)}MnO_3$+delta cathodes of solid oxide fuel cells," *Int. J. Hydrogen Energy*, vol. 35, pp. 2477–2485, 2010.

[86] H. L. Cao, Z. H. Deng, X. Li, J. Yang, Y. Qin, –Dynamic modeling of electrical characteristics of solid oxide fuel cells using fractional derivatives," *Int. J. Hydrogen Energy*, vol. 35, pp. 1749–1758, 2010.

[87] Z. S. Lv, D. H. Xie, X. J. Yue, C. H. Feng, C. H. Wei, –Ruthenium oxide-coated carbon felt electrode: A highly active anode for microbial fuel cell applications," *J. Power Sources*, vol. 210, pp. 26–31, 2012.

[88] W. Yuan, Y. Tang, X. J. Yang, B. Liu, Z. P. Wan, –Structural diversity and orientation dependence of a liquid-fed passive air-breathing direct methanol fuel cell," *Int. J. Hydrogen Energy*, vol. 37, pp. 9298–9313, 2012.

[89] Y. H. Bai, M. F. Liu, D. Ding, K. Blinn, W. T. Qin, J. Liu, et al., "Electrical and electrocatalytic properties of a $La_{0.8}Sr_{0.2}Co_{0.17}Mn_{0.83}O_3$-delta cathode for intermediate-temperature solid oxide fuel cells," *J. Power Sources*, vol. 205, pp. 80–85, 2012.

[90] Y. Tang, W. Yuan, M. Q. Pan, Z. P. Wan, "Feasibility study of porous copper fiber sintered felt: A novel porous flow field in proton exchange membrane fuel cells," *Int. J. Hydrogen Energy*, vol. 35, pp. 9661–9677, 2010.

[91] D. H. Zeng, M. Q. Pan, Y. Tang, "Qualitative investigation on effects of manifold shape on methanol steam reforming for hydrogen production," *Renewable Energy*, vol. 39, pp. 313–322, 2012.

[92] S. L. Li, W. Chen, G. Luo, X. B. Han, D. M. Chen, K. Yang, et al., "Effect of hydrogen absorption/desorption cycling on hydrogen storage properties of a $LaNi_{3.8}Al_{1.0}Mn_{0.2}$ alloy," *Int. J. Hydrogen Energy*, vol. 37, pp. 3268–3275, 2012.

[93] Y. H. Cai, T. Chen, T. Q. Yang, J. S. Xiao, "Mechanism of water transport in serpentine cathode channels of proton exchange membrane fuel cells," *J. Power Sources*, vol. 209, pp. 90–104, 2012.

[94] L. Guo, D. M. Zhang, L. T. Duan, Z. Y. Wang, W. H. Tuan, "Formation of nano-contacts on Fe-Ni-Cr alloy for bipolar plate of proton exchange membrane fuel cell.," *Int. J. Hydrogen Energy*, vol. 36, pp. 6832–6839, 2011.

[95] Y. Jun, H. Zarrin, M. Fowler, Z. W. Chen, "Functionalized titania nanotube composite membranes for high temperature proton exchange membrane fuel cells," *Int. J. Hydrogen Energy*, vol. 36, pp. 6073–6081, 2011.

[96] Q. H. Chen, L. J. Gao, R. A. Dougal, S. H. Quan, –Multiple model predictive control for a hybrid proton exchange membrane fuel cell system," *J. Power Sources*, vol. 191, pp. 473–482, 2009.

[97] X. D. Wang, X. X. Zhang, W. M. Yan, D. J. Lee, A. Su, –Non-isothermal effects of single or double serpentine proton exchange membrane fuel cells," *Electrochim. Acta*, vol. 55, pp. 4926–4934, 2010.

[98] X. D. Wang, Y. X. Huang, C. H. Cheng, J. Y. Jang, D. J. Lee, W. M. Yan, A. Su, –An inverse geometry design problem for optimization of single serpentine flow field of PEM fuel cell," *Int. J. Hydrogen Energy*, vol. 35, pp. 4247–4257, 2010.

[99] X. D. Wang, W. M. Yan, Y. Y. Duan, F. B. Weng, G. B. Jung, C. Y. Lee, –Numerical study on channel size effect for proton exchange membrane fuel cell with serpentine flow field," *Energy Convers. Manage*., vol. 51, pp. 959–968, 2010.

[100] X. D. Wang, Y. Y. Duan, W. M. Yan, D. J. Lee, A. Su, –Channel aspect ratio effect for serpentine proton exchange membrane fuel cell: Role of sub-rib convection," *J. Power Sources*, vol. 193, pp. 684–690, 2009.

[101] X. D. Wang, Y. Y. Duan, W. M. Yan, X. F. Peng, –Local transport phenomena and cell performance of PEM fuel cells with various serpentine flow field designs," *J. Power Sources*, vol. 175, pp. 397–407, 2008.

[102] L. P. Duan, –Analysis of the relationship between international cooperation and scientific publications in energy R&D in China," *Appl. Energy*, vol. 88, pp. 4229–4238, 2011.

Chapter 7 Conclusion and Future Work

7.1 Summary and conclusion

The major contributions of the thesis are summarized corresponding to the chapters of the thesis, followed by the main conclusions for each chapter.

The major contributions of chapter 2 include: (1) the empirical model of PEMFC is developed using support vector machine (SVM); (2) the hybrid modelling approach is proposed by combining the empirical submodel and mechanistic submodel.

The main conclusions are:

- SVM is a powerful tool for nonlinear system identification and modelling due to its excellent performance in function regression. Using SVM, the proposed empirical model shows some desirable properties, including good accuracy, fast response and low computational burden. These characteristics lay the solid foundation for the control study.

- Using the hybrid modelling approach, the proposed combined model overcomes the disadvantages of both the empirical model and the mechanistic model. Compared with pure empirical model, the combined model can be built with less operational data due to the reduction of input dimensions. In addition, unlike pure empirical model, the combined model has generalization ability, which means the combined model is not limited to a specific application or a narrow corridor of operating conditions. On the other hand, unlike pure mechanistic model, the combine model has simple expressions and provides low computational burden.

The major contributions of chapter 3 include: (1) the model predictive control (MPC) strategy is developed using Model Predictive Control Toolbox of the MATLAB program; (2) the novel MPC strategy is designed by employing the particle swarm optimization (PSO) algorithm; (3) the constrained MPC strategy is designed and the standard PSO algorithm is modified to hand the constraints.

The main conclusions are:

- Using Model Predictive Control Toolbox, the MPC strategy proposed shows good performance with respect to maintaining the performance outputs at the nominal value during the transit operating conditions. More precisely, when step changes occur in the stack current as a result of uncontrollable load, the oxygen excess ratio and the stack voltage are able to be maintained at 2.33 and 250V, respectively. Besides, the proposed MPC strategy causes no overshoot. However, the proposed controller has some drawbacks in terms of response speed, resulting long settling time.

- Due to its fast convergence speed and strong robustness, PSO is suitable to solve the real-time optimization problem formulated by MPC. Using PSO as optimizer, the novel MPC strategy achieves robust control of PEMFC voltage with good performance in tracking both constant and dynamic set points. In addition, due to the introduction of reference trajectory, the novel MPC avoids excessive movement of control inputs and achieves smooth tracking performance.

- The constrained MPC strategy is proposed to prevent reactant starvation and excessive pressure difference across the membrane. The standard PSO algorithm is not able to solve the constrained optimization problem formulated by the constrained

MPC. Therefore, it is modified by introducing a constraint violation checking procedure to handle the constraints. In addition, the modified PSO is accelerated by improving the initialization process based on the optimal control sequence obtained by MPC receding strategy at the previous sampling period. The constrained MPC strategy with the modified PSO algorithm achieves robust control of stack voltage. Meanwhile, the constraints are not violated, which means the reactant starvation and excessive pressure difference across the membrane are effectively prevented.

The major contributions of chapter 4 include: (1) the efficiency curves of PEMFC under different operating conditions are obtained and analyzed; (2) the maximum efficiency point tracking (MEPT) controller is designed based on the extremum seeking control (ESC) theory.

The main conclusions are:

- The steady-state analysis shows that the efficiency curves of PEMFC are unimodal with the peak determined by the combination of the stack current and the oxygen excess ratio. This implies that improved performance may be achieved by identifying the maximum efficiency point and regulating the system about this point.

- MEPT problem is a so-called extremum seeking control or self-optimizing control problem. It means the control objective is the optimization of an objective function which may depend on unknown model parameters, or the selection of the desired inputs to keep a performance function at its extremum value. Particularly for MEPT problem, the maximum efficiency points depend on the changing stack current caused by the uncontrollable load. Therefore, when varriations in the stack current occur, the oxgyen excess ratio has to be adjusted to achieve the maximum efficiency.

- Based on extremum seeking control theory, the MEPT controller is designed. By searching for the optimal oxygen excess ratio in real-time, the proposed MPET controller shows good performance in tracking the maximum efficiency point under changing stack current conditions. Compared with traditional methods, the proposed controller has three advantages. First, the optimization problem is solved by feedback control law. Hence, it has a main advantage of strong robustness over other open-loop control methods. Second, it is a real-time control method. Therefore, it can be used for real-time optimization of time-varying systems. Third, it does not require prior knowledge of system model. In other words, it is a non-model based control method. Despite these desirable properties, it also comes with drawback. The periodic perturbation will bring oscillations into the system. Thus, when the system reaches the extremum, the system oscillates about this value rather than converging to it exactly.

The major contributions of chapter 5 include: (1) the control-oriented thermal model of PEMFC is developed; (2) the model-based thermal controller is designed.

The main conclusions are:

- The control-oriented thermal model that considers both PEMFC stack and coolant is developed based on the energy conservation principle. The model is nonlinear with disturbances and uncertainty. The main reasons are: (a) the stack current is modelled as disturbance, which corresponds to the uncontrollable load; (b) many physical parameters may vary to a large extent under different operating conditions.

- Since the model is formulated in nonlinear affine form with disturbance, the input/output linearization method is employed by introuducing a dynamic feedforward/static state feedback law. The temperature controller is then designed based on the linearized model. The proposed controller shows better performance than PID controller in terms of accuracy.

The major contributions of chapter 6 include: (1) China‘s main drivers for the transition towards the hydrogen economy are indentified; (2) China‘s energy supply matrix is reviewed and the potential role of different energy resources in future hydrogen economy is analysed; (3) China‘s policy and government support programs for the R&D of hydrogen and fuel cell technologies are reviewed. Research achievements are also summarized.

The main conclusions are:

- Four main drivers are indentified: (1) energy security; (2) climate change; (3) urban air pollution; (4) competitiveness. China considers the energy security as its first priority, with special concern for ensuring continuous and sufficient oil supply. Hydrogen can be produced from diverse resources, both renewable (solar, wind, hydro, biomass) and non-renewable (coal, oil, natural gas). Therefore, hydrogen can diversify the energy supply and reducing the dependence on oil imports. Meanwhile, China has huge greenhouse gas and other pollutant emissions due to its heavy industry background and large population of vehicles. Hydrogen serves as a potential solution to these problems as it is a clean and efficient fuel, causing low CO_2 or other pollutant emissions. China‘s global competitiveness will also be fostered if China companies are able to forge a lead in hydrogen and fuel cell technologies

- Coal is the backbone of China‘s current energy system. China‘s coal-based energy system is both beneficial and detrimental to the transition towards hydrogen-based economy. In favor of hydrogen economy is the availability of so much potential hydrogen fuel, while the current reliance on coal, the low price of ―dirty‖ energy delivery and the established infrastructure of the coal power industry may make it difficult to increase industrial momentum towards the hydrogen economy. On the other hand, oil and natural gas are not ideal sources for hydrogen production due to their high price and limited reserve. In the long term, renewable energy resources are likely to play a more important role in hydrogen production due to their abundant reserves in China. The major barrier to the commercialization of renewable energy is the high cost of infrastructures, which results in the high electricity tariff and the low market acceptance. Under such circumstances, government incentive is an effective way to encourage renewable energy production.

- China government has made ambitious plan and provides strong financial support for hydrogen and fuel cell technology development. All of China‘s top-tier institutes and universities are conducting hydrogen and fuel cell research. Of the various fuel cell types, the high temperature variants—SOFC and MCFC—are most suitable for hydrogen that is derived from hydrocarbon sources. Unlike low temperature cells such as the PEMFC, both the SOFC and MCFC can tolerate carbon oxides in the fuel and indeed are able to oxidise CO directly. Studies have shown that fuel produced from coal gasifiers can be used in the SOFC and MCFC. Considering China‘s coal-based energy system, this may be an important application in the future.

In sum, the thesis's main contributions to new knowledge are:

- Modelling methods: (a) A new empirical model of PEMFC is developed using SVM. (b) A novel hybrid modelling approach is applied to PEMFC for the development of the combined empirical and mechanistic model.

- Control methods: (a) A new MPC strategy is proposed by integrating PSO algorithm. (b) A new constrained MPC strategy of PEMFC is formulated and solved by the modified PSO algorithm. (c) The maximum efficiency point tracking problem of PEMFC is first analysed and solved based on extremum seeking control theory. (4) The input/output linearization method is applied to the nonlinear affine model of PEMFC thermal system to derive a new dynamic feedforward/static state feedback control law.

7.2 Future work

The major part of this work focuses on the modelling and control of PEMFC system. However, PEMFC has limitations on its dynamic response. This is because of the mechanical delays of the fuel delivery system such as valves and pumps and also the limited rate of heat release. Therefore, an additional energy source is needed to complement the slow dynamics of PEMFC when rapid load variations occur. This energy source could be an ultracapacitor or a battery pack.

The modelling and control of the hybrid power system that consists of PEMFC and secondary energy source are critical issues for future research. The dynamic behaviour of each component must be carefully considered and modelled in order to ensure sufficient power flow. The power flow control strategy of the hybrid power system should be optimized to supply the required power with the highest efficiency.